Sensitive Soils of the Puketoka Formation, Hamilton, New Zealand

A thesis submitted in partial fulfilment

of the requirements for the degree

of

Master of Science (Research) (Earth Sciences)

at

The University of Waikato

by

Emily Charlotte Kitchen

2021

THE UNIVERSITY OF
WAIKATO
Te Whare Wānanga o Waikato

Dedicated to my dear mum,

Thank you from the bottom of my heart for everything you have done and continue to do for me, and for encouraging me to become who I am today.

Abstract

Sensitive soils are known to cause significant issues in the infrastructure and civil engineering industry, and are prone to sudden, oftentimes catastrophic failures following long periods of stability. The Walton Subgroup soils deposited through volcanic activity and partially reworked by the ancestral Waikato River are identified within the Hamilton Basin. These materials are of interest to the engineering community, and consultancy groups in the Hamilton area, due to their identified sensitivity. The Puketoka Formation was focused on in this study.

Sampling of material was undertaken at two active construction sites in Hamilton: Dixon Road Roundabout, and Temple View Urban Development. A series of classification tests were completed to determine the samples' mineralogical and geotechnical characteristics.

Mineralogical testing found that all the materials were silt dominated (55.06 – 81.12 %), with sub-ordinate clay (13.10 – 18.85 %) and sand (5.56 – 25.35 %) fractions. The moisture contents were variable (49 – 65 %). The field moist bulk density varied throughout the samples (1069 – 1576 kg/m^3), as did the oven dry bulk densities (645 – 1057 kg/m^3). The porosity as a result also varied (36 – 51 %). The void ratios followed the same trend as the porosity values (0.56 – 0.88). The particle densities of the materials also showed variation (1935 – 2487 kg/m^3). The activities of all three samples were variable, ranging from inactive (0.60) to active (1.79). The X-Ray Diffraction (XRD) analysis determined that the main clay mineral present within the samples was a kaolinite group clay, either halloysite or kaolinite. The Fieldes & Perrott NaF test to determine the presence of allophane was also completed on the samples. Both tests were negative, confirming the dominance of halloysite. Bulk analysis also determined other constituents of the samples to include quartz, plagioclase, augite and volcanic glass. Scanning Electron Microscopy (SEM) indicated the main halloysite morphologies present to be a combination of short and long tubules, spheroids, plates and book formations. The microstructure was analysed, and the main clay minerals, grains, microaggregates, and pores within the materials described. The microfabric was consistent for all three samples, with each showing an abundance of small pores (< 20 μm). These pores hold significant amounts of water in not readily accessible locations, leading to the highly porous, but poorly permeable nature of the materials. DRAB1 and TV1 showed microstructures consistent with Huppert (1986) and Beattie's (1990) 'matrix' structures, whilst TV2 showed a more dominant 'skeletal' to 'matrix' structure.

Atterberg limits testing found that the samples had a high liquid limit (59 – 75 %) and plastic limit (41 – 53 %), but a variable plasticity index (8 – 34 %) and liquidity index (0.1 – 2). This placed all three samples within the high plasticity "MH" category upon the Casagrande chart. Consolidated undrained triaxial testing of DRAB1 and TV1 indicated a characteristic normally consolidated response to shear, with the majority of cores showing shear band formation. Only TV1 at 170 kPa displayed an intermediate failure type, potentially occurring due to a combination of material being tested, confining pressure, and the low shear rate allowing time for pressure dissipation. The percentage of axial strain the cores failed at varied (1.81 – 16.35 %), and the peak deviator stress (129 – 277 kPa) and pore water pressure values (717.2 – 879.7 kPa) tended to increase as the confining pressures increased. Graphical outputs show a moderate strain, contractive (MSC) style of failure. The effective shear strength values produced were in keeping with the varying ranges of previously published values (effective cohesion: 0 – 37 kPa, effective friction angle: 27 - 38°). The permeability for all three samples was estimated to

be ~10^{-9} – 10^{-10}. Thin section analyses of failed core sections for DRAB1 at 270 kPa confining pressure and TV1 at 130 and 230 kPa confining pressures found that some degree of shear formation and propagation occurred. The calculated R' angle for DRAB1 was closely observed in the thin section, however was not for TV1. This was hypothesised to have occurred due to a true shear band failure not occurring, rather the development of intermediate to juvenile shear bands within the soil.

The sensitivity of the Puketoka Formation and wider Walton Subgroup is hypothesised to have been derived from the reworking and weathering the materials experienced. This in turn influenced the porosity and permeability of the materials, which I believe govern the sensitivity of the soils to a degree. Therefore, I believe the Puketoka Formation materials are representative of a silt-dominated, minimally reworked deposit of volcanic origin, that showed appreciable differences compared with the previously studied Tauranga soils.

The remediation strategies used in the engineering industry were also analysed, and the suitability of the strategies in the context of the Puketoka Formation discussed. This assessment provides an overview of why traditional strategies for remediation may not be beneficial in some cases for the Walton Subgroup materials, which could be of benefit to key engineering groups that encounter these soil materials.

The results of this study provide a set of data which can be used as an initial reference point. The findings and hypotheses made could be of use to key groups including local engineering consultancies, who handle these materials regularly.

Acknowledgments

I would like to extend a massive thank you to every single person that has helped me throughout this experience. I am so grateful to each and every one of you.

I would first like to give my wholehearted thanks to my supervisor, Dr Vicki Moon, for the way in which you supervised the study throughout. Letting me run wild with this research and allowing me to write to my heart's content, before reining it all back into a piece of work that is concise (ish!) and relevant is truly commendable, and I am very grateful for all your help. Sorry for making your red pen run out of ink!

To AECOM Hamilton, in particular, Principal Engineering Geologist Darren Maxwell and Senior Engineering Geologist Nick Lethborg for being so accommodating and allowing me to gather samples from Dixon Road Roundabout. To Kyron Day for casting your engineering eye over my (often wrong) maths and for reading and listening through my thesis ramblings, always providing thoughtful and useful feedback. And to the rest of the geotech team for chatting to me about my thesis, your collective knowledge and experience was of great help. I hope this work provides some useful information to the team. To CMW Geosciences for allowing me to "jump the fence" and gather samples from the Temple View Urban Development site. Thank you to Associate Engineering Geologist Kori Lentfer for kindly organising for me to come along and take samples, and to Izzy for spreading the word about my thesis. I couldn't have done it without you! Hopefully this makes for some interesting reading. To Schick Civil Construction Limited for allowing me access to these sites.

To the University of Waikato for awarding me a Postgraduate Research Masters Scholarship, First Tier.

To all of the staff at university who have helped me. To Thomas Robertson for your unending patience in teaching me how to use the triaxial apparatus, and for answering all the ridiculous questions I came up with along the way. To Kirsty Vincent for your continued help with a number of lab-based tests I needed over the course of this study. Your expertise and skill in getting some difficult soils to behave helped this thesis significantly. To Helen Turner of the Scanning Electron Microscope unit for your expertise in helping produce imagery of some challenging soil material. To Annette Rogers and Holly Harvey-Wishart, for helping me with all the mineralogical testing needed for my thesis. And to Cheryl Ward, for helping me format my thesis.

A big thank you is needed for my dear friends who have supported me throughout the course of this study. You are some of my most fervent supporters, always encouraging and believing in me both in this research, and elsewhere in life. Thank you for taking a genuine interest in my work, and for letting me talk your ears off about it for the past year and a half! Hopefully I haven't given you tinnitus.

To my dad. Although things have been difficult the past few years, I hope this work makes you proud.

Finally, I would like to express my utmost thanks to my mum, whose constant support and encouragement helped me exceed all my expectations and produce this piece of work of which I am so proud. Hopefully it makes for some enjoyable light reading!

Table of Contents

Please see supplementary document for appendices.

List of Figures

List of Tables

Chapter 1
Introduction

1.1 Background and research motivation

Soil sensitivity is defined by the ratio between the measured peak and remoulded strength values, assuming that the soils are at the same moisture content, where high sensitivity corresponds with a dramatic loss of strength on remoulding. This leads to very fluid, high mobility debris flows. As a result, sensitive soils have long been identified as posing threats to infrastructure and human livelihood, due to their unpredictable nature.

In the Northern Hemisphere, sensitive soils have been found to generally form from glacial outwash clays that have been deposited in a shallow sea, followed by uplift into a subaerial environment after which they have experienced significant leaching and weathering. The majority of these sensitive clays have been identified in Canada and Scandinavia, therefore a large amount of research and supporting information has been developed for these regions (Gillot, 1979; Thakur et al., 2017). Typical landslide features include extensive, retrogressive flowslides with large, low-angle source areas leading to long run-out debris flow deposits (Thakur et al., 2017).

Other areas of the world that also have identified sensitive soils include Indonesia, Japan, and more locally, New Zealand, particularly in the volcanic soils of the North Island. Many of these sensitive soils do not share the mode of formation of the sensitive clays seen in the Northern Hemisphere, rather, forming from rhyolitic and andesitic tephra material. The presence of the clay minerals halloysite and allophane governs the sensitivity of the materials (Joussein et al., 2005; Lowe et al., 2012; Moon, 2013; Moon et al., 2015, Kluger et al.., 2017), in contrast with the illite clays dominant in Northern Hemisphere sensitive soils.

The Hamilton Basin contains significant volcanically-derived materials sourced from the Taupo Volcanic Zone (TVZ). There are a number of differing groups of soil material, classified mainly through their relative location within the landscape, predominant method of deposition, composition and mineralogy, and inherent soil properties. One group in particular, the Walton Subgroup, contains the Puketoka and Karapiro Formations, a pair of recognised

sensitive soil formations whose weathering has allowed for the development of halloysite-rich soil. These materials have been identified to have low remoulded strengths, low permeabilities, and a tendency to release excess moisture when disturbed, making them unsuitable for a number of uses in an engineering sense. The Puketoka Formation materials will be analysed in depth throughout this thesis.

1.2 Aims

The main aim of this thesis is to determine the geomechanical, mineralogical, and microstructural properties of samples of Puketoka Formation soils in order to determine if similar geological controls influence the sensitive response of these soils to other studied New Zealand sensitive soils. A secondary aim is to provide a base set of engineering data for these materials through laboratory based testing, and to consider the current engineering remediation practices for Puketoka Formation materials.

Objectives defined to achieve the aims of this thesis research are to:

1. sample sites within Hamilton with exposed sensitive Puketoka Formation soils;
2. undertake geomechanical testing the samples using standardised laboratory testing methods;
3. determine the characteristic microstructural and mineralogical properties of the tested materials;
4. hypothesise the main factors governing sensitivity within the Puketoka Formation; and
5. use the results and observations of the samples tested to provide potential insights from an engineering perspective.

1.3 Benefits of the thesis research

The benefits for the completion of this thesis research include:

a) recent, quantitative and qualitative data gained for the Puketoka Formation materials that provides information that could be of use to a number of key groups including consultancies and academic organisations;

b) a detailed analysis of the microstructure of the soils, filling a gap in previous knowledge and providing a basis for future focused research determining the relationship between halloysite morphologies and sensitivities;

c) an hypothesis into the factors governing sensitivity in the Puketoka Formation materials; and

d) an insight into the current remediation strategies being applied to soils such as the Puketoka Formation, and how these may not be effective in some cases.

1.4 Layout of thesis

Following the introduction (**chapter 1**), **chapter 2** outlines the background information for the study, identifying the Walton Subgroup, which contain the Puketoka and Karapiro Formations. The history of sensitive soil classification is explored, in addition to the common regions of the world where sensitive soils occur, and how these differ between the Northern and Southern Hemispheres. The common clay minerals that cause sensitivity are then discussed, along with the common engineering issues relating to sensitive soils *in situ*.

Chapter 3 then discusses the methods used in the laboratory. The site selection processes and rationale are also detailed.

Chapter 4 describes the sampling sites in greater detail and discusses the sampling procedures undertaken. **Chapter 5** summarises the results of the Atterberg Limits testing completed for the samples, and discusses the calculated bulk density, particle density, moisture content and porosity values. **Chapter 6** summarises the results of x-ray diffraction and particle size analysis tests. **Chapter 7** summarises triaxial test results including analysis of the primary mode of failure, and the characteristic graphical responses. Thin sections of the failed cores are

also analysed. **Chapter 8** summarises the scanning electron microscope results, further analysing the dominant clay mineral in the samples. The microstructure of the materials is also assessed.

Chapter 9 reverts to a broader discussion, analysing all the findings and research gained over the course of the thesis, and compares the findings to relevant literature present surrounding the topic. The controls of sensitivity in the Puketoka Formation are also explored. The implications of these findings within an engineering context are also discussed. Any limitations encountered during the study are also discussed here. Finally, **chapter 10** closes the study with concluding statements surrounding the research completed, and the information gained throughout the course of the study, reiterating key findings and conclusions made regarding the Puketoka Formation materials.

Chapter 2
Literature Review

2.1 Introduction

Sensitive soils can cause significant damage to the landscape and infrastructure when large-scale failure events occur. The identification of sensitive soils, and the subsequent management practices to ensure the risks of the soil behaviours are minimised, is a critical factor in engineering geology as a result. This chapter is split into several sections. First, the geological background to the Hamilton Basin is described, with the characteristic landscape units, and the characteristic material types identified. Then, sensitivity in soils is defined, and the characteristics of sensitive soils are described before sensitive soils identified in New Zealand are compared with soils in the Northern Hemisphere. The clay minerals that cause sensitivity in soils are then defined before the hazards are outlined. Finally, the current remediation strategies for sensitive soils are identified, and the lack of literature supporting this issue is demonstrated.

2.2 Background to study area

2.2.1 Geological background of the Hamilton Basin

The Hamilton Basin is an oval shaped depression that is greater than 80 kilometres in length running from north to south, and over 40 kilometres wide (Selby & Lowe, 1992). The basin is bounded in nearly all directions by various mountain ranges, except to the south (**Figure 2.1**). The Hakirimata and Taupiri Ranges bound the basin to the north, the Pakaroa Ranges to the east, and the Alexandra Volcanics and Kawhia Syncline (Western Uplands) to the west of the basin (Selby and Lowe, 1992). In the southern direction, the basin floor material rises and connects with the land of the King Country Plateaux (Selby & Lowe, 1992). The Hamilton Basin was initially produced around 5 million years ago (Ma) as a direct result of normal faulting that produces tectonic features including the Hauraki Graben across the now defined Waikato Region (Selby & Lowe, 1992). The Waikato River runs through the Hamilton Basin and is responsible for much of the more recent landscape development (McCraw, 2011).

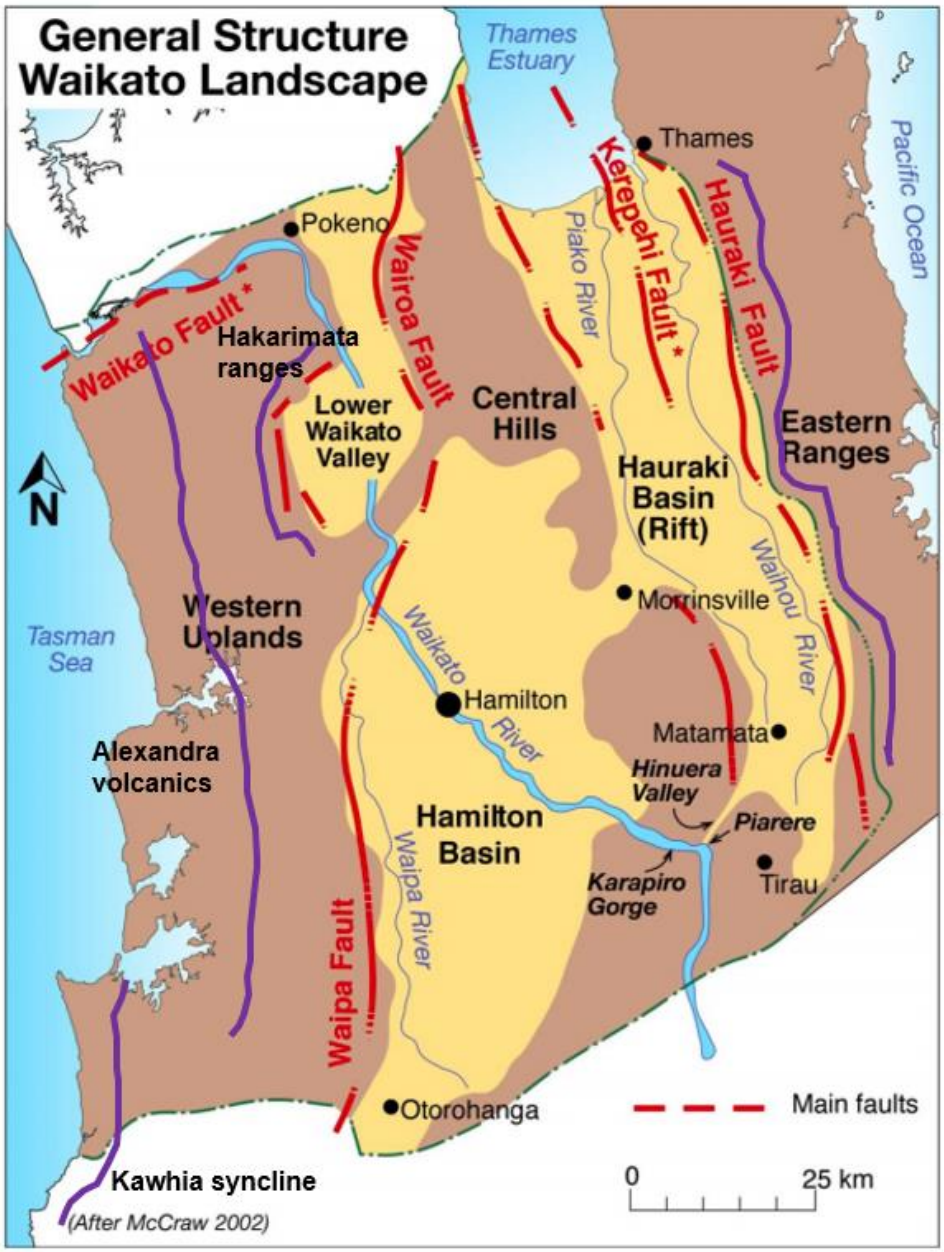

Figure 2.1. Schematic of the Hamilton Basin, detailing the general basin structure. The purple lines indicate the mountain ranges of the region, as described above (Lowe, 2010).

2.2.2 Landscape units of the Hamilton Basin

There are four main distinctive landscape units identified within the Hamilton Basin. These landscape units characterise the materials that constitute the units and the geomorphic processes that formed them over geological time (Lowe, 2010). The units consist of low rolling hills, flat to gently undulating alluvial plains, lowland terraces, and gullies (**Figure 2.2**). The low rolling hills are mantled by Walton Subgroup airfall ash layers that were deposited from

around a million years ago and tend to consist of the airfall tephric deposits of the Hamilton Ash Formation, and the older Kauroa Ash Formation. The alluvial plains represent the alluvium deposits derived from the volcanic activity of the Taupo Volcanic Zone (TVZ) from around 100ka that were deposited within an ancestral Waikato River and are classified as the Hinuera Formation. The lowland terraces are comprised of pumice alluvium deposited as a direct result of a breakout flood event from a TVZ eruption that occurred in 232 $\pm$ 5AD and is classified as the Taupo Pumice Alluvium. The gullies are indicative of fluvial downcutting from the path of the ancestral Waikato River, and expose the alluvial Hinuera Formation, and tend to cut towards the current path of the Waikato River (Lowe, 2010).

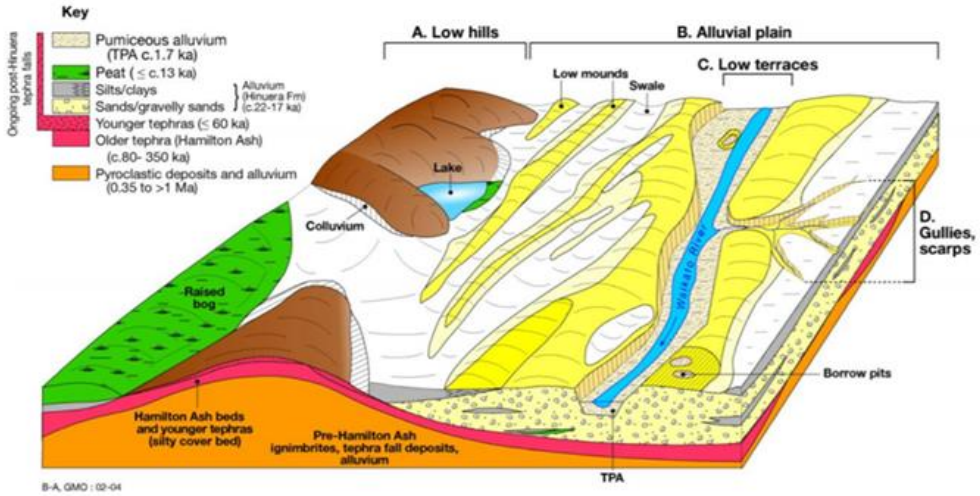

Figure 2.2. Schematic diagram showing the main landscape units within the Hamilton Basin, showing the predominant materials comprising each unit (Lowe, 2010).

2.2.2.1 Walton Subgroup

The Walton Subgroup are a group of formations deposited in the early Quaternary, and are Pleistocene age, terrestrial deposits that make up the low rolling hill formations which rise above the more recent alluvial plains of the basin. The Quaternary period of deposition extends from around 1.8 million years before present. The Walton Subgroup is dominated by formations of poorly welded ignimbrites and tephra deposits, which characterise a sequence of interfingering pumiceous lenses of fine-grained sands and silts, with interbeds of peat, pumiceous gravelly sands, and mud (White et al., 2015).

The Walton Subgroup includes three formations: the Puketoka Formation, the Waeranga Gravels, and the Karapiro Formation (Kear et al., 1978). The oldest of the subgroup deposited is the Puketoka Formation, characterised by both well-sorted, pumiceous clays, sands and breccias, in addition to unsorted beds which make up the distal portions of the rhyolitic ignimbrite sheets (Selby & Lowe, 1992). The Puketoka Formation often produces bluff formations, due to the deposition of silica on the surface pumiceous beds (Kear et al., 1978).

The pumiceous clays, sands and breccias representing fluvatile and lacustrine sediments are characterised by fine, light coloured pumice sands and silts that were formed from a fine, argillized volcanic glass (Kear et al., 1978). These glass particles are cylindrical in shape, and often contain small deposits of light clays within them (Kear et al., 1978). These glass particle concretions provide evidence of agitated water (Kear et al., 1978). The greatest outcrops of this variant are found upon the north-eastern lowlands of the Hamilton Basin.

The unsorted pumice variant is more common than the sorted materials. This variety consists of unsorted, coarse white pumice ignimbrite in a coherent form, with around 25% quartz fragments (Kear et al., 1978). This variant is characteristic in that it contains a large proportion of rhyolitic volcanic glass, which is commonly argillized. This relates to its' method of formation and deposition, during periods of extreme rhyolitic volcanism.

The Waeranga Gravels is a localised unit consisting of weathered greywacke debris, which likely originated from the surrounding mountain ranges and was deposited via alluvial fans. The Waeranga Gravels are restricted to old valleys that have cut into the ranges of Hokanui greywacke rocks (Kear et al., 1978). The distinctive features of the Waerenga Gravels includes the locally derived constituents, usually from portions of Hokanui rocks, which are embedded in the sandy matrix. The Waerenga Gravels are characteristically highly weathered, with most of the greywacke pebble fragments being broken by hand (Kear et al., 1978). The Waeranga Gravels are also assumed to be the lateral equivalents of the Karapiro and Puketoka Formations (Kear et al., 1978).

Any sediments younger than the Puketoka Formation that underlie the eroded aggraded plains are included in the Karapiro Formation. The formation can often lie unconformable over the Puketoka Formation and can be somewhat compared with the Hinuera Formation in its' spatial extent and origin through fluvial alteration and deposition (Kamp & Lowe, 1981).

As a result, it is widespread in the Hamilton Lowlands and the lower Waikato region. The Karapiro Formation tends to be multicoloured, containing white, grey, orange, pink, red and browns (Kear et al., 1978). Most of these hues are caused by deep weathering processes.

The Karapiro Formation is geologically very similar to the Hinuera Formation, as they are current-bedded volcanic grits which show similar lithologies to the well described Hinuera Formation (Kear et al., 1978). The Karapiro Formation likely had complex modes of formation and had the influences of eustatic fluctuations and sediment supply changes (Kear et al., 1978).

In most cases, however, the Puketoka and Karapiro Formations are challenging to distinguish between one another due to the interfingering nature of the formations and differing spatial extents and thicknesses, as first discovered by Kear and others (1978) works makes it hard to distinguish between the two formations. In practice, the Karaprio Formation is assigned to any material with clear fluvial origin, whilst the Puketoka Formation classification is applied to inferred pyroclastic flow deposits (Moon, V., Personal Communication, 10th August 2021). This classification is an oversimplification, as the Puketoka Formation contains reworked materials that were influenced by local alluvial processes. For the purposes of this study however, any materials being tested will be referred to as the Walton Subgroup, to minimise the risk of misclassification.

2.2.2.2 Kauroa and Hamilton Ash

A time discontinuity between the deposition of the Kauroa and Hamilton Ashes has been observed, and the units deposited below this surface have been determined to be the Kauroa Ash Formation (Ward, 1972). The younger beds are identified as the Hamilton Ash Formation (Ward, 1972). The Kauroa and Hamilton Ash depositions occurred in the Quaternary contemporaneously with basin infilling by fluvial, lacustrine and ignimbrite deposits from the Taupo Volcanic Zone (TVZ) and the ancestral Waikato River. Within this time, a series of air-fall tephras were deposited, mainly from volcanic activities relating to the TVZ (Selby & Lowe, 1992). Two key formations can be identified, with the first being the Kauroa Ash Formation.

The Kauroa Ash beds are clay rich, highly weathered tephras, and many of the deposits have been largely removed by erosion due to a long delay between depositions. Following erosion, another tephra was deposited, and mantled the landscape. A 3 to 5 m thick layer was deposited, and is classified generally as being strongly weathered, with a clay texture, and tends to be firm in strength (Selby & Lowe, 1992).

The Hamilton Ash Formation is around 36,000 years old in age, is loessic in origin, and mantles the landscape (Lowe, 1981). The ash beds are patchy across the region, because of

erosional processes that occurred following the deposition of the formation (Ward, 1972). The Hamilton Ash Formation has been identified to be subaerial in depositional nature, formed from a volcanic event that occurred within the Taupo Volcanic Zone (TVZ) (Lowe, 1994). The Hamilton Ash units have been shown to be strongly weathered, clay-textured tephric layers and paleosols (Lowe, 1994). There are several distinctive beds within the Hamilton Ash Formation, with the oldest bed typically being pale yellowish-brown colour (Lowe, 1994). Overlying this bed, the rest of the beds are more reddish yellow to strong brown in colour, are characteristically clayey in texture, and range from friable to firm consistency (Lowe, 1994). These ash beds are determined to be rhyolitic in origin, and generally contain halloysite clays.

2.2.2.3 Hinuera Formation

Following the deposition of the tephra layers, the surface layers began to be deposited. This originated from the depositional products of the ancestral Waikato River. The Hinuera Formation is low angled, and was deposited around ~20,000 years ago, and generally consists of bedded and cross bedded pumice sands, silts and gravels with interbedded peats (Edbrooke, 2005). The dominant sediments making up the Hinuera Formation consist of quartz, feldspars, rounded rhyolitic rock fragments, pumice and heavy minerals (Hume et al., 1975; Selby & Lowe, 1992).

2.3 Sensitivity

2.3.1 Sensitivity definition

Sensitive soils are defined as soils that alter from a stiff and brittle material when dry, into viscous liquids when stresses are applied to remould the soil (Thakur et al., 2017). Sensitive soils can stay stable in situ for thousands of years, before suddenly losing all strength. Sensitivity is triggered by disturbances and occurs through the transferral of effective stress onto the water contained within the inter-pore spaces of the soil, leading to a reduction in the cohesive forces between particles (Thakur et al., 2017). The soil can then potentially behave as a liquid, leading to often catastrophic levels of failure (Selby, 1993).

2.3.2 Sensitivity calculation

Sensitivity is defined using a specific **equation (2.1)**, that assumes two samples being tested in a laboratory or in the field, both undisturbed and remoulded, have the same water content (Selby, 1993).

$$sensitivity = \frac{undisturbed, undrained\ stength}{remoulded, undrained\ strength} \qquad (2.1)$$

Sensitivity is presented as a ratio; and a large degree of variability can be experienced within tests, even in differing soils of the same origin (Selby, 1993). Therefore, in terms of geotechnical testing in New Zealand, the New Zealand Geotechnical Society (NZGS) in 2005 published a set of numbers characterising sensitivity in soils, based upon basic field testing (shear vane testing) (New Zealand Geotechnical Society, 2005). **Table 2.1** shows the ratio thresholds that define the differing levels of sensitivity within the soil. The term 'quick' is generally not used to describe soil sensitivity in modern literature, however, it is still used as a classification description by the New Zealand Geotechnical Society.

Table 2.1. Sensitive soil values determined by the NZGS to define different levels of sensitivities for a soil in-situ (New Zealand Geotechnical Society, 2005).

Descriptive Term	Shear Strength Ratio $\frac{\text{undisturbed}}{\text{remoulded}}$
Insensitive, normal	< 2
Moderately sensitive	2 – 4
Sensitive	4 – 8
Extra sensitive	8 – 16
Quick	> 16

International classifications of sensitive soils differ somewhat from those used in New Zealand. The Canadian Foundation Engineering Manual outlines how the seismic hazard is assessed, and tends to use the spectral format for assessment, which considers the soil class and the probability of the soil failing at ~2 % chance every 50 years (Abuhajar et al., 2010). This

manual gives a value of sensitivity, S_t, which can then be used to identify the level of sensitivity with a range of pre-defined values (**Table 2.2**).

Numerous methods are used to determine the sensitivity of a soil, including unconfined compression tests, optimum moisture content estimation, amongst other lab-based testing methods. These value ranges are much broader than the New Zealand classification scheme, and the values are significantly larger. This is the case because sensitivity can vary greatly in soils in different countries (Abuhajar et al., 2010). Sweden, for example, includes soils in the 'low sensitivity' category, which would produce an 'extra' or 'highly' sensitive rating in New Zealand or the USA. The Swedish and Canadian classes reflect the extent of very sensitive soils in Scandinavia and Canada (Abuhajar et al., 2010).

Table 2.2. Comparison table of the American, Canadian and Swedish classification of soil sensitivity, in relation to testing criteria of the soils (Abuhajar et al., 2010).

	S_t		
Classification	**USA**	**Canada**	**Sweden**
Low sensitivity	2-4	< 10	< 10
Medium sensitivity	4-8	10-40	10-30
High sensitivity	8-16	> 40	30-50
Quick	-	-	50-100
Extra quick	-	-	> 100

2.3.3 Sensitive soil characteristics

Sensitive soils can often be identified based upon the characteristics they display *in situ*, in addition to the characteristic behaviours they display. Generally, a sensitive soil can be identified within the laboratory by looking for the following key characteristics (Lefebvre, 1996):

- open fabric;
- high moisture content;
- high amounts of clay minerals within soil body;
- sensitivity value of greater than 30; and

- remoulded shear strength less than 0.5kpa.

Sensitive soils typically display a metastable structure prior to disturbance. Several factors can cause disturbance within the soils: through an earthquake or some smaller scale action such as traffic movement, or more commonly in the case of New Zealand sensitive soils, through the reduction of pore water pressures within the soil body (Gillott, 1979). The open, flocculated structure, held together by edge to edge bonding of the aluminosilicate layers to one another is destroyed, allowing the materials to assume a closer structure (Gillott, 1979). This opens the voids between the layers that contain pore water, which can then be freely released, leading to an oversaturation of water within the soil profile, which produces a net positive pore water pressure, and greatly reduces the strength of the soil profile (Gillott, 1979).

2.3.4 Sensitive soils in New Zealand, in comparison to the Northern Hemisphere

Sensitive soils tend to be found in portions of the world where glaciation events occurred in the Pleistocene and consist predominantly of marine sediments that were deposited following the retreat of the ice sheets that covered the landscape (Gillott, 1979). This method of formation is predominant in the sensitive soils in the Northern Hemisphere (Gillott, 1979).

Sensitive soils documented in literature within the Northern Hemisphere are predominantly found in regions of Scandinavia and Canada and are often termed as ‘quick clays’. This term is outdated and is no longer used in literature. Clays in these areas were formed in depressions of the topography, where bodies of marine or brackish waters were present, prior to the retreat of the glacial ice sheets that blanketed the landscape, between 18,000 and 6,000 years ago (Lefebvre, 1996). As a result of the glacial sheets, the mean sea level at the time was comparatively lower than modern levels. Glacial sheet retreat led to the emergence of these clay deposits above sea level, which in turn altered the groundwater regimes of the soil bodies. The materials were then exposed to the subaerial environment, causing weathering.

The actions of the hydraulic gradients within the groundwater regimes led to the eventual reduction of salt ion concentrations within the soil, which led to drops from concentration levels of around 32 g/L to the modern observed values of less than 1g/L (Lefebvre, 1996). The reduction of the soils’ salinity led to the subsequent reduction in the

liquid limit of the soil, and the remoulded shear strength, making them more susceptible to strength failure (Lefebvre, 1996).

As a result of this formation process, the 'quick clays' of Norway and Canada have a characteristic stratigraphic profile (**Figure 2.3**). A weathered, broken clay crust makes up the top layer, followed by an intact clay layer that is slowly permeable, a thin till layer, before a bedrock bottom layer (Thakur et al., 2017). The intact clay layers experience a characteristic open, flocculated structure, caused by the colloidal particles present within the deposited material. The colloidal particles interact with the salt rich waters surrounding them to produce a loose aggregated, open structure through the process of gelation of flocculation (Gillott, 1979). The leaching of the salt ions present within the interlayer space of the clay minerals leads to a reduction in the strength of the clay structure (Moon et al., 2015).

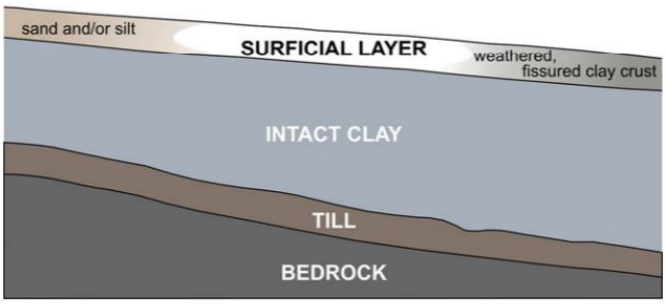

Figure 2.3. Diagram showing simplified stratigraphic column of glacial marine deposits characteristic of Eastern Canada (Thakur et al., 2017).

However, in New Zealand, sensitive soils form differently, being derived from volcanic eruptive deposits. Tauranga, in the Bay of Plenty region, is one of the main areas containing sensitive soils in New Zealand. In recent history, numerous large-scale landscape failures have occurred around the region. The Tauranga basin has a complex stratigraphy, with several distinctive 'sets' of material producing the differing stratigraphic layer observed (Moon et al., 2013). The topmost layer seen within the Bay of Plenty region are defined as Pleistocene and Holocene aged sediments, which have been derived from the volcanic eruptive events of the Taupo Volcanic Zone (TVZ) and are indicative of modern soil materials (Moon et al., 2013. The main component of this identified layer is the Rotoehu Ash, which was deposited around 60,000 years ago (Moon et al., 2013). Below the Rotoehu Ash, is a paleosol which formed upon the Hamilton Ash. The Hamilton Ash is identified to be made up of a series of deposits that are dated between 0.08 and 0.38 million years old (Moon et al., 2013). Below the bottom

of the Hamilton Ash formation, a distinctive Pahoia Tephra sequence can be seen. The tephra is made up of both primary and reworked volcanic materials, which range in age between 0.35 and 2.18 million years old (Moon et al., 2013).

Sensitivity in these soils occurs due to the weathering of certain constituents of the volcanic products, namely the volcanic glass and pumiceous deposits, leading to the formation of short-range order clays that trigger sensitive soil behaviours.

However, despite the differences in formation for sensitive soils in New Zealand in comparison to the Northern Hemisphere, the chemical composition of the soils is qualitatively similar (Gillott, 1979). This indicates that the measures applied internationally may have some local application in New Zealand and may aid in this research.

2.3.5 Clay minerals

Clay minerals are defined as nanoscale ($\sim 2\mu m$), negatively charged particles with a large surface area that are a constituent of soil. Clay minerals are layered silicate minerals and make up the fine-grained fraction of soils (Theng, 2012). Clay minerals can either be crystalline or non-crystalline in structure, and the non-crystalline minerals are responsible for a soils' reactivity (Theng, 2012). The short-range order aluminosilicate clay minerals tend to control a soils' sensitivity (Theng, 2012).

Aluminosilicate clay minerals can have a number of forms, based upon the number and arrangement of the parallel aluminosilicate layers; the silica tetrahedral (Si^{4+}) and alumina octahedral sheets (Al^{3+}/Mg^{2+}). These sheets can share cations and water molecules to produce the clay structures (Theng, 2012).

The clay minerals that tend to cause sensitivity in soils are short range order aluminosilicate minerals, which have a 1:1 ratio of alumina sheets to silica sheets arranged parallel to one another in repeating layers and share differing interlayer cations. These minerals predominantly include halloysite and allophane.

2.3.5.1 Halloysite

Halloysite is a dioctahedral 1:1 clay mineral with an interlayer of water molecules between the alumina and silica adjacent layers. This layer of water molecules can be easily removed, to produce a number of hydrated and dehydrated forms (Cunningham et al., 2016). Halloysite is around 10 Å in thickness between layers when hydrated, and around 7 Å in thickness when dehydrated (Joussein et al., 2005). Multiple halloysite forms have been identified in the literature: tubules, spheroids, plates, and vermiform books (Joussein et al., 2005; Wyatt, 2009; Cunningham et al., 2016) Additional forms including books and mushroom-capped spheroids have also been identified in recent research (Kluger et al., 2017).

Table 2.3 summarises the relationship between the forms of halloysite found within the soil body, in relation to the properties of the soil in differing countries.

Table 2.3. Table showing the different forms halloysite can be found in within a soil body, relating to the formation and weathering processes the soil underwent, and where in the world these soils were found (after Joussein et al., 2005; Wyatt, 2009; Cunningham 2012). Sketches of the key halloysite morphologies are also included.

Sketch	Morphologies	Occurrences
	Tubular, long and thin, short and stubby tubes	Cryptokarstic sediment, volcanic glass and pumice, feldspar and mica alteration.
	Pseudo spherical and spheroidal	Weathered volcanic ash and pumices, volcanic glass in marine environment, (eg. Guatemala soils, New Zealand).
	Platy	Volcanic ash soils, weathered pyroclastic, lateritic profiles, fissures within granite, hydrothermal alteration, tuff bed (e.g. Texas, Brazil, Guatemala).
	Fibre	Lateritic soil, weathered granite (e.g. Australia, Brazil).
	Prismatic, rolled, crinkly, walnut-meat	Volcanic ash soils, weathered granite (Japan)
	Cylindrical, disk	Rhyolitic tephra (New Zealand)
	Spherulitic, regular lath with rolling edge	Weathered granite/gabbros (Scotland)
	Crumpled lamellar	Weathered pumices (Japan)
	Lath, scroll	Altered volcanic glass (Japan)
	Glomerular or ‘onion like’	Volcanic ash (Cameroon)
	Book	Volcanic airfall tephra (New Zealand)

2.3.5.2 Halloysite formation

Halloysite is hypothesised to form through the actions of cations that were derived from early stage weathering of volcanic materials (Moon, 2016). Halloysite favours development within a silicon (Si) rich environment, within materials that have a lower permeability, therefore encouraging a higher, potentially stagnant moisture regime (Churchman & Lowe, 2012). In the Central North Island (Tauranga and Waikato), the volcanic deposits are generally rhyolitic, and as a result, halloysite clays can form from rapid, low-temperature alterations of the volcanic glass fragments within the material (Churchman & Lowe, 2012).

Halloysite is of interest due to the geomechanical properties it imparts upon soils. The small mineral size, and capabilities to form varied morphologies provides a set of engineering characteristics quite distinctive from other soil materials (Moon, 2016). As a result, this sensitivity can often be complex, with open microstructures, high porosity and a high natural moisture content encouraging the release of water from the pore spaces following failure, with the low cation exchange capacity, low cohesion and low plasticity of halloysite exacerbating the failure (Moon, 2016).

2.3.5.3 Morphologies

2.3.5.3.1 Variability in morphologies

Because halloysite forms through weathering processes, several external factors contribute to the variability in the forms seen. The concentrations of iron (Fe) within the soil have been suggested to influence morphology, with platy forms being attributed to higher concentrations of Fe, conversely, tubular forms having lower concentrations (Joussein et al., 2005). Recent studies have attempted to explain how the differing morphologies of halloysite form over time. Cunningham and others in 2016 looked in depth at the likely formation hypotheses for halloysite. Churchman and others (2010) summarised the process as being favoured in a locally wet environment enriched with silica, which allows for the thermodynamically and kinetically favoured formation of halloysite. Published theories (Churchman et al., 2010; Cunningham et al., 2016) have hypothesised the formation evolution of the differing halloysite morphologies (**Figure 2.4**).

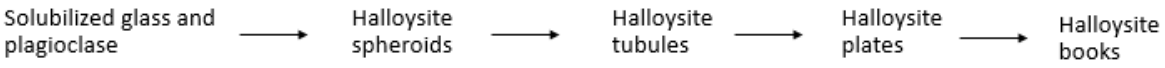

Figure 2.4. schematic showing the hypothesised formation process for differing forms of halloysite through time (adapted from Cunningham et al., 2016).

Initially, halloysite spheroids form from the silica rich solution (Lowe, 1986). Over time, these spheroids reform, either through coalescence, or through the process of dissolution and precipitation to produce halloysite tubules (Churchman et al., 2010). These tubules then unroll and merge into plate-like structures under correct conditions, via neoformation (Cunningham et al., 2016). This explains the formation of the halloysite spheroids, tubules and plates. The formation of the 'book' structures is still not well understood, however. It has been hypothesised that a specific period of drying aids in the coalescence of the plates into vermiform structures through shrinkage and isostatic pressure alterations (Cunningham et al., 2016). This drying and shrinkage process is visually noticeable by manganese dioxide (MnO_2) redox concentrations, indicative of seasonal drying (Cunningham et al., 2016). The drying, if prolonged, favours kaolinite formation rather than halloysite however.

2.3.5.3.2 Morphology and sensitivity

Studies by Smalley et al., (1980) and Tanaka (1992), hypothesised that a higher spheroidal halloysite count imparted greater sensitivity. This was again observed in Kluger and others' 2017 study on the Bramley Drive slip in Omokaroa, where landsliding occurred in a soil layer later identified to contain high spheroidal halloysite content. It was also noted there was an absence of identifiable allophane within the soil material (Kluger et al., 2017). Kluger and others compared sensitivities through quantification of the amount of halloysite within the material using a point count method first adapted by Frolor and Manning in 1969 (Kluger et al., 2017). This involved the use of planar SEM images with a grid overlay, where particles were then counted (Kluger et al., 2017). The results found that at different depths, the material they were analysing (Pahoia tephra sequence) had differing halloysite morphologies and percentage by weight. The spheroidal halloysite concentration increased further down the profile, reaching a maximum at the sensitive layer identified to have potentially caused the

landslide. Interestingly, the morphology also differed down the profile. Initially tubular halloysite was identified, before spheroidal halloysite began to dominate, becoming larger in size further down the profile (Kluger et al., 2017).

This large diameter has been hypothesised to additionally dictate sensitivity (Kluger et al., 2017). This sensitivity was found to relate to the shape of the spheroids, and their behaviours following failure and remoulding. In an undisturbed state, the spheroidal halloysite are aggregated into distinctly connected particle chains. However, upon failure and remoulding the aggregates have fallen apart into smaller clusters/aggregates or even individual halloysite particles (Kluger et al., 2017). The study was of importance due to the identification of the 'mushroom-capped' spheroid morphology within the sensitive layer of the Pahoia Tephra sequence (**Figure 2.5**).

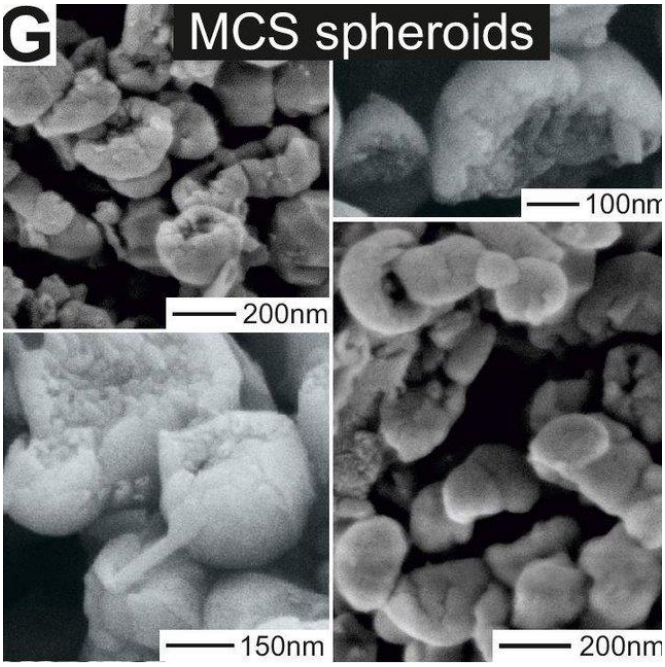

Figure 2.5. SEM images showing the presence of 'mushroom capped' spheroidal halloysite particles identified within the sensitive layer of the Lower Pahoia tephra analysed from the Bramley Drive landslide by Kluger and others in 2017. The images show the spheroids in different magnifications and contrasts.

These mushroom caps are produced by deformities within the spheroidal particles, creating openings to give the spheroids to give a unique shape, which is hypothesised to control some mechanical aspects of halloysite behaviours (Kluger et al., 2017). The presence of opposite charges within different portions of the mushroom shape (weakly positively charged in concave openings, weakly negatively charged upon convex surfaces) promotes weak Van

Der Waals or electrostatic forces to attract and promote aggregation of the individual spheroids (Kluger et al., 2017; Moon et al., 2017). These attractions are short range however, and can easily be detached through remoulding, thus leading to a low remoulded strength (Kluger et al., 2017).

2.3.5.3.3 Morphology interactions and microfabric

Soil microfabric defines the small scale interactions between differing fractions of a soil material. Numerous differing microfabrics can be observed, including skeletal, matrix, turbostratic, honeycomb and laminar, dependent upon the behaviours of the differing clay and grain fractions observed.

The hierarchical classification of terms used for microfabric analysis is defined below.

Primary structural elements are defined as the particles which form the main 'building blocks' of the soils (Beattie, 1990). For the purposes of this study, in a similar manner to that undertaken by Wyatt, 2009, the primary structural elements are classified as either clay minerals or grains. Clay minerals are single crystalline clay units, usually defined based upon morphology (Beattie, 1990; Wyatt, 2009). Conversely, grains refer to sand or silt-sized particles (Huppert, 1986; Beattie, 1990; Wyatt, 2009).

Elementary particle arrangements classify the interactions of each primary structural element (clays and grains) with one another within the sample (Beattie, 1990; Wyatt, 2009).

Particle associations represent interactions between the primary structural elements and the elementary particle arrangements. These can be classified into a number of different forms (**Table 2.4**).

Pores are classified by size, with their boundary elements or shapes being of less importance in this study. The pore size classification is based upon that of Huppert (1986). The pore sizes affect the retention of the water (ie. smaller pores hold water more tightly than larger pores). Huppert (1986) and Beattie (1990) classified the thresholds for different pore sizes (**Table 2.5**).

The culmination of terms can be used to define the microfabric of the materials. **Table 2.6** below defines the different microfabrics as a result of the combination of differing factors. The arrangements are defined using Huppert's 1986 definition of the differing microfabrics. These classifications also relate to continuity of the groundmass. These terms were used by

Beattie (1990) in their study of Waikato coal measures, and by Wyatt in his 2009 study on sensitive soil materials. It is similarly adopted in this study (**Table 2.7**).

Table 2.4. Table summarising the different kinds of overall particle associations expected and historically observed within a material. Adapted from Wyatt, 2009.

Type	Definition
Connectors	Clusters of clay-sized minerals which forms bridges between clay microaggregates and the non-clay materials (Collins & McGown, 1974).
Embedded	Grains are completely surrounded by groundmass material (Wyatt, 2009).
Grain coatings	Material coats the surface of a grain along the fracture surface (Wyatt, 2009).
Pluck marks	Grains are removed by specimen preparation techniques leaving a hollow depression (Moon, 1989).
Loose material	Grains are observed in the groundmass but are loose, with physical separations between the grains (Moon, 1989).
Lapping	Groundmass laps against the surface of the grain to form a direct contact (Wyatt, 2009).

Table 2.5. Table summarising the thresholds for different pore sizes within a material, based upon historical literature (Huppert, 1986).

Pore class	Size (μm)
Ultra-pore	<0.1
Micro pore	0.1-5
Meso pore	5-30
Macro pore	>30

Table 2.6. Table summarising the five main microfabric types, as defined by Huppert in 1986, and further by Beattie in 1990. The different microfabric classifications are dependent upon the matrix, grain orientation, and pore type.

Microfabric type	Description
Skeletal	Discontinuous matrix; material is essentially granular. Clay either organised into regular or irregular aggregates which behave as silt-sized entities, or form connector assemblages and coatings between and around grains. The pore space is dominated by isometric but irregular mesopores (Huppert, 1986; Beattie, 1990).
Matrix	Continuous structure where grains are completely immersed, but intramatrix edge to face contact angles are large. Pore space is dominated by isometric micropores (Huppert, 1986; Beattie, 1990).
Turbostratic	Continuous matrix, with intramatrix edge to face contact angles small with a significant number of face to face contacts. Orientation is not a necessary criterion however. Pore space is dominated by elongated micropores (Huppert, 1986; Beattie, 1990).
Honeycomb	Continuous matrix, the situation where clay microaggregates interact to form open, loose networks (Tergahzi, 1925; Casagrande, 1932; Beattie, 1990).
Laminar	Continuous, highly orientated matrix where grains are completely immersed. Intramatrix contacts are predominantly face to face and pores are predominantly fissure shaped (Beattie, 1990).

Table 2.7. Table summarising the definitions for both continuous and discontinuous groundmasses (after Beattie, 1990; Wyatt, 2009).

Groundmass type	Definition
Continuous	No clearly definable boundaries between differing structural units, with individual grains being immersed within clay-sized groundmass (Beattie, 1990; Wyatt, 2009).
Discontinuous	Particle associations and structural units have definable boundaries, or discrete domains (Beattie, 1990; Wyatt, 2009).

In the case of halloysite, multiple morphologies can interact with one another to produce differing microstructures. The interactions of halloysite tubules, spheroids, plates and books with one another can have a number of orientations: face to face (FF), face to edge (FE) and edge to edge (EE). **Figure 2.6** details those interactions, based upon the study completed by Wyatt (2009). The differing microfabric arrangements produced by the clay minerals when interacting with one another is also depicted. These arrangements are seen in SEM imagery taken of soil samples, and provide a basis for determination of factors including the degree of weathering and geological history of the samples.

In addition to the clay particles within the soil material, there are often larger mineral grains that interact with the clays to further develop the microfabric. There are characteristic clay particle morphologies and orientations, in addition to the characteristic grains observed in weathered pyroclastic deposits. Arthurs (2010) completed a study on various pyroclastic deposits across Tauranga and characterised the main components identified in the samples (**Figure 2.7**) (Arthurs, 2010).

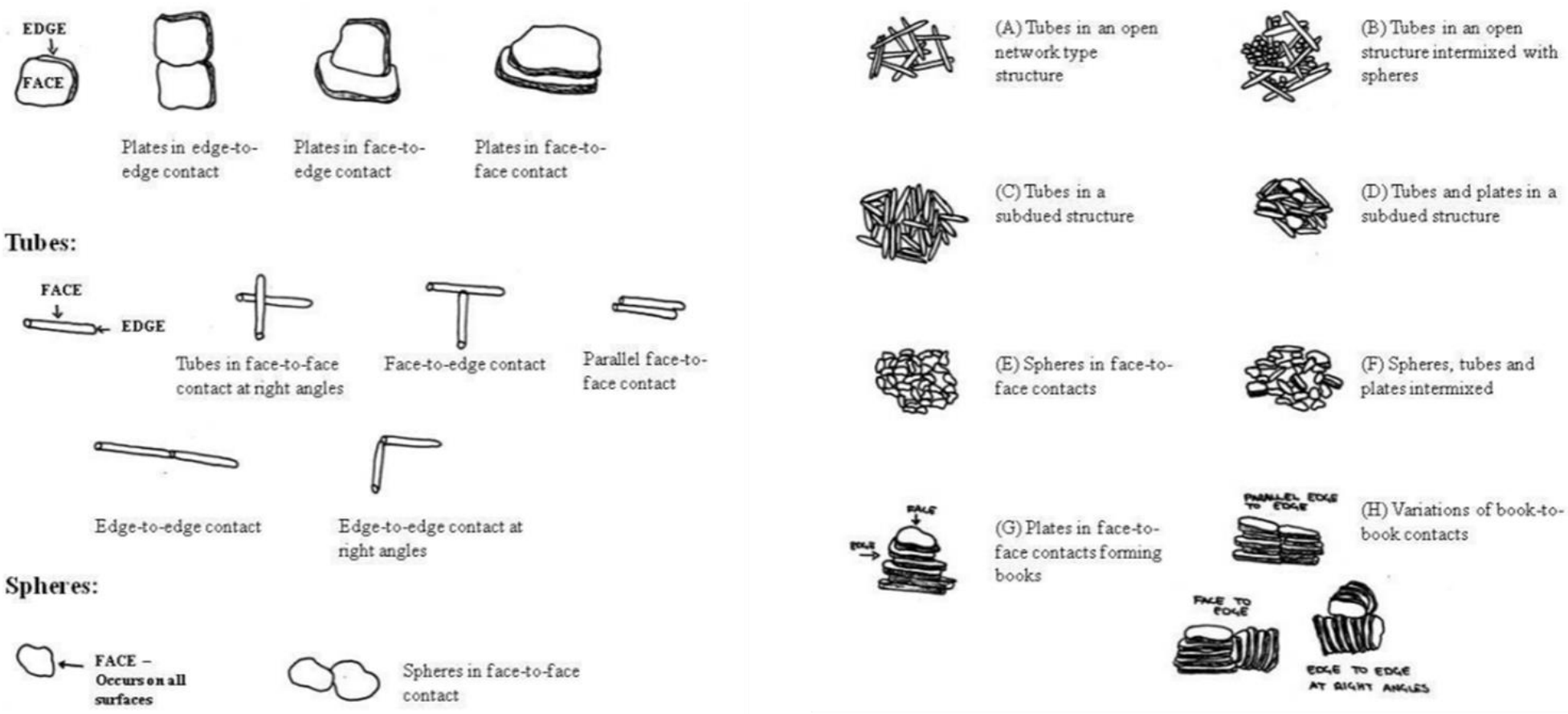

Figure 2.6. Images showing the range of differing contact arrangements between differing clay morphologies. Image A shows the orientations commonly adopted by different morphologies, and image B shows these interactions in-situ within a clay matrix. (Wyatt, 2009)

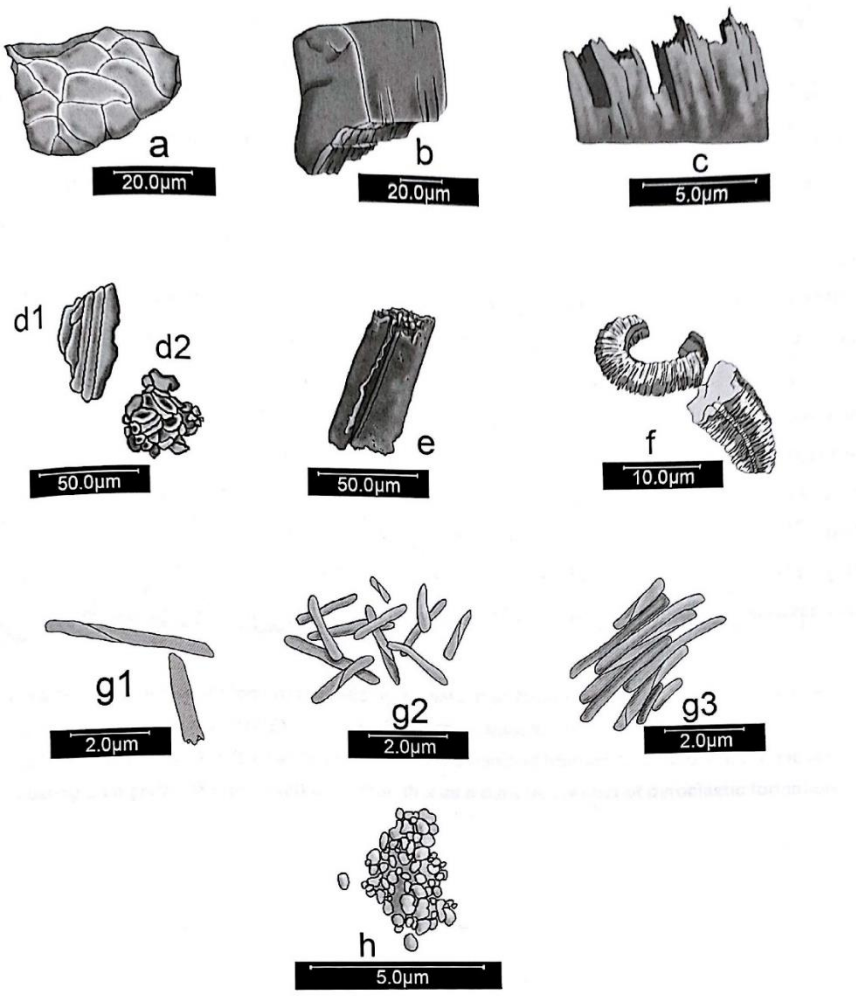

Figure 2.7. Diagram identifying the common mineral components identified within weathered pyroclastic soils, as identified by Arthurs in 2010. A) Quartz grain with concoidal fractures. B) Feldspar grains with cleavage planes and a blocky morphology. C) Fractured mica grains with cleavage planes. D1) bubble wall shards. D2) Pumice grain. E) Pipe like grain. F) veniform book formations. G1) tubular clay particles. G2) Lattice microaggregates. G3) Bundle like aggregates. H) Globular microaggregates of spheroidal clay particles. (Arthurs, 2010).

Halloysite can be characterised in a number of ways using quantitative lab techniques, including x-ray diffraction (XRD) through the use of formamide, ethylene glycol and various heat treatments to identify the hydrated and dehydrated forms, infrared spectroscopy, and scanning electron microscopy (SEM) to determine the dominant morphologies present within a material (Hillier & Ryan, 2002; Joussein et al., 2005). These techniques are to be used in this research.

2.3.5.2 Allophane

Allophane is a short order clay mineral which contains silica, alumina and water molecules within it's' structure (Parfitt, 1990). Allophane tends to derive from volcanic ash tephras and is a weathering product of the short order clay mineral imogolite (Theng, 2012).

In New Zealand, three types of allophane have been found to exist; Al-rich allophane with an Al:Si ratio of ≥ 2, Si-rich allophane with an Al:Si ratio ≈ 1, and stream deposit allophane, which has an Al:Si ratio ≈ 0.9 to 1.8 (Parfitt, 1990). In particular, the Al-rich allophane is predominant in New Zealand soils (Parfitt, 1990). Both the Al and Si rich varieties of allophane contain nanotubular imogolite fragments. These fragments assume a spherical shape, which measures around 4 – 5 nanometres (nm) (Lowe, 1995). The spherule has water molecules within its' centre, in addition to being absorbed into the surface. The 'holey' structure of the allophane molecule allows for a massive surface area to be achieved, with numerous active sites on the inside and outer portions of the spherule structure. **Figure 2.8** shows the structure of allophane, and the spherical form it takes (Lowe, 1995).

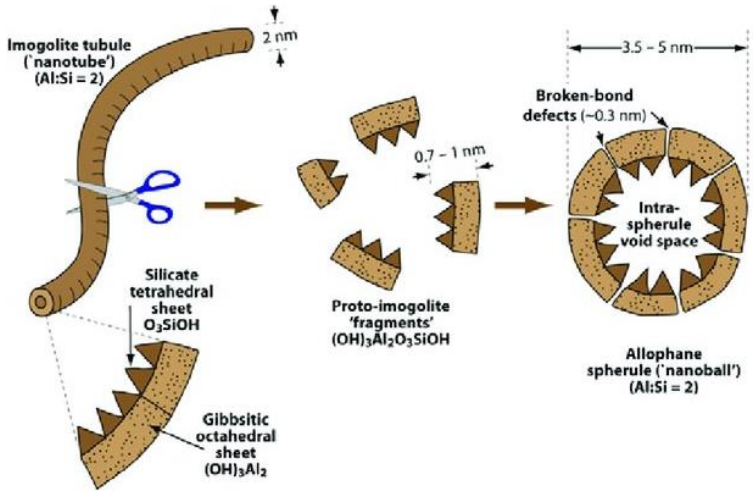

Figure 2.8. Diagram detailing the structure of allophane, formed from the weathering of volcanogenic soil fragments, in particular, volcanic glass (Lowe et al., 2012).

2.3.6 Short range order clay mineral formation

Both halloysite and allophane clay minerals described here originate from volcanic depositional products, typically of rhyolitic origin (Robinson, 2016). The main volcanic centre from which these deposits derive from is the Taupo Volcanic Zone (TVZ), which has been defined by Robinson (2016), as a 'complex series of overlapping calderas, of differing ages'

(p.1967). The local environmental processes, in addition to the composition of the soils deposited, are critical factors in determining the type of clay mineral formed.

Under the generalised silicon (Si) leaching model, it is stated that both allophane and halloysite can form directly from the combining of the products of weathering from the volcanic glass and primary minerals deposited from the volcanic depositional events, under the correct local environmental conditions (Cunningham et al., 2016). Halloysite formation is favoured in local environments of high Si content that is not well drained. Allophane, however, forms in a lower Si concentrated environment, where the soils have a good drainage regime (Cunningham et al., 2016). This produces more aluminium rich allophane.

2.4 Hazards and management

2.4.1 Hazards caused by sensitivity from an engineering perspective

Sensitivity in soils has been well documented to be associated with several serious engineering problems, relating to mass movement events and flow liquefaction. Many large-scale events have occurred in New Zealand in recent history, particularly in the Tauranga Region. As a result measures need to be taken in order to minimise the risk of damage that can be inflicted by sensitive soils. Common remedial measures that are taken by firms either during or upon the completion of projects include erosion control using fragmented portions of rock stacked at the toe of the slope in order to reduce the physical area exposed to environmental conditions. During construction, measures such as counter filling using portions of rock allows for the counter balancing of weight upon the slope by large machinery. Additional measures such as pile installations for large infrastructure projects, such as the Skaudal Bridge in Norway, can also be installed to produce additional stability. Removing physical loads at the top of the slope is also commonly completed to increase the stability, if construction occurs at the top of the slope (Thakur et al., 2014). Current practices for determining the slope stability *in situ* have been deemed as often unreliable in the past, as in a large number of cases, no particular initial mode of failure can be defined (Gillott, 1979).

2.4.2 Landslides

Landslides are defined as the rapid downward movement of earth materials down a sloped surface under the influence of gravity (Selby, 1993). Landslides, or mass movement events, occur due to a number of factors, including but not limited to, heavy rainfall events, movement by earthquakes, and in some cases, anthropogenic activities upon the top of a slope feature (Cuomo, 2014). Two distinctive landslide features are related to the activities of sensitive soils; translational and flow slides (Moon et al., 2017). These slide types have both been documented in New Zealand in recent history and have predominantly occurred in the Bay of Plenty Region, in Tauranga. The Pahoia Tephras of the Bay of Plenty stratigraphy tends to be the stratigraphic unit responsible for the sensitivity seen within the Tauranga region, and causes many of the large-scale landslide events seen (Moon et al., 2013). Literature detailing landslides within a number of East Asian and Pacific countries have commonly detailed the failed landslide materials as pyroclastic deposits (Chau et al., 2004; Chigira, 2014; Kluger et al., 2015; Moon, 2016; Kluger at al., 2017). These studies also identified the clay minerals present within the materials were a product of chemical weathering, through pedogenesis (soil development) or diagenesis (chemical water-rock interactions) (Kluger et al., 2017). In particular, spheroidal halloysite was identified within the landslide prone layers of failure-prone pyroclastic material, commonly upon the rupture surfaces (Smalley et al., 1980; Tanaka, 1992; Joussein et al., 2005; Kluger et al., 2017; Kluger et al., 2020).

2.4.2.1 Translational landslides

Translational landslides are defined as shallow surface, large scale soil movement features that have essentially straight slide planes that occur following large-scale rainfall events, where the water table can rapidly fill to saturation point at a rate more rapid than drainage can occur within the soil profile (Selby, 1993). Any existing tension cracks produced from previous landslide events may also be filled with excess water during these rainfall events (Selby, 1993). As a result of this, soil particles can lose the cohesion strength between particles, leading to the initiation of sensitive soil behaviours. Translational landslides typically experience increased deformation and water content further downslope of the initiation site, which can lead to different ‘zones’ of flow down the slope, i.e., a fairly dry debris slope at the top of the slope may become a ‘blockier’ avalanche of smaller rock debris pieces within a

liquified flow towards the bottom of the slope (Selby, 1993). These events can range from smaller to large scale.

2.4.2.2 Flow events

Flow events occur due to liquefication within coarse debris, fine-grained soil materials, or clay minerals (Selby, 1993). To distinguish between these flow types, the terms debris flow, earth flows and mud flows are assigned to each process (Selby, 1993). The general movement of flow events tends to be retrogressive, as the activities of each soil block failing from the slope surface destroys the lateral supports of the soil bodies above it (Selby, 1993). The tendency of these flows is reliant on several factors, including the:

- the remoulding of the soils' structure during landslide events;
- presence of clays with high resting liquid limits, in topographical areas of high rainfall;
- presence of clays with low resting liquid limits, in topographical areas of low rainfall;
- presence of soils with an open fabric structure that originated from depositional flocculation; and
- thawing events of ice (occurs in glacial regions, not of particular issue in most areas of New Zealand).

The liquid limit (LL) is defined as the typically observed water content at which a soil can pass from a liquid to plastic state (International Organization for Standardization (ISO/TS 17892-12:2004, 2004).

2.5 Triaxial testing

The geomechanical properties a soil experiences *in situ* can be simulated through the use of a triaxial apparatus. The use of the triaxial allows for the determination of the shear strength of a material (Rees, 2013). Multiple different triaxial tests can be performed, in relation to differing engineering applications. These include:

- Unconsolidated Undrained test (UU)
- Consolidated Undrained test (CU)
- Consolidated Drained test (CD)

Dependent upon what parameters need measurement, differing tests will be completed. **Table 2.8** summarises the main differences between the tests, based on different parameters being measured. Triaxial testing can be used to simulate how a soil will fail *in situ*, and the characteristic failure type the soil would experience.

Table 2.8. Table summarising the key differences between Unconsolidated Undrained (UU), Consolidated Undrained (CU), and Consolidated Drained (CD) tests for triaxial testing (Head & Epps, 1980; Wyatt, 2009).

	Unconsolidated Undrained	Consolidated Undrained	Consolidated Drained
Pore water pressure measurement, during testing	No	Yes	Yes
Saturate Sample until B = 95%	No	Yes	Yes
Consolidate until 95% PWP dissipation	No	Yes	Yes
Drainage	No	Only during consolidation	During consolidation and shear.
Normal stresses	Cell Pressure	Cell Pressure – Back Pressure	Cell Pressure – Back Pressure
Strain rate	Failure within minutes	Slow enough to allow pore water pressure equalisation and measurement	Slow enough to prevent pore water pressure build up.
Duration test time per sample	Minutes to Hours	Day to days	Days to a week
Cohesion	Total	Total and Effective	Total and Effective
Friction Angle	Total	Total and Effective	Total and Effective

2.5.1 Failed core appearance

Based upon the methodology outlined by Selby (1993), four main modes of deformation failure were used to characterise the failures seen within the samples tested in triaxial tests. These failures are classified as shear failure (a), wedge failure (b), intermediate failure (c), and barrel failure (d). **Figure 2.9** shows the characteristic external appearances of these failure types.

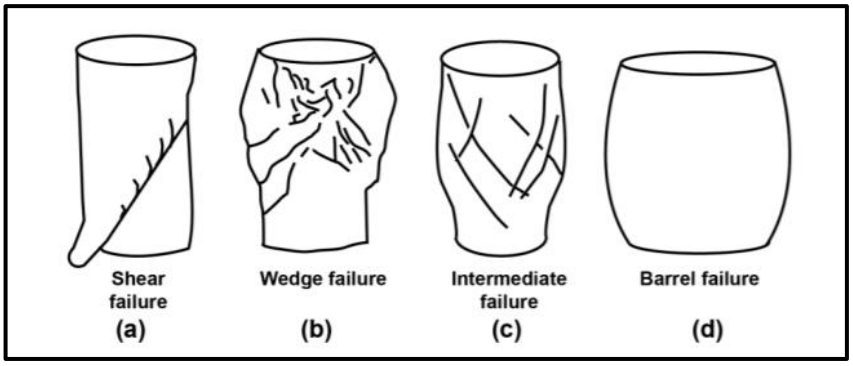

Figure 2.9. The types of deformation failure conditions outlined by Selby in 1993 that typically occur under triaxial testing conditions (Mills, 2016).

The type of failure that occurs within the sample can be related to the failure mechanisms it experiences. Shear failure, which is defined by the failure of a sample at an angle on a single plane, is characteristic of brittle deformation (Selby, 1993; Mills, 2016). Wedge failures, however, which have two failure planes that fail ~ perpendicular to one another, can be classified as both brittle and ductile forms of deformation failure (Selby, 1993; Mills, 2016). Complete ductile deformation can be classed as intermediate failure, or outwards bowing into a barrel failure (Selby 1993; Mills, 2016).

The occurrence of both brittle and ductile deformation during triaxial testing can create an area of shear zones, which occur because of the soil accommodating the majority of the deformative stress (Gylland et al., 2014). These zones are called principal shear zones (hereafter referred to as PSZ) (Gylland et al., 2014; Mills, 2016). Secondary shear zones (SSZ) accommodate a reduced amount of these deformation stresses. Additional features including minor shears also occur, but are smaller in size, and are shallower than the features developed for the PSZ and SSZ. Microshears are associated with these zones (Mills, 2016).

Depending upon the type of material being tested, different responses to deviator stress, effective stresses and pore water pressure changes are expected. **Figure 2.10** summarises the response expected from a normally consolidated material (orange), an over-consolidated clay (green), and an over-consolidated sand (pink) (Boulanger & Idriss, 2006). **Figure 2.11** summarises the pore water pressure responses of normally consolidated, slightly over-consolidated and heavily over-consolidated materials.

A combination of response factors of the soil material can lead to the development of concentrated areas of soil deformation, known as strain localisation (Gylland et al., 2014).

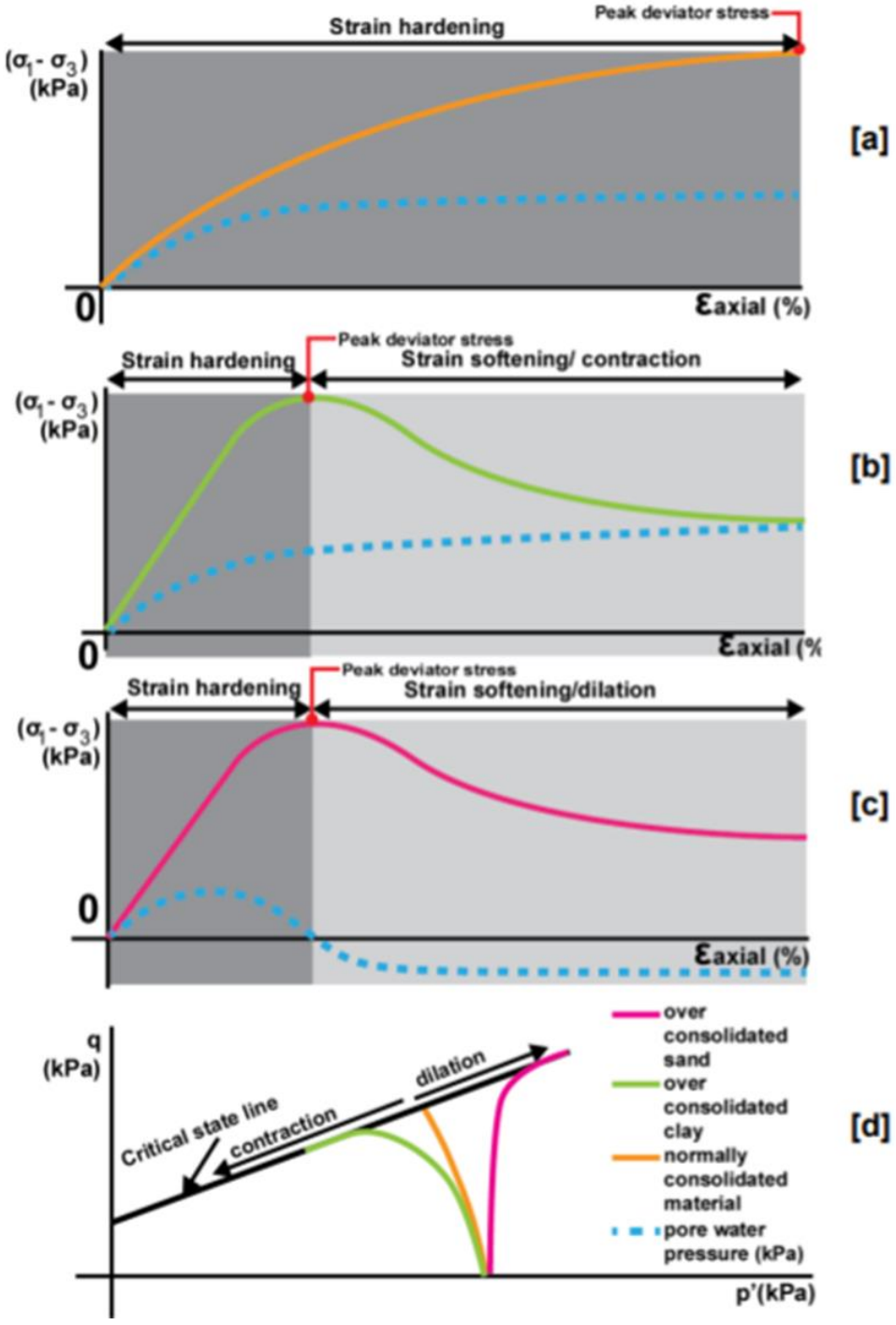

Figure 2.10. Schematics a-d (top to bottom) diagrams of the differing stress behaviours that are expected for differing materials, including over consolidated sands (pink), over consolidated clays (green), and normally consolidated material (orange) for both the deviator stress values (q) versus the ε_{axial}, and p' vs q plot (Boulanger & Idriss, 2006; Briaud, 2013; Mills, 2016).

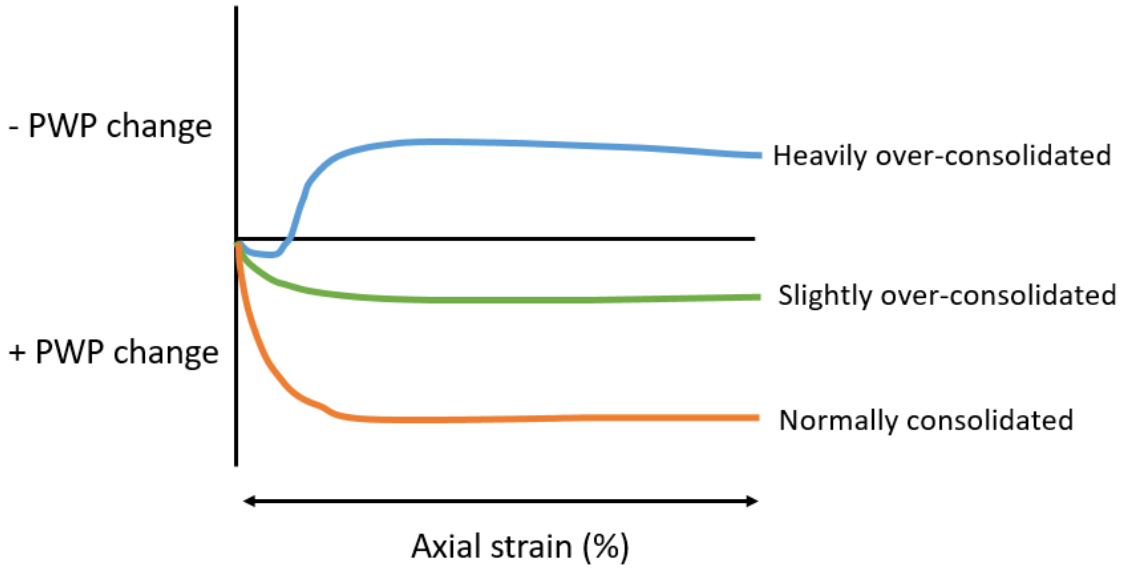

Figure 2.11. Graph summarising the response of pore water pressure (PWP) changes in response to changes in axial strain (%), relating to the degree of consolidation within clay materials (after Tan, 2010).

2.5.2 Strain localisation

Strain softening, contractive failure (hereafter referred to as SSC) failure types can generally be classified by p'-q' curves with contraction at failure, a stress-strain plot that have a defined peak followed by an identifiable strain softening region, and a pore water pressure response that slowly rises following failure (Gylland et al., 2013a; Mills, 2016). Dominant physical failure modes include shear band formation and wedge failures (Gylland et al., 2014; Mills, 2016). SSC failures are associated with strain localisation in tested samples. Strain localisation is recognised as the onset of instability, and strength loss between particles is initially concentrated into specific areas within the soil material (Rudnicki & Rice, 1975; Derues & Viggiani, 2004; Gylland et al., 2013b).

The trends observed on the stress-strain plots relate to the different phases of failure. During the initial straight portion of the stress-strain plot, prior to the peak deviator stress being reached, deformation is hypothesised to be elastic, with little influence of plastic deformation (Nova, 2012; Mills, 2016). This straight portion increases rapidly, and a similar trend can be observed upon the corresponding pore water pressure graphs. This rise occurs irrespective of the confining pressure of the test (Mills, 2016). Following shear band formation, contraction and deformation of the soil microstructure produces further increases in pore water pressure, which either moves through the deformed material within the strain band, or out of the sample

itself (Mills, 2016). This is observed on the p'-q' plots, indicated by the almost immediate sample contraction at the peak deviator stress value. This in turn can be correlated to an observed peak in pore pressure at the peak deviator stress value, and the formation of visual external shear band features (Mills, 2016). SSC failures have characteristic graphic responses.

Literature has observed in more depth the formation and propagation characteristics of shear band features (Thakur et al., 2014). Strain localisation occurs prior to the strain softening portion of the shear stage in triaxial testing, where the strain is concentrated within a specific area of the sample, usually along one or two specific planes that are more predisposed to weakness (Rudnicki & Rice, 1975; Derues & Viggiani, 2004; Gylland et al., 2013b; Mills, 2016; Robertson, 2017). The amount of strain visually expressed has been hypothesised to relate to the failure type, shear rate, and the type of material being tested (Wyatt, 2009; Cunningham, 2012; Thakur et al., 2014; Mills, 2016) (**Figure 2.12**).

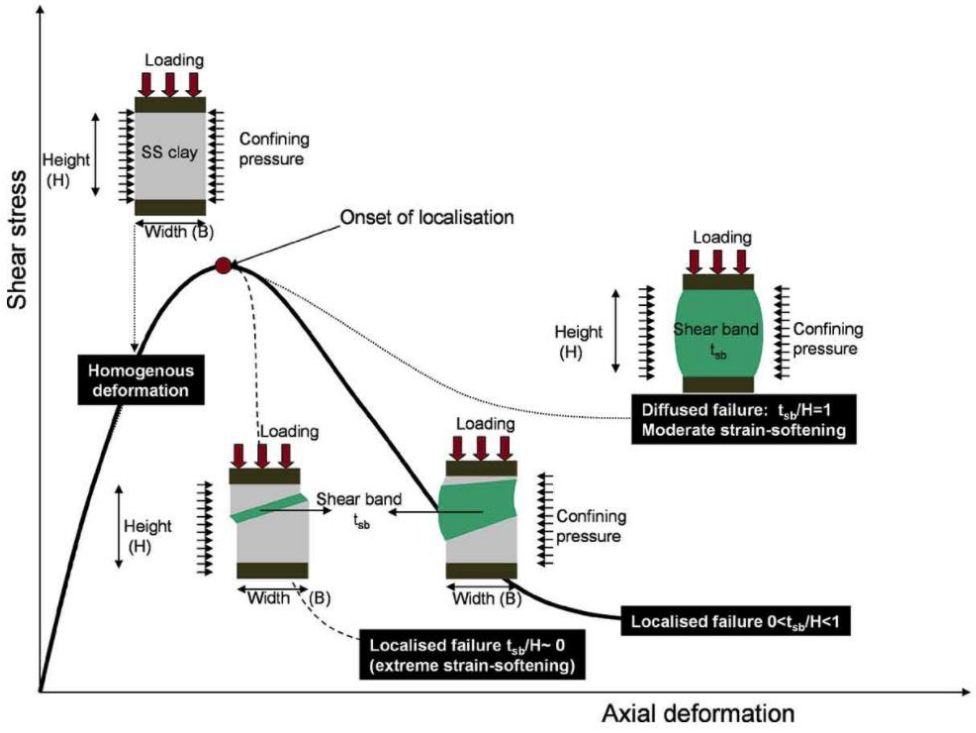

Figure 2.12. Image depicting an idealised formation and propagation of strain localisation, depicting the formation of a shear band at differing deformation rates and intensities (Thakur, 2011). The thickness of the shear bands are dependent upon the post-peak strain softening response of the sensitive clay soil material (Thakur, 2011).

Strain localisation can be identified upon stress strain curves, and the material brittleness being identified by rapid strain softening following failure. This leads to a high

degree of contractive failure, identified by a rapid drop in deviator stress following the peak (Gylland et al., 2013b; Gylland et al., 2014; Thakur et al., 2014; Mills, 2016).

More ductile failure is associated with the strain not necessarily concentrating into one specific area, leading to reduced strain softening within the sample, and a lesser degree of contractive failure (Gylland et al., 2013b; Gylland et al., 2014; Thakur et al., 2014).

The development of strain localisation and shear bands within a soil core can lead to the development of Riedel shears.

2.5.3 Riedel shears

First described by Riedel in 1926, following experiments in clay cake models, Riedel shears, or R-shears, as they will henceforth be referred to, are indicative of strike-slip, divergent and convergent fault systems (Ahlgren, 2001). R-shears represent the embryonic response to shear failure and can commonly be identified within shear zones of failed soil material (Katz et al., 2004).

The basic geometry of an R-shear feature is summarised in **Figure 2.13**. At the scanning electron microscope (SEM) level of preciseness, it should be expected that the microstructure of the shears displays these characteristic failure angles and the bands should create angles of $\phi/2$ and $90 - \phi/2$ to the general shear zone direction (Katz et al., 2004). There should also be a characteristic interception of an acute angle at $\beta = 90 - \phi$, where ϕ is indicative of the angle of internal friction (Katz et al., 2004).

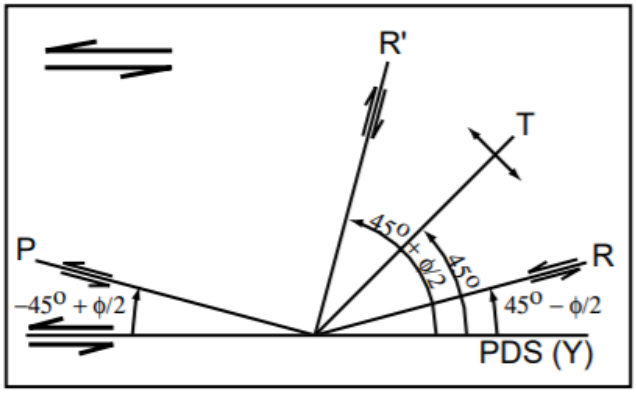

Figure 2.13. Diagram showing the idealised Riedel shear (R-shear) failure geometry within a sample. Additionally, the primary displacement discontinuity (PDS, Y), conjugate R' and P shears, and tension fractures (T) The assumption is that this geometry could be identified at a scanning electron microscope (SEM) level (Ahlgren, 2001).

Riedel shears are made up of three individual shears; R shears, the lesser observed R' shears, and P shears (Fossen, 2010; Mills, 2016). R shears are the most common form of shear, and have been hypothesised to form first, followed by the rarer R' shear, and subsequently the P shears. These shears link together to form a final large shear (Morgenstern & Tchlenko, 1967; Gylland et al., 2013b; Mills, 2016). R shears can usually be seen externally if a core has experienced shear band deformation (Gylland et al., 2013b).

These shears resemble several shears identified in different studies of vastly different magnitudes. These include the large-scale brittle deformation observed within the San Andreas Fault (Byerlee, 1992), and on the other extreme, was observed in the microscale deformation of kaolin clays (Morgensten & Tchalenko, 1967; Mills, 2016). More locally, Mills discovered Riedel shear morphology in failed sensitive soils sampled from the Tauranga region in her 2016 study. This is not coincidence, rather a common mode of formation in each scenario. The main factors governing formation include the friction angle of the material, and the principal stresses acting on the soils which produce shear bands (Gylland et al., 2013a; Gylland et al., 2013b; Mills, 2016).

2.5.4 Material componentry and failure type

The componentry pf the materials can influence how the materials behave during triaxial testing, and the characteristic responses observed on the graphs produced for different parameters (**Figure 2.14** and **2.15**). This is important, as reworked soils such as the Walton Subgroup may contain varying proportions of different particle sizes.

A study completed by Anantanasakul & Roth in 2018 using lab-produced silt and clay soil mixtures found the more silt content, the less compression the soil experiences during vertical consolidation. Silt particles are generally much larger and often more angular compared with clays, allowing for transferral of effective stresses across the surface area. (Anantanasakul & Roth, 2018). How the silts interlock and interact through frictional forces influences the undrained shear strength and effective friction angle measurements. This response is most apparent at lower over-consolidation ratios (the ratio between effective consolidation stresses experienced in the past and the current consolidation stresses being experienced) (Anantanasakul & Roth, 2018).

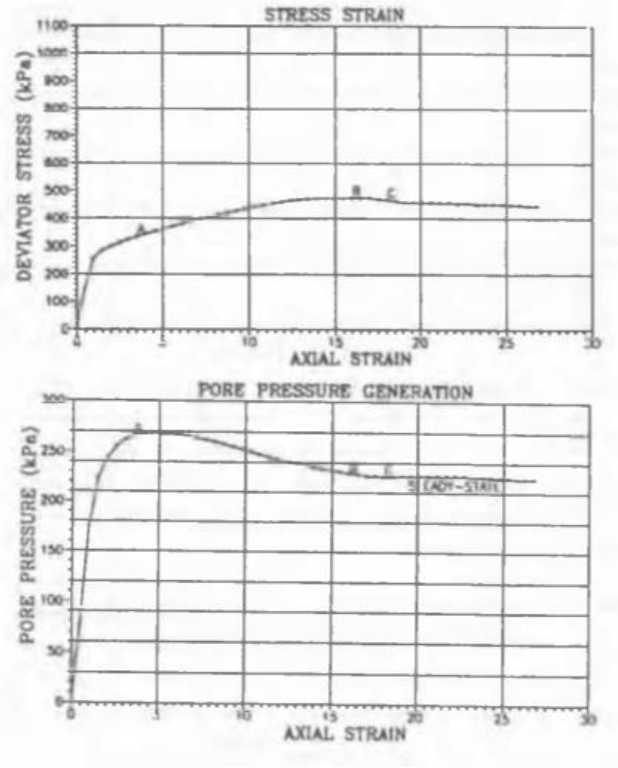

Figure 2.14. Graphs summarising the deviator stress and pore water pressure (kPa) response of a material in relation to axial strain for a shear band failure (Konrad & Sawitzki, 1994).

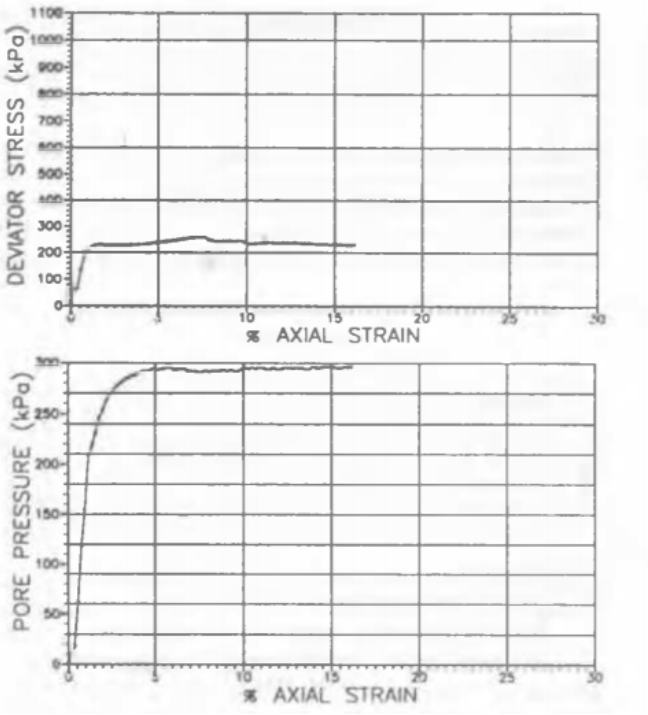

Figure 2.15. Graphs summarising the deviator stress and pore water pressure (kPa) response of a material in relation to axial strain for a barrel failure (Konrad & Sawitzki, 1994).

2.5 Current remediation methods for sensitivity

Sensitivity in soils can become problematic in an engineering sense. In order to remediate these materials, and make them suitable for infrastructure and building works, several basic strategies are currently relied upon, including compaction of the material to increase density, mixing of soil material with stabilising agents to increase desirable material properties, or the installation of external infrastructure such as prefabrication drains (PVD) to reduce the impact of undesirable material properties.

2.5.1 Identifying sensitive soil materials

Presently, the risk of failure within soils which are deemed sensitive (lose strength following disturbance and remoulding) are usually modelled using earthquakes as the trigger event for failure (Åhnberg et al., 2013). However, whilst this may apply in some cases, many sensitive soil failures occur for other reasons, including excess pore water pressure (Moon et al., 2016). Therefore, additional methods and parameters for modelling sensitive soil risk and failure are sought after, however, there are still gaps in published literature and research regarding this topic (Åhnberg et al., 2013).

2.5.2 Identified remediation strategies

The current identified remediation strategies recommended by many engineering consultancies rely upon external materials and methods to increase stabilisation (compaction, lime addition, potassium dosing and prefabrication vertical drains). These methods in particular are to be reviewed, as potential viable methods for sensitive soil stabilisation.

2.5.2.1 Compaction

Compaction is the process whereby density of the soil material is mechanically increased, in order to increase strength and stability (Trenter, 2001). Soil compaction increases soil bearing capacity and stability, in addition to reducing the levels of settlement experienced (Multiquip, 2012). Compaction is achieved through the movement of specific construction plant across the target area, rearranging the soil particles into a tighter configuration (MBIE, 2017). Compaction can be achieved by simply driving the deadweight of a machine over the soil material in a static manner, or through vibrations via an additional machine attached to the construction plant (Multiquip, 2012). Compaction is dependent upon the geomechanical properties of the soil material and can vary as a result. Compaction is a common, fairly cost-effective method of improving soil materials in-situ but relies on certain characteristics of the soil for the determination of suitability (Multiquip, 2012). Compaction occurs rapidly to a soil material following movement.

2.5.2.2 Consolidation

Consolidation similarly aims to increase a materials' density as with compaction, but through the movement of water from the pores within a soil. Consolidation is one of the main methods of improving the geotechnical properties of a soil (Meilani & Fikri., 2020). The fundamental controls of sediment consolidation are determined by the bulk properties of the soil including grain size, grain packing soil permeability and soil strength parameters (Lowe, 1975). Consolidation occurs in soils over a long period of time, as water moves through the small inter-connected pores of the material. The time consolidation takes within a soil material is influenced by the moisture content of the soil, in addition to the soils' porosity (Meilani & Fikri, 2020). Consolidation can be accelerated in certain materials through the use of external measures such as prefabricated vertical drains (PVDs).

2.5.2.3 Lime application

One of the most widespread and common methods for remediation in problem soils globally is the use of lime to increase the strength of cohesive soil materials (Firoozi et al., 2017; Torrance, 2017; Thakur et al., 2017). Broms and Borman first investigated this method in 1979 and mixed unslaked lime together with the sensitive soil material, triggering a series of cementation reactions between the calcium oxide (CaO) compounds and any silica or aluminium bearing elements within the soil (Broms & Borman, 1979; Firoozi et al., 2017; Torrance, 2017; Thakur et al., 2017). The effects of stabilisation are dependent upon a number of variables, including the nature of the material, the type and kind of lime used, the temperature and water conditions, and the degree of compaction, and water content during compaction (Dibble, 1991).

Lime acts to stabilise material through the chemical reactions with clay minerals under alkaline conditions. The available silica within the soil reacts the most strongly (Bell, 1988; Bell, 1989). These reactions impart cation exchange, flocculation and aggregation of clays, carbonation and pozzolanic reactions, which alter engineering properties (Lees et al., 1982; Choquette et al., 1987; Bell; 1988; Dibble, 1991). **Table 2.9** summarises the effects these mechanisms have.

Table 2.9. Table summarising the mechanisms altering engineering properties within lime-stabilised soils, as discussed in the literature.

Mechanism	Description
Cation exchange	Exchange of ions at clay surface to produce Ca-clays (Dibble, 1991).
Flocculation/aggregation of clays	Ca-clays attract to one another, changing soil plasticity, workability and shrinkage properties (El-Rawi & Awad, 1981; Dibble, 1991).
Carbonation	Exposure of lime to air, producing $CaCO_3$. Reduces ability of lime to stabilise (Dibble, 1991).
Pozzolanic reactions	Interactions between lime and available silica and alumina in soil. Usually readily available from clay minerals. Produces water-insoluble calcium gels which crystallise into calcium silicate and aluminate hydrates (Hilt & Davidson, 1960; Dibble, 1991).

Lime stabilisation increases the plastic limit of a soil, but reduces the plasticity index (Bell, 1989). The maximum dry density attainable is also reduced through alteration of the optimal moisture content, meaning compaction can be achieved at a wider range of moisture contents (Bell, 1989). Lime curing increases the strength of soils through the increase in cohesion, with some increase in friction angle (Transport Research Board, 1976; Dibble, 1991). The materials also become more brittle, decreasing strain at failure, but increasing the stress (Transport Research Board, 1979; Bell, 1989). Permeability is initially increased through greater friability, but as curing time increases, permeability decreases through insoluble cement growth and grains gaining larger films of bound water (Brandl, 1981; Dibble, 1991). The shrink-swell ability of the soils are also reduced (Bell, 1988; Bell, 1989; Dibble, 1991).

Research has also proven that in some cases, dependent on soil properties, lime-stabilised soils can revert to pre-stabilised conditions over a period of 6-12 months following application (McNamara, 2003). The 2003 study completed by McNamara upon allophanic soils beneath Fijian roads found that at low-level dosages, the soils reverted to original behaviours between 6-12 months after application, likely due to the unique mineral structures of the soil (McNamara, 2003). Little research has been completed upon the impacts of lime stabilisation in halloysite-rich soils.

2.5.2.4 Potassium salt dosing

Potassium chloride is a common salt solution used globally since the early 1970s. Potassium salt dosing has been proven effective in long-term studies completed on Norwegian glacial sensitive soils (Helle et al., 2015). Around 2600 potassium chloride wells were installed in a quick clay deposit in Ulvensplitten, Norway in 1972 (Helle et al., 2015). The long term impacts of salt dosing found an increase in the undrained and remoulded shear strength, in addition to increased Atterberg limits (Helle et al., 2015).

However, this method of stabilisation has also been tested at a local scale, by Robertson in his 2017 thesis research of Tauranga sensitive soils. The use of potassium chloride (KCl), potassium hydroxide (KOH), and potassium carbonate (K_2CO_3) to treat triaxial soil cores over a period of months found that K_2CO_3 was the most beneficial compound in increasing the measured strength parameters by triaxial testing, and it was hypothesised this occurred due to the intercalation of the ions into the basal spacings between the halloysite mineral, thus displacing the water, and subsequently widening the space (Robertson, 2017). This then was hypothesised to increase the cohesion and friction angles, as a direct result of the need to overcome an increased grain-grain friction relationship (Robertson, 2017). The increased basal spaces also accommodate more pore fluid, which allows for a reduction in pore water pressure when the material is placed under stress (Robertson, 2017). **Figure 2.16** shows a hypothesised scenario whereby sensitive clay materials, such as those encountered by Robertson in 2017 (labelled here as ‘quick clay’) are stabilised upon a slope through the injection of potassium chloride, which intercalates into the interlayer spaces between the clay particles (Helle, 2017).

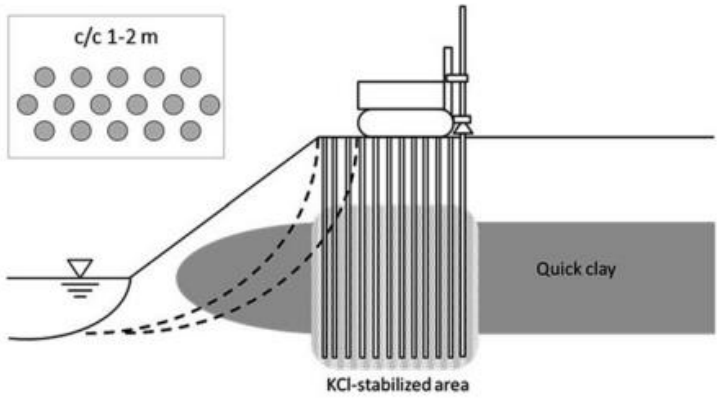

Figure 2.16. Diagram depicting the impact stabilisation with KCl solution has upon identified 'quick clays' (sensitive soil material) within a soil slope (Helle, 2017).

This methodology was proven to be so successful, based upon the inherent properties halloysite imparts (Helle, 2017). Halloysite rich soils tend to have an efficacy for intercalation of poorly hydrated cations, including NH_4^+, Cs^+, and K^+ (Joussein et al., 2005). As a result, these cations are more readily intercalated into the interlayer spaces between halloysite particles, in comparison to other ions (Joussein et al., 2005).

2.5.2.5 Prefabrication vertical drains (PVD)

Prefabrication vertical drains (PVDs) are installed vertically within a material to aid in the shortening of the pore water pressure drainage path from a low permeability soil layer (Turukmane et al., 2019). Installation of drains in susceptible layers reduces the time taken for primary consolidation to occur (Turukmane et al., 2019). The installation process, depth and width of the drains is dependent on soil properties.

PVDs are generally made of a plastic core, encased by either a geotextile non-woven or woven fabric (Turukmane et al., 2019). The drains are used to accelerate the settlement of the materials, to reduce the construction period of a project (Turukmane et al., 2019). PVDs are also beneficial for use with stabilisation of sensitive soils by increasing the shear strength of the materials (Turukmane et al., 2019). PVDs have a number of advantages and disadvantages, summarised in **Table 2.10**. For effective remediation of soil materials using PVDs, a combination of preloading to encourage primary consolidation and drainage installation is recommended (Meilani & Fikri, 2020).

Therefore, PVDs could potentially be a viable option for sensitive soil remediation, particularly with soils of a high water content brought about by high porosity, but low permeability.

Table 2.10. Table summarising the advantages and disadvantages of PVDs (Thurukmane et al., 2019).

Prefabrication vertical drain (PVD)	
Advantages:	Disadvantages:
Greater assurance of vertical drainage at 20 – 30 m depth.	Installation of drains could be challenging in situations where fill, sand or stiff clay overlies target material
Can withstand appreciable amounts of lateral displacements	Where sensitive soils are present, disturbance by drain installation may be challenging and lead to strength loss.
Fairly cost effective, dependent upon the scale of the project	

2.6 Summary of chapter

The geological background to the Hamilton basin, the characteristic landscape units of the basin and the characteristic materials making up the units, sensitivity and the sensitive soil characteristics, differences in sensitive soils in New Zealand compared to soils in the Northern Hemisphere, the clay minerals that cause sensitivity (halloysite and allophane), hazards that sensitive soils cause, and the management strategies to reduce sensitivity, and current remediation strategies for sensitive soils have been reviewed.

The hazard for sensitive soils in an engineering sense is high, especially within areas such as the Hamilton Basin, where infrastructure demands are increasing, leading to large deposits of Walton Subgroup materials being exposed. These materials cause issues throughout the engineering process, due to a lack of specific engineering parameters designed to accommodate and account for the behaviours of these materials. It is these issues that motivates this thesis research.

Chapter 3
Methodology

3.1 Methodology introduction

Samples were taken from sites that were deemed suitable for sampling. A number of lab-based procedures were carried out on the samples taken to determine the geomechanical and mineralogical properties characteristic to the Walton Subgroup materials. The following discussion outlines the parameters measured and the standards used for these methods. Detailed procedures for each of these methods can be found in **Appendix 3.1**, and are split up into individual sections.

3.2 Site selection

The sites selected for use in the analysis of sensitive soils within the Hamilton Basin required a site with an easily accessible sampling area, with a defined Walton Subgroup portion that could be sampled, and a broad, definite field area that clearly displayed the soil layers *in situ*. Identification of the sites tested relied upon prior knowledge and connections to sites through engineering consultancies.

3.3 Geotechnical analyses

3.3.1 Moisture content and Atterberg limits

Soil moisture content and Atterberg limits were determined and tested following strict guidelines based upon the ISO/TS 17892:2004 methodology (ISO/TS 17892:2004a; ISO/TS 17892:2004b; ISO/TS 17892:2004c). Moisture content (**Appendix 3.1.1**) was calculated using **equation 3.1**. The determination of Atterberg limits is a key process to laboratory investigation and testing of soils. The Atterberg limits are transitional boundaries between the different states of soil matter within a fine-grained soil material, which is defined as any soil with 50% or more

of the materials below the 0.075mm grain size threshold (Germaine et al., 2009). **Figure 3.1** shows the different stages of soil defined by Atterberg limits, with the different units being identified using the abbreviations seen upon the diagram. From this point onwards, the stages will be defined using the ISO/TS 17892-12:2004 methodology.

The different stages defined by Atterberg limits include the shrinkage limit (SL), which marks the point between a solid and semi-solid soil material (Seed et al., 1964). The next boundary is the plastic limit (PL), which is the boundary between a semi-solid soil material and more plastic soil behaviour. This transition occurs slowly in most soils *in situ* (Seed et al., 1964). The next boundary is the liquid limit (LL), which marks the boundary between plastic soil behaviour and liquid behaviours. Finally, the uppermost boundary is the fluidization limit (FL), which is the boundary between the liquid behaviours of a soil body, and the suspension of soil particles within a fluid suspension (Seed et al., 1964). Most soils, however, sit between the plastic and liquid limits within their natural states (Seed et al., 1964). The plasticity index (PI) is also commonly measured and indicates the values over which the soil behaves in a plastic manner. Atterberg limit parameters were calculated using **equations 3.2 and 3.3** in **Appendix 3.1.1.**

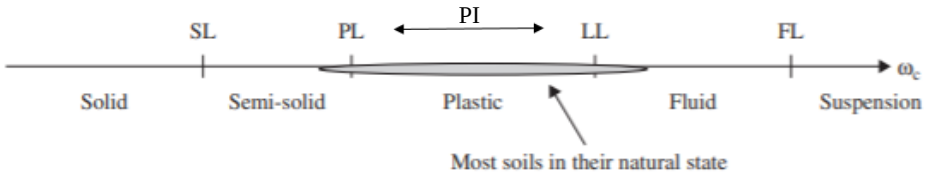

Figure 3.1. Diagram showing the boundaries between the different defined Atterberg limits, and the associated soil behaviour observed at each boundary.

Atterberg limits were used to determine the classification of the soil being tested, in order to relate to the sensitivity of the soil. The Atterberg limits tests were completed using homogenous soil pastes under a cone penetrometer. The cone penetrometer was used to minimise variability, which is commonly experienced using the Casagrande cup (**Appendix 3.1.1).**

3.3.2 Bulk density, dry density and particle density

Bulk density is the measure of material density, considering the physical mass of the material being measured including pore space. Field moist density and oven dry density determination was completed following standard ISO/TS 17892-2:2004 (**Appendix 3.1.2**) and both field moist and oven dry density were calculated using **equations 3.4, 3.5 and 3.6.**

Particle density, however, is the measurement of the density of individual particles classes within the material being tested. Particle density was completed and calculated using **equation 3.7** in line with standard BS1377: Part 2:1990:8.3., the standardised Density Bottle (Small Pyknometer) Method (**Appendix 3.1.2**).

3.3.3 Triaxial testing

Triaxial testing was completed upon the sensitive soils of the Hamilton Basin in order to determine the stress-strain relationship of the soils under confining stress with pore water pressure measured (**Appendix 3.1.3**). The failed samples were subsequently tested to determine the failure mechanisms that sensitive soils typically undergo when external pressures are applied. The triaxial tests were beneficial, as the results gained could be compared to recent and relevant New Zealand-based literature, including the works completed by Mills in 2016 and Robertson in 2017.

The triaxial test type was also important. Consolidated drained, unconsolidated undrained, and unconsolidated undrained tests are common tests undertaken, dependent upon the parameters needed. The Consolidated Undrained (CU) test was used for this study, as both the total and effective friction angle and cohesion was measured.

The methodology used for triaxial testing at the University of Waikato adheres to the British Standard (1990) part 8: Shear strength tests (BSI, 1990). The testing procedure took around a week to complete for each testing run. This was due to the inherent properties of the soil, as the sensitivity of the soil meant that an extended period of consolidation was needed, in addition to a seven-day shear stage, to ensure sufficient failure of the sample. This differed significantly from the testing times of previously tested sensitive soil samples, such as those tested by Mills in 2016, and Robertson in 2017. Four stages of testing were completed: saturation, B-check, consolidation and shear. The effective strength exerted on the samples and

the estimated coefficient of permeability were also calculated. The values needed for these various stages were calculated using **equations 3.8, 3.9, 3.10 and 3.11**.

3.4 Mineralogical analyses

3.4.1 Thin section production

Thin sections were produced of the failed triaxial material in order to gain additional information regarding the location, orientation, distribution and thickness of the shear zones following the example of Gylland et al., (2013b). These observations give a better understanding of the likely propagation pathways of the shear features and provide indication of areas of weakness (**Appendix 3.1.4**)

3.4.2 Particle size analysis

A particle size analysis (**Appendix 3.1.5**) was completed upon a small subsample of homogenous paste to determine the dominant particle size, in addition to the percentage of particles that were "sand-sized", "silt-sized" and "clay-sized". The particle sizer analysis was completed using the University of Waikato SOP (Standard Operating Procedure) to determine the percentage of particles under defined particle size grading. The analysis was completed using the Malvern Mastersizer laser size analyser. Activity was also calculated using the results of the clay-sized fraction of the particle size analysis, in addition to the plasticity index calculated from Atterberg limit testing, using **equation 3.12** (**Appendix 3.1.5**).

3.4.3 X-ray diffraction (XRD)

X-ray diffraction (XRD) is a known technique for the quantitative and qualitative analysis of the mineralogical properties of a soil sample (Harris & White, 2008). Soil mineralogy is a critical property to be measured, due to the soils' reliance on these properties in its' behaviour under differing conditions (Harris & White, 2008). XRD is one of the most effective strategies of identification of minerals within fine grained materials, such as soil (Harris & White, 2008). XRD is also useful as it allows for changes to be measured regarding

additions of stabilisation agents such as lime or cement, to determine the potential mineralogical alterations of the soil (Goodary et al., 2012). The main principle of measurement for the XRD is that each crystalline substance within a sample has a characteristic atomic arrangement which diffract X-Rays in a unique manner, allowing for identification.

Small subsamples of soil had the clay fractions separated and pipetted onto a ceramic tile for use in clay analysis. Calgon was used as a flocculent to disperse the clay particles into solution. Four testing runs were completed for the clay analysis: untreated, ethylene glycol; heated to 110°C for one hour prior to testing and heated to 500°C one hour before testing. Formamide was also added to determine between halloysite and kaolinite (**Appendix 3.1.6**).

Oven dried, unsorted powder was prepared and used for bulk sample analysis. These samples were oven dried at 105°C before being run through the XRD. Therefore, the use of XRD was critical in the determination of the main minerals present within the soil samples taken, both in the bulk samples tested, and in determining the predominant clay mineral present within the samples.

Allophane testing was additionally completed (**Appendix 3.1.6**) to determine the presence within the samples, due to the x-ray amorphous nature of allophane clays.

3.4.4 Scanning electron microscope

The scanning electron microscope (SEM) (**Appendix 3.1.7**) is a specialist microscope used for the characterization of the internal structures of a material (Podor et al., 2012). The use of the SEM on soils for the analysis of engineering properties allows for the identification of the microfabric of the soil at a range of differing magnifications, from 20 times to 50,000 times magnification (Podor et al., 2012).

In the case of this study, the SEM was largely used to analyse the microstructure of the failures, and how the different particle size fractions interact with one another. These results could then be related to real life scenarios, of how the material will fail if subjected to specific conditions.

3.5 Summary of chapter

Lab based tests were completed for the testing of the soils to provide an in-depth dataset that determined the main properties of the soil, in relation to the geomechanical results seen from lab testing. In particular, the failed triaxial cores were made into thin sections, then analysed further. These identified properties are critical for the subsequent determination of why sensitive soils fail in the ways documented, and how this affects the soils in an engineering capacity.

Chapter 4
Site descriptions and field observations

4.1 Introduction

This chapter outlines the process of selecting sites, and the observations made. Multiple sites were considered for sampling, however only two sites contained an accessible deposit of suitable Puketoka Formation sample, and that could be accessed and sampled within the timeframe of both the construction project and this study. As a result, only two sites were sampled. At each site, samples were taken for Atterberg limit testing, triaxial core testing, and bulk density testing. This meant taking a large bulk sample of sensitive material from the cuttings to be made into homogenous pastes for Atterberg limits, in addition to several cores being driven into horizontal ledges of the cutting to provide intact cores for triaxial and bulk density testing. This chapter provides more comprehensive and detailed descriptions on how the sites were selected, and how the soils were sampled, along with any limitations that were encountered during the sampling process.

4.2 Site selection

To identify where potential accessible deposits of Puketoka Formation materials could be found, geological maps of the region were studied before discussions were had with geotechnical consultancies that were involved in large-scale construction projects across Hamilton. AECOM offered access to several sites, including Dixon Road Roundabout, which had identified Puketoka Formation materials at depth where slope cuts had been performed. Additional sites, including The Meadows stages 3 and 5, and North City Park were considered, but were deemed unsuitable due to difficulty in accessing the materials and constraints on project timelines deeming sampling windows too small. For The Meadows however, hand auger and handheld shear vane data were still obtained.

Care was taken to ensure that samples were as undisturbed as possible, through the scraping of pads to expose deeper materials, and ensuring the cores were hammered vertically

into the material. However, external factors including excavation of the site and plant activity that could have led to some disturbance of the material also need to be considered in this case.

CMW Geosciences also provided access to the Temple View site, which was proven to provide a viable source of Walton Subgroup material within the exposed levelling cuts completed in early 2020.

The sites sampled were chosen due to compliance to the suitability criteria:

- within areas of the Hamilton Basin where Walton Subgroup, in particular the Puketoka Formation, materials had previously been identified;
- they had an accessible source of sensitive Puketoka Formation materials (identified by visual appearance and shear vane results); and
- consultancy and contractor groups allowed access to the site, allowing sampling to occur.

4.3 Site one – Peacocke State Highway 3/Dixon Road roundabout

The first samples were taken from the in-construction Peacocke State Highway 3 (SH3) site (hereafter referred to as the Dixon Road Roundabout site), which began construction in January of 2020. The samples were obtained in July 2020. The roundabout aims to link Ohaupo Road/SH3 and the not yet built Peacocke Road (Hamilton City Council, 2020). The project is being built as a partnership between the New Zealand Government and Waka Kotahi New Zealand New Zealand Transport Agency, as part of the Southern Links project (Hamilton City Council, 2020). The project was being completed by Schick Civil Construction, with an AECOM lead engineering consultant supervising the stages of construction. (Hamilton City Council, 2020). The roundabout was completed during this study (**Figure 4.1**).

Figure 4.1. Diagram showing the site of the construction of the Peacocke State Highway 3 (SH3) roundabout in Southern Hamilton (Hamilton City Council, 2020).

The site was suitable for sampling sensitive soils, as there were several deep cuts into the material that exposed the Puketoka Formation materials and were relatively easy to access and sample. **Figure 4.2** shows the extent of the cuts being made at different parts of the site, in order to allow for retaining walls to be built to reduce erosion and create a level area.

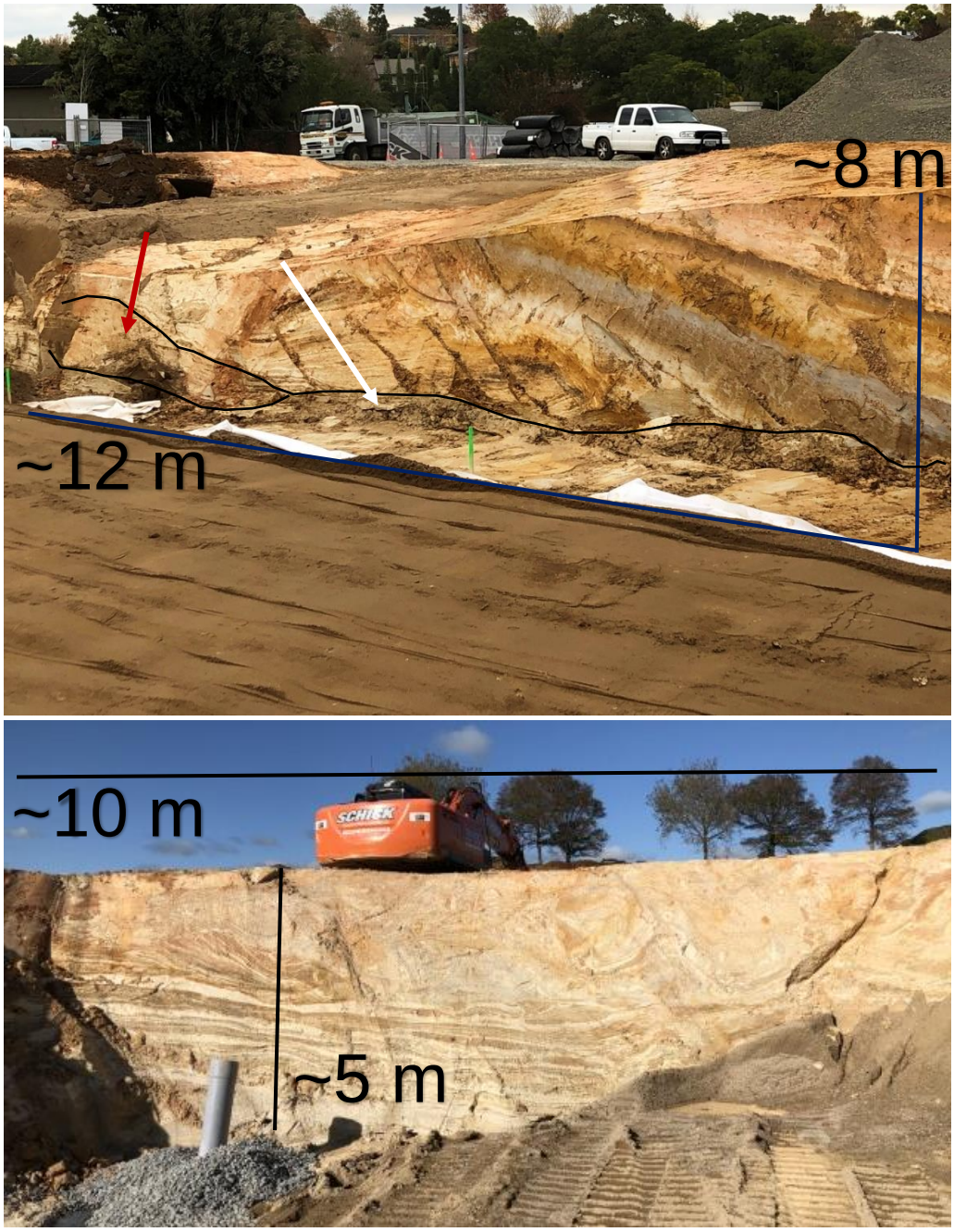

Figure 4.2. Images taken at the Dixon Road Roundabout site showing the scale and size of the cuts being made within the sediments. Top image depicts the bedded layers observed at the site, showing from the top down a sequence starting at the Lower Hamilton Ash formation, the Karapiro Formation, and the upper (red arrow) and lower Puketoka Formation (white arrow) layers. The lower Puketoka beds were sampled for this study. (Lethborg, 24th July 2020).

The site also exhibited the presence of a small fault identified running through one of the exposed cuts, indicative of seismic history. **Figure 4.3** shows the extent of the faulting within an exposed cut segment.

Figure 4.3. Image showing evidence of the faulting found within the Dixon Road Roundabout site cuttings, which could pose an issue to the sensitive sediments within the site if seismic activity were to occur. Note the bedding of the layers observed, separated by dark brown layers (Lethborg, 24th July 2020).

4.3.1 Site characteristics

The site showed an extensive number of layers due to the ~10m cuts made in order to accommodate future underpass installations. **Figure 4.4** shows the approximate location of the samples taken for the Dixon Road Roundabout site, hereafter referred to as DRAB1.

Figure 4.4. Google Earth image showing the approximate location of sampling for the Dixon Road Roundabout (DRAB1) site, in relation to the now constructed roundabout (Google Earth, 2021).

A comprehensive depositional stratigraphy could be observed on-site (**Figure 4.5**). The lower Hamilton Ash formation was identified by the characteristic brownish orange colour, and clayey SILT consistency. The upper Karapiro Formation was observed with faint pink mottles, above a series of greyish brown Kauroa Ash beds. A dark brown paleosol layer was also observed between the Kauroa Ash and Karapiro Formations. The lower Karapiro Formation was then identified with orange mottles, and a dominantly SILT texture, with some sand and trace clay. The upper and lower Puketoka Formations differed in colouration, with the lighter greyish-yellow layer representing the upper Puketoka formation. This layer was cohesive in nature and showed evidence of redox reactions and manganese concretions upon the surface. The lower Puketoka Formation, sampled for this study, appeared to be more orange

in colouration, with black streaks indicative of the manganese inclusions. It also appeared to have more granular inclusions than the upper Puketoka Formation based upon in-situ characteristics. **Table 4.1** summarises the classification of the sampled DRAB1 material.

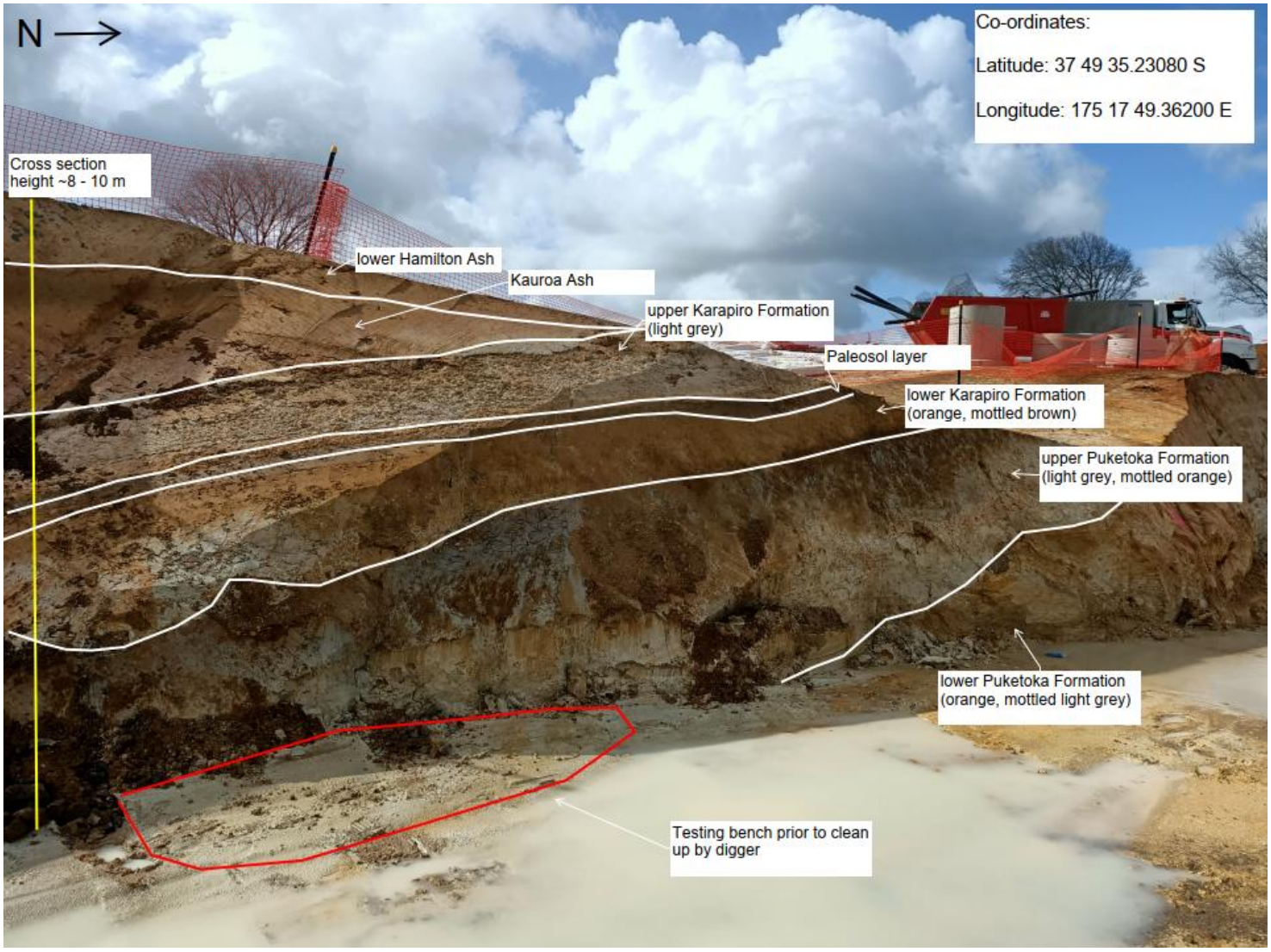

Figure 4.5. Annotated diagram showing one of the exposed cross-sections present at the Dixon Road Roundabout site, showing the main sedimentary units present, in addition to the sale of the exposure, and location of the triaxial and bulk density core bench (Co-ordinates in WGS, 1984).

Table 4.1. Table summarising the classification of the material sampled upon the Dixon Road Roundabout (DRAB1) site, following NZGS 2005 conventions.

Classification of material sampled (NZGS, 2005):	SILT, some sand, minor clay: light brownish orange, streaked black. Stiff; moist; high plasticity; sensitive; manganese nodules, subangular to subrounded, less than or equal to 2mm in diameter; breaks down when worked.

4.3.2 Site sampling

Twelve undisturbed triaxial cores and ten bulk density cores were taken from the testing bench seen in **Figure 4.5** in addition to two bags of bulk material to test Atterberg limits, particle density, particle size distribution and X-Ray Diffraction.

Handheld shear vane data was taken from the site, and the results are summarised in **Table 4.2.**

Table 4.2. Table summarising the handheld shear vane results and sensitivity ratings for Dixon Road Roundabout site, taken from two locations of the cut testing bench. Additional results gained from AECOM hand auger logs from a 2018 investigation at Dixon Road, fsourced from the New Zealand Geotechnical Database (NZGD) have also been included.

Depth of shear vane (m)	In-sit/remoulded results (un-corrected, kPa)	Calculated sensitivity	Sensitivity classification (NZGS, 2005)
0.00m (surface)	62/20	3.1	Moderately sensitive
	66/14	4.7	Sensitive
1.8 m (AECOM, 2018)	69/15	4.6	Sensitive
2.1 m (AECOM, 2018)	47/15	3.1	Moderately sensitive

For the triaxial and bulk density cores, a horizontal bench was cut into the sensitive material (**Figure 4.5**), before the cores were spread across the bench 15 cm apart from one another, making sure that the surface was as flat as possible, and free of any evident cracks or iron pan features. The cores were then gently pushed in and hammered into the soil, until the core top sat flush with the surface of the soil (**Figure 4.6**). A wooden block was placed on top of the samples to minimise the vertical deviation when being driven down (Mills, 2016; Robertson, 2017). The excess soil surrounding the core was then dug away using a spade and retrieved. This excess soil was used as bulk sample. Once removed, the cores were wrapped in clingfilm to ensure that the soils remained as close to field moist conditions as possible.

Figure 4.6. Figure showing ten of the twelve triaxial cores hammered into the cleared bench of Puketoka Formation material (30cm mallet for scale) (Kitchen, 2021).

Because the materials being tested were sensitive in nature, extra measures were needed to ensure that the soil retained the moisture content experienced in-situ. This was also completed to minimise the risk of the soil cores drying out prior to testing.

Therefore, a particular sampling methodology was adopted to ensure these conditions were met, and the cores were kept as field moist as possible:

1. once the sample was extracted within the core, the core was thoroughly squirted with distilled water, to ensure it was moist;
2. the ends of the core were wrapped with a layer of clingfilm, with care being taken to remove air from both ends;
3. the core was then coated with another layer of clingfilm, which was then moistened with more distilled water;
4. step 3 was completed multiple times, until the middle of the core was wrapped around eight times with dampened layers of clingfilm;
5. following this, the ends of the core were then covered again with another layer of clingfilm; and

6. finally, the wrapped cores were then placed in a resealable bag, with all air being pushed out to ensure a tight seal.

4.4 Site two – Temple View Urban Zone Development

The second set of samples taken for this study was from the Temple View suburb of western Hamilton in February 2021. Temple View is a suburb established in the 1950s, before coming under the legal control of the Hamilton City Council in 2004 (Hamilton City Council. 2021). The Urban Zone Development aims to provide new housing and infrastructure that is in keeping with the values identified within the Temple View community. The Hapori Park subdivision is the area of interest for this thesis, as it was the area in development at the time of sampling.

4.4.1 Site geomorphology and characteristics

The site at Temple View was once agricultural land that had been excavated and prepared for development at the time of sampling.

The site at the time of sampling was in the cut/fill portion of the development, and therefore widely exposed. The site was once part of a ridge that has been cut down to create a level surface for future development of the subdivision. The cuts had been exposed for around a year at the time of testing and have therefore developed a weathered crust. As a result, a freshly scraped pad was required, to sample the more undisturbed in-situ materials present. Co-ordinates for the three testing locations can be found in **Table 4.3**.

4.4.2 Site sampling

Two areas were sampled from within the Temple View site (referred to as TV1 and TV2) in order to capture some of the variance seen within the site (**Figure 4.7**).

Figure 4.7. Annotated map showing the sampling areas within the Temple View site, where TV1 and TV2 materials were sampled from (Google Earth, 2021).

Table 4.3. Table showing the co-ordinates for the testing sites within the Temple View sampling site (coordinates in WGS, 1984).

Testing location area:	Latitude (decimal degrees, minutes and seconds):	Longitude (decimal degrees, minutes and seconds):
TV1	37°49’12.35”S	175°13’40.05”E
TV2 area 1	37°49’10.26”S	175°13’41.42”E
TV2 area 2	37°49’11.41”S	175°13’42.77”E

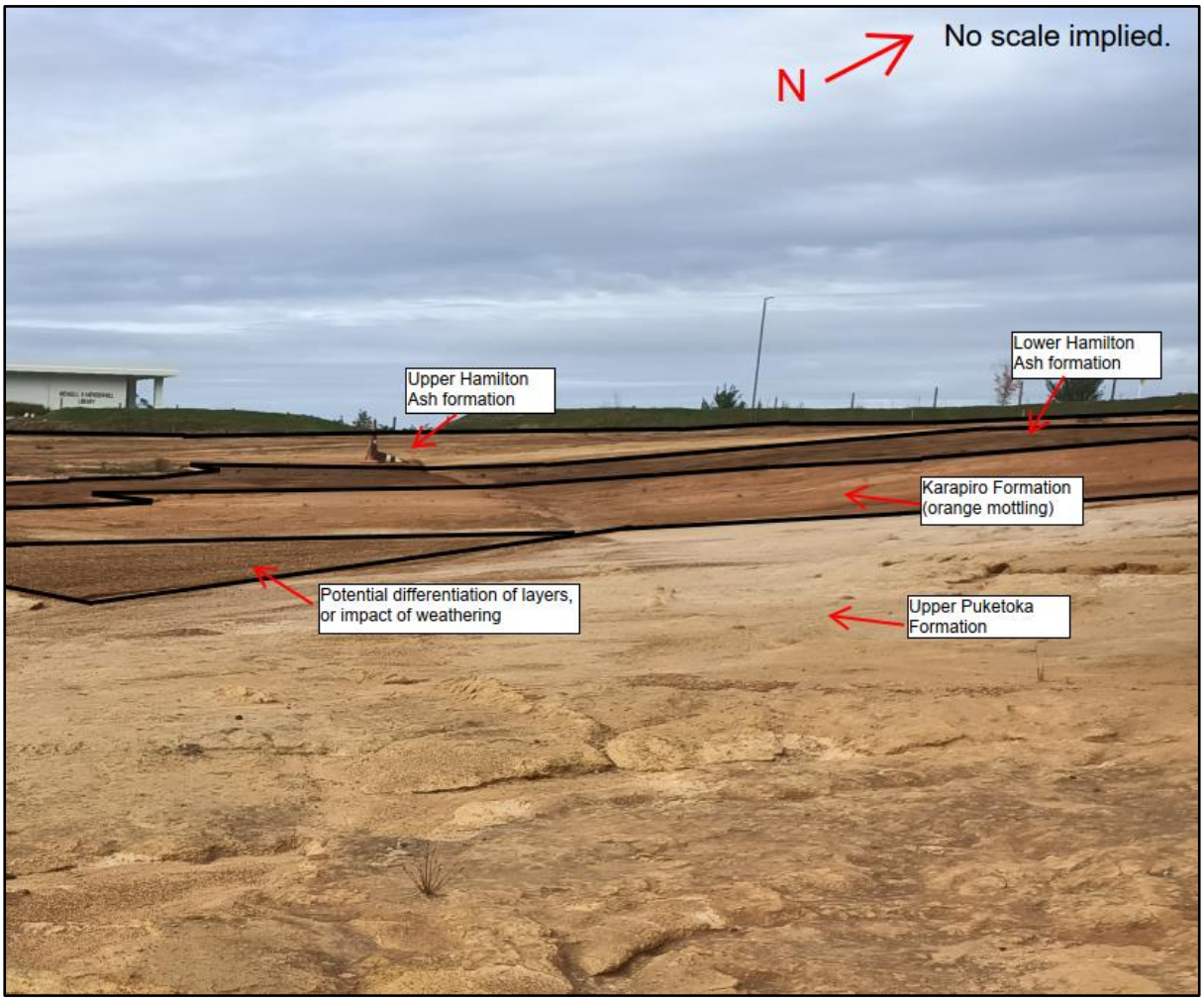

Figure 4.8. Image depicting the sequence of deposition interpreted within the Temple View site, based upon physical characteristics of the material. Note that this material has been exposed to weathering conditions to upwards of a year, therefore the colourations may not be truly representative of the formations. No scale implied.

A similar sequence of material compared with Dixon Road Roundabout could be observed (**Figure 4.8**). However, the layers were somewhat less visible, likely due to weathering effects. The upper and lower Hamilton Ash formations were present, identified by the distinctive brownish orange colouration and clayey SILT consistency. The probable Karapiro Formation was identified below this, with no clear Kauroa Ash layer above this. The Karapiro Formation had distinctive orange mottling, and was dominantly SILT, with some sand and trace clay. Below this was the hypothesised upper Puketoka Formation, identified by the pink mottling and manganese concretions, and a dominance of SILT, with some clay. The lower Puketoka Formation, identified in **Figure 4.7**, was sandier in composition, but still contained manganese concretions.

Handheld shear vanes were also completed on the surface of the material. A summary of the results and associated sensitivity classification is summarised in **Table 4.4**.

Table 4.4. Table summarising surface shear vanes completed at various sampling locations across Temple View.

Depth of shear vane and material tested	Peak/remoulded values (un-corrected, kPa)	Calculated sensitivity	Sensitivity classification (NZGS, 2005).
0.00m (surface) -TV1	120/32	3.8	Moderately sensitive
0.00m (surface) – TV2 area 1	90/40	2.3	Moderately sensitive
0.00m (surface) – TV2 area 2	92/42	2.2	Moderately sensitive

These slopes were identified to have exposed Walton Subgroup materials, therefore could provide a viable source of material suitable for sampling. Three locations were sampled for this site, following the gradient of the cut to the upper and lower Puketoka Formations (**Figure 4.7**). This allowed for some variation to be assessed upon a small scale. **Figure 4.9** Figure **4.10** and show the visual differences between the two samples.

The classification of the materials sampled on this site are summarised in **Table 4.5**, using the NZGS system of classification.

Table 4.5. Table summarising the classification of the materials sampled at Temple View, using the NZGS 2005 classification.

Classification of materials (NZGS, 2005)	**TV1** – SILT, some sand, trace clay; pink, mottled orange, streaked black. Very stiff; moist; low plasticity; sensitive; manganese nodules, subangular to subrounded; breaks down when worked.
	TV2 – Sandy SILT; light greyish yellow, streaked black. Stiff; moist; low plasticity; sensitive; manganese nodules, subangular to subrounded, breaks down when worked.

Sampling was undertaken in the same manner to that of Dixon Road Roundabout. Twelve triaxial cores were taken, in addition to 12 bulk density rings. However, parafilm was used to wrap the ends of the cores, rather than clingfilm, due to the parafilm's better capacity to wrap and retain moisture within the core for transportation and storage. Three bags of bulk sample were also collected.

However, due to the length of time these materials had been exposed to external elements, a degree of drying out and weathering had occurred. Whilst care was taken to scrape off any crusted and dry material, sampling of some of the lower Puketoka Formation materials was unsuccessful, as the cores were too dry to have any appreciable cohesion. This impacted the number of tests that could be completed.

Figure 4.9. Image showing the level platform scraped prior to triaxial core extraction of the upper Puketoka Formation materials (20 cm shearvane to scale).

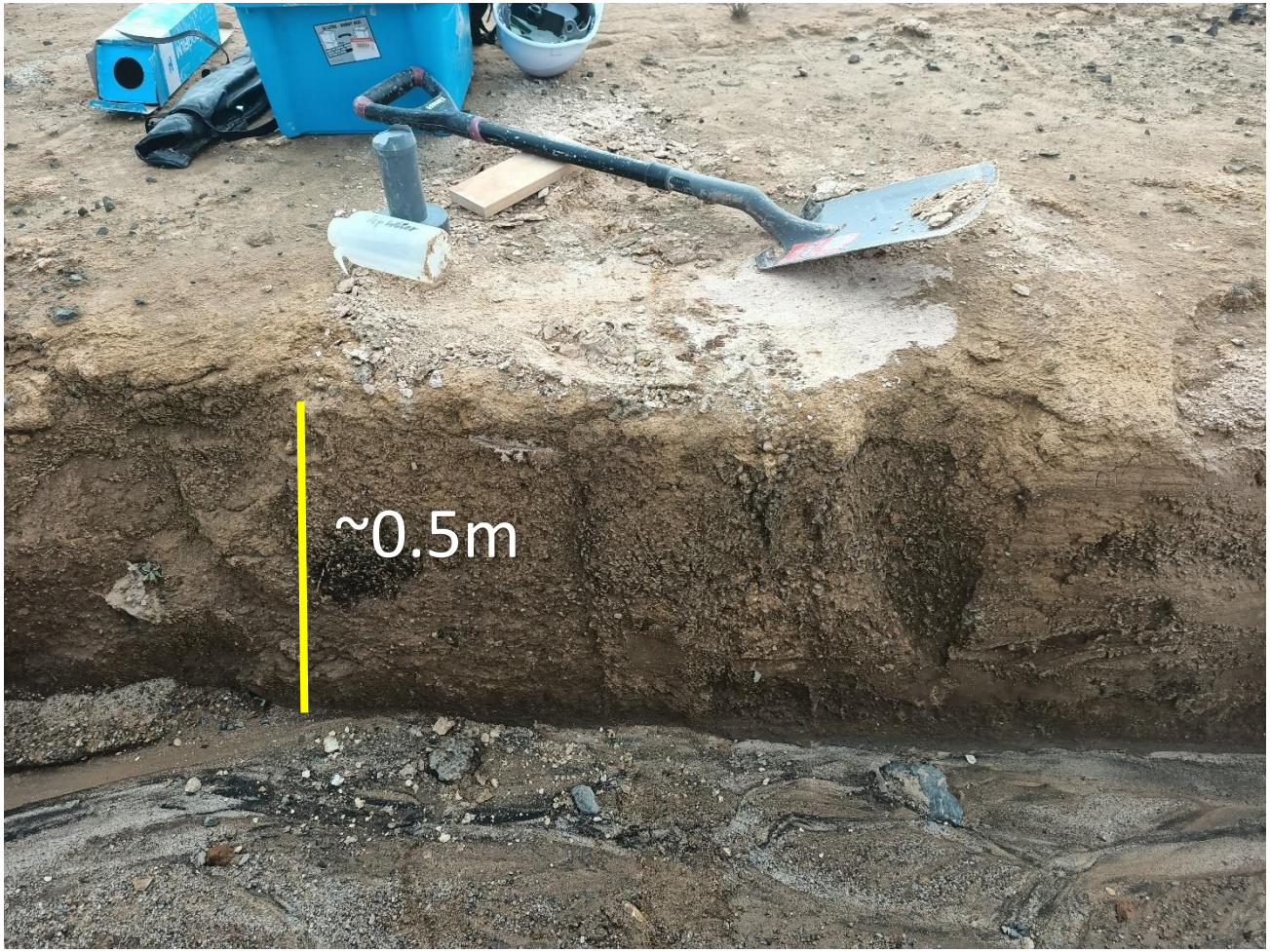

Figure 4.10. Image showing the bench scraped and used for sampling of the lower Puketoka Formation materials within the Temple View Site (water bottle for scale).

4.5 Comparison of sites

The two sites used within this study are located around 6 kilometres away from one another, therefore provide some potential level of variability in the extent of the Puketoka Formation. **Figure 4.11** compares the locations to one another.

Figure 4.11. Google earth image comparing the locations of the two sites sampled for this study. The large outline indicates the Temple View site, and the smaller outline indicates the Dixon Road Roundabout site (Google Earth, 2021).

The material gathered from each site showed some variation in the colouration of the material, and the apparent cohesive and granular fractions identified, indicating that potentially differing materials had been sampled. This provided the opportunity to gain results that were representative of a wider range of Puketoka Formation materials.

4.6 Site three – The Meadows Subdivision, Stages 3 and 5

The Meadows Subdivision Stages 3 and 5, part of a larger scale 11 stage subdivision, is located in Flagstaff, and serves as a critical part of the Rototuna Growth Cell. Deposits of Walton Subgroup material have been identified at the site (Blue Wallace Surveyors Limited, 2021). The site was once a 60ha dairy farm, which was bought 17 years ago. Pemberton Civil Limited have been contracted to complete the earthworks upon the subdivision, with AECOM's lead consultant supervising the operations. **Figure 4.12** shows the scale of stages 3 and 5.

Figure 4.12. Google Earth image showing the extent of the stages 3 and 5 development stage of The Meadows subdivision (Google Earth, 2021).

No lab samples were taken from The Meadows. However, hand augers were completed within Walton Subgroup materials, gaining geological and engineering strength data for the formation. The hand auger data are displayed in **Figure 4.13**

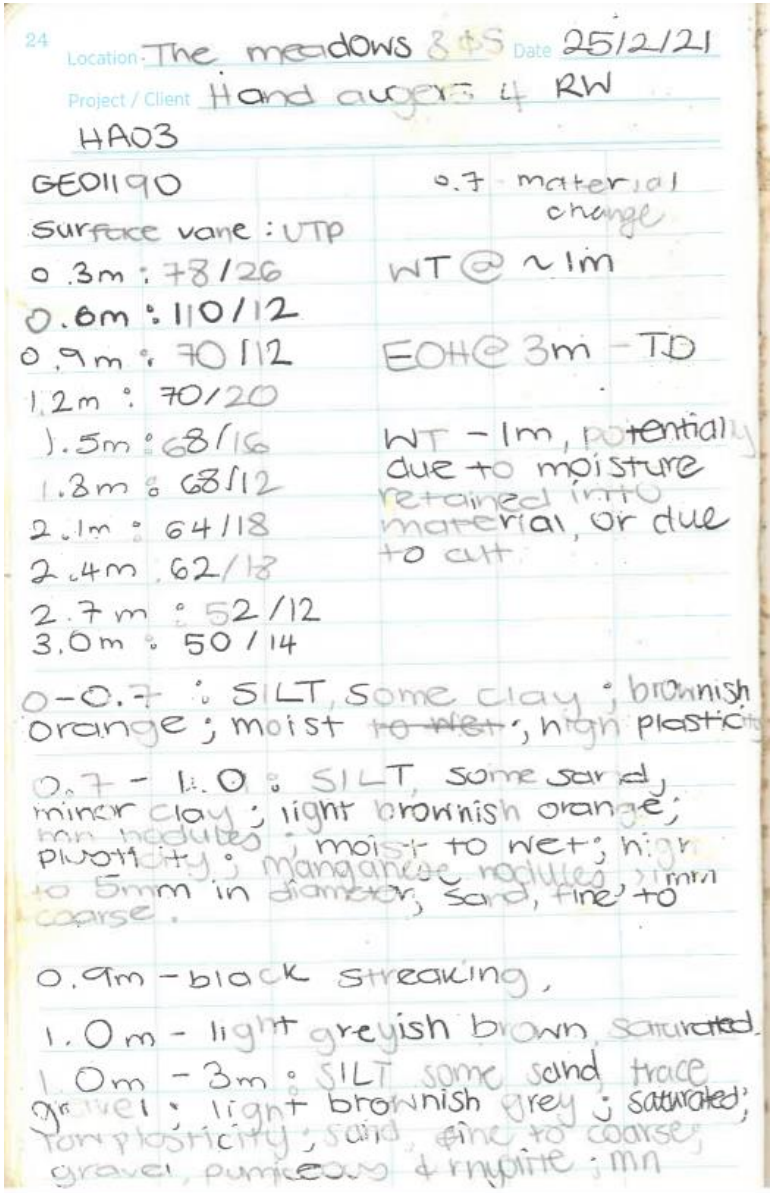

24

Location: The meadows 3 & 5 Date: 25/2/21

Project / Client: Hand augers 4 RW

HA03

GE01190

Surface vane: UTP

0.3m: 78/26

0.6m: 110/12

0.9m: 70/12

1.2m: 70/20

1.5m: 68/16

1.8m: 68/12

2.1m: 64/18

2.4m: 62/18

2.7m: 52/12

3.0m: 50/14

0.7 material change

WT @ ~1m

EOH @ 3m - TD

WT - 1m, potentially due to moisture retained in the material, or due to att

0-0.7: SILT, some clay; brownish orange; moist ~~to wet~~, high plasticity

0.7 - 1.0: SILT, some sand, minor clay; light brownish orange; mn nodules; moist to wet; high plasticity; manganese nodules >1mm to 5mm in diameter; sand, fine to coarse.

0.9m - black streaking,

1.0m - light greyish brown saturated.

1.0m - 3m: SILT some sand trace gravel; light brownish grey; saturated; low plasticity; sand, fine to coarse; gravel, pumiceous & rhyolite; mn

Figure 4.13. Photo showing a typical hand auger completed within the Puketoka Formation, to 3 metres depth (0.9m hand auger rod for scale), with rows laid out from left to right, in addition to field notes logging the formation, using New Zealand Geotechnical Society 2005 logging conventions.

4.7 Summary of chapter

Multiple sites were assessed for suitability to obtain Puketoka Formation materials, however only two sites fit all the criteria and could be accessed within an appropriate timeframe. Sampling for viable Puketoka Formation samples was undertaken at two large scale construction projects within the Hamilton area. These sites were within the southern area of Hamilton, around 6 kilometres apart. The material obtained from both sites were consistent with documented Puketoka Formation materials. Samples were taken to test both the geomechanical and mineralogical properties of the materials to provide a set of data that characterises the materials.

Chapter 5

Soil classification tests

5.1 Introduction

This section analyses the results gained from the laboratory-based classification tests; Atterberg limits, bulk density, particle density and particle sizer tests, and identifies the key trends seen. Raw results for this section can be found in **Appendix 5.1**.

5.2 Atterberg limits results

Soil pastes were produced for all three samples through the addition of water. The presence of fine to coarse sand-sized grains (**chapter 7**) within all the samples made complete removal challenging. As a result, the soil was worked to as homogenous a state as possible, where ~ 90% of visible grains were removed. This took around six hours to complete.

The paste was then left to sit for around 30 minutes before being tested, at eight differing moisture contents. The amount of water added was measured throughout, to ensure accuracy when replicate tests were completed.

Figure 5.1 shows the relationship between the cone penetration and the measured moisture content for the samples studied. The trend lines of the graph shows a strong positive correlation (R^2 = 0.85 - 0.98), and a relatively shallow increase in cone penetration as the moisture content of the soil increases.

Table 5.1 summarises the Atterberg limits calculated for the materials of this study, in addition to previous studies completed with Tauranga sensitive soils. DRAB1 had the highest liquid limit (LL) value (75 %), whilst TV1 had the lowest (59 %). The plastic limits were fairly comparable between samples, with TV2 having the greatest value (53 %), and DRAB1 the lowest (41 %). The plasticity index varied appreciably between DRAB1 and TV1 and TV2 (34 % versus 11 and 8 % respectively). The liquidity indexes for DRAB1 and TV1 were low (0.14 and 0.1 respectively), whilst TV2 was appreciably higher (1.50).

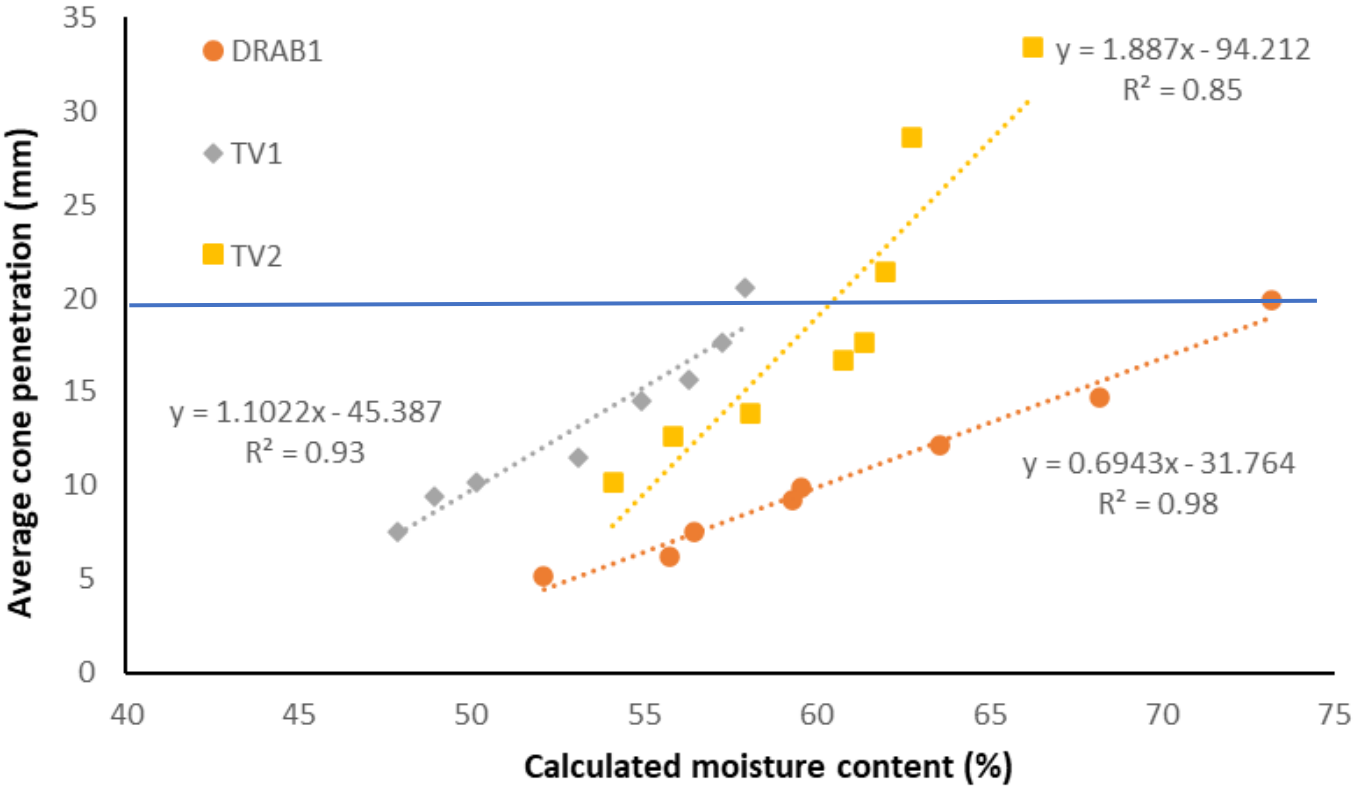

Figure 5.1. Graph showing the relationship between the average cone penetration (mm) and the moisture content (%) for the soils of this study. The blue line indicates penetration at 20 mm.

Table 5.1. Table summarising the measured Atterberg Limits results gained for the materials tested in this study, in addition to previous studies completed with soil materials from Tauranga and Hamilton.

Study	Liquid limit (LL) (%)	Plastic limit (PL) (%)	Plasticity index (PI) (%)	Liquidity index (LI)
This study, DRAB1	75	41	34	0.1
This study, TV1	59	48	11	0.1
This study, TV2	61	53	8	2
Moon & Blackstock, 2004	77	43	34	-
Wyatt, 2009	86	52	34	2
Cunningham, 2012	72	43	43	2
Mills, 2016	66	41	25	3
Robertson, 2017	92	78	10	0.4
CMW, BH05 (1), 2015	66	48	18	-
CMW BH05 (2), 2015	65	44	21	-
CMW BH06 (1), 2015	75	45	30	-
CMW BH06 (2), 2015	64	42	22	-

- = Not measured in this study.

A concept discussed in some literature, in particular, a study completed by Briaud in 2013, details Atterberg limit indices used in American classifications of soils. The plasticity index (PI) is the most used parameter in estimating soil behaviours, therefore, will be used for comparison in this study. **Table 5.2** summarises the Atterberg limits indices outlined by Briaud in their 2013 publication.

Table 5.2. Table showing the characteristic Atterberg limit indices for classifying 'low', 'medium' or 'high' liquid limit, plastic limit or plasticity index values (Briaud, 2013).

Parameter	Low	Medium	High
Liquid limit	10-40	40-80	**>80**
Plastic limit	10-20	20-30	**>30**
Plasticity index	0-20	20-50	**>50**

DRAB1 had a medium liquid limit (75 %), a high plastic limit (41 %), and a medium plasticity index (34 %). TV1 also had a medium liquid limit (59 %), a high plastic limit (45 %), but a low plasticity index (8 %). TV2 similarly had a medium liquid limit (61 %), a high plastic limit (53 %), but a low plasticity index (8 %), in keeping with TV1.

All three samples produced plasticity indexes in keeping with published values for the presence of inactive halloysite dominated volcanic soils (13 – 44 %) (Moon et al., 2013). The liquidity indexes tended not to follow the same trend in relation to the published values (1.2 – 2.4); being 0.14 for DRAB1 and 0.1 for TV1. However, TV2 fell within these values (1.5).

Comparison of the indices between the two sites samples indicates the similarities between the two, which was expected, due to the similarity of the materials tested. However, TV1 and TV2 were found to have lower plasticity indexes compared to that of DRAB1. This could be indicative of the main particle types within the materials.

5.2.1 Comparison with previous studies

5.2.1.1 Tauranga and Hamilton soils

The results produced are comparable to the previous studies on sensitive soils completed in Tauranga Region by Moon and Mills in 2016, and Robertson in 2017 (***Table 5.1***). However, these results also differ slightly from previous measurements.

Looking at the variability in the liquid limits (LL), the values recorded for DRAB1 are the most similar to Wyatt (2009), Cunningham (2012) and Mills' 2016 studies (66 – 86 % in versus 75 % in this study). This is also true with the plastic limit (PL) values (41 – 52 % in versus 41 % in this study). TV1 similarly produced comparable results to those of Wyatt (2009), Cunningham (2012) and Mills' (2016) studies for the liquid limit and plastic limit values (59 % and 48 %). The liquid and plasticity index values are appreciably different from the results gained in previous years, however. TV2 showed similarities to Mills' liquid limit (61 %), however produced a plastic limit more in keeping with Wyatt's (2009) study (52 % versus 53 % in this study).

The plasticity and liquidity indexes for DRAB1 and TV1 are appreciably lower than all of the calculated values from the Tauranga studies (**Table 5.1**). TV2 however produced a result in keeping with the results of Wyatt (2009) and Cunningham (2012) (2 % versus 2 % in this study).

Moon and Blackstock's (2004) study assessed the Walton Subgroups' Atterberg limits results. The results of DRAB1 are comparable with the liquid limit (75 versus 77 %), plastic limit (41 versus 43 %) and plasticity index (34 versus 34 %) results obtained by Moon and Blackstock (2004). TV1 and TV2 show general agreement with the plastic limit (48 and 53 % versus 43 %) but show appreciable differences in the liquid limit and plasticity index (**Table 5.1**).

A 2015 report completed by CMW Geosciences Ltd., provided results based upon the Puketoka Formation in Hamilton, taken from the Temple View site. These results can be used for comparative analysis in this study, particularly for the samples taken from the Temple View site. Based upon the Atterberg limit results (**Table 5.1**) gained from the report, the values calculated for DRAB1 are somewhat comparable to those from the CMW report, in particular the values gained from the testing of BH06. Interestingly, the samples gained from Temple View (TV1 and TV2) show variation from the results gained from the CMW study. This is further discussed in **chapter 9**.

In terms of classification on the Casagrande plasticity chart, the results from DRAB1, TV1 and TV2 all fit within the same classification as previous studies' results, based upon the calculated liquid limit and plasticity index values. The "MH" classification was given for all three samples tested (**Figure 5.2**) indicative of silts and clays with a liquid limit value of greater than 50, and has characteristics of inorganic silts, micaceous or diatomaceous fine sands or silts, or elastic silts (Carter & Bentley, 2016).

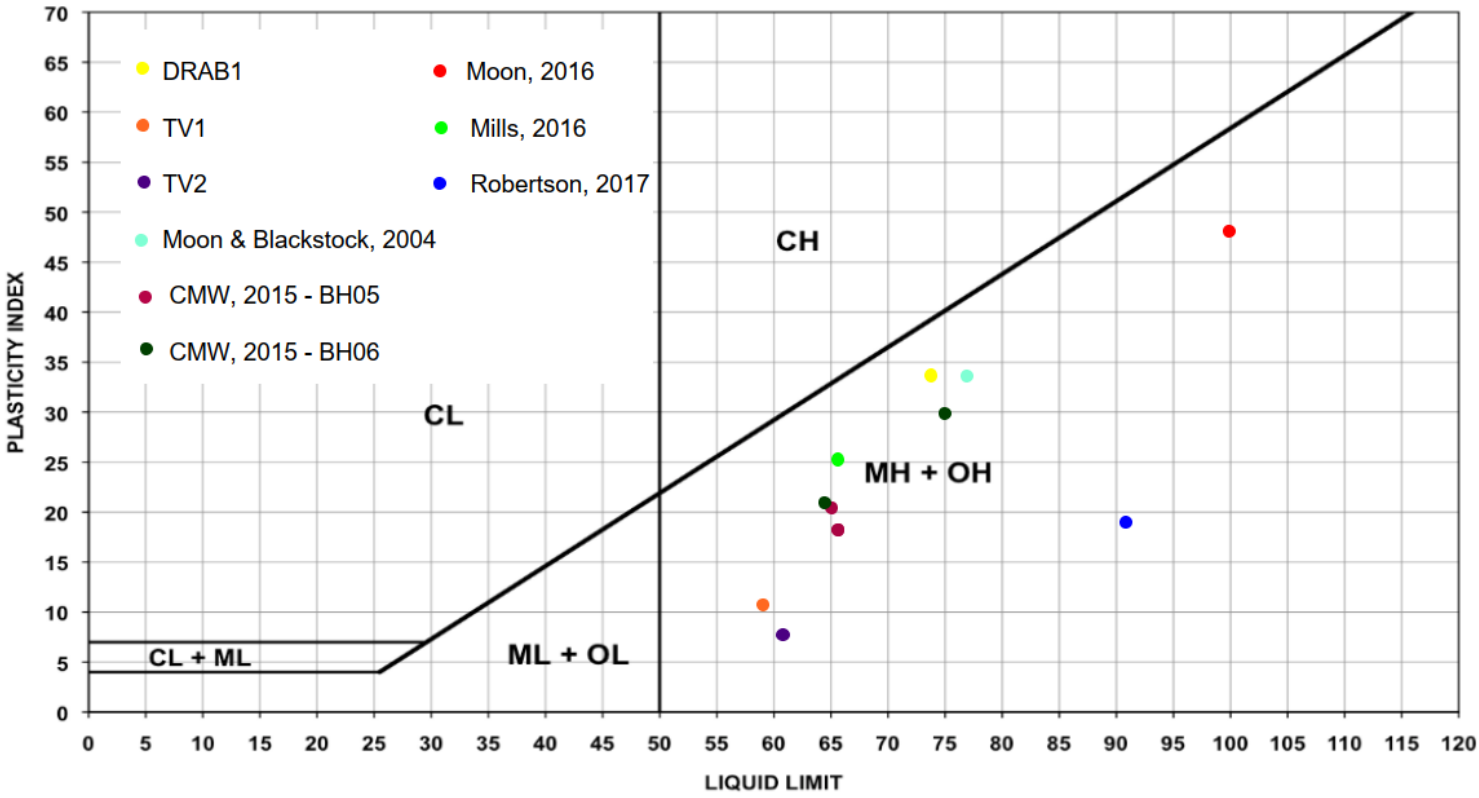

Figure 5.2. Graph summarising the Atterberg limits results for tests completed on DRAB1, TV1 and TV2 samples, in addition to results of previous studies (Casagrande, 1948).

5.3 Bulk density, moisture content and porosity

The bulk density of the soil material also needed to be calculated to provide a basis for subsequent effective stress calculations. Bulk density and subsequently dry density were calculated according to (ISO)/TS 17892:2004. The average moisture content and porosity values were also calculated (**Table 5.3**).

Table 5.3. Table showing the calculated average field moist (*p*) and oven dry (*pd*) bulk density values (kg/m^3), moisture contents, porosity (*n*) values (%) for the samples collected for this study. Void ratios (e) were also calculated. Material descriptions are also included.

Sample name	Description of material (NZGS, 2005)	Average field moist bulk density value (*p*, kg/m^3)	Average oven dry bulk density (*pd*, kg/m^3)	Average moisture content (%)	Average porosity value (*n*, %)	Calculated void ratio (e)
DRAB1	Sandy SILT, minor clay; sand, fine to coarse.	1576 ± 12	1057 ± 8	49 ± 16	36 ± 11	0.56
TV1	SILT, some sand; sand, fine to medium.	1460 ± 13	980 ± 9	49 ± 0.1	41 ± 11	0.69
TV2	Sandy SILT; sand, fine to medium.	1069 ± 138	645 ± 83	65 ± 0.2	51 ± 9	0.88

DRAB1 and TV1 were seen to have relatively high wet bulk density values (**Table 5.3**), whilst TV2 was considerably lower. The dry bulk density values similarly followed these trends. TV2 was also seen to have a higher average moisture content percentage (65 %), and a higher porosity value (51 %). DRAB1 and TV1 conversely have the same lower moisture content (49 %), with TV1 having a higher porosity compared to DRAB1 (41 % versus 36 %). Interestingly, the porosity values for DRAB1 and TV1 are below previously published values for halloysite-dominated volcanic soils (51 – 77 %) (Moon et al., 2013) TV2 had a porosity consistent with published values (51 %). TV2 had the greatest void ratio (0.88), whilst DRAB1 had the lowest (0.56). This was expected, as porosity and void ratio are interrelated.

5.4 Particle density

The compiled particle densities for the three samples are summarised in **Table 5.4**.

Table 5.4. Table of the average calculated particle density values for DRAB1, TV1, and TV2 samples, measured in kg/m^3. Standard error values for the results are also included.

	DRAB1	TV1	TV2
Calculated particle density value (kg/m^3):	2452 ± 490	2487 ± 280	1935 ± 250

Both DRAB1 and TV1 samples displayed particle density values consistent with published halloysite-dominated sensitive soil values from studies completed in Tauranga (2220 – 2663 kg/m^3) (Mills, 2016). However, TV2 produced a notably lower value compared with DRAB1 and TV1.

5.5 Summary of chapter

The results compiled in this chapter represent the soil classification from identified sensitive soil materials obtained from two large scale infrastructure project sites across Hamilton. DRAB1 was found to have the lowest porosity and moisture content, however had the highest bulk density value. TV1 had the highest particle density value, however. TV2 had the highest porosity and moisture content values, and as a result, the lowest bulk density values. This relates to the inversely proportional relationship between bulk density and porosity within a soil volume.

Chapter 6
Mineralogy and grain size

6.1 Introduction

The results of the mineralogical analyses undertaken upon the samples provided a suite of useful information that can now be analysed further to determine the predominant features of the sensitive soils. This chapter details the main minerals and particles within the samples.

6.2 Particle sizer results

Particle size analysis was completed upon samples from all of the Dixon Road Roundabout (DRAB1) and Temple View (TV1 and TV2) sites. The classification of grain sizes was based upon the New Zealand Geotechnical Society (NZGS) system, where the particles are separated into three different classes, dependent upon size. These thresholds, in μm, are > 2 μm for clay, 2 and 60 μm for silts, and between 60 and 2000 μm for sands (**Table 6.1**) (NZGS, 2005).

Table 6.1. Particle size divisions, in both mm and μm, based upon the NZGS 2005 classification, in accordance with NZS 4402 (1986) (NZGS, 2005).

Description	Particle Size (mm)	Particle Size (μm)
Clay	< 0.002	< 2
Silt	0.002 – 0.06	2 – 60
Sand	0.06 - 2	60 - 2000

Further differentiation between particle sizes was completed to give a more detailed analysis, splitting the silt sized particles up into fine silts (2 – 6 μm), medium silts (6 – 20 μm), and coarse silts (20-60 μm), and the sand particles into fine sand (60 – 200 μm), medium sand (200 – 600 μm) and coarse sand (600 – 2000 μm).

Table 6.2 summarises the distribution of particles in the DRAB1, TV1 and TV2 samples. See **Appendix 6.1** for raw particle sizer results. All three samples had high silt contents (> 40 %) (**Table 6.2**). TV1 had the highest silt content (81.12%), compared to TV2 and DRAB1 (76.01 % and 55.06 % respectively). The silt content is generally much higher in the Temple View samples, compared to Dixon Road Roundabout, with the silt being predominantly fine in size. DRAB1 had a subordinate fine sand content (25.35 %) compared to TV1 and TV2, which had minor fine sand (5.56 and 10.89 % respectively). All three samples had some clay, but DRAB1 had the highest clay content (18.85 %) when compared to TV1 and TV2 (13.32 % and 13.10 % respectively). These results are somewhat in agreement with the field classification of these samples (**chapter 4**), but some alterations to the classifications is required following this information (**Table 6.3**).

Table 6.2. Table summarising the particle size distribution within the samples analysed with the Malvern particle sizer.

	Clay sized particles (< 2 μm) (%)	**Silt sized particles (2-60 μm) (%)**				**Sand sized particles (60 – 2000 μm) (%)**			
Sample name:	**Total:**	Fine	Medium	Coarse	**Total:**	Fine	Medium	Coarse	**Total:**
DRAB1	18.85	22.70	21.05	11.31	55.06	14.79	10.37	0.19	25.35
TV1	13.32	34.95	34.38	11.79	81.12	5.56	0.00	0.00	5.56
TV2	13.10	34.46	32.15	9.40	76.01	7.85	3.04	0.00	10.89

Table 6.3. Table summarising the updated geological classification for the samples of this study.

Sample	Classification
DRAB1	Sandy SILT, some clay
TV1	SILT, some clay, minor sand
TV2	SILT, some clay, minor sand

6.3 XRD Results

The results of the X-ray diffraction analysis for these materials allowed for the determination of clay minerals within the sample, in addition to the main minerals present overall. Both clay and bulk analyses were completed. XRD results are interpreted through the identification of the main peaks produced throughout the runs, which are then correlated to the basal spacing of the clay minerals within the sample (Whitton & Churchman, 1987).

6.3.1 Bulk sample analysis

The results from the dried bulk samples (**Figure 6.1**) determined the main minerals within each sample (**Table 6.4**). The presence of these particular minerals were determined by the location, intensity, and morphology of the peaks observed. Crystalline materials can be identified by sharp, narrow peaks upon the graph (Kuman, 2019). The identification of clay minerals is more challenging than more crystalline structures, as clays generally are characterised by broad diffraction patterns (Whitton & Churchman, 1987).

DRAB1 (**Figure 6.1**) shows a distinctive peak at ~10.1 °2Theta (~7.3 Å) (identified by black circle on graph), indicating the presence of potential hydrated halloysite. The lack of any significant peak at ~7 °2Theta indicates a potential absence of dehydrated halloysite, or kaolinite clays (Sachan & Penumadu, 2007). A series of peaks between ~20 and 32 °2Theta (indicated by green circle on graph) is indicative of the defined crystalline elements, including quartz, plagioclase feldspar, augite, mica and some cristobalite. The high intensity peak at 20 °2Theta indicates the presence of quartz. The apparent triple peak at moderate intensity identified at ~25 °2Theta is indicative of the presence of plagioclase. The distinctive high intensity peak at 27 °2Theta, and the two smaller peaks at 31 and 32 °2Theta are indicative of either augite or micaceous minerals (Marcucci & Hynek, 2014). No distinctive high intensity trace identifying cristobalite (~23 °2Theta) could be identified. The broad peaks identified from ~35 to ~75 °2Theta (identified by red circle) are classed as ceramic minerals derived from the tile the sample was tested on, therefore are not considered in the overall mineralogy.

TV1 (**Figure 6.2**) only showed definite traces for dehydrated halloysite or kaolinite (black circle), identified by a peak at 10.1 °2Theta (~7.3 Å) (Joussein et al., 2005; Sachan & Penumadu, 2007). A series of peaks between 20 and 30 °2Theta (green circle) can be seen, and the distinctive peak at ~27 °2Theta is indicative of quartz. The peak observed at ~31 °2Theta

is indicative of either augite or micaceous minerals. The peaks observed from ~35 °2Theta onwards are again classified as ceramics from the tile tested (identified by red circle).

TV2 also showed evidence of halloysite at 10.1 °2Theta (~7.3 Å) (identified by black circle, **Figure 6.3**). TV2 also showed the strongest evidence of potential kaolinite, identified by a characteristic double peak at ~34 °2Theta (Sachan & Penumadu, 2007). Quartz was again identified, by the characteristic peak at ~ 27 °2Theta (identified by green circle). Potential mica or augite was also identified, with the double peaks at ~31 and 33 °2Theta. The ceramics were also identified, from ~32 °2Theta onwards (identified by red circle).

Table 6.4. Table summarising the differing minerals identified in each of the samples tested in this study.

Sample name	Minerals identified
DRAB1	Quartz, halloysite, augite, mica, potentially cristobalite, potentially kaolinite.
TV1	Quartz, mica, augite, halloysite, potentially kaolinite.
TV2	Quartz, mica, augite halloysite, kaolinite.

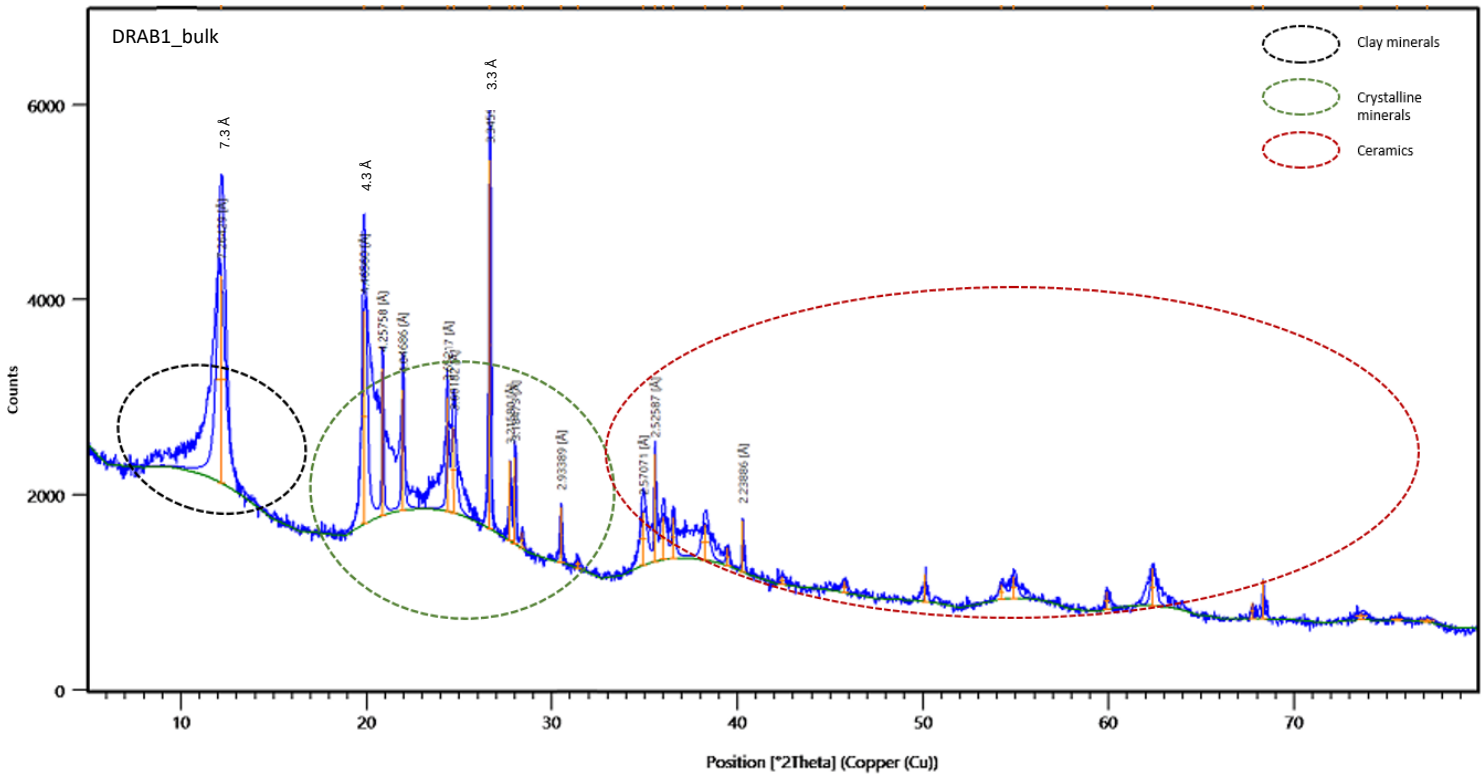

Figure 6.1. XRD bulk sample analysis for the DRAB1 sample.

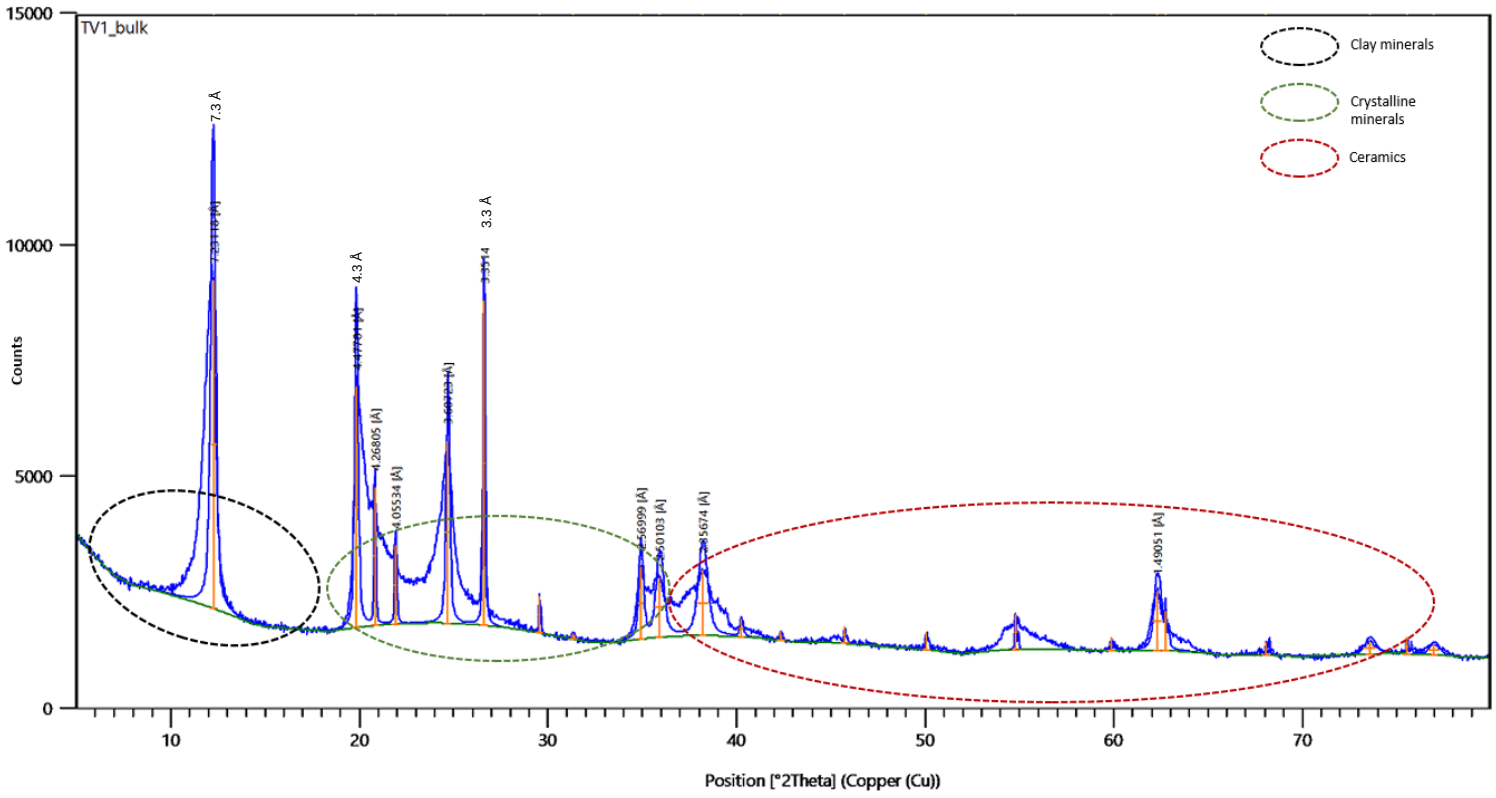

Figure 6.2. Bulk sample XRD graph produced for TV1.

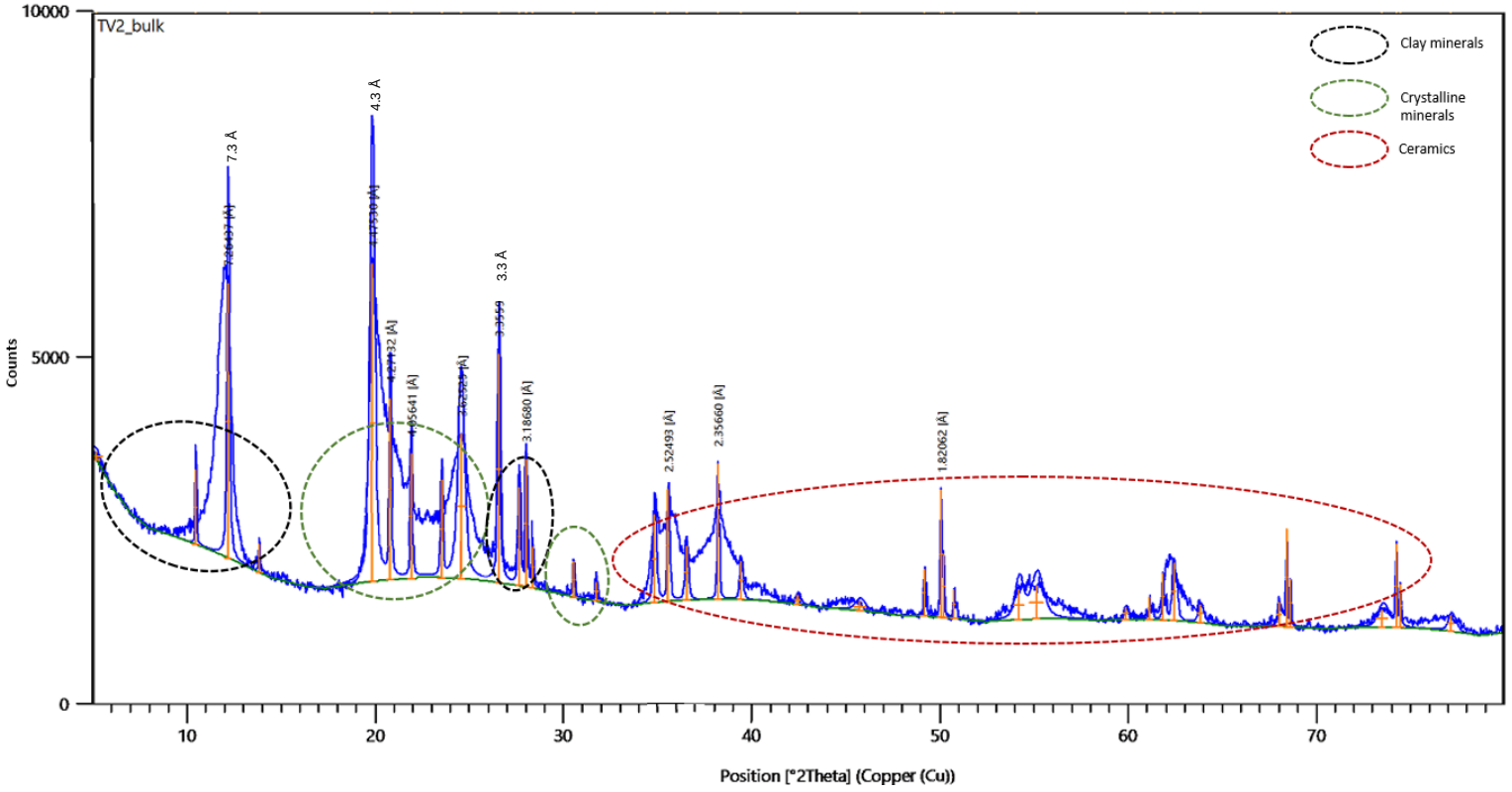

Figure 6.3. Bulk sample XRD graph produced for TV2.

6.3.2 Clay sample analysis

The clay analysis was completed over four differing runs (**Figure 6.4**). The samples were first run untreated (blue line), before being dosed with glycerol (green line), heated to 110°C (red line) before finally being heated at 550°C (pink line).

The determination of the main clay mineral was also determined. **Table 6.5** summarises the characteristic spacing of differing clay minerals, highlighting the response of halloysite and kaolinite.

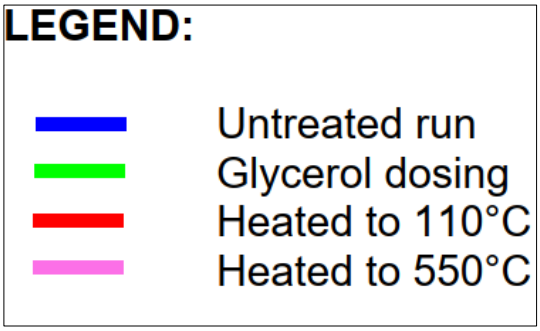

Figure 6.4. Legend summarising the four clay identification XRD runs completed upon the samples in this study (after Mills, 2016).

Table 6.5. Table showing the characteristic spacings differing minerals display in reference to each testing stage of XRD, which aids in identification. Halloysite, of interest, is outlined in red (Whitton & Churchman, 1987).

I Discrete minerals

Mineral	Mg⁺⁺–air	Mg⁺⁺–glycerol	Treatments K⁺	Heated 550°C	Formamide
(a) Mica*	10	10	10	10	–
(b) Chlorite	14	14	14	14	–
(c) Vermiculite	14–10	14	10	10	–
(d) HIV**	14	14	14	10	–
(e) Smectites	15–10	18	10	10	–
Kaolinite	7.2	7.2	7.2	No peak	7.2
Halloysite	7.2	10–11 (not all)	7.2	No peak	10.4

For DRAB1 (**Figure 6.5**), a large peak (~30,000 count) was identified for the untreated clay trace graph at 10 °2Theta (~10 Å), which then altered to a moderate peak at 8 °2Theta (~ 11 Å) for the glycerol and 110 ° C heating runs. The 10 Å peak only persisted within the untreated run before merging into one smaller peak at ~11 Å. The 10 and ~11 Å peaks completely collapsed following heating at 550 ° C. These results infer that there is a presence of hydrated halloysite within the DRAB1 samples, as identified by the 10 Å peak, which then expands to 11 Å following various treatments (Joussein et al., 2005). A smaller peak could be seen at ~7.3 Å (12° 2Theta) that was asymmetrical in nature, and persisted for the first three runs before collapsing following heating at 550 °C, indicating the presence of either dehydrated halloysite or kaolinite. Due to the similar nature of the peaks, the clay cannot be explicitly defined from these results alone.

The graph produced for TV1 (**Figure 6.6**) showed similarities to DRAB1. A large peak was again identified at 10 Å (~40,000 count, 10 °2Theta) with another moderate peak identified at ~11 Å (8 °2Theta). The 10 Å peak persisted for the first testing run, before combining to produce an intermediate peak between 10-11 Å (12 °2Theta) for the glycerol and 110°C tests, prior to collapse following heating at 550°C. This is consistent with the behaviour expected for hydrated halloysite (Joussein et al., 2005). One small peak was present at around ~7.3 Å (12° 2Theta) which only persisted within the 110 °C test, unlike DRAB1. This provides evidence of dehydrated halloysite or kaolinite (Joussein et al., 2005).

For TV2 (**Figure 6.7**), the peaks identified at ~10 and ~11 Å (8-10 °2Theta) were extremely significant (over 40,000 count). The 10 Å peak persisted for the untreated run only, before collapsing to combine with the 11 Å peak. The 11 Å peak persisted for the glycerol and 110°C runs, before collapsing following the 550°C heating run. This again indicates strongly the presence of hydrated halloysite within the sample. A very small peak was identified at ~7.3 Å (12° 2Theta) which only persisted for the 110°C run, but did not react strongly to other any other testing runs. This is consistent with the trend observed for TV1, and is indicative of either dehydrated halloysite or kaolinite (Joussein et al., 2005).

An extended series of peaks was identified between ~4 Å and ~2.6 Å (~20 - ~27° 2Theta). The higher peaks persisted for all four runs, whilst the lower peaks persisted for the glycerol and 110°C runs but were not present for the untreated and 550°C runs. This is consistent with dehydrated kaolinite, and shows the strongest evidence of the presence of kaolinite. Additional peaks were similarly identified between ~3.2 Å and ~2.8 Å. The extremely high peak at ~2.75 Å, 25°2Theta indicates the stronger presence of quartz minerals in the TV2 sample, compared to DRAB1 and TV1. This indicates a greater concentration of fine quartz minerals (< 2 µm) beyond the background levels created by the blank sample.

The results observed are in agreement with the expected mineralogies observed in previous studies concerning volcanically-derived soil materials (Joussein et al., 2005; Kuman, 2019).

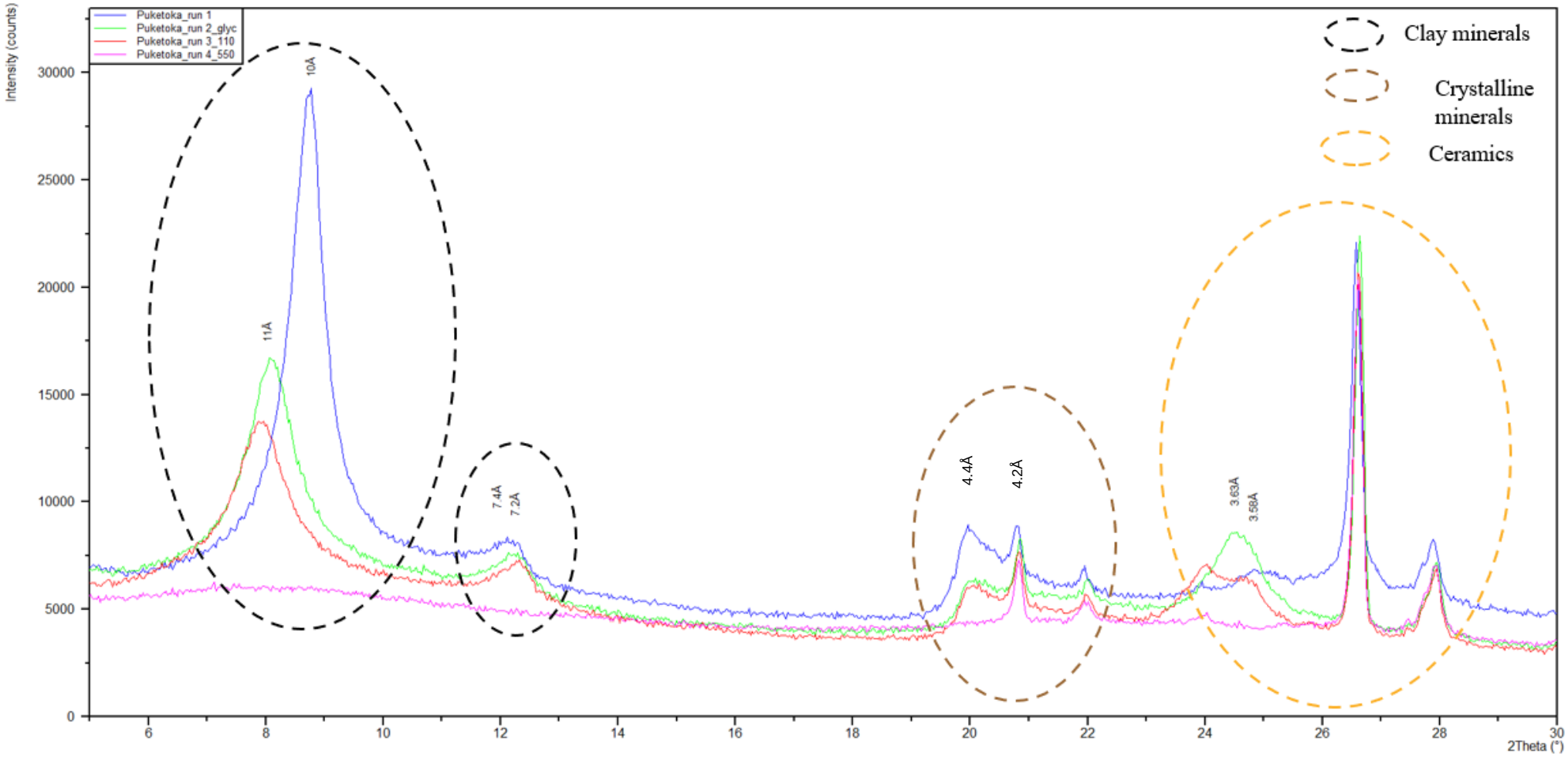

Figure 6.5. XRD trace plot determining the presence of clay minerals within the DRAB1 sample, for different treated and untreated runs.

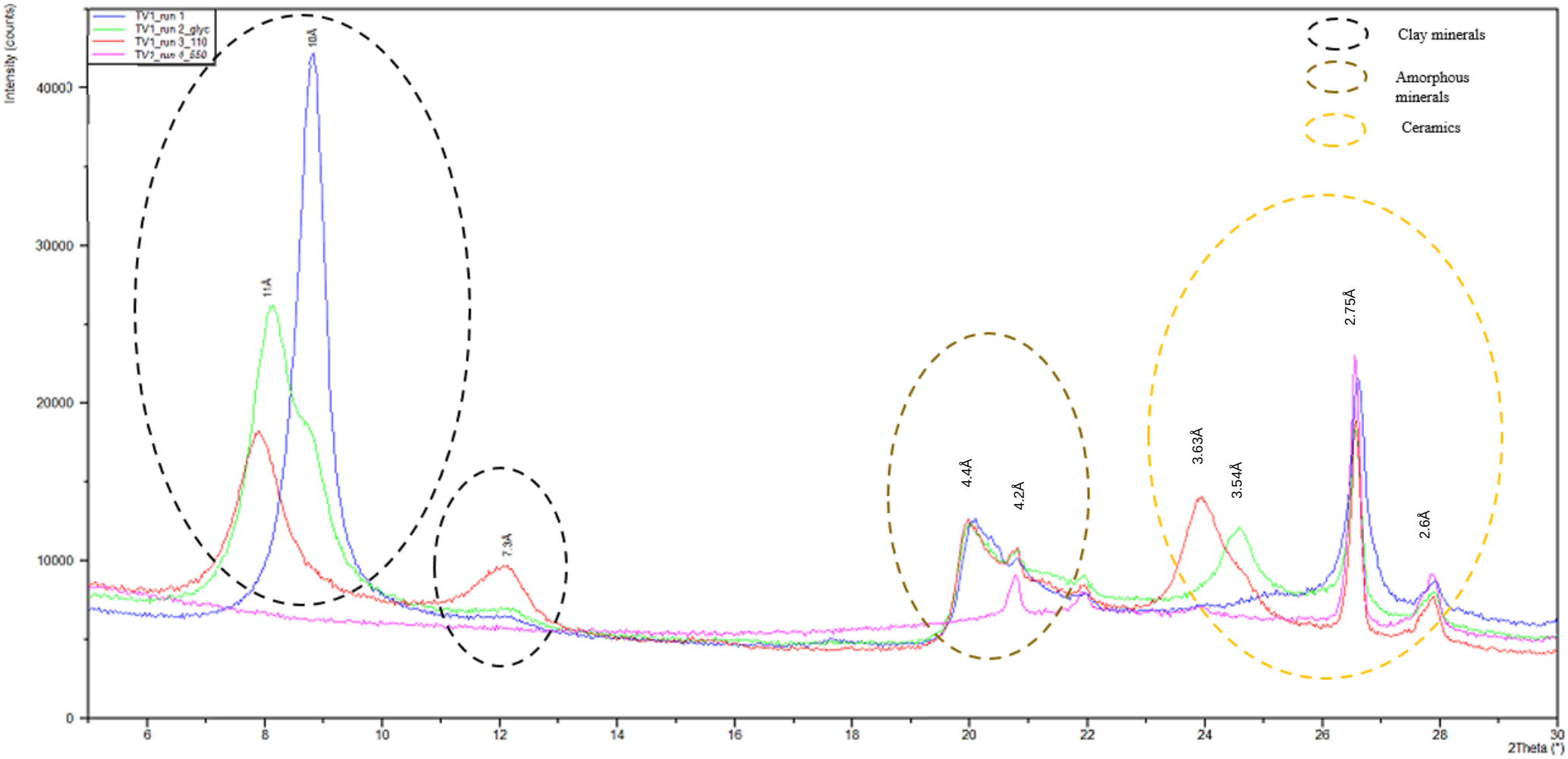

Figure 6.6. Summary XRD graph detailing the response of the TV1 material following different sampling runs.

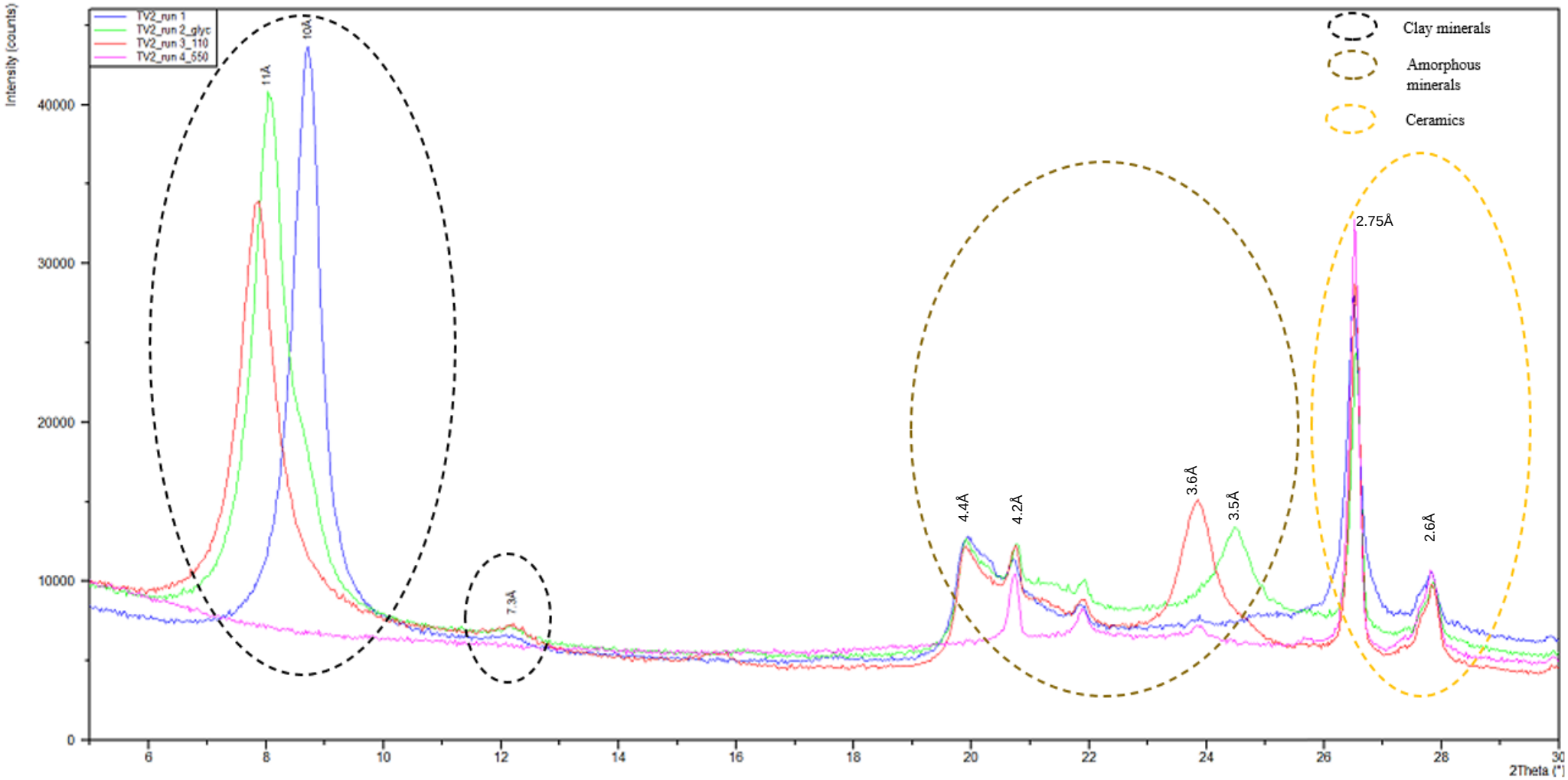

Figure 6.7. Summary XRD graph showing the TV2 material response to differing sampling runs.

6.4 Allophane identification

Due to the incredibly small nature of allophane, it is x-ray amorphous (Lowe et al., 2012). Therefore, qualitative testing was needed. The NaF test, developed by Fieldes and Perrott, was conducted for all three samples, and the results found no presence of allophane within either site after 1 minute, 3 minutes and 5 minutes of exposure to NaF (**Figure 6.8** and **6.9**).

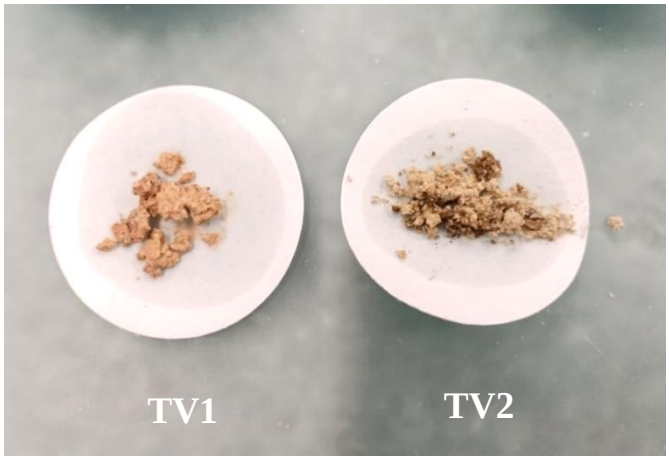

Figure 6.8. Image showing the results of the Fieldes and Perrott NaF test for allophane. The lack of pink colouration upon the paper indicates absence of allophane after 5 minutes of exposure.

Figure 6.9. Image showing the results of the Fieldes and Perrott NaF test for allophane. The lack of pink colouration upon the paper indicates absence of allophane after 5 minutes of exposure.

6.5 Activity

Activity can be classified into three critical groups: inactive, normal, and active (Selby, 1993). This activity rating can then be used to classify the behaviour of the soil. **Table 6.6** shows the critical values for classification, and **Table 6.7** summarises the calculated activity values for DRAB1, TV1 and TV2.

Table 6.6. Table showing the characteristic activity values distinguishing between clays of inactivity, normal behaviour, and activity (Selby, 1993).

Activity level	Classification term
< 0.75	Inactive
0.75 – 1.25	Normal
> 1.25	Active

Table 6.7. Table summarising the calculated activity values for the samples tested in this study.

Sample name	Calculated activity value	Activity classification
DRAB1	1.79	Active
TV1	0.81	Normal
TV2	0.60	inactive

DRAB1 was calculated to have an activity of 1.79, indicating an active clay following Selby's 1993 classification. TV1 was found to have an activity value of 0.81, placing it into the "normal" category. TV2 had a calculated activity of 0.6, placing it into the "inactive" category. **Figure 6.10** summarises these classifications into graphical form.

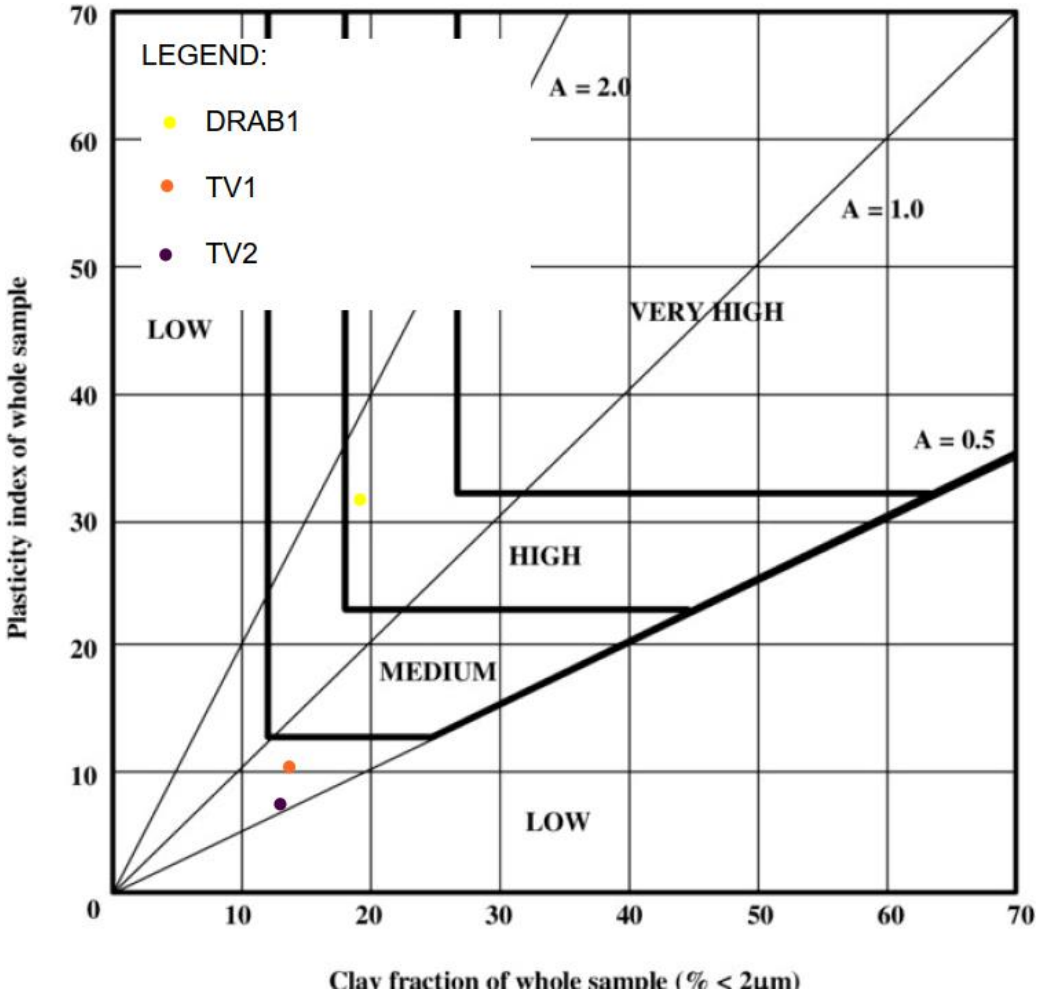

Figure 6.10. Graph summarising the classified activity levels for the tested samples, based upon the clay fraction within the soil, and the calculated plasticity index.TV1 and TV2 are classified as 'low' activity, whilst DRAB1 is classed as 'high' activity. Note that rather than "inactive", "low" activity is used (Selby, 1993; Toksoz & Yilmaz, 2019.).

6.6 Summary of chapter

The results gained from the particle sizer and X-ray diffraction tests have identified the dominant particle size within each of the samples tested to be silt-sized. Halloysite and potentially kaolinite were found to be the main clay minerals for the samples, which is consistent with what is expected of the Walton Subgroup materials, being volcanogenic derived soils. The activity of the samples were also calculated. Additional minerals found included quartz, plagioclase and potential cristobalite.

Chapter 7
Triaxial results

7.1 Introduction

This chapter summarises the results of the static triaxial test. The triaxial tests completed upon these samples were consolidated, undrained (CU) tests, and this section detail the results for stress-strain, stress path and pore water pressure plots, the post-failure characterisation of triaxial cores, and thin section analysis.

It should be noted that the triaxial tests completed for this study follow similar procedures as previously observed in Wyatt's 2009, Cunningham's 2012 and Robertson's 2017 theses, by using slower testing rates, calculated from each samples' consolidation stage results. This differs from Mill's 2016 testing procedure, where a defined shear rate was applied for all samples.

7.2 Testing conditions

The testing conditions for each triaxial stage for the six samples, in addition to the approximate amount of time each test took, are summarised in **Table 7.1**.

Table 7.1. Table summarising the effective stress calculation parameters used in this study, in addition to the calculated confining pressures, and cell and back pressures controlling each of the testing stages. The calculated shear rates and the approximate testing time in days is also included.

Sample	Depth in profile (m)	Estimated force of overlying soil (kN/m^3)	Water table depth (m)	*In situ* effective stress (kPa)	Confining pressure values used (kPa)	Saturation	B-check	Consolidation	Shear rate (mm/hr)	Approximate testing time (days)
						Cell/back pressure	Cell/back pressure	Cell/back pressure		
					100	670/660	720/705	860/760	0.0044	5
DRAB1	~10	18	~0.2	177	170	700/690	750/732	950/780	0.0029	7
					270	700/690	750/736	980/710	0.0039	6
TV1	~5-8	12	~1.2	73	130	650/640	780/660	800/670	0.0025	8
					170	750/740	800/780	950/780	0.0118	4
					230	750/740	800/787	990/760	0.0537	3

7.3 Consolidated undrained triaxial test response

Dependent upon the particle componentry of the material, differing methods of failure can be expected. Dense, hard and over-consolidated soils tend to show a brittle type of failure, which is characteristically seen as the stress-strain curve reaching its' peak stress value at less than 5% total strain (Boulanger & Idriss, 2006).

Because the samples in this study are clay and silt dominated, they are expected to behave as soft or loose soils, therefore are expected to exhibit ductile failure behaviours (Briaud, 2013). This means that the peak deviator stress is generally reached at a value range of between 15-20%, with the pore water pressure gradually increasing prior to failure, subsequently reducing the effective stresses within the sample, leading to failure. Some of the graphs produced were incorrect due to loading errors during testing. Additionally, incorrect responses observed on the p'q' plots for the samples were also included. These graphs can be observed in **Appendix 7.3**.

7.3.1 Deviator Stress response

The deviator stress versus axial strain graphs produced (**Figure 7.1**) for DRAB1 and TV1 samples generally show a similar trend of an initial rise in deviator stresses as the strain percentage increases, before reaching a peak deviator stress value, and subsequently decreasing as strain percentage increases. Both the DRAB1 and TV1 samples show the same trend of the initial increase rising to reach a peak value, before subsequently decreasing as strain percentage increases.

DRAB1 tended to show a more defined drop in deviator stress following the peak value, identified by a drop in the graph line following the identified peak between ~5 and 8 %. It should be noted however that the 270 kPa test only reached a strain of around 14.8 % before the triaxial apparatus malfunctioned and no longer recorded readings. This will have an influence on the trends seen and should be considered when analysing the graph.

TV1 shows a greater plateau in the measured deviator stress following the identified peak, before eventually beginning to drop between ~13 and ~18.5 %. The peak deviator stress values (**Table 7.2**) experienced during each test tended to increase as the confining pressures increased, with the exception of the DRAB1 170 kPa test. The deviator stress values measured

for the soils in this study are generally in keeping with results gained from previous studies (**Table 7.2**).

The pore water pressure response was generally consistent with the deviator stress responses, increasing as the confining pressure increased (**Table 7.2**). The DRAB1 270 kPa test did not reach completion however, therefore the pore water pressure does not match the increasing trend observed for the rest of the samples as a result. The pore water pressure values observed at failure for the samples of this study are appreciably higher compared with the Tauranga soils (**Table 7.2**).

The percentage of strain at failure varied between the two samples. DRAB1 experienced strain at failure between ~1.8 and ~6.5% (**Table 7.2**), whilst TV1 was comparatively higher, between ~4.8 and ~16.3%. Whilst the values tended to increase as the DRAB1 confining pressures became higher, TV1 fluctuated, with the highest value being gained from the 170 kPa test. The values for DRAB1 are in keeping with previous studies (**Table 7.2**), but TV1 generally shows appreciable differences compared with the Tauranga soils, with the exception of tests completed by Wyatt (2009) (**Table 7.2**).

Table 7.2. Table summarising the shear stage failure results gained for the samples of this study.

Sample name and confining pressure (σ_3)	Percentage axial strain at failure (%)	Pore water pressure at failure (kPa)	Peak deviator stress (σ_1 - σ_3) (kPa)
DRAB1 – 100 kPa	1.81	795.2	129
DRAB1 – 170 kPa	2.44	865	122
DRAB1 – 270 kPa	6.51	855.1	277
TV1 – 130 kPa	4.82	717.2	145
TV1 – 170 kPa	16.35	862	164
TV1 – 230 kPa	10.35	879.7	233
Wyatt, 2009 – 20 – 300 kPa	1.7 – 20.1	-	64 - 368
Cunningham, 2012 – 100 – 300 kPa	1 - 9	-	105 - 268
Mills, 2016 - 75-355 kPa	1.9 – 3.5	27 - 462	131 - 383
Robertson, 2017 – 205 – 355 kPa	0.78 – 1.63	50 - 195	151 - 313

- = Not measured in this study

7.3.2 Pore water pressure response

The change in pore water pressure in relation to axial strain percentage for DRAB1 and TV1 is summarised in **Figure 7.2**. Generally, a positive increase in pore water pressure was experienced by both DRAB1 and TV1 the samples. Due to loading issues with the triaxial apparatus, the tests can be seen to start between 1 and 2 % strain, rather than zero. Again, it should be noted that due to the strain reading error for the DRAB1 270 kPa test likely influenced the results displayed on the graph.

7.3.3 Stress path responses

7.3.3.1 DRAB1

The p' q' plots produced for DRAB1 (**Figure 7.3**) indicates that generally, all three samples experienced initial dilation as the deviator stress increased during shear. This dilation is then followed by a contractive response prior to the yield point. The graphs then show a contractive response following the yield value being reached, identified by a left-hand tracking of the graph (**Figure 7.3**). Generally, up to the yield value, the pore water pressure increased at the same rate, as identified by the relatively straight upwards tracking of the line prior to the yield value being reached. The samples all track above the critical state line before correcting (identified by red circles on graph), a characteristic consistent with sensitive soils.

7.3.3.2 TV1

The p' q' plots produced also reflect the failure modes for TV1 (**Figure 7.4**). The 130 and 170 kPa tests for TV1 show an initial contractive response prior to the yield point, where pore water pressure is increasing at a faster rate than the applied stress. Following the yield value being reached, the 130 kPa sample follows the critical state line. The 170 kPa test appears to go beyond the critical state line and appears to begin experiencing strain softening but does not complete a full loop to follow the critical state line. The 230 kPa test appears to show a path consistent with a total stress path, where pore water pressure increases at the same rate as the applied stress, similar to that of the DRAB1 130 and 170 kPa tests. Upon reaching the critical state line, the sample appeared to go past this point to the yield limit, before strain

softening back to the critical state line, resulting in the characteristic loop being seen (black circle).

Generally, all of the samples show a total stress to contractive response to stress. In particular, the TV1 230 kPa test shows a response characteristic of a sensitive soil, where a strain softening loop brings the sample behaviour back to the critical state line following the path to the yield point.

The max deviator stresses experienced for DRAB1 were between 128 and 276 kPa, and TV1 between 144 and 233 kPa (**Table 7.2**). These values are comparative to the results gained by Mill's (2016) (131-383 kPa) and Robertson's 2017 studies (151-313 kPa), likely due to the similar confining pressures used. The deviator stresses increased with the confining pressure values.

7.4 Effective strength

Effective strength, consisting of effective friction angle and effective cohesion, were also calculated for the samples (**Table 7.3**). The Mohr circles can be seen in **Appendix 7.1**.

The peak effective values differed between DRAB1 and TV1. DRAB1 had a low effective friction angle (27°), but high effective cohesion (37 kPa). TV1 conversely had a moderate effective friction angle (38°), but no effective cohesion (0 kPa) (**Table 7.3**). The total shear strength values calculated for this study can also be observed in **Appendix 7.1.**

Table 7.3. Table summarising the effective cohesion and friction angles calculated for the samples of this study.

	Effective shear strength	
	Cohesion, C' (kPa)	Friction angle, Ø' (°)
DRAB1	37	27
TV1	0	38

Comparison of the effective shear strength values of this study with other studies completed upon Tauranga sensitive soils (**Table 7.4**) shows that the values are generally in keeping with the values expected for volcanically-derived soil materials containing halloysite.

Table 7.4. Table summarising the peak effective cohesion and friction angle results gained from a number of New Zealand based studies undertaken upon halloysite-rich soils (2.s.f.).

Study	Location	Peak c' (kPa)*	Peak φ′ (°)
This study, 2021	Hamilton, NZ	0-37	27-38
Jacquet, 1990	New Zealand	55-60	2-8.5
Keam, 2008	Bay of Plenty, NZ	0-43	50-56
Wyatt, 2009	Bay of Plenty, NZ	11.8-24	27.3-31.1
Arthurs, 2010	Bay of Plenty, NZ	0-70	25-37
Mills, 2016	Bay of Plenty, NZ	17-26	31-32
Robertson, 2017	Bay of Plenty, NZ	26.6	19.3

* effective cohesion values in kPa; kN/m3 is equivalent value.

7.5 Estimated permeability

The coefficient of permeability could be estimated from the triaxial consolidation. The calculation used serves as an indirect method of calculation, based upon principles linking the coefficient of consolidation and the coefficient of compressibility, and the variance and errors in the calculations is high, therefore the values should be used as an indicative estimate only.

Table 7.5 summarises the results. The samples of this study are generally lower than previously published values (Moon, 2013 = 10^{-8} – 10^{-9}, this study = 10^{-10}), with the exception of TV1 130 and 230 kPa. The calculations completed to gain these values can be observed in **Appendix 7.2**.

Table 7.5. Table summarising the estimated coefficient of permeability (kz) values for the samples tested in this study, in addition to previously published values (Moon, 2013).

Sample	Confining pressure (kPa)	Calculated coefficient of permeability k_z (m/s)
DRAB1	100	10^{-10}
	170	10^{-10}
	270	10^{-10}
TV1	130	10^{-9}
	170	10^{-10}
	230	10^{-9}
Moon (2013)	-	In the order of 10^{-8} – 10^{-9}

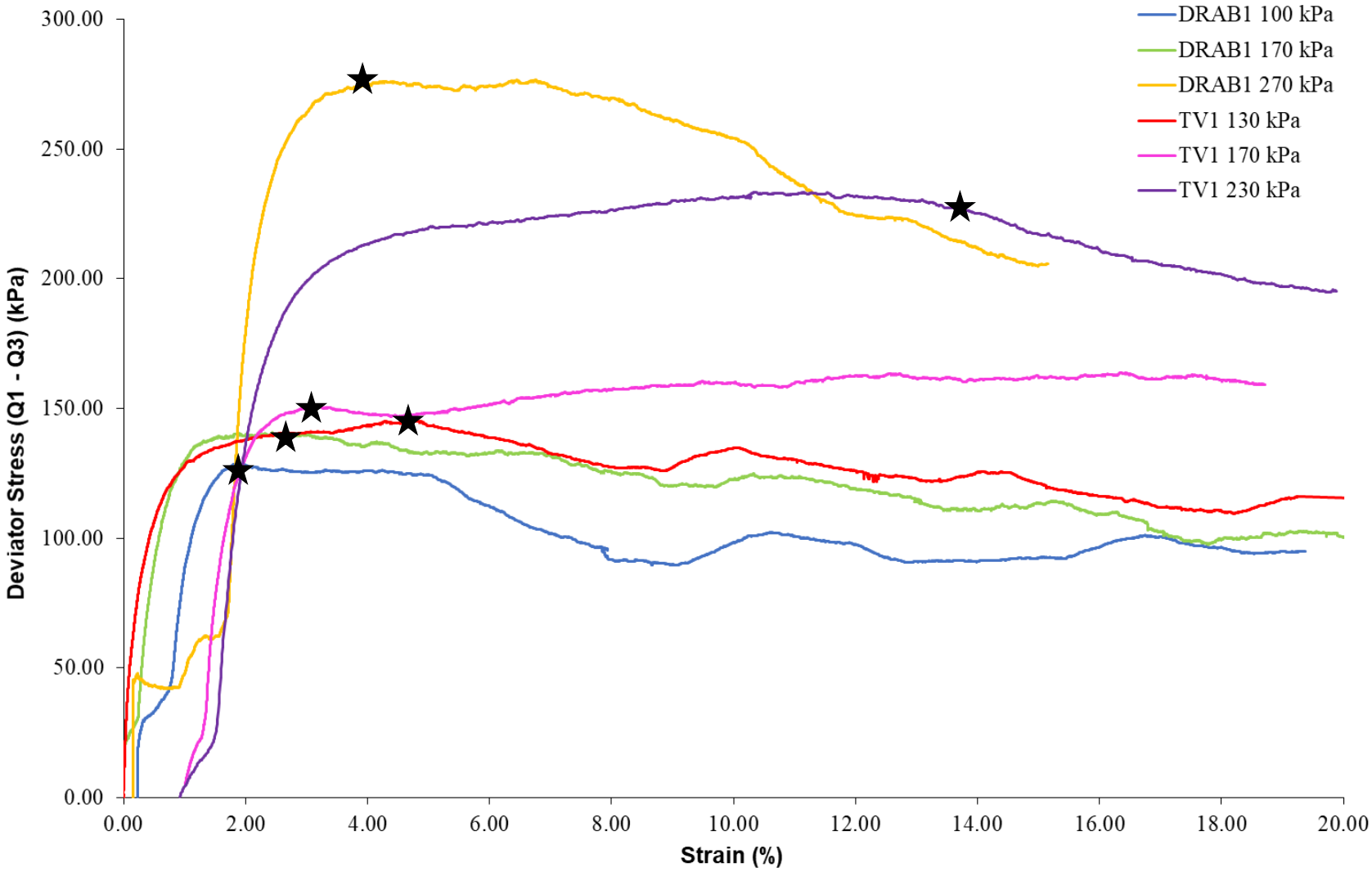

Figure 7.1. Graph summarising the deviator stress response to changing axial strain, for DRAB1 and TV1 failed cores at differing confining pressures. Black stars indicate the identified peak values for each confining pressure.

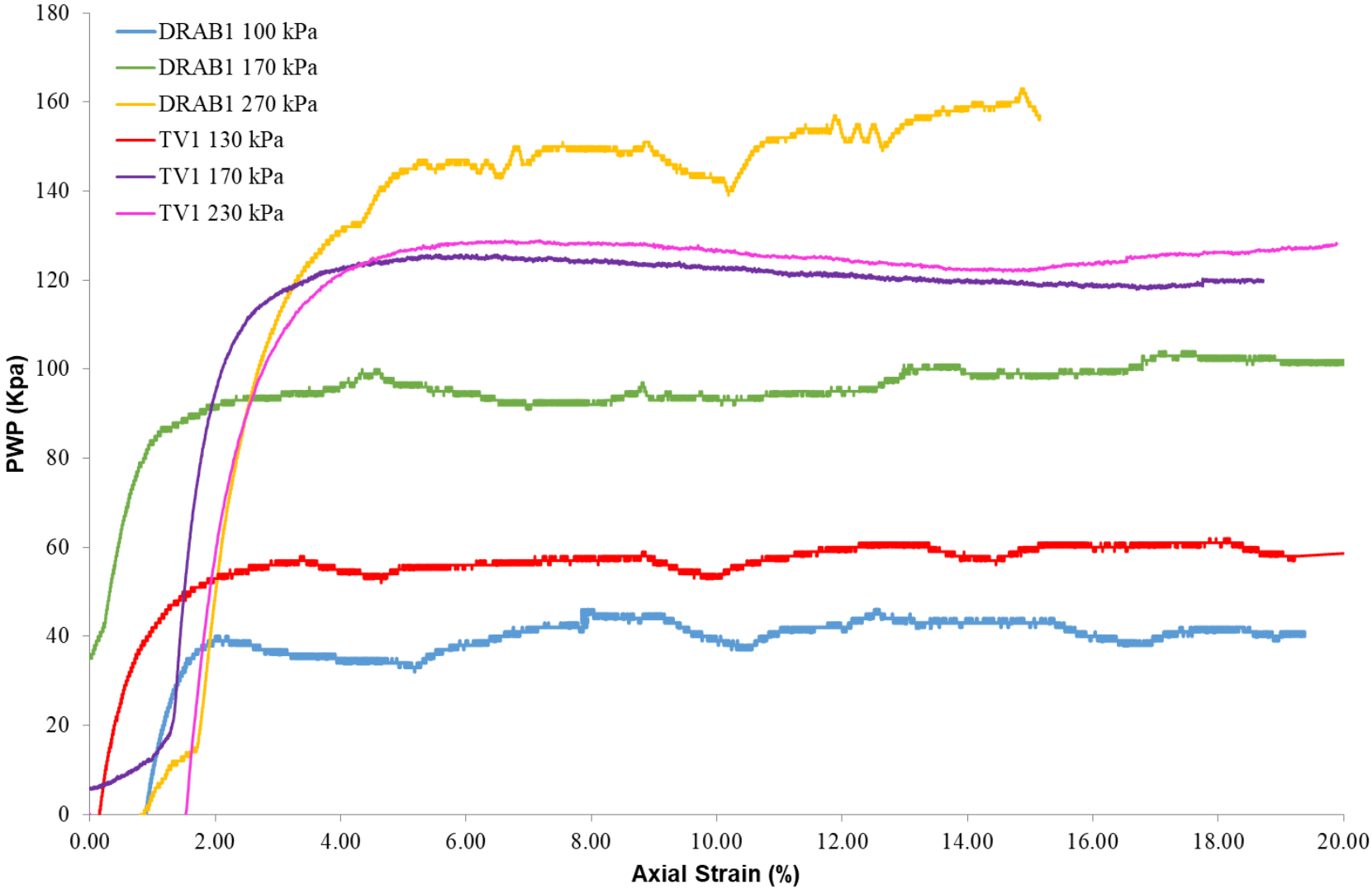

Figure 7.2. Graph summarising the pore water pressure (PWP) response to changing axial strain for DRAB1 and TV1 cores at differing confining pressures.

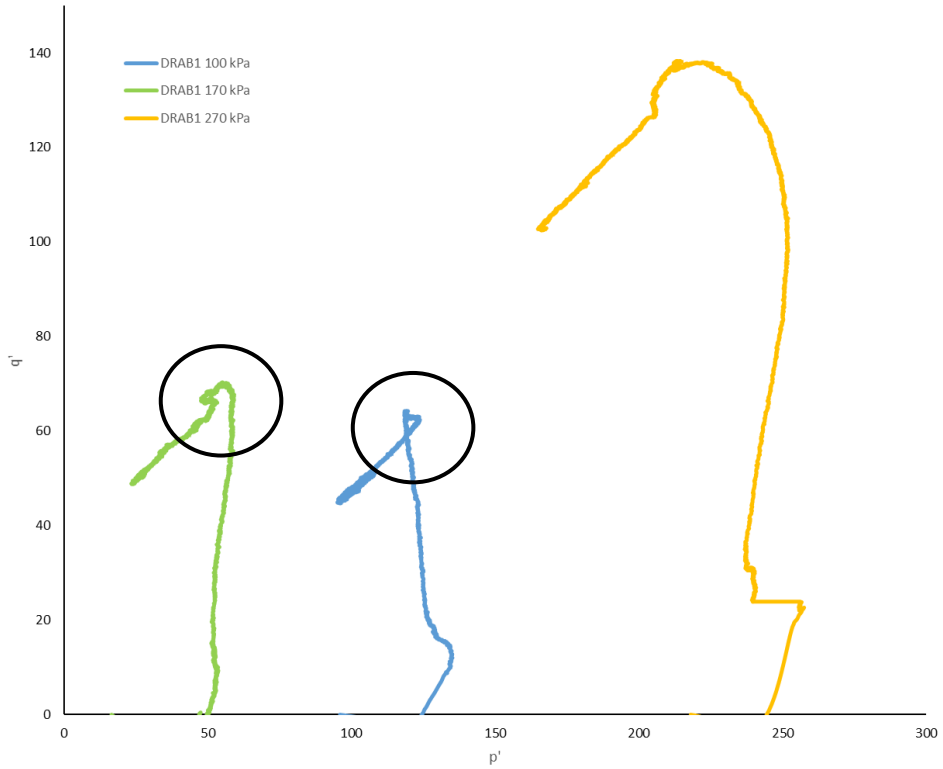

Figure 7.3. Graph summarising the p' versus q' response for DRAB1 failed triaxial cores, at differing confining pressures. Black circles indicate the correction made by the materials, after travelling above the critical state line.

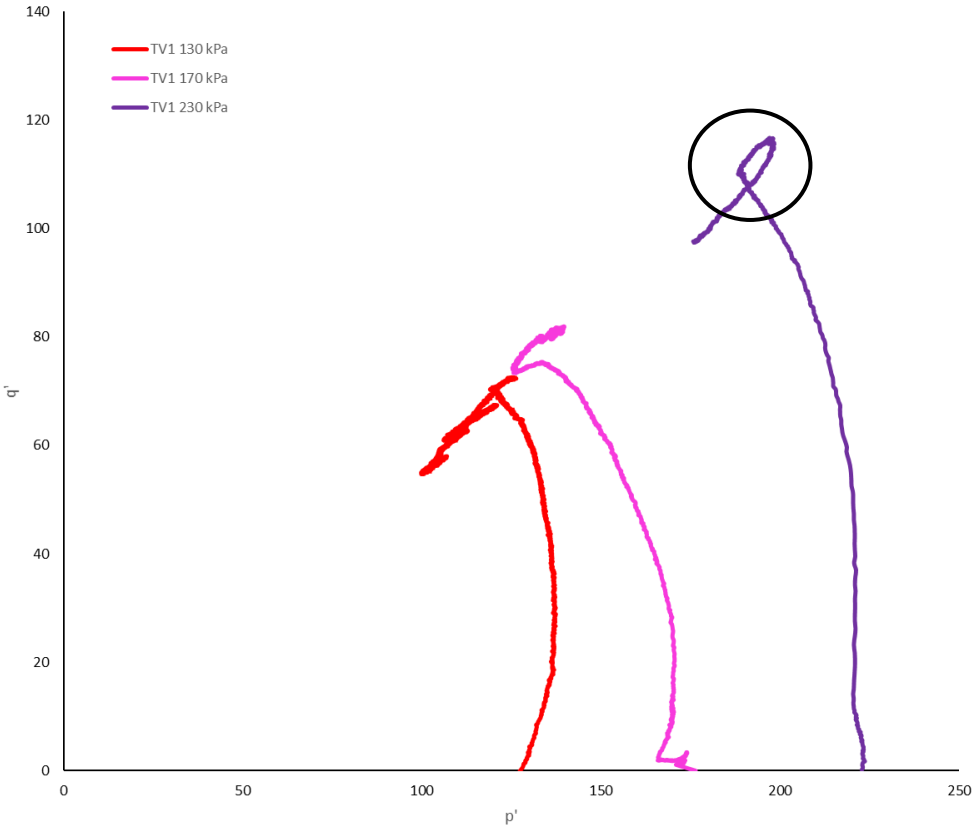

Figure 7.4. Graph summarising the p' vs q' response of the TV1 triaxial cores at differing confining pressures. The black circle indicates the correction of the material following travel above the critical state line to the yield point.

7.6 Failed triaxial core appearance

Following triaxial testing, failed cores were removed, sketched, and photographed. The way in which the sample failed is potentially indicative of the main forms of deformation that lead to sensitive soil failure events (Selby, 1993; Mills, 2016). The PSZ, SSZ, minor shears and surface deformations were also denoted upon the sketched cores. Two planes, the left and right of the failed soil cores, defined as plane 1 (left side of the core) and plane 4 (right side of the core) are used for analysis in this study. A legend denoting these zones and colours used in this study is summarised in **Figure 7.5**.

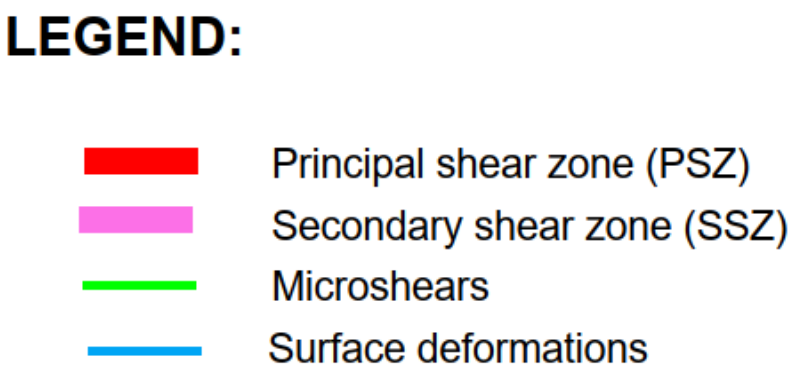

Figure 7.5. Legend denoting the colours used for characterising the principal shear zones (PSZs), secondary shear zones (SSZs), microshears, and surface deformations (after Mills, 2016).

7.6.1. Dixon Road Roundabout (DRAB1)

DRAB1 cores produced characteristic failures at different confining pressures. Shear band development (**chapter 2**) was observed for 100, 170 kPa and 270 kPa tests.

7.6.1.1 100kPa confining pressure

Figure 7.6 shows shear band formations in the DRAB1 100 kPa core. A distinct PSZ can be seen propagating diagonally across the sample, evidenced by the external physical deformation of the sample and the large "crack" occurring at the top right (plane 1) and left (plane 4) of the core. Microshears are observed running laterally across the middle of the failure zone in plane 1. Surface cracks and deformations on the lower left of the core (plane 1, identified by green lines) potentially indicate formation of secondary shear zones (SSZs). Plane 4 shows a more discrete PSZ propagation across the sample. Surface deformations can be seen upon the failure zone in both planes 1 and 4, and "bunching" of material to accommodate downward movements through the lateral movement of the material. A zone at the base of the sample shows deformation and bulging, potentially indicative of the formation of a secondary shear zone. Manganese streaking can also be seen within the failure zone of plane 1.

7.6.1.2 170kPa confining pressure

Figure 7.7 again shows a shear band formation can be observed propagating diagonally across the sample in a similar manner to the 100 kPa core. Material cracking can be observed upon the upper portion of the sample (planes 1 and 4). Deformation of the iron bands within the failure zone running diagonally across the sample in planes 1 and 4 are also indicative of the movement of material to accommodate the deformation. Microshears spread laterally within the PSZ in plane 1 indicate a potential relief of stress following core failure. An SSZ could potentially be forming beneath the PSZ (plane 1). This can similarly be seen on plane 4. Manganese streaking can be observed below the PSZ for both planes, although it is more predominant on plane 4. Multiple surface deformations can be observed, likely occurring from loading and unloading of the sample.

7.6.1.3 270 kPa confining pressure

Figure 7.8 displayed a very pronounced shear band formation which is observed propagating diagonally across the sample. A significant downward movement can be observed of displaced material. Microshears propagate across the length of the PSZ indicating an

extensive failure zone and need for lateral stress release. Bulging above the PSZ could indicate the formation of an SSZ (plane 1). Plane 4 shows similar characteristics, however bulging occurs upon the more deformed portion of the core in this case. Surface deformations can be observed at the base (plane 1) and top of the samples (plane 4) but due to their distance from the PSZ and potential SSZ, were isolated minor surface deformations.

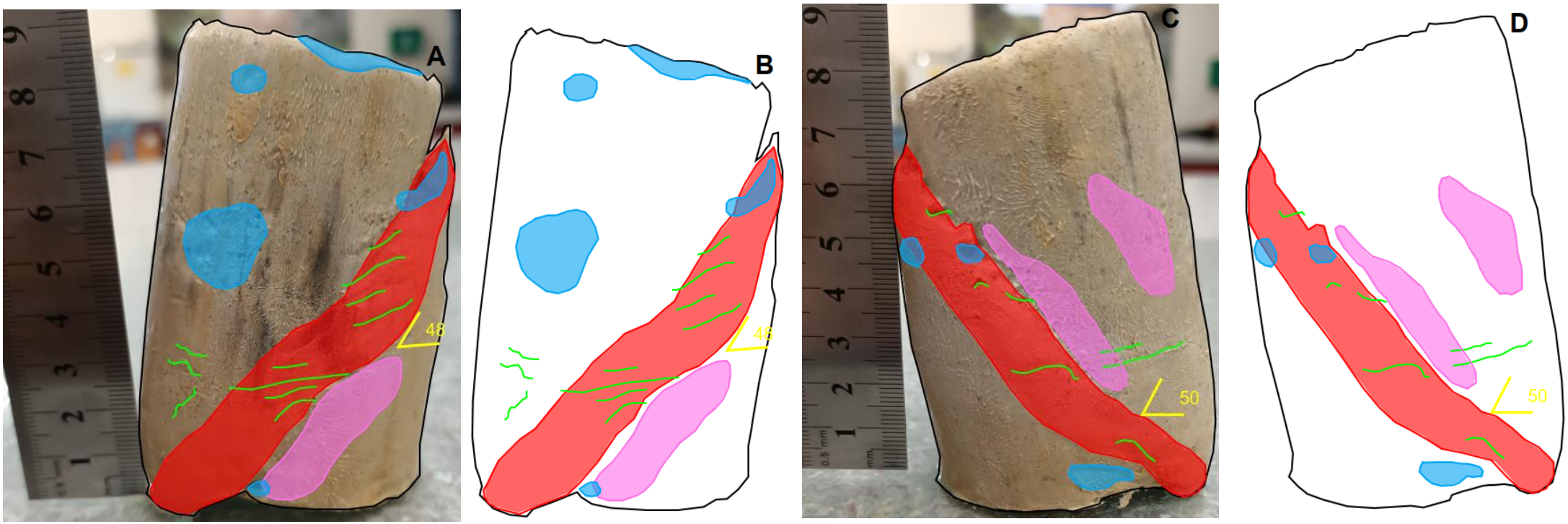

Figure 7.6. Annotated images of plane 1, overlain on an image of the soil core (**A**) and blank (**B**) and plane 4 (**C**) and (**D**), of the failed DRAB1 triaxial core, at 100 kPa confining pressure.

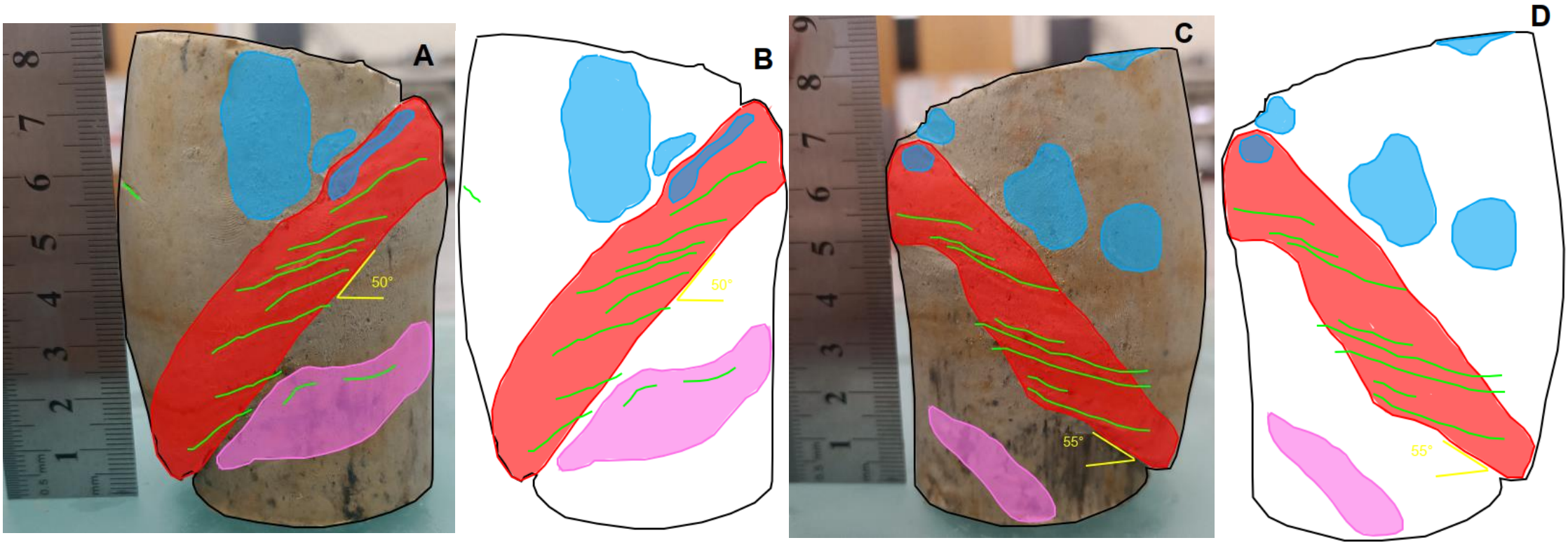

Figure 7.7. Annotated images of plane 1, overlain on an image of the soil core (**A**) and blank (**B**), and plane 4 (**C**) and (**D**), of the failed DRAB1 triaxial core, at 170 kPa confining pressure.

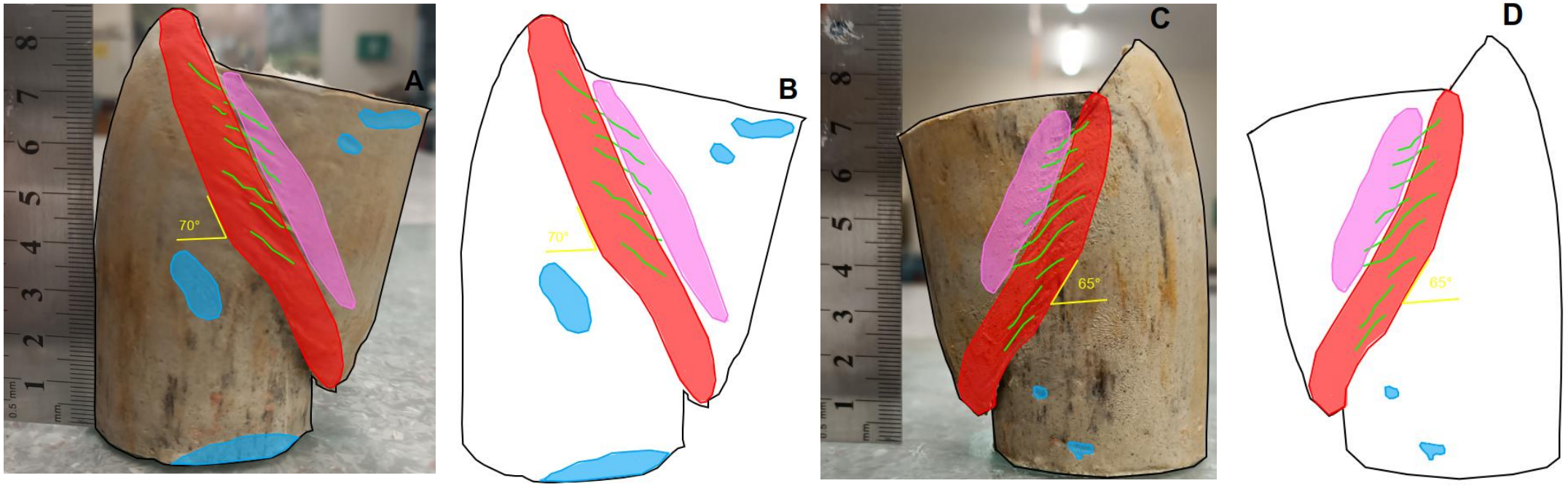

Figure 7.8. Annotated images of plane 1, overlain on an image of the soil core (**A**) and blank (**B**), and plane 4 (**C**) and (**D**), of the failed DRAB1 triaxial core, at 270 kPa confining pressure.

7.6.2 Temple View

The Temple View cores generally produced a combination of intermediate failure types with immature shear band formation, and overall intermediate failures. Manganese concentrations were again observed to occur in proximity to zones of failure.

7.6.2.1 130 kPa confining pressure

An intermediate to immature shear band formation was observed (**Figure 7.9**) on the TV1 130 kPa core. A small discontinuous PSZ was identified propagating diagonally across the sample with a small lateral PSZ propagating across the top of the sample (plane 1) aiding in the formation of the barrel failure. Microshears were identified within the zone of failure with a crack propagating laterally across the PSZ. This could indicate the formation of an SSZ (plane 1). Plane 4 doesn't show this trend with quite the same intensity. Manganese nodules concentrate at the shear band portion of failure. These are indicated by the black circles upon figure 6.7. These nodules are less prominent on plane 4.

7.6.2.2 170 kPa confining pressure

Again, an intermediate formation could be observed (**Figure 7.10**). As a result no distinctive PSZ can be identified, rather generalized areas of deformed material. No distinctive large scale shears could be observed moving across the samples. The upper part of the sample is hypothesised to be the PSZ due to the presence of microshears laterally across the sample, observed in the upper portions of both planes 1 and 4, in addition to deformation zones, indicative of contraction following failure. Additional lateral microshears below the lateral PSZ could potentially indicate the formation of an additional zone of SSZ failure. A similar trend can be observed on planes 1 and 4, with plane 1 being slightly more pronounced. Iron streaking can be observed propagating vertically through the zones of failure within plane 4. This is not observed in plane 1.

7.6.2.3 230 kPa confining pressure

Figure 7.11 shows an intermediate to immature shear band formation in a similar manner to the 130 kPa core. General zones of deformation and weakness are again identified as a result. A PSZ and SSZ feature can be identified within the middle of the sample, propagating laterally on plane 1 and diagonally on plane 4. Microshears were observed within these zones of failure. A number of surface deformations can be seen upon the core (plane 1) as a result of “bunching” of material following failure, in order to accommodate for deformation of material. Plane 4 shows the intermediate formation in more detail, with more microshears within the PSZ. A secondary SSZ can also be identified with more clarity upon plane 4. Manganese nodules can also be identified within the hypothesised SSZ upon plane 4 but is noticeably absent in plane 1.

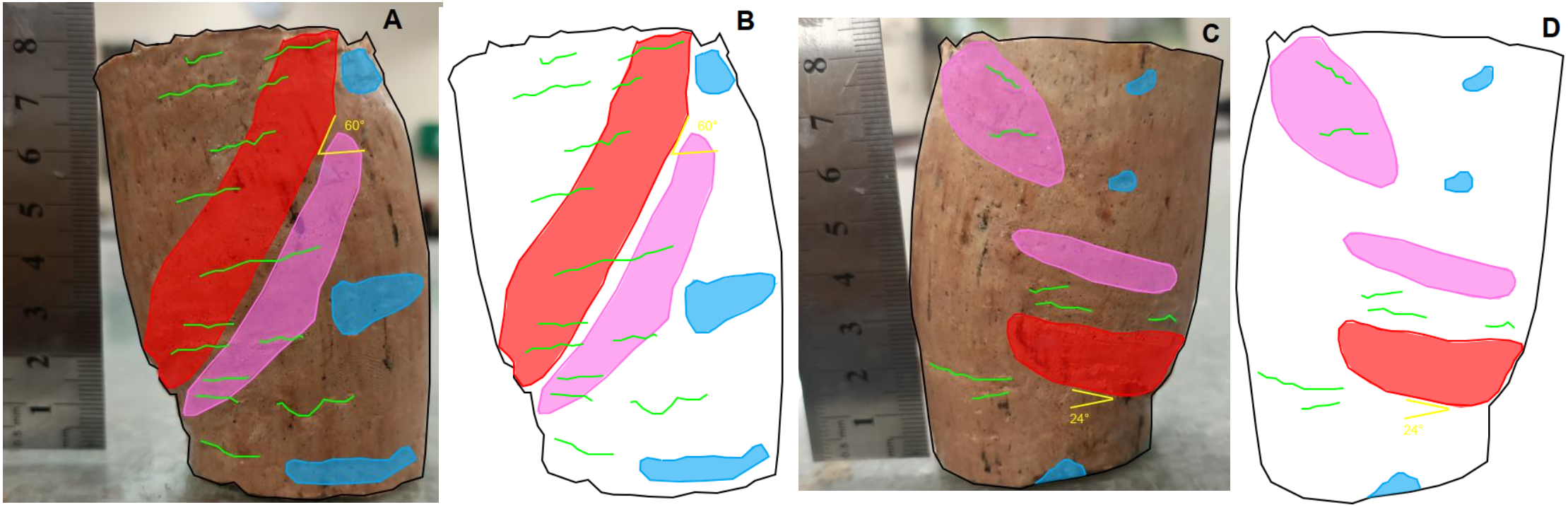

Figure 7.9. Annotated images of plane 1, overlain on an image of the soil core (**A**) and blank (**B**), and plane 4 (**C**) and (**D**), of the failed TV1 triaxial core, at 130 kPa confining pressure.

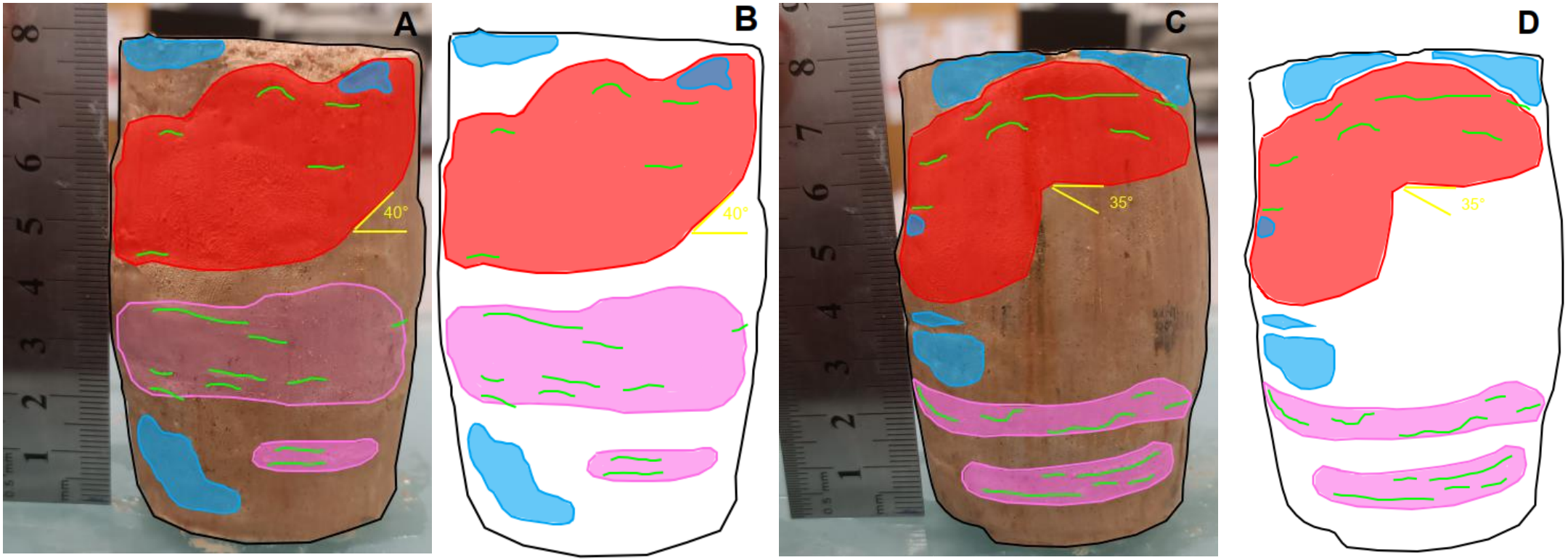

Figure 7.10. Annotated images of plane 1, overlain on an image of the soil core (**A**) and blank (**B**), and plane 4 (**C**) and (**D**), of the failed TV1 triaxial core, at 170 kPa confining pressure.

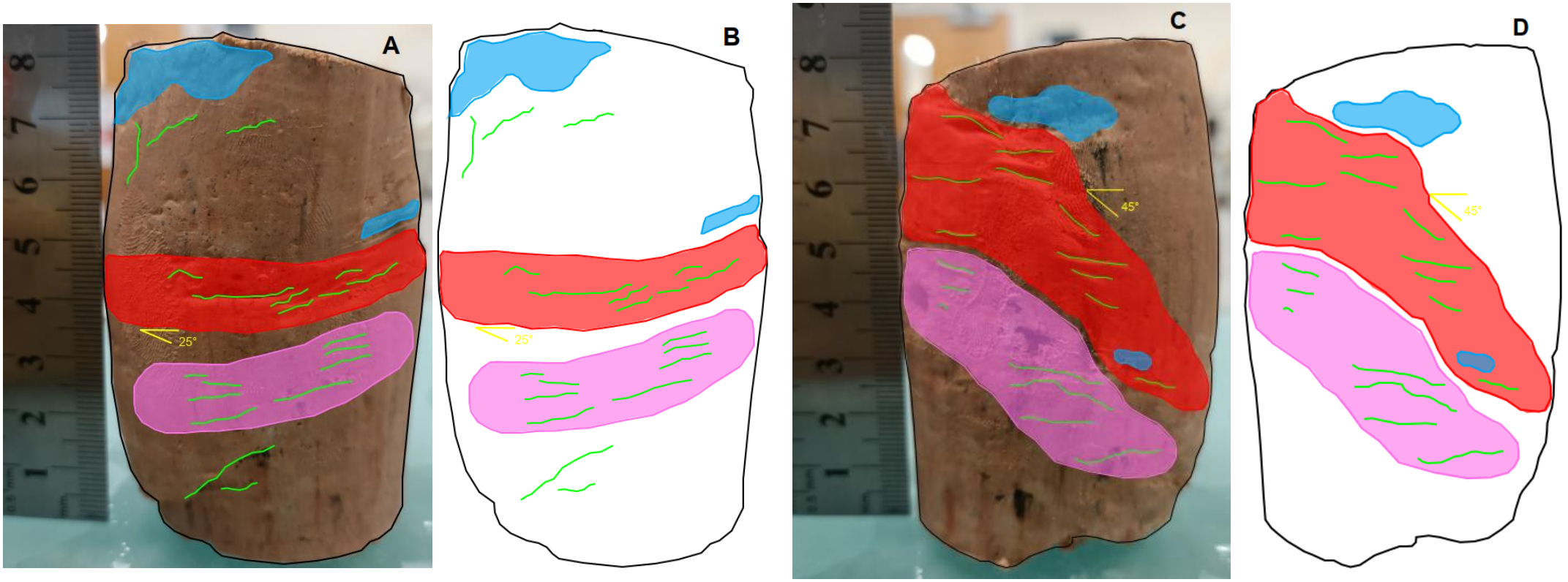

Figure 7.11. Annotated images of plane 1, overlain on an image of the soil core (**A**) and blank (**B**), and plane 4 (**C**) and (**D**), of the failed TV1 triaxial core, at 230 kPa confining pressure.

7.7 Thin section analysis

Thin sections were attempted for the failed triaxial core materials using a number of methods. The full process is detailed in **Appendix 3.1.4.** In the end, DRAB1 produced a 270 kPa thin section, and TV1 produced 130 and 230 kPa thin sections. Images can be observed in **Appendix 7.4.**

7.7.1 Mineral abundances

The thin sections (**Appendix 7.3**) were analysed and the visual relative mineral abundances of the samples quantified (**Table 7.6** and **7.7**). The samples were ~60-70 % matrix, and ~20-25 % grains that were generally silt-sized. Varying proportions of cristobalite, augite, hematite, magnetite and lithics were also observed.

Table 7.6. Table summarising the mineralogy of the DRAB1 270 kPa thin section.

Sample name	Mineral type	Relative abundance (%)	Shape	Size (mm)
DRAB1	Clay-sized material	73	-	Less than 0.002
	Silt-sized material	20	-	0.002-0.06
	Lithics	Rare	Sub-angular	1.4
	Cristobalite	5	Angular to sub-angular	0.2-0.6
	Magnetite	1	Sub-angular to subrounded	0.2-0.35
	Augite	Rare	Sub-angular	0.2
	Hematite	1	Sub-angular	0.08-1.8

Table 7.7. Table summarising the mineralogy of the TV1 thin sections, at 130 and 230 kPa confining pressures.

Sample name	Mineral type	Relative abundance (%)	Shape	Size (mm)
	Clay-sized material	65	-	Less than 0.002
	Silt-sized material	25	-	0.002-0.06
	Lithics	<1	Sub-angular to subrounded	3.1
TV1	Cristobalite	5	Angular to sub-angular	0.4-1
	Magnetite	5	Sub-angular to subrounded	0.12-0.25
	Augite	<3	Sub-angular	
	Hematite	3	Sub-angular	0.15-0.5

7.7.2 Riedel shears

One of the characteristic features observed was the presence of Riedel shears (**chapter 2**). In an idealised testing situation, the orientation of the Riedel shears is dependent upon the friction angle (φ) (Ahlgren, 2001). The idealised shear orientation has been detailed in existing literature to be around 45° ± φ/2 (Riedel, 1929; Ahlgren, 2001). However, due to the variable nature of the triaxial test from external factors altering the pressures being exerted (**chapter 2**) will produce a more variable environment than that of an idealised situation (Mills, 2016).

Schematics based upon the effective friction angles of this study (**Table 7.3**) have been produced (**Figure 7.12**).

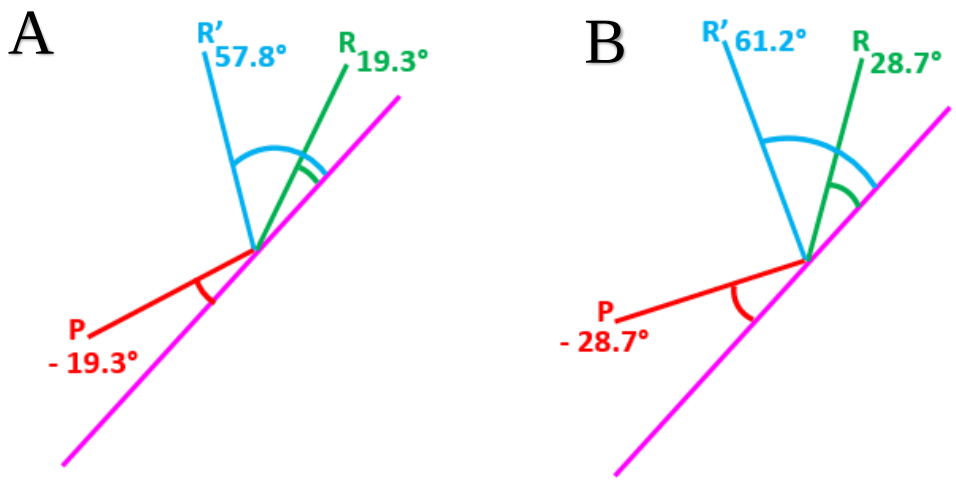

Figure 7.12. Expected Riedel shear orientations calculated for DRAB1 (**A**) and TV1 (**B**), based upon the calculated friction angle of the materials. PDS indicated the primary displacement discontinuity.

7.7.1.1 DRAB1 – 270 kPa

The thin section produced for the 270 kPa sample was taken adjacent to the failure surface (**Figure 7.13**). The shears were not prominent, with the overall thin section having few fracture zones visible. The large main PSZ shear was connected to the conjugate shears by several small lateral shears. These shears had a measured angle of between 30 and 40°. These measured angles did not closely match the calculated angle values for Riedel shear propagations detailed in **Figure 7.12**, A). The shears were infilled with a dark substance, potentially hematite, as observed in **Figure 7.16**, image B.

Figure 7.13. Image depicting the location on the core where the thin section was taken from, adjacent to the failure surface.

7.7.1.2 TV1 – 130 kPa

The thin section produced for the 130 kPa confining pressure was taken adjacent to the failure surface (**Figure 7.14**) This thin section was found to exhibit more visible shears, compared with the DRAB1 270 kPa sample (**Figure 7.17**). One PSZ zone could be seen propagating across the sample, with two conjugate shear zones connected by R' shears. The interaction between these shears had a measured angle of ~50 - 60°. The measured angles were in agreement with the calculated Riedel shear propagations detailed on **Figure 7.12**, B). One conjugate shear passes through a highly weathered, high relief cristobalite crystal (**Figure 7.17**, **B)**). Infilling of the fracture within the crystal was also observed. There is a lower degree of shear infilling compared to the DRAB1 270 kPa sample (image B), bottom left corner).

Figure 7.14. Image showing the location the 130 kPa thin section, adjacent to the failure surface.

7.7.1.3 TV1 – 230 kPa

The TV1 230 kPa thin section was taken adjacent to the failure surface (**Figure 7.15**) produced shows the main hypothesised PSZ propagating laterally across the sample (**Figure 7.18**) but did not show any infilling with dark material, unlike DRAB1 270 kPa and TV1 130 kPa samples. The shear zones within the TV1 230 kPa sample were not developed enough to accurately define and measure the Riedel shear propagation zones and interactions between different shear types. Therefore, only the main identified shear zone within the sample is marked on **Figure 7.18**.

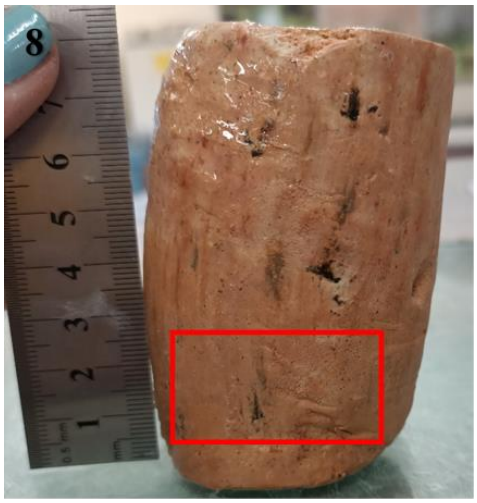

Figure 7.15. Image showing the location of the thin section taken from the TV1 230 kPa thin section, adjacent to the failure surface.

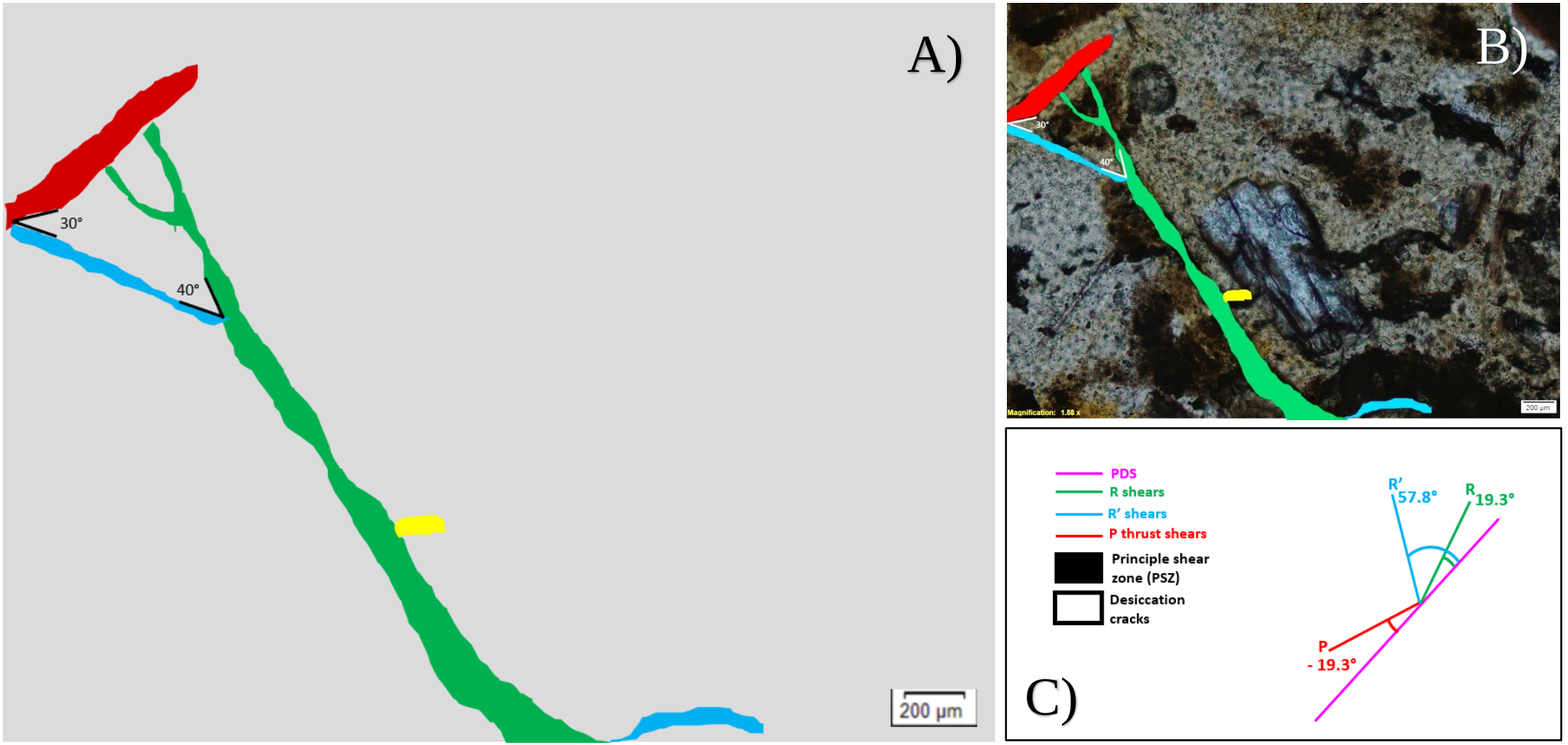

Figure 7.16. Thin section images depicting shears within the DRAB1 270 kPa sample. A) Shears identified, PSZ denoted by green line, R' shears as blue, and conjugate shears (P) as red. Additional R shears are yellow. B) shows shears overlain on thin section. C) depicts the legend produced for this sample.

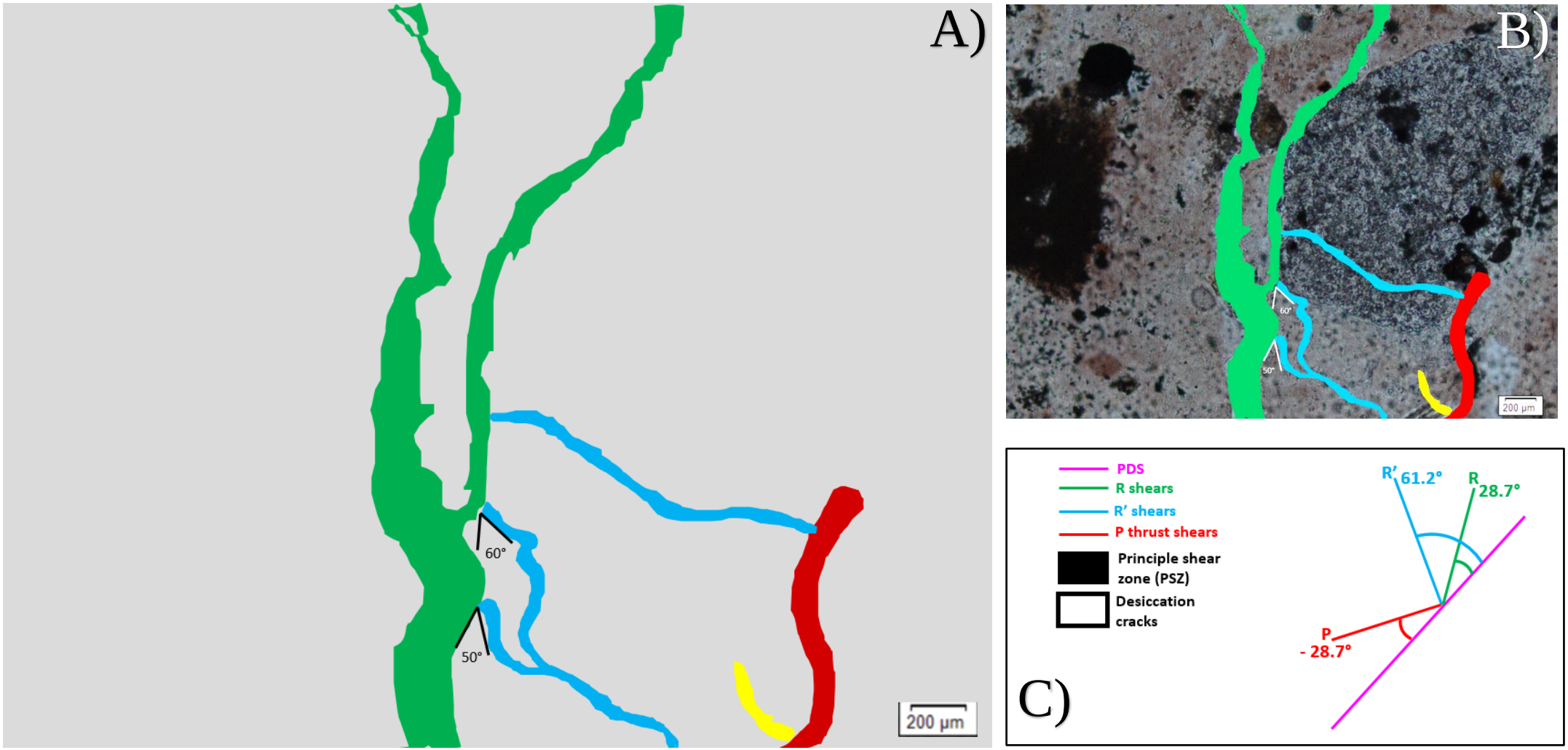

Figure 7.17. Thin section images depicting shears within the TV1 130 kPa sample. A) shears identified, PSZ denoted by green line, R' shears as blue, and conjugate shears (P) as red. Additional R shears are yellow. B) shows shears overlain on thin section. C) depicts legend produced for this sample.

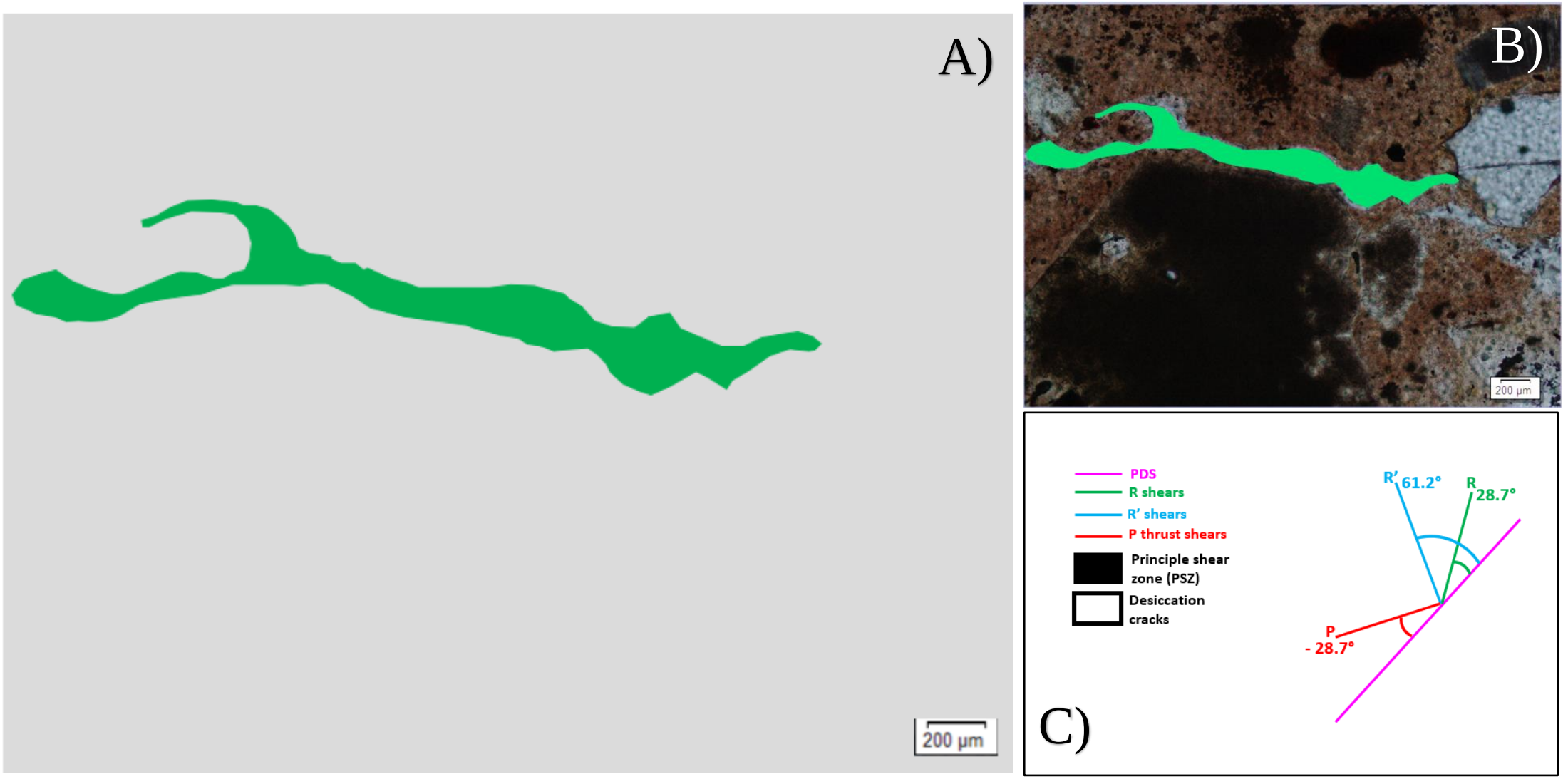

Figure 7.18. Thin section images depicting shears within the TV1 230 kPa sample. A) shears identified, the PSZ denoted by green line. B) shows shears overlain on thin section. C) depicts legend depicted for this sample.

7.8 Limitations in the triaxial procedure

The limitations of the experiment must be considered. Whilst great care was taken to produce accurate, consistent results, some limitations may have arisen during the testing procedure.

7.8.1 Collection of field samples

The use of the steel push tubes for the collection of samples, whilst effective in retaining the samples shape, can result in the compaction within the middle of the sample, as a result of the hammering action (Gylland et al., 2014). This hammering can also lead to sample disaggregation which can decrease strength (Mills, 2016).

To combat and minimise this risk of error, any samples that showed any significant outward signs of fracture following sampling were not used for testing. Any internal fractures, however, could only be discovered post-failure, therefore, were impossible to detect prior to testing. Because the samples were tested using the same methodology, the test results are as uniform as possible.

Because of the highly spatially variable nature of soil material, the need for differing soil samples being as similar as possible was very challenging to achieve. The multitude of differences within the soil profile, including differences in inclusions, inclusion sizes, presence of differing materials and so forth needed to be considered whilst testing. The high spatial variability of soils within a small sampling area explains irregularities or differences seen within the results. To determine any differences, post-failure triaxial cores were cut open and observed, to identify factors that may have influenced the results.

The time of year the cores were collected and the depth of testing influenced the quality of the samples obtained. The TV2 samples collected were too dry to be used for triaxial testing, crumbling when cut (**Figure 7.19**).

Figure 7.19. Image showing the condition of the TV2 cores during extraction. The granular nature of the cores in addition to the moisture content disallowed successful core extraction and trimming.

7.8.2 Temperature interference

The potential of external interference of temperature upon the triaxial apparatus also may have potentially led to diurnal fluctuations on the measured specimen volume change, due to waters' expansive and contractive behaviour under different temperature conditions. This produced a distinctive diurnal sinusoidal wave being displayed on the consolidation graphs (Moon, V, personal communication, 18th September 2020). To reduce the impact of diurnal cycles upon the data, only the initial portion of the graph, showing the correct trends, was analysed to determine the critical time needed for the shearing portion of the triaxial testing procedure.

The triaxial apparatus also experienced seating issues during the shear phase of testing, meaning deviator stress and pore water pressure responses to strain did not start at zero, rather at 1 – 2 % strain. This was accounted for through the omission of data reflecting the loading issue in the graphs produced.

7.8.3 Error in the shear phase of testing

I hypothesise that during the loading process, despite the loading ram and back pressure sensor appearing to line up exactly, the ram may have been offset to one side. Upon the shear phase, as a result, the initial loading was offset to one side, prior to slipping down into place for the remainder of the tests (**Figure 7.20**). As a result, some lag was likely experienced between the deviator stress reading and the load the soil was experiencing. This only occurred generally within the first 2 % of strain within a test however, so it can be said with some confidence that it did not impact the peak deviator stress point to much of a degree. To account for this however, the data showing no change in strain was omitted from the graphs, to give a more accurate depiction of the response over time. I believe that further experience would rectify this issue. This was proven in a final test I completed upon TV1 at 130 kPa, where I ensured some axial force was being applied by the loading ram into the back pressure sensor. The results of this test removed the 'steps' that were commonly observed on the incorrect graphs (**Appendix 7.3**).

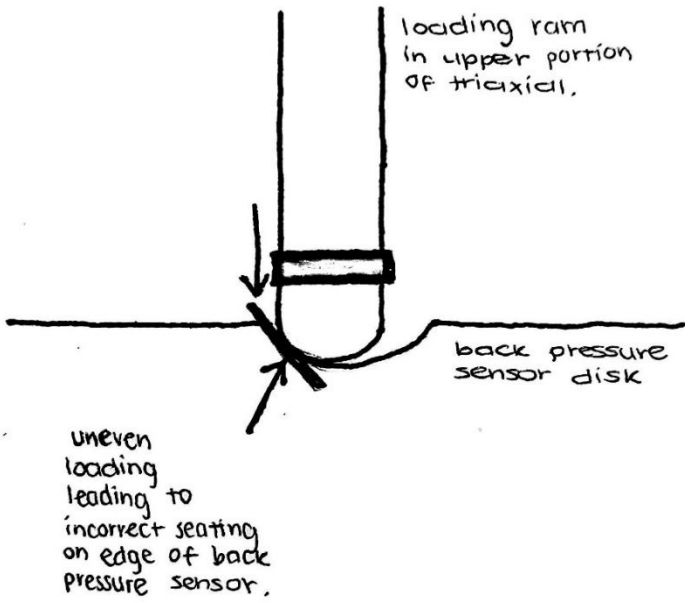

Figure 7.20. Diagram depicting the likely scenario occurring during the shear phase of the triaxial tests undertaken during this study. Note the uneven seating of the upper ram within the back pressure sensor disc, thus leading to an uneven loading being applied upon the samples in the first 1-2 % strain, before the ram forced its way to seat evenly within the disc.

7.9 Summary of chapter

The completion of the triaxial testing, and the associated calculations and graphic modelling allowed for the determination of the behaviour of samples under a range of confining pressures and allowed for the determination of the expected response upon a stress strain curve, stress path, and pore water pressure changes. The failed cores showed a combination of failure modes, including more concentrated shear failure modes, or more generalised wedge or barrel failure modes. The variation in these modes of failure could be attributed to a number of factors, including the proportions of silt and clay sized materials within the soil matrix, the effective stresses acting upon the samples, and the void ratio within the sample (Konrad & Sawitzki, 1994).

Generally, testing went well, however loading issues during shear meant strain was measured from 1-2 % onwards, and issues with measurements during the DRAB1 270 kPa test meant strain was only measured to ~ 14.8 %. The analysis of the thin sections was also completed. Gylland and others' 2013 method to air dry the samples following cutting was chosen as the best method to use, based upon the results of Mills' 2016 study. The majority of the sample was made up of clay-sized groundmass and silt-sized particles, too small to distinguish. Cristobalite, magnetite, hematite, quartz and augite were also identified in differing quantities between samples. Analysis also showed the presence of shears within the samples, and how they interact with one another in some cases.

Chapter 8
Mineralogical properties – Scanning Electron Microscope results

8.1 Introduction

This chapter summarises the results gained from the use of the scanning electron microscope (SEM). The SEM has the capabilities to identify clay, silt and sand sized particles directly, and how they interact with one another (Wyatt, 2009). As a result, the SEM used determine the predominant clay mineralogy of the particles within the sample, in addition to the microstructures of the particles. For the purpose of this investigation, both interactions between differing clay morphologies within the samples analysed and the greater interaction between the clay minerals and the larger grains within the samples.

8.2 Clay morphologies

The samples from this study had a high density of halloysite clay minerals identified, with a number of different morphologies: tubules, spheroids, plates and books. The abundances observed in this study are qualitative rather than quantitative, completed by observation only.

8.2.1 Tubes

Figure 8.1 to **8.4** shows the main halloysite tubules identified within DRAB1, TV1 and TV2 samples respectively. The tubular form of halloysite was the most abundant in all three samples analysed, with DRAB1 containing the highest abundance of short tubules, between 0.2 and 0.64 μm in length. TV1 and TV2 had comparative abundances of short tubules, between 0.1 and 0.4 μm in length, but contained longer tubes compared with DRAB1, between 0.4 and ~1 μm in length (**Figure 8.2** and **8.3**). The tubes were identified to be hollow in many cases. (**Figure 8.1** and **8.2**). The arrangement of the tubules was fairly consistent across all three

samples, but the densities of the arrangements differed. Face to edge, parallel face to face and face to edge at right angles orientations were observed, with a dominance of face to edge at right angles occurring in DRAB1 and TV1 (**Figure 8.4**). TV2 predominantly showed both edge to edge and right angled face to edge orientations (**Figure 8.3**).

The tubule morphology is consistent with those found in the sensitive Pahoia Tephra and Matua Subgroup materials analysed in Moon and others 2015 study within the Tauranga region.

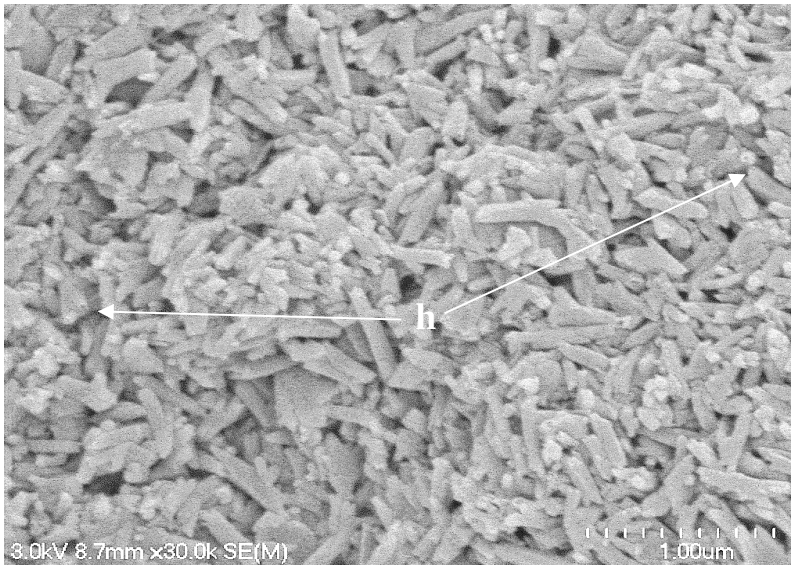

Figure 8.1. SEM image of DRAB1 depicting the abundance of loosely packed short halloysite tubules identified within the sample. The h denotes the open end of the tubule, indicating the tubes are hollow. The sizes of the tubes generally ranged from 0.2 to 0.6 μm in length, although some tubes greater than 0.6 μm could be identified, however these were rare.

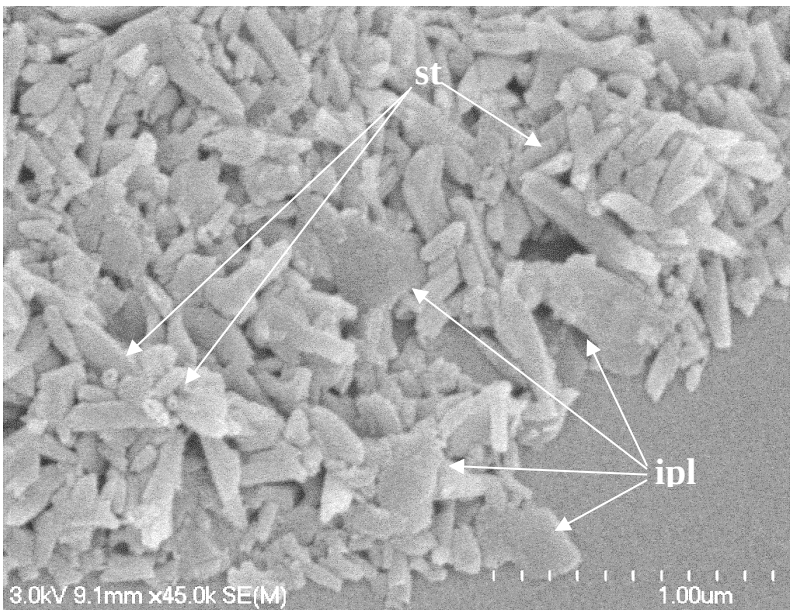

Figure 8.2. SEM image showing a closer resolution of the DRAB1 short tubules, their hollow nature (denoted by st) and their chaotic packing arrangement. Interestingly, some platy formations can also be identified, denoted by ipl, and are irregularly shaped. The size of the tubes ranged between 0.2 and 0.6 μm.

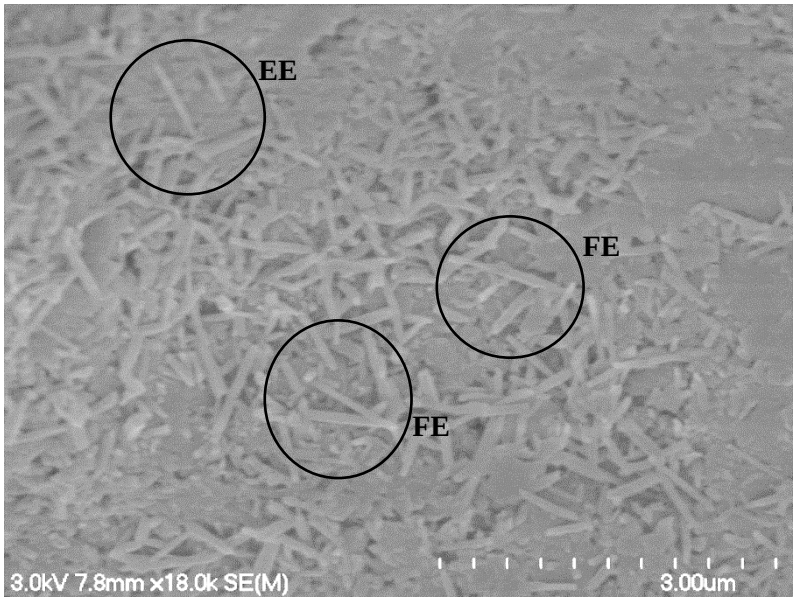

Figure 8.3. SEM image showing the long tubules identified within TV2. These tubules have a loosely packed arrangement. The tubules measure between 0.7 and 1.2 μm in length. The predominant interactions (face to edge, FE and edge to edge, EE) are also identified upon the image, as black circles.

8.2.2 Plates

Plate morphologies were also present within all three samples analysed (**Figure 8.5** to **8.9**). Plates appeared to be less abundant than the tubules identified, but the abundances appeared to be similar in all three samples analysed, with differing shapes. The plates appear to either be hexagonal or irregularly shaped in DRAB1 (**Figure 8.5**, **8.6**, and **8.7**). Plates that are hexagonal in shape normally associated with halloysite. The plates appeared to be more irregular in shape for TV1 and TV2 (**Figure 8.8** and **8.9**). The sizes of the plates varied in all three samples. (Dixon, 1989; Wyatt, 2009). The plates tended to be edge to edge (EE) and face to face (FF) in contact in all three samples.

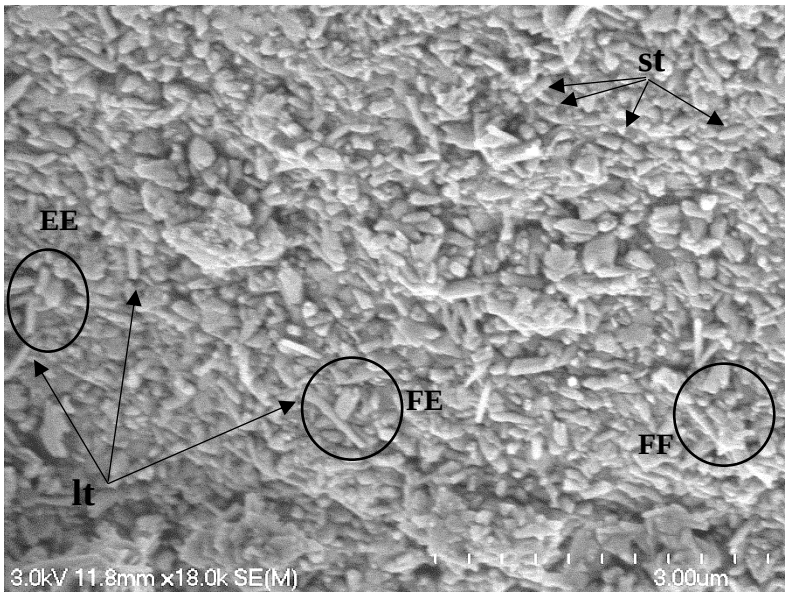

Figure 8.4. SEM image showing the tubule formations within TV1. Note the combination of shorter tubules (st) (0.1 to 0.2 μm in size) and longer tubules (lt) (0.4 to 0.7 μm in size) interacting with one another. Though it is difficult to identify explicit contacts in this image, it appears that wide angled face to edge (FE) and edge to edge (EE) contacts dominate, with some rare parallel face to face (FF) contacts.

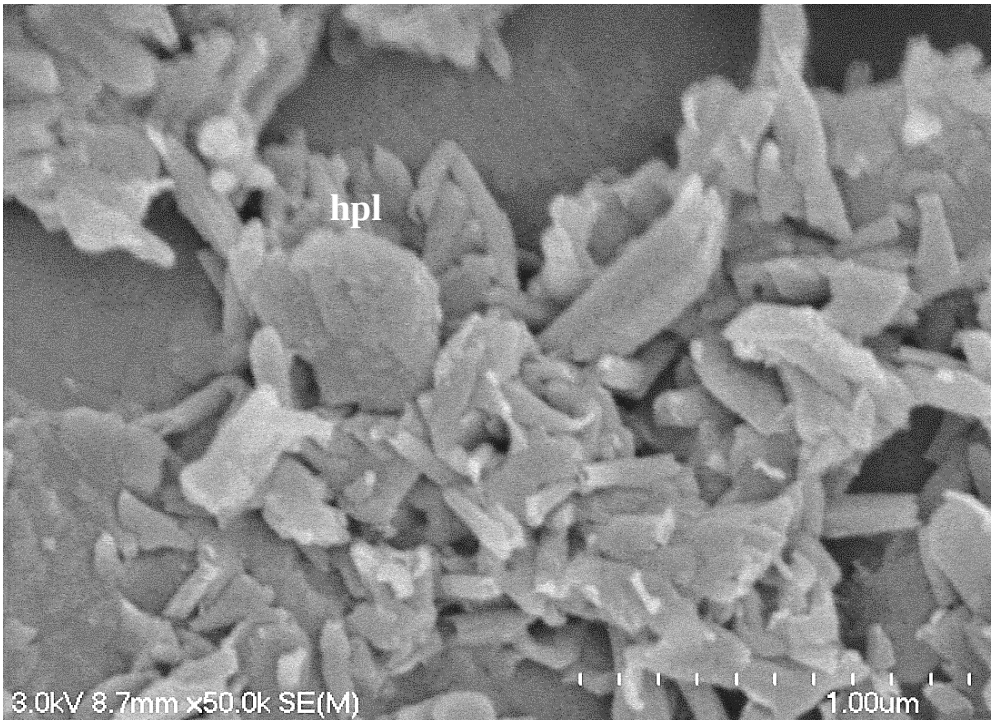

Figure 8.5. SEM image depicting the presence of more hexagonal plates (hpl) within the DRAB1 sample analysed. These plate formations predominantly were found within the open structure of the halloysite tubules, somewhat blocking the gaps within the open structure. The plate pictured measured 0.5 µm in length and 0.4 µm in diameter.

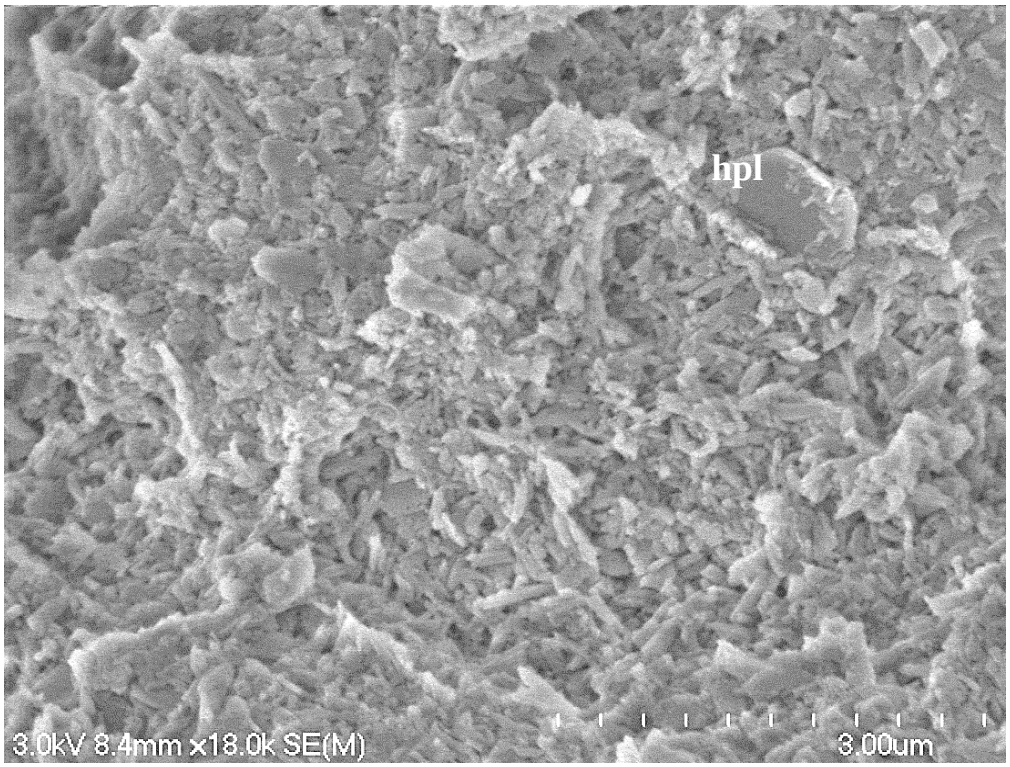

Figure 8.6. SEM image depicting a larger hexagonal plate (hpl) formation within DRAB1, measuring ~1 µm in diameter. The length of the plate is unknown, due to the base being buried within the halloysite tubules structure.

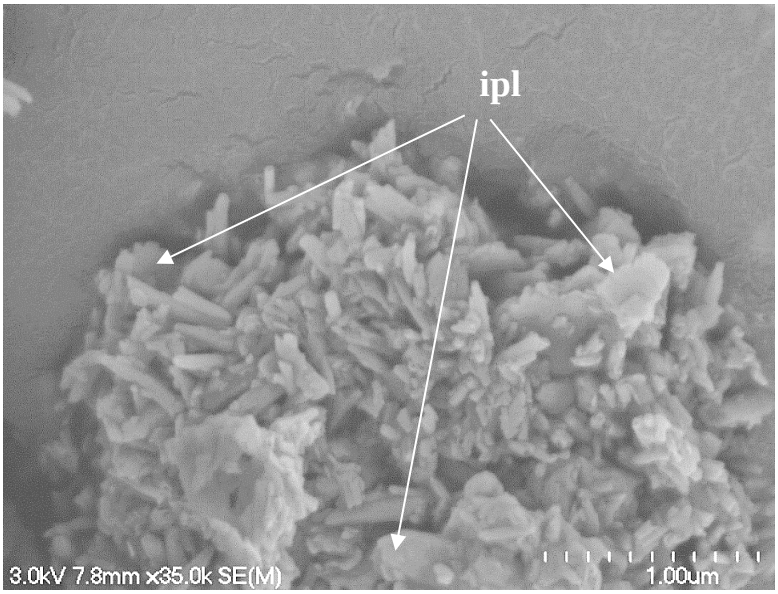

Figure 8.7. SEM image showing the presence and relative abundance of irregularly shaped plates within the DRAB1 sample, denoted by ipl. Due to the results of the XRD analysis, it is likely these plates could be kaolinite, which commonly adopt this form (Wyatt, 2009). Sizes of plates within this sample ranged between 0.3 to 0.5 μm in diameter.

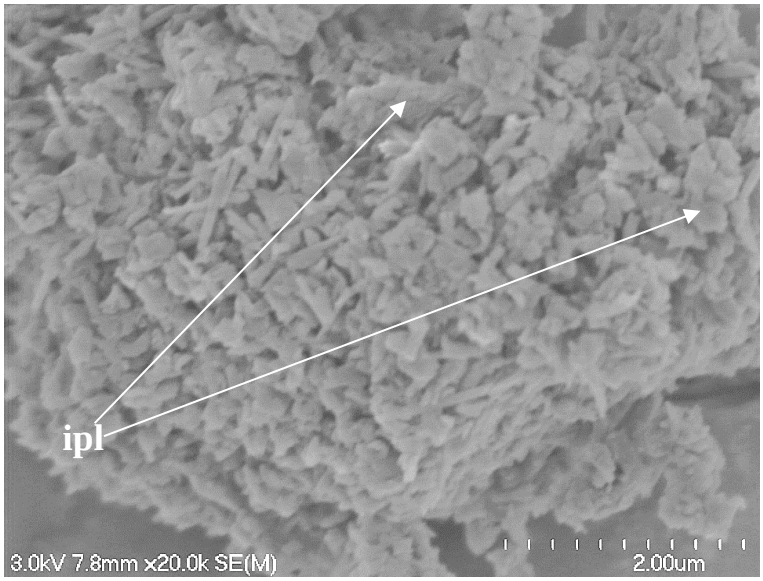

Figure 8.8. SEM image of TV2, showing the combined presence of halloysite nanotubules and irregular plates, denoted as ipl. Sizes in TV2 ranged from 0.1 to 0.2 μm in size. Due to limitations in the depth imaging upon the SEM however, it is challenging to differentiate between plates and spheroidal shapes (Wyatt, 2009).

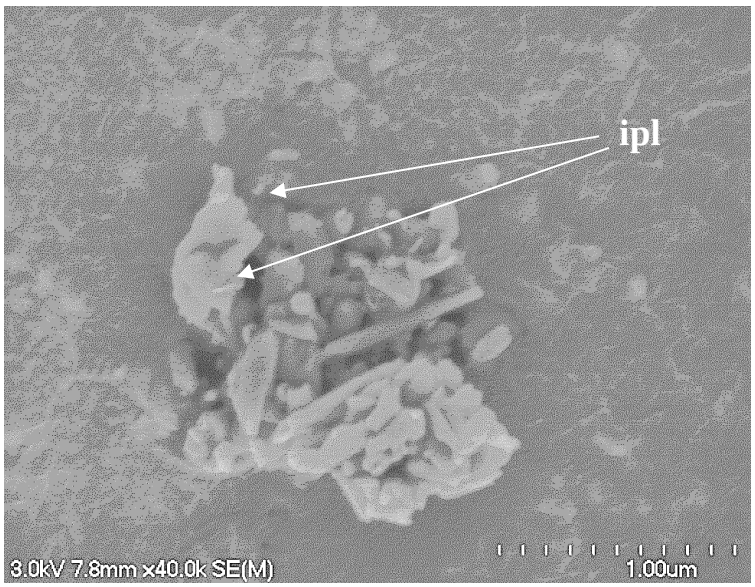

Figure 8.9. SEM image showing the presence of irregularly shaped plates within TV1, denoted by ipl. The plates range between 0.3 and 0.6 μm in TV1. Due to the limitations of the SEM it is challenging to determine the depth and true shape of the plates.

8.2.3 Spheroids

There were also spheroid morphologies identified within all samples (**Figure 8.10**). The low apparent abundance of these formations appeared similar in all three samples tested (**Figure 8.10**, **8.11**, **8.12** and **8.13**). These spheroids appeared to predominantly be polygonal in shape. Due to the limitations of SEM imagery, in most cases it was difficult to differentiate between spheroids and plates. The spheroid shape is a common indicator of halloysite (Joussein et al., 2005; Wyatt, 2009; Kluger et al., 2015). All three samples showed a similar arrangement, with the spheroids being in face to face contact with one another, intermixed with halloysite tubules in a subdued arrangement (Wyatt, 2009). In some cases, clusters of spheroids were identified, in a somewhat globular formation. This observation was consistent with Arthur's (2010) observations (**chapter 2**).

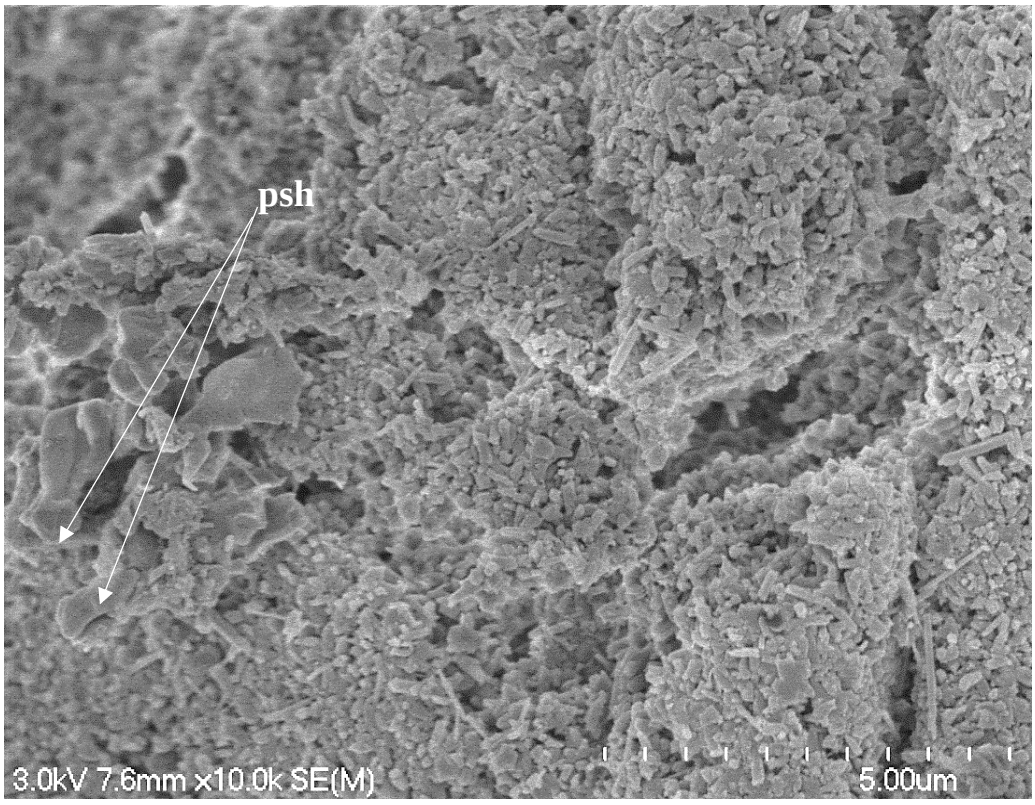

Figure 8.10. SEM image depicting the presence of polygonal spheroids in TV2 (psh).

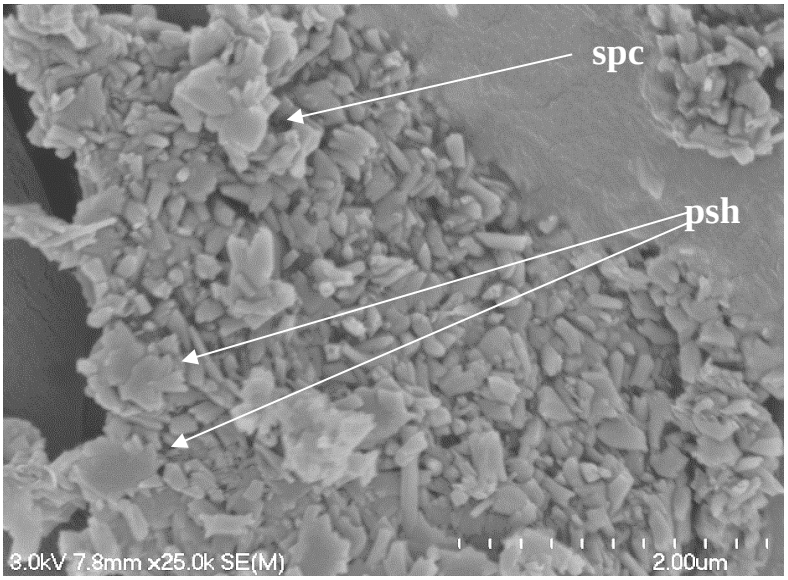

Figure 8.11. SEM image showing the presence of polygonal spheroids within TV2, denoted by psh. Note the apparent cluster of spheroids, denoted by spc. These spheroids measured between 0.1 and 0.2 μm in size. Due to the limitations of SEM imagery made it challenging to define between spheres and plates with 100 % certainty.

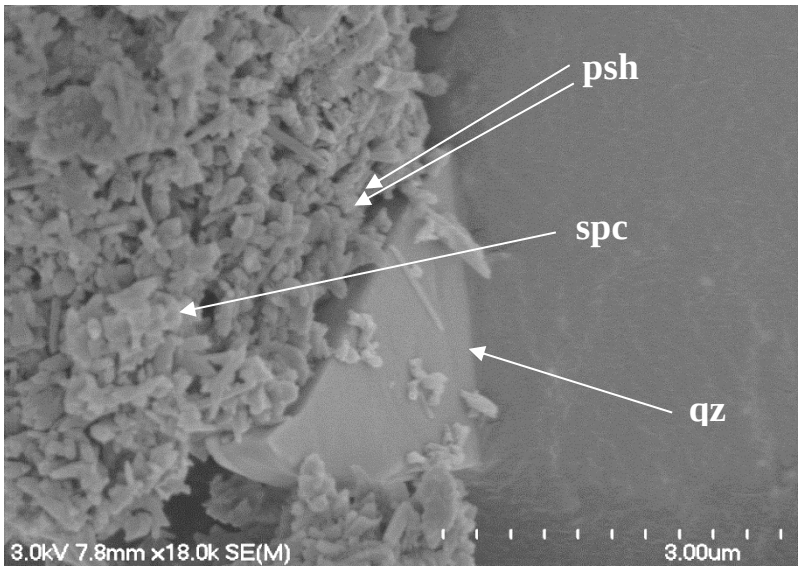

Figure 8.12. SEM images taken of TV1 showing the polygonal spheroids identified within TV1, denoted by psh. The spheroids identified were between 0.1 and 0.2 μm in size. Note the spheroid cluster upon the material, identified by spc. The spheroids appear more polygonal in shape compared to that of DRAB1. A potential angular quartz crystal has been identified to the right of the image, denoted by qz. The crystal measures 1.1 μm in length and 0.5 μm in diameter.

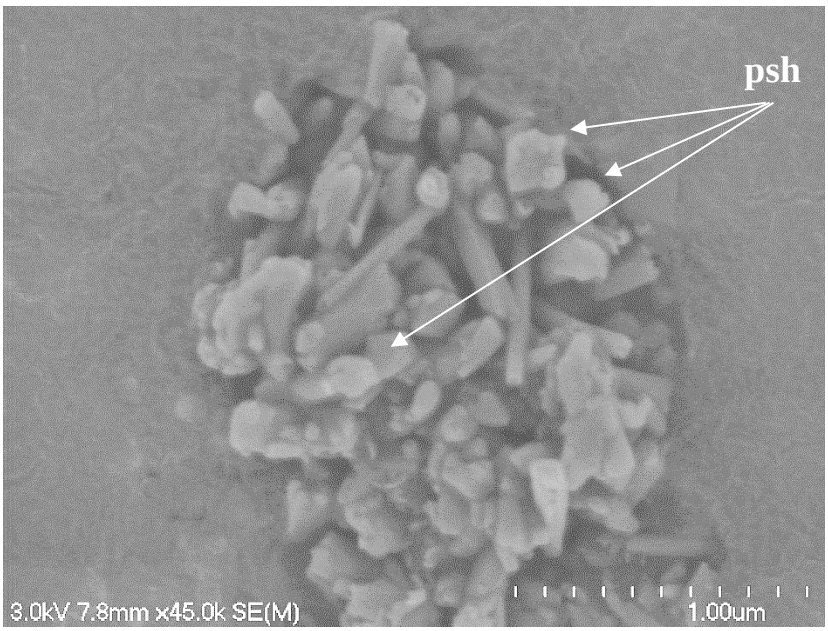

Figure 8.13. SEM image taken of DRAB1 showing some potential spheroid formations within the material, denoted by psh. However, due to the limitations of the SEM imagery, it is challenging to differentiate between spheroid and irregular plate morphologies.

8.2.4 Vermiform plates – 'books'

Whilst the identification of singular plates occurred in all three samples, stacked plates in a vermiform arrangement (books) were only observed in TV1 and TV2 and were seemingly absent within DRAB1. TV2 had the greatest observed abundance. The books observed were identified to be blocky and square to vermicular curved books, varying in size between 75 and 250 μm in length, and 0.5 to 100 μm in diameter (**Figure 8.14**, **8.15** and **8.16**). Book formations were identified within Tauranga sensitive soils in Wyatt's 2009 study, and in the pyroclastic soil materials studied across Tauranga in Arthur's 2010 study (**chapter 2**). I hypothesise the books identified in TV2 are kaolinite, observed on the XRD bulk and clay graphs (**chapter 6**).

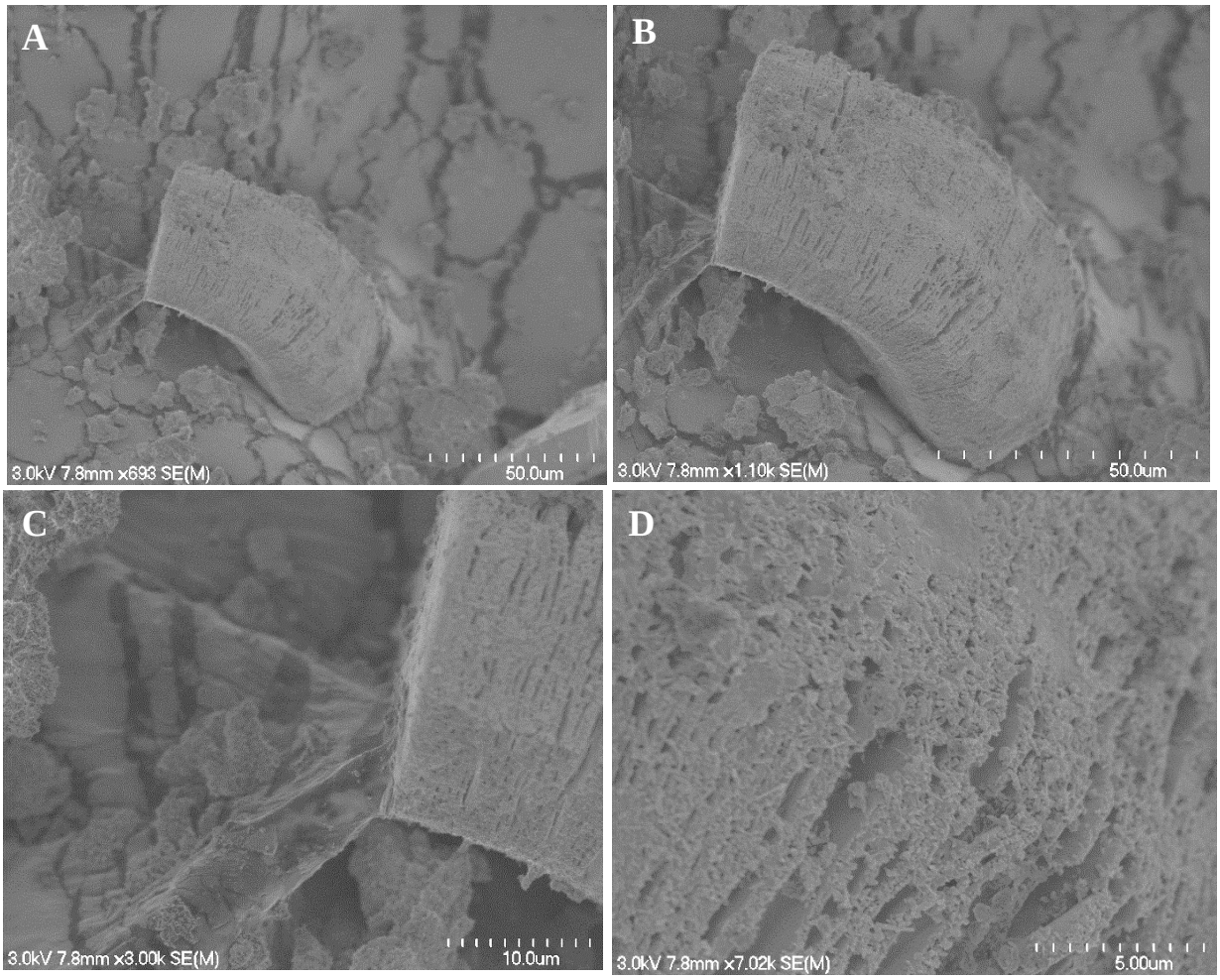

Figure 8.14. SEM images displaying the discovery of a potential vermiform 'book-like' formation within TV2. Images A-D show increased magnification to show the fabric of the stacked plates. The book formation is 75 μm in length, with the plates being 45 μm in diameter. The plates are closely packed together, with only isolated areas of delamination in portions of the structure (see image D).

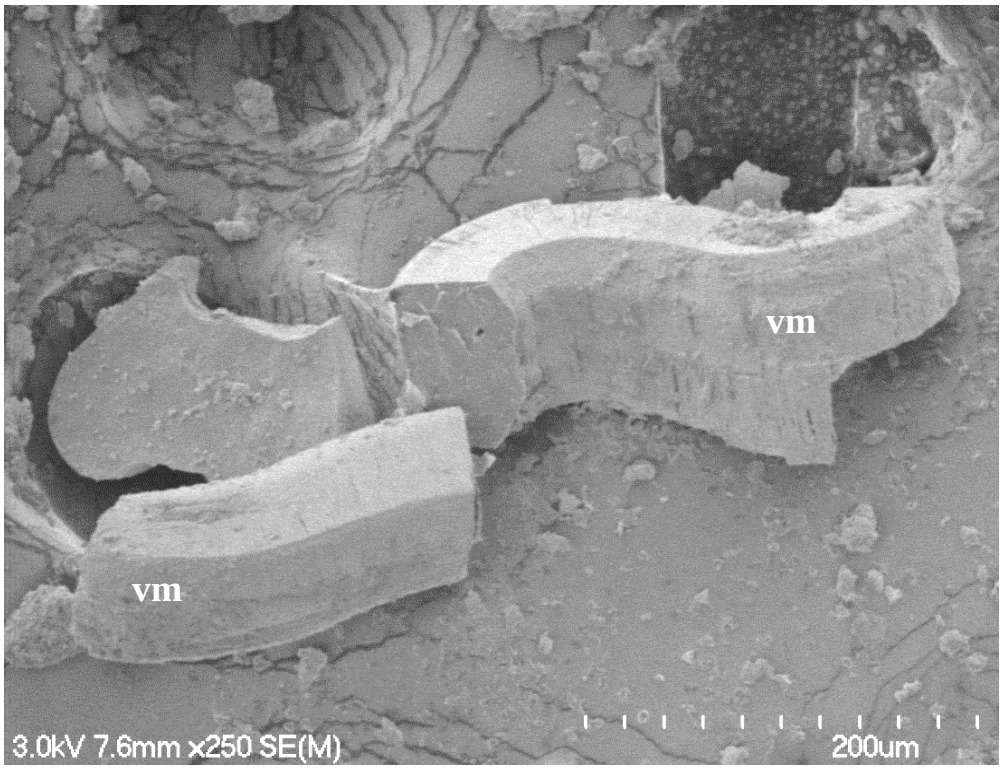

Figure 8.15. SEM image depicting the presence of two vermiform book (vm) forms radiating away from one another at a common point in TV2. The books range from 200 to 250 μm in size, and display face to edge contacts.

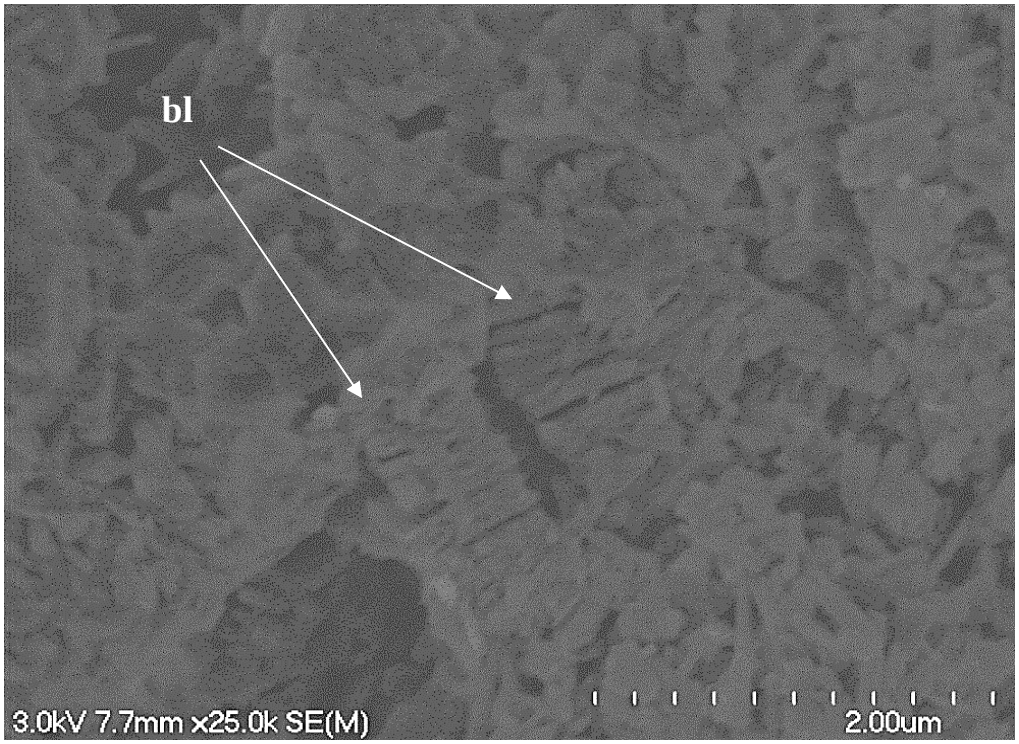

Figure 8.16. SEM image of the potential blocky book formations within TV1, denoted by bl. These books measured between ~1 μm in length, and ~0.5 μm in diameter.

8.3 Microstructure

Until now I have just described the interactions purely of the clay minerals with one another. In a more granular, silt dominated material such as the Walton Subgroup, it is also necessary to consider the interactions of the more granular materials and the clay minerals together (**chapter 7**), the main minerals contained within the materials include quartz, cristobalite, feldspars and volcanic glass. The microfabric interactions of these grains in relation to one another, and the evidence of the degree of weathering can indicate the relative strength these arrangements impart upon the soil material. Both the more cohesive and granular portions of the soils were analysed. The hierarchical classification of microstructural terms is defined in detail in **chapter 2.**

8.3.1 DRAB1

8.3.1.1 Primary structural elements

8.3.1.1.1 Clay minerals

The interaction of the differing halloysite morphologies show that the tubules tended to display a combination of somewhat loose and more closely packed parallel associations, with the plates and spheroids infilling any gaps in many cases (**Figure 8.17**, **8.18** and **8.19**). These materials are classified as clay minerals for the remainder of this analysis.

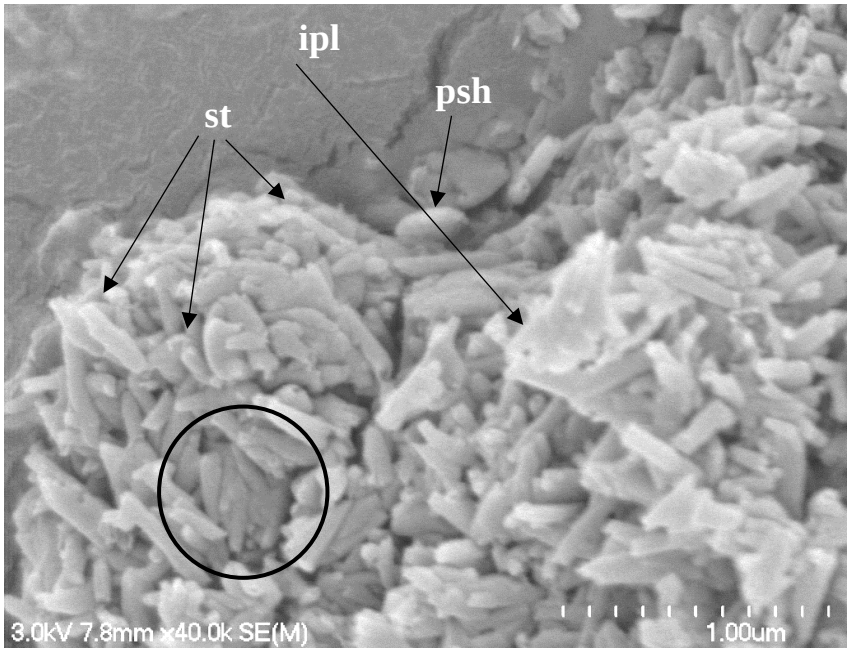

Figure 8.17. SEM image showing the dominant halloysite morphologies identified within the DRAB1 samples analysed (short tubules (st) in a loose edge to edge contact arrangement, with polygonal spheroids (psh) and irregular plates (ipl) filling in the spaces between the tubules). In this case, some parallel contacts between tubules can be observed (identified by black circle).

8.3.1.1.2 Grains

Sand-sized grains of quartz and weathered glass appeared to dominate the granular fraction of DRAB1. These grains were predominantly angular in shape and tended to be found surrounded by the clay-sized matrix. The grains generally ranged between 1 and 3.5 μm in size, but some isolated larger grains could also be identified within the sample (**Figure 8.20** and **8.21**). The grains did not show any dominant orientation, and tended not to touch one another, always being surrounded or covered by groundmass. Particle size analysis indicated silt-sized particles dominated the DRAB1 sample, thus indicating the potential for additional silt-sized aggregations of grains being masked by the occurrence of smaller clay-sized materials.

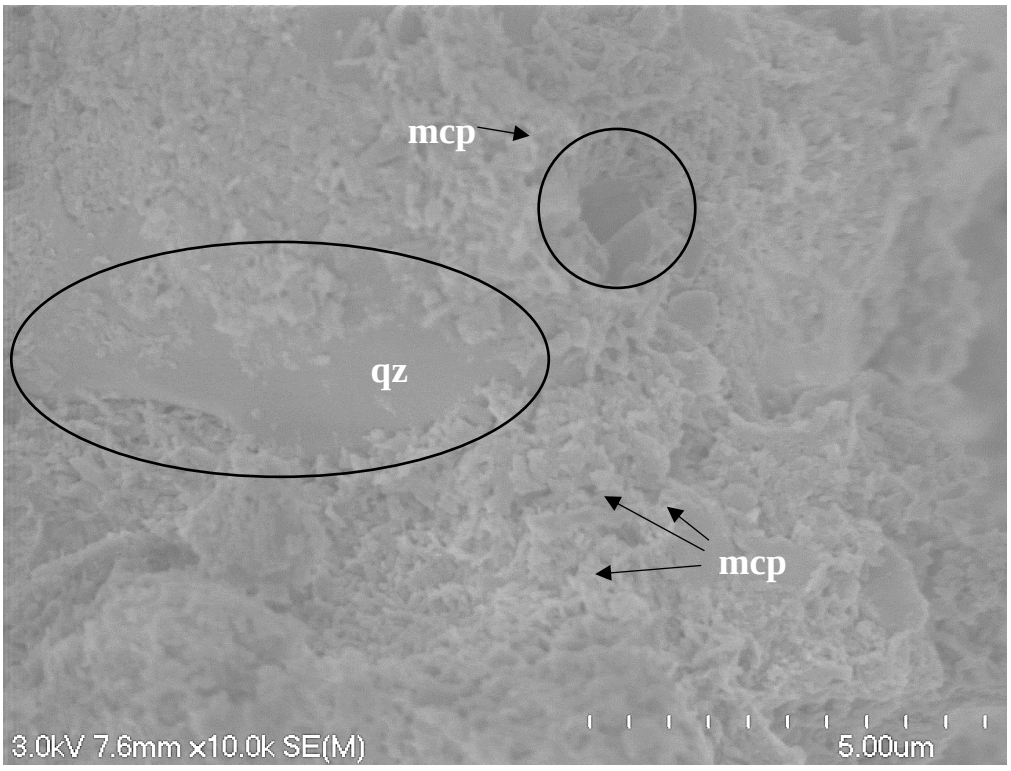

Figure 8.18. SEM image showing the presence of a potential quartz crystal, being lapped by the clay-sized matrix within the DRAB1 material (denoted by large black circle). This grain is 6.5 μm in length, with the diameter unknown. Also note the presence of a pore-like structure to the right of the quartz crystal (denoted by small black circle; mcp). This opening is 1.3 μm in size, thus classifying it as a micropore. The pore appears to have formed through collapse of the material. Several smaller micropores can be identified to the lower half of the image (mcp). These range between 0.2 and 0.5 μm in size.

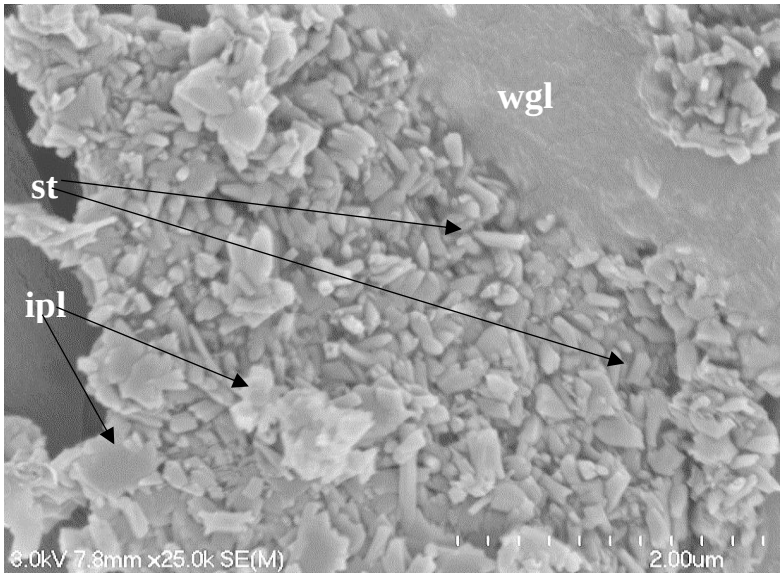

Figure 8.19. SEM image showing the presence of a hypothesised weathered glass grain (wgl) amongst a clay-sized matrix consisting of short halloysite tubules (st) and irregular plates (ipl). The weathered glass particle measured 3.59 μm in length, and 1.59 μm in diameter at its' widest point.

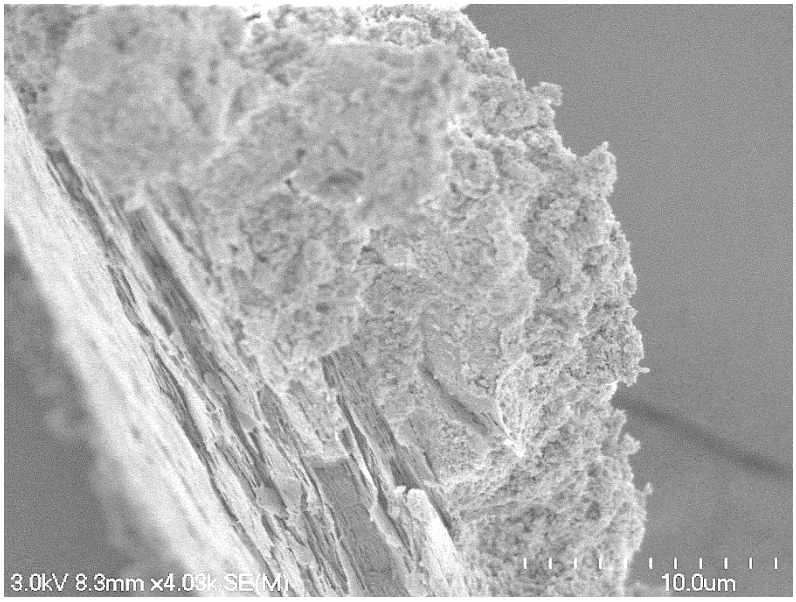

Figure 8.20. SEM image showing the presence of an apparent weathered mineral present within the DRAB1 sample. Note the presence of clay-dominated matrix coating the topmost portion of the grain.

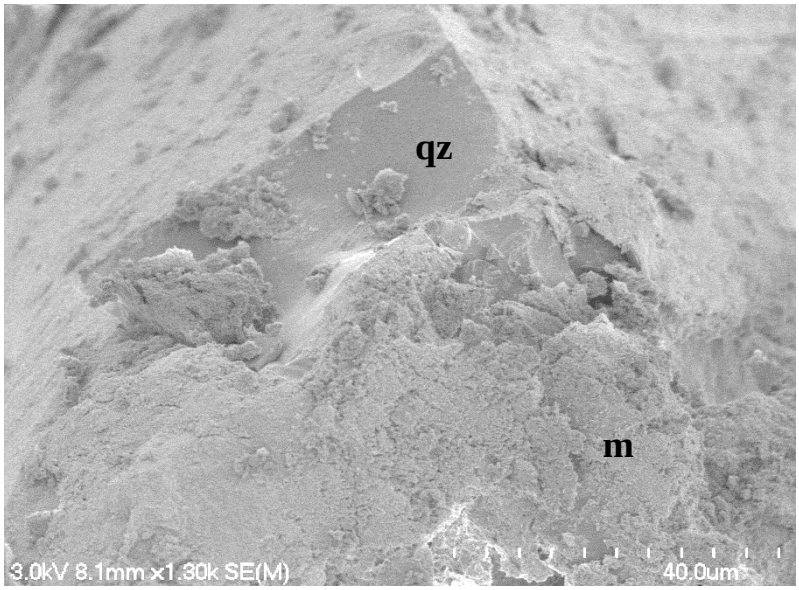

Figure 8.21. SEM image depicting a potential quartz (qz) grain covered by the clay sized matrix (m).

8.3.1.2.1 Matrix

In all the DRAB1 samples analysed, because of the range of morphologies present in the matrix, and their somewhat irregular shapes, it was sometimes challenging to define exact particle contact orientations. However, tubes could be identified in edge to edge (EE) and face-to-face parallel (FF) contacts with some accuracy, and the plates could be identified in face-to-face (FF) contacts (**Figure 8.22** and **8.23**). The polygonal spheroids tended to dominantly show FF contacts, due to the overall shape of the morphologies. It is likely that additional contacts exist, but due to the limitations of the SEM imagery, cannot be seen with clarity.

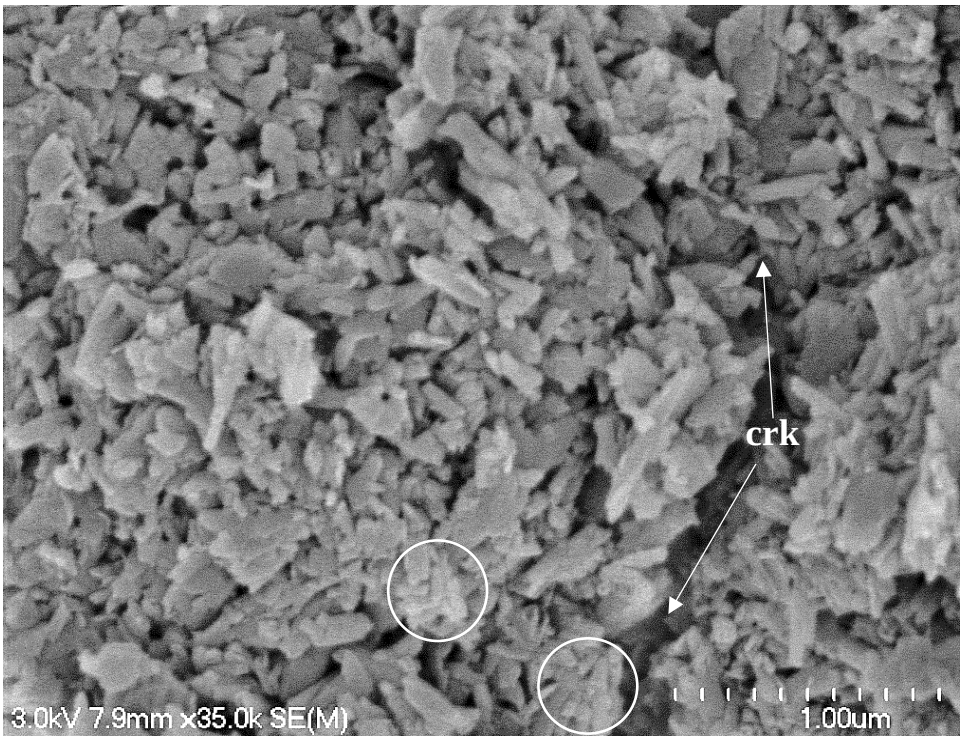

Figure 8.22. SEM image showing typical matrix of DRAB1 material. Note the predominance of sort halloysite tubules and irregular plates. A dominance of edge to edge (EE) contacts can be observed between the tubules, with the plates infilling gaps in the loose arrangement. Also note the presence of some parallel tubule contacts (denoted by white circles) and the presence of a large crack (crk), likely occurring due to desiccation as a direct result of sample

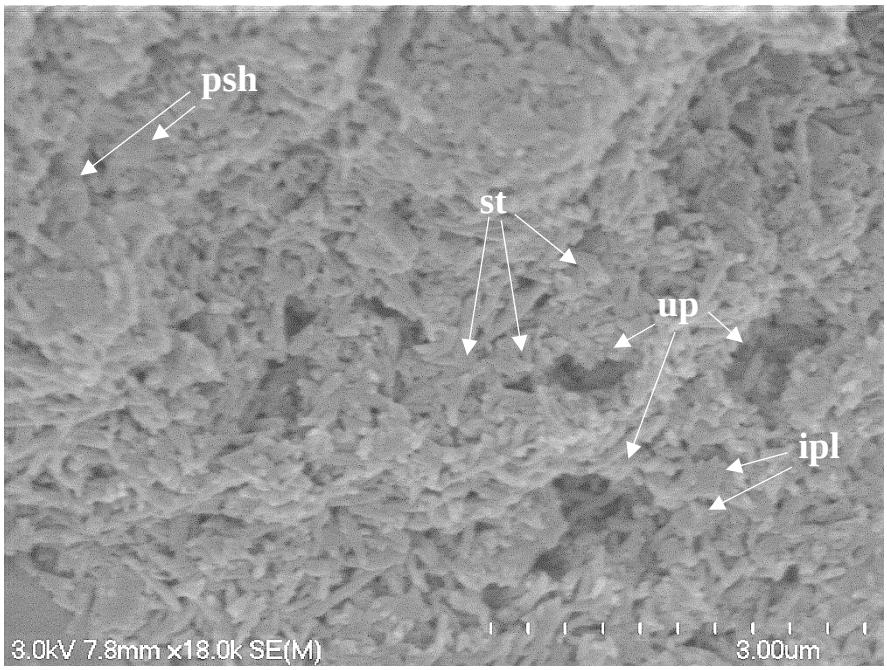

Figure 8.23. SEM image depicting the range of halloysite morphologies identified within the DRAB1 matrix. Note the presence of short tubules (st), polygonal spheroids (psh), and irregular plates (ipl). Additionally, several ultrapores (up) were identified to the bottom right of the sample, ranging between 0.90 and 0.97 μm in size.

8.3.1.2.2 Microaggregates

The main microaggregates identified within the DRAB1 samples appears to be clusters of clay minerals with poorly defined boundaries (**Figure 8.24**). These clusters were somewhat challenging to identify at times due to the irregular boundaries of the materials, and the limitations of the SEM apparatus. When identified, the clusters tended to be ~5 - 10 μm in size and consisted of the same materials as present in the matrix.

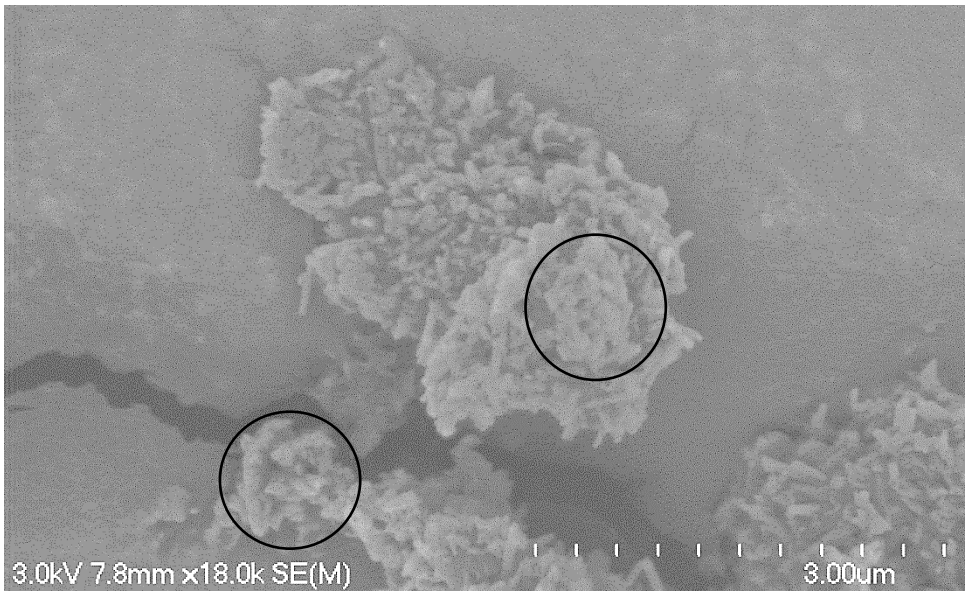

Figure 8.24. SEM image showing the presence of individual clay-sized material clusters within the material (denoted by black circles). These clusters, hereafter referred to as microaggregates, are discrete of one another, and tend to be attached to other material through clay connector bridges.

Apparent defoliated layers were also identified within the sample, emanating out of the clay-sized matrix. These appear to differ from the halloysite book formations identified in TV1 and TV2, rather representing large scale plate formations loosely stacked upon one another (**Figure 8.25**). These plates display loose face to face contacts, unlike the halloysite book formations. This material has been hypothesised to be micaceous in nature.

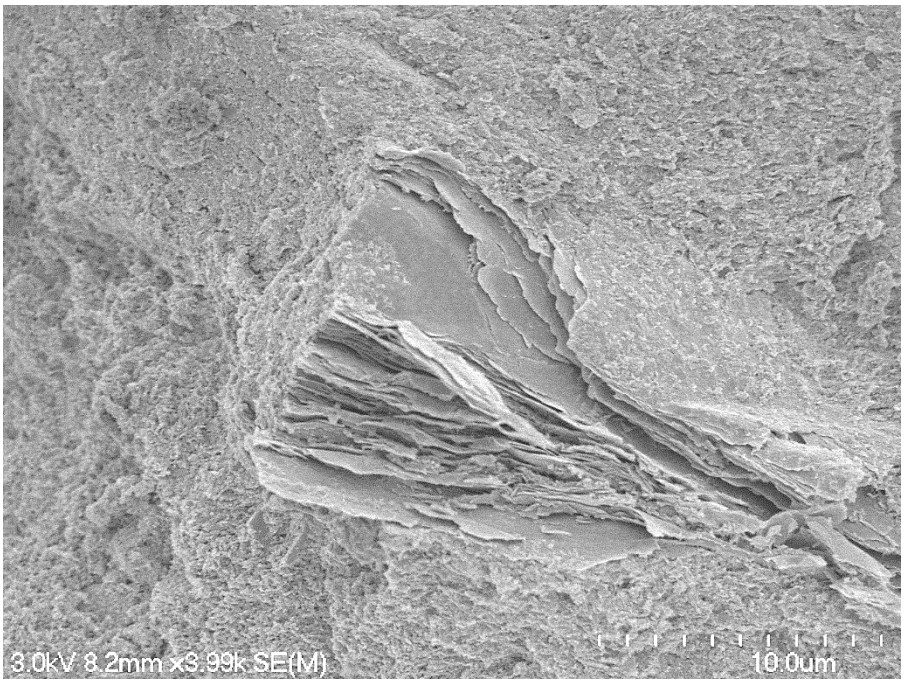

Figure 8.25. SEM image depicting the presence of apparent large-scale plates emanating out of the clay-sized matrix. These plate features show a large degree of defoliation, and range between 14.3 µm and 20.5 µm in size.

8.3.1.3 Overall particle associations

Individual grains were typically either embedded into the clay-sized matrix, or on the edges of aggregates with the matrix lapping around the edge of the grain (**Figure 8.18** and **8.19**). Minimal grain coatings could be observed upon the surface of identified grains, leaving a predominantly clean surface (**Figure 8.19** and **8.26**). The grains appeared to be tightly held within the matrix, with little to no evidence of pluck marks or disturbances.

The arrangements of the primary particles appeared to be fairly consistent and tended to form the background matrix microfabric to hold large grains when they were present. As a result, the samples depicted a continuous matrix, consistent throughout. A number of connector assemblages could be observed connecting the larger grains to the clay-sized matrix as a result (**Figure 8.26**).

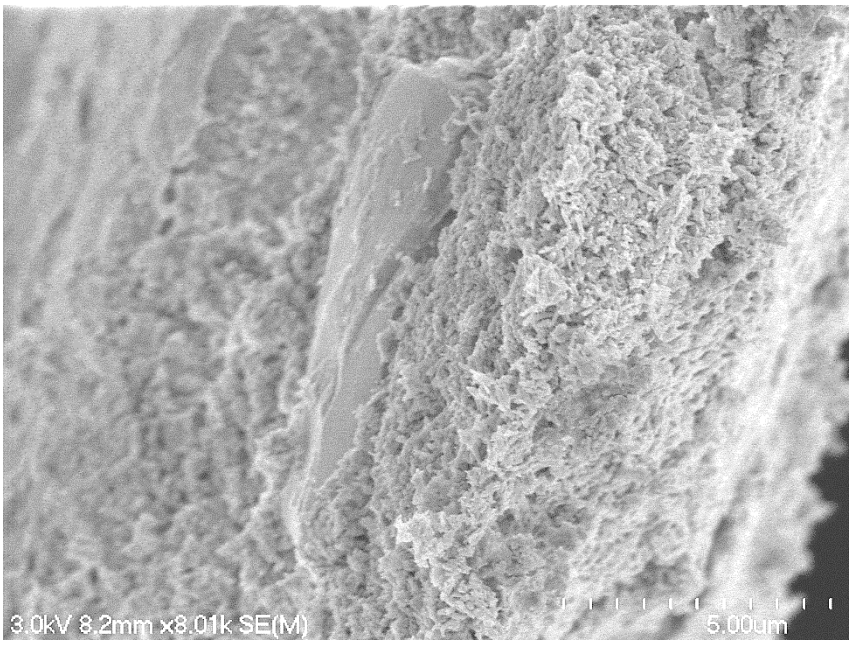

Figure 8.26. SEM image depicting the complete embedment of a sand - sized grain within a clay-sized matrix. The grain measured 7.8 μm in length, and 1.7 μm in diameter. The groundmass has a large number of connector assemblages upon the grain surface as a result.

8.3.1.4 Pore shapes and sizes

The porosity of the DRAB1 samples was calculated to be 41 %. This porosity can be observed in the open, loose structure of the DRAB1 materials, in the clay-sized matrix and clay microaggregates. Generally, the pores were between 0.2 and 0.9 μm in size, classifying them as micropores. However, some ultra-pores were also identified. Porosity could also be identified within the hollow ends of the halloysite tubules, and these were predominantly ultra-pore in size (< 0.1 μm). (**Figure 8.27** and **8.28**).

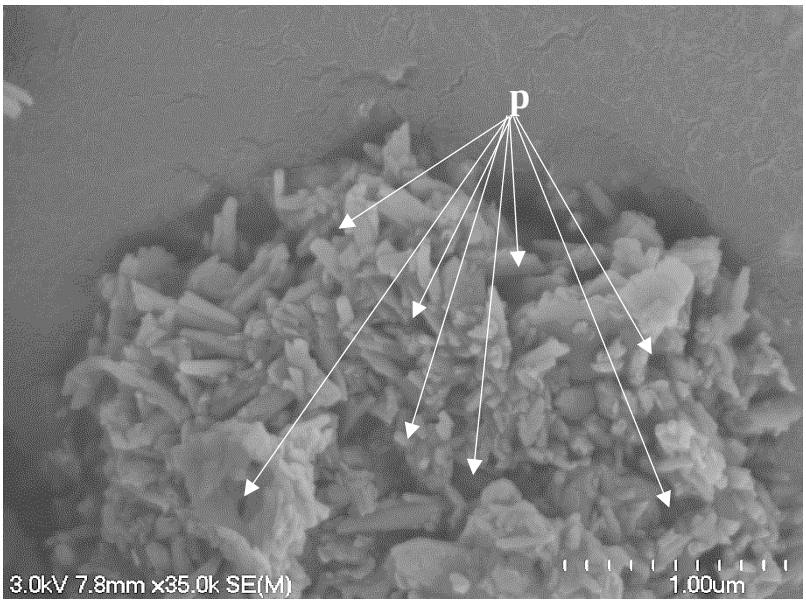

Figure 8.27. SEM image depicting the extent of the porosity (p) identified within the DRAB1 sample analysed. These pores measure between 0.04 and 0.4 μm in size, classifying them as ultra- to micropores.

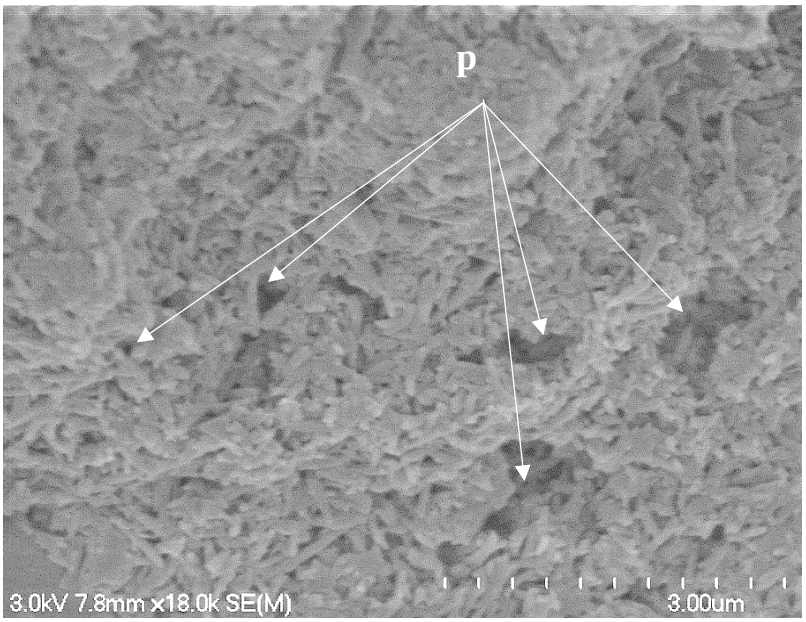

Figure 8.28. SEM image displaying another example of the porous nature of the DRAB1 materials analysed. The pores (p) ranged between 0.13 and 0.97 μm in size, classifying them as micropores.

8.3.2 TV1

8.3.2.1 Primary structural elements

8.3.2.1.1 Clays

The main clay mineral identified within the TV1 samples was again halloysite, similarly with a number of interacting morphologies (**Figure 8.29** and **8.30**). These particles are described in detail earlier in the chapter. The different morphologies were seen to extensively interact with one another, and displayed no distinctive orientation, rather having differing orientations

within different areas. Plates (between 0.3 and 0.6 µm in size) tended to stack in face to face (FF) contacts, whilst shorter tubules (between 0.1 and 0.15 µm) tended to have either parallel FF contacts, or face to edge (FE) contacts, encouraging an open structure. The longer tubules (between 0.5 and 0.6 µm) tended to show FE or edge to edge (EE) contacts. The angles of these interactions tended to be quite large, larger than those observed in DRAB1. Tubules appeared to be the most abundant in the samples analysed, with an appreciable number of plates also being observed, similar to DRAB1. The plates tend to be more irregular in shape. Polygonal spheroids were similar in abundance to DRAB1. The spheroids (between 0.1 and 0.13 µm) tended to interact predominantly with FF contacts when isolated and in the globular arrangements, due to the inability to differentiate between different surfaces upon the individual spheres (**Figure 8.29** and **8.30**).

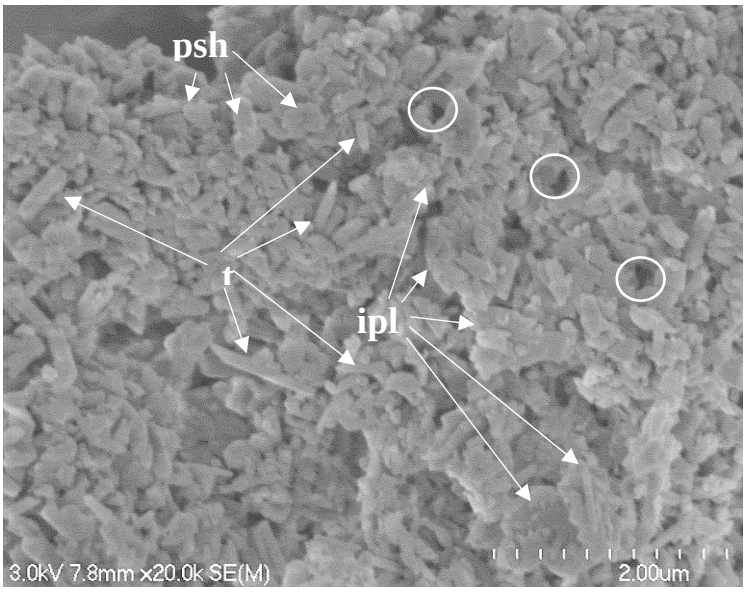

Figure 8.29. SEM image showing the range of interacting halloysite morphologies identified within the TV1 samples. Note the apparent greater densities of irregular plates (ipl) compared to tubules (t), compared to the DRAB1 samples. Polygonal spheroids (psh) are also identified. Multiple pores can also be identified to the right of the samples, denoted by the white circles.

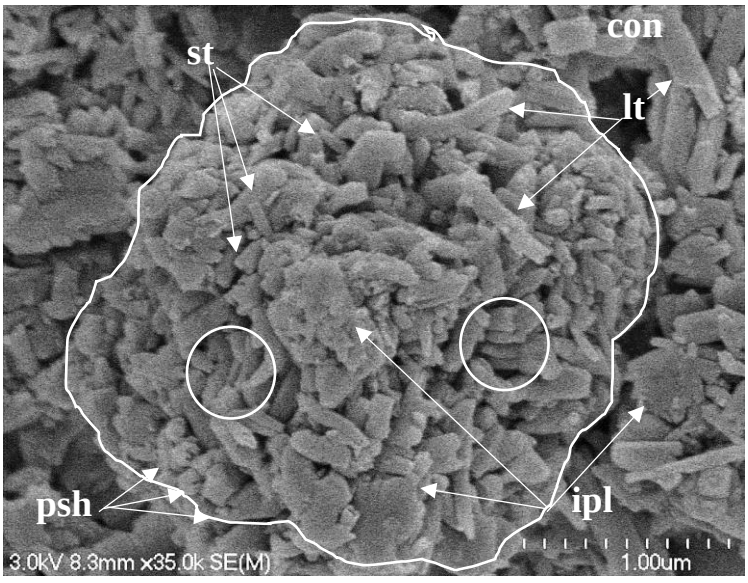

Figure 8.30. SEM image depicting a clay microaggregate structure within TV1 (white outline), with a combination of halloysite short (st) and long (lt) tubules, apparent flattened irregularly shaped plates (ipl), and rare polygonal spheroids (psh) interacting with one another. Note the presence of parallel face to face (FF) contacts between the tubules in multiple spots upon this structure (denoted by white circles). A clay connector bridge can also be observed to the top left of the image (con).

Grains were frequently observed in the TV1 samples analysed, more frequently than DRAB1. Both sand and silt-sized grains were present, predominantly quartz and volcanic glass (**Figure 8.31** and **8.32**). Both the sand-sized grains and volcanic glass appeared angular. The grains were fairly random in orientation and tended to be isolated from one another, being embedded within the matrix. Several large, isolated grains could also be observed within the more granular portion of the sample, ranging between ~450 to 870 µm in size (**Figure 8.33** to **8.35**), and showed various degrees of weathering. A hypothesised example of blocky feldspar was also identified (**Figure 8.34**). An unidentified blocky grain was also identified (**Figure 8.36**) that appeared to have a foliated structure, similar to that of the halloysite books identified in TV1 and TV2. I hypothesise this grain is either a blocky feldspar grain with identified cleavage planes, or a mica grain with foliated cleavage planes.

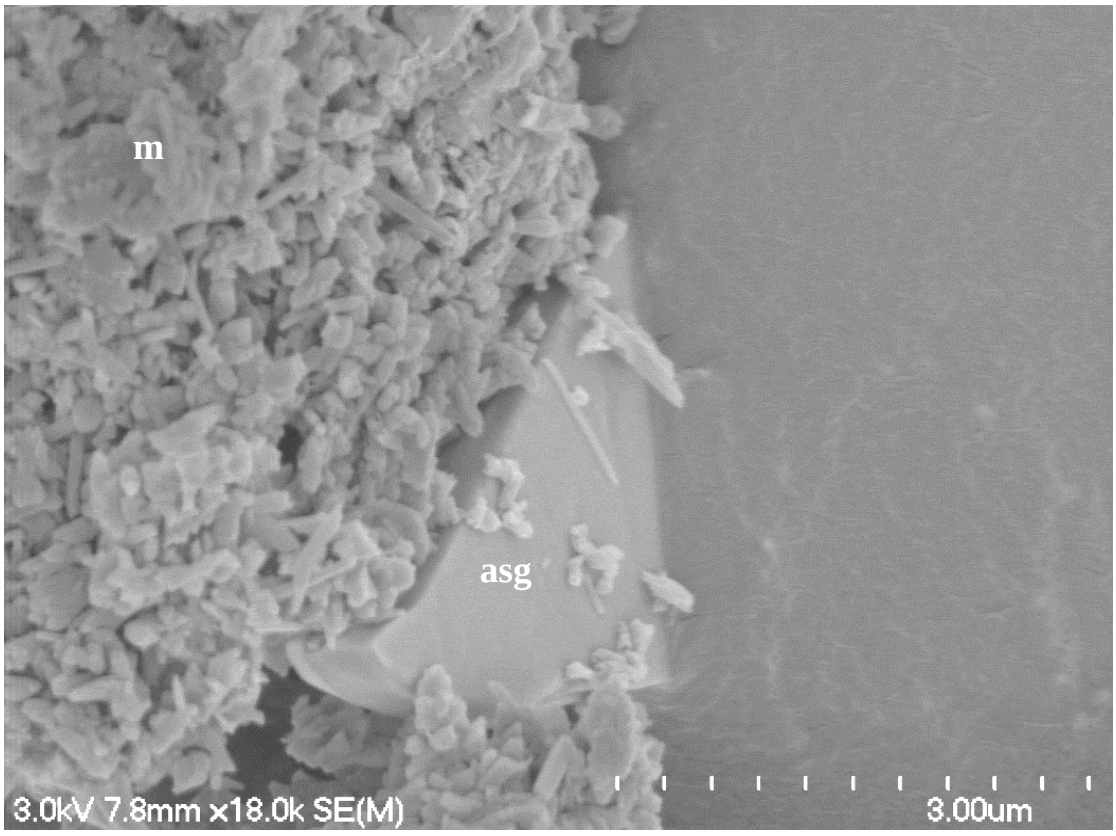

Figure 8.31. SEM image showing the presence of an angular sand-sized grain (asg) embedded within the clay-sized matrix (m). The quartz grain measured 3.1 µm in length, and 1.8 µm in diameter.

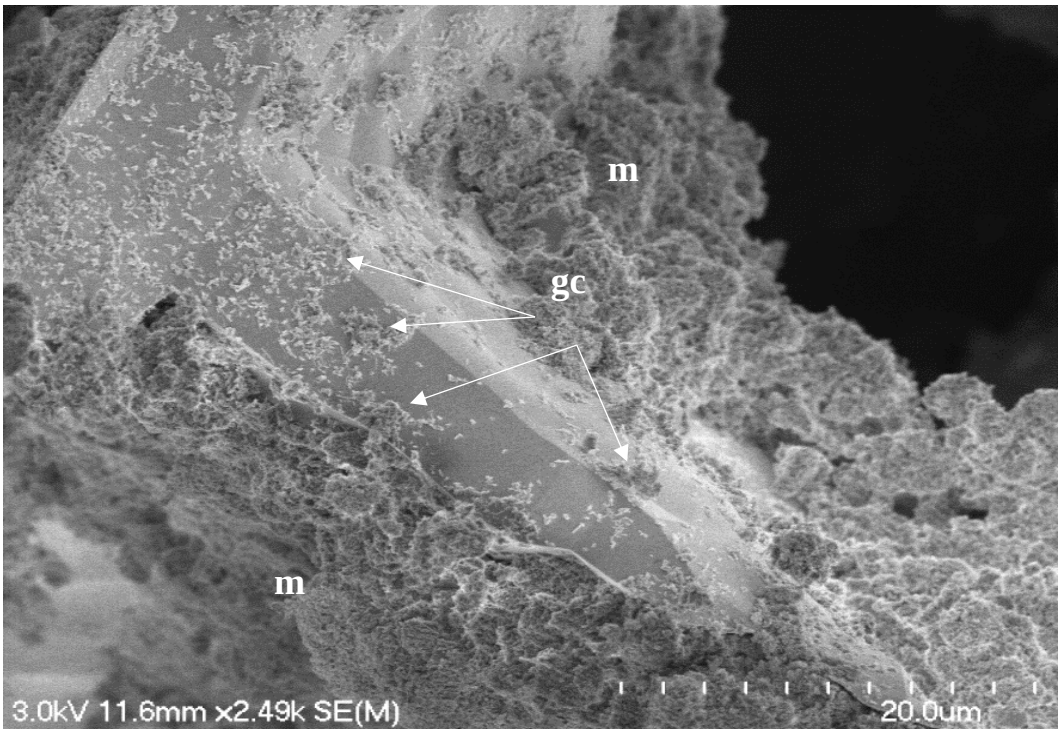

Figure 8.32. SEM image depicting a large sand-sized grain embedded within the clay-sized matrix (m). The surface of the grain was also observed to be heavily covered with grain coatings (gc). The grain appears to be a portion of a Y-shaped glass shard, a characteristic form of glass observed in pyroclastic materials.

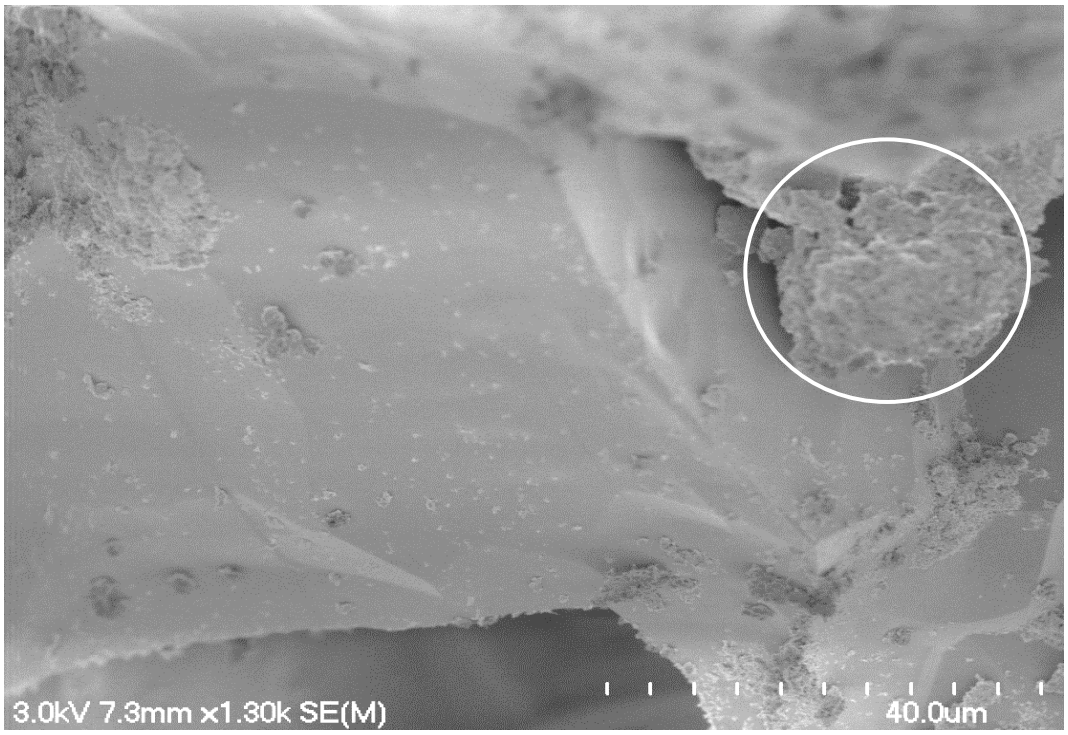

Figure 8.33. SEM image depicting the presence of a large sand grain fragment, partially covered with clay-sized matrix. Note the presence of a clay microaggregate (denoted by white circle) present upon the surface of the grain.

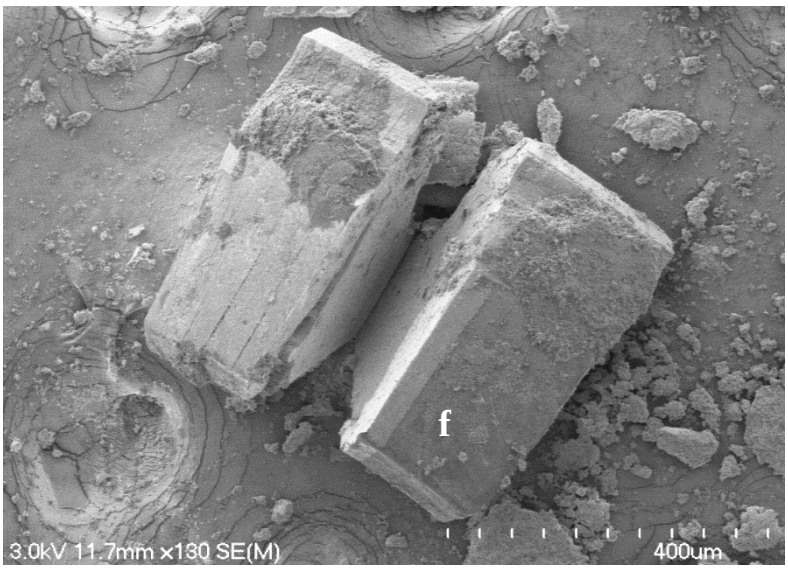

Figure 8.34. SEM image showing a hypothesised feldspar (f) grain identified within the more granular portion of the TV1 sample. This grain is extremely large in size (458 µm), and appears to have split down the middle as a result of sample preparation.

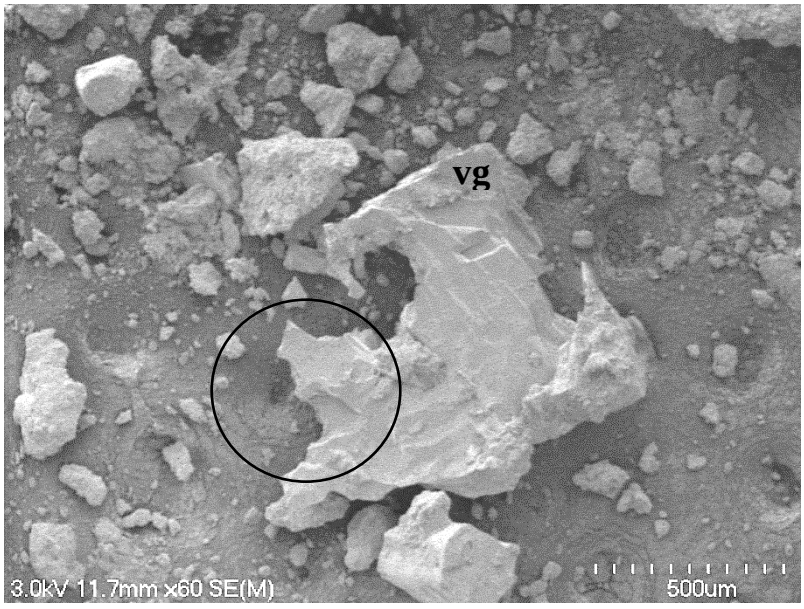

Figure 8.35. SEM image depicting a highly weathered isolated volcanic glass grain (vg) within the TV1 sample. This grain shows cleavage planes upon the surface and shows gaps (denoted by circles) that appear to have contained material that has since weathered away. The grain measured ~870 µm in length, and ~830 µm in width.

Figure 8.36. SEM image depicting a large, blocky grain identified within the more cohesive portion of the TV1 sample. The grain is 180 µm in diameter, and appears to be foliated, similar to the book formations identified in TV1 and TV2. The grain is also finely covered in grain coatings across the exposed surfaces. This grain is hypothesised to be micaceous.

8.3.2.2 Elementary particle arrangements

8.3.2.2.1 matrix

The groundmass making up the TV1 samples tended to be diverse in morphologies (**Figure 8.37** and **8.38**). The interactions of the polygonal spheres, irregular plates and tubules made it somewhat challenging to define explicit point to point contacts.

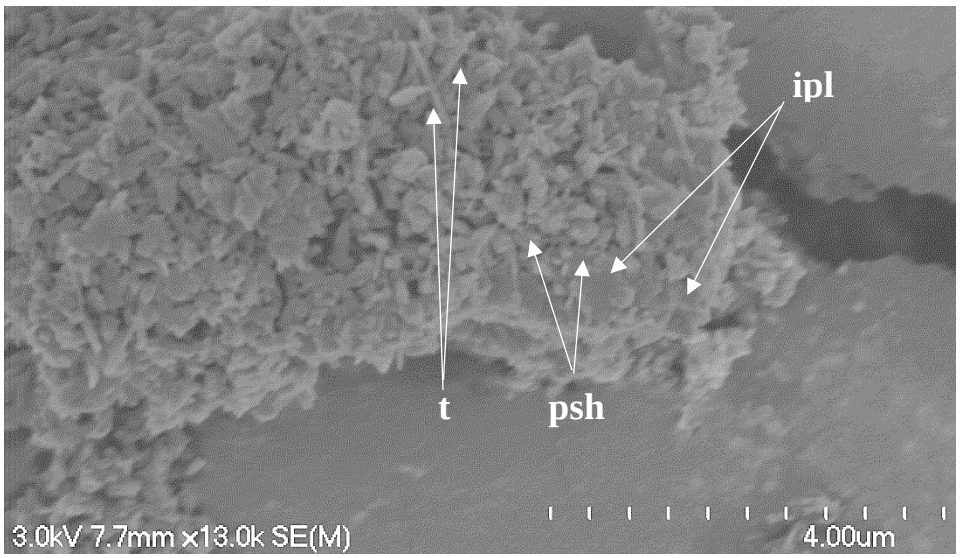

Figure 8.37. SEM image showing an example of the matrix making up the TV1 samples. Note the subdued tubule (t) contacts, covered and connected with irregular plates (ipl) and polygonal spheroids (psh).

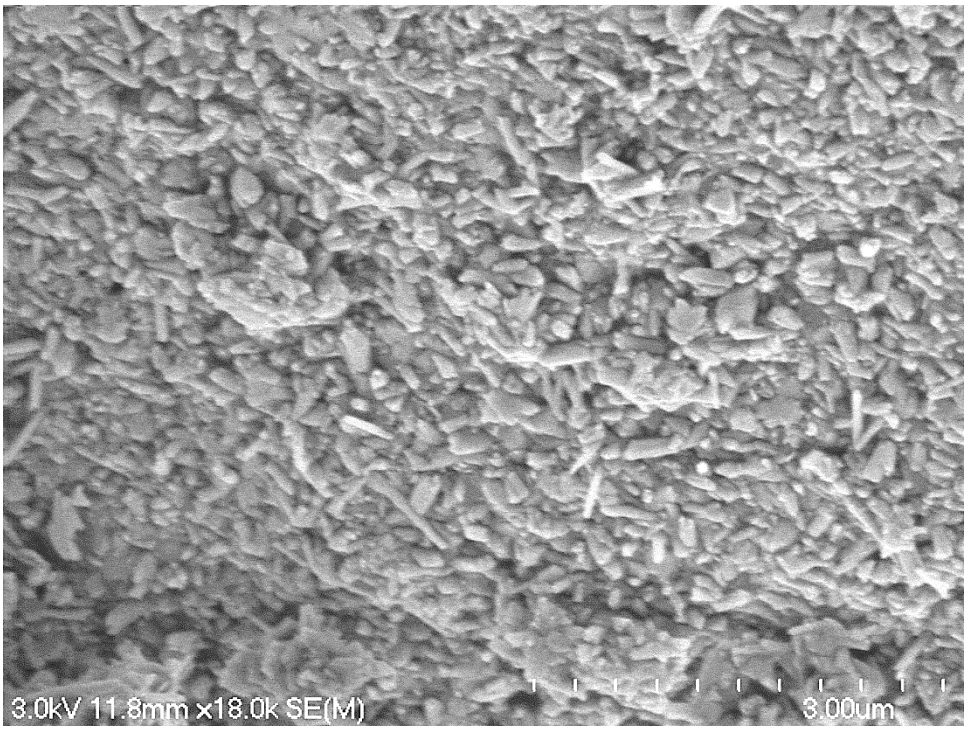

Figure 8.38. SEM image depicting the interactions of the clay-sized matrix dominating the TV1 samples.

8.3.2.2.2 Microaggregates

Two main microaggregate features existed; individual clay assemblages, in addition to hypothesised halloysite books. The clusters of clay minerals tended to be made up of the same material as the clay-sized mineral matrix. The boundaries of these microaggregates were irregular and were difficult at times to identify (**Figure 8.39**). The halloysite books could be seen embedded within the clay-sized matrix (**Figure 8.40**) and were rarely identified within TV1, but more than that of DRAB1. The books tended to not have a dominant orientation, and could be seen in singular formations, and in close contact with one another in parallel edge to edge (EE) contacts.

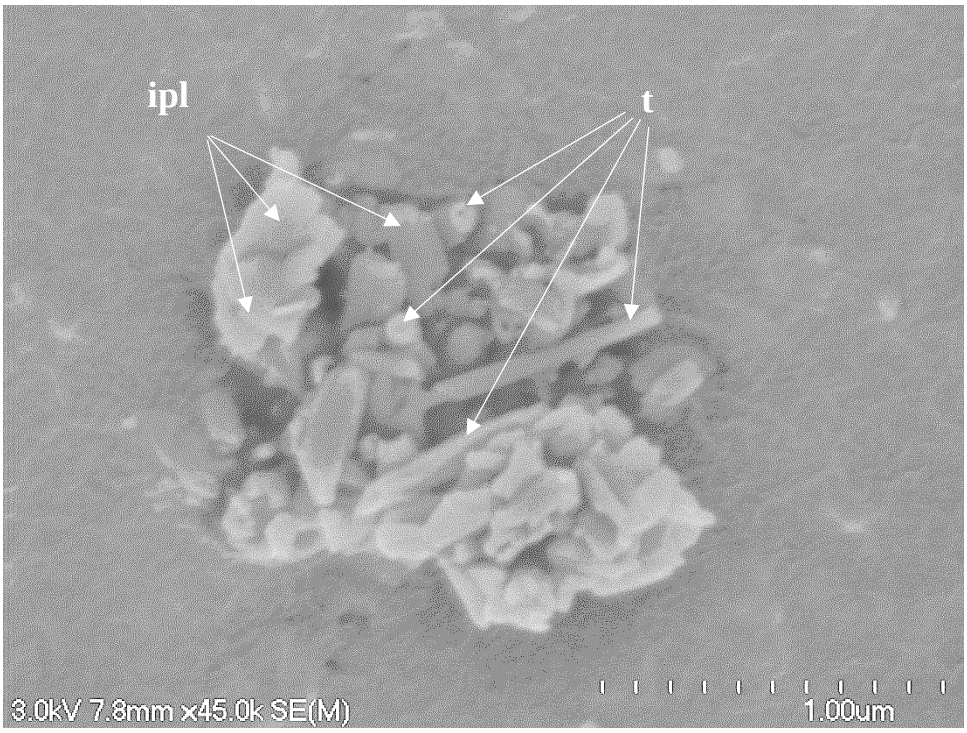

Figure 8.39. SEM image showing an example of the clay-sized microaggregates present within the TV1 samples analysed. Note the interactions between the halloysite tubules (t) and irregular plates (ipl) in this case. The microaggregate measures 1.57 μm in length, and 1.42 μm in diameter, making it clay-sized.

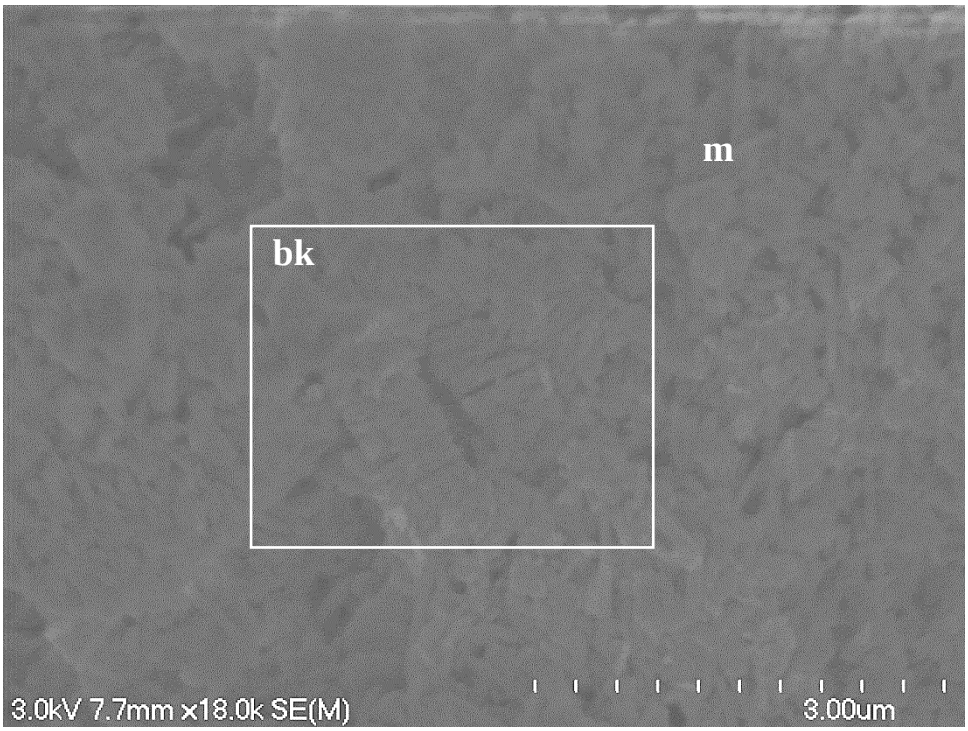

Figure 8.40. SEM image showing potential 'book' morphologies embedded within the clay-sized matrix (m). The 'book' morphologies (bk) represent multiple halloysite plates stacked in a face to face (FF) arrangement with one another (indicated by white square). The book formation measured 1.3 μm in length, and 0.6 μm in diameter.

8.3.2.3 Overall particle associations

The associations in TV1 generally showed larger grains embedded within a surrounding clay-sized matrix, with the clay matrix lapping up the sides of the larger grains. The grains also tended to have minimal grain coatings upon the surfaces of the cut areas (**Figure 8.31** and **8.33**).

The books were seen to be deeply embedded and somewhat covered by the clay sized matrix and tended to be more covered in grain coatings. This is potentially indicative of the general location halloysite takes within the samples. The connector assemblages observed between these grains were populous, holding the grains within the matrix (**Figure 8.41**).

The microstructures of the TV1 samples were dominated by irregularly shaped microaggregates, some blocky book formations, silt and sand sized grains, and clay-sized groundmass dominated by tubes, smaller irregular plates and some polygonal spheres (**Figure 8.42**).

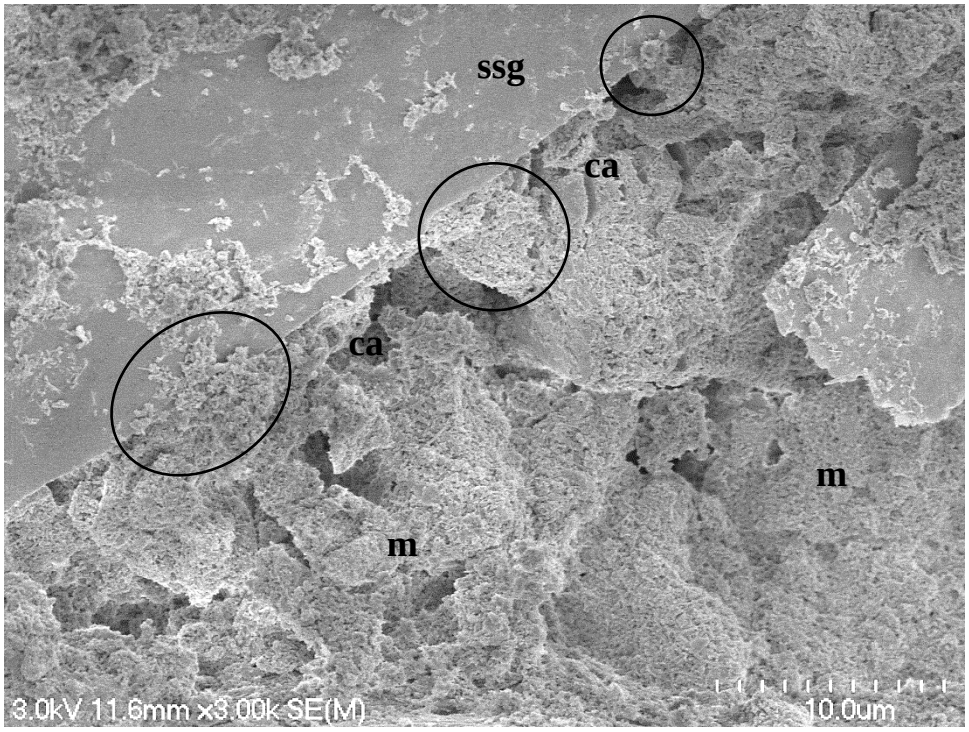

Figure 8.41. SEM image depicting a large sand sized grain (ssg) embedded within a dense clay sized matrix (m). A number of clay connector assemblages (ca) can be identified, denoted by the black circles.

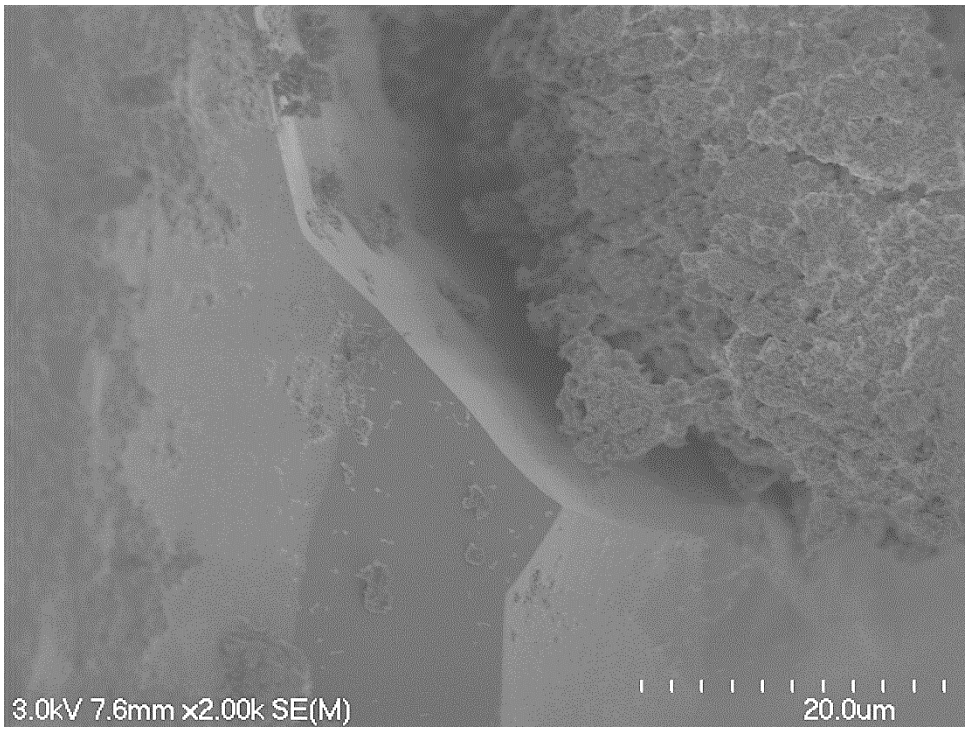

Figure 8.42. SEM image showing the presence of the clay-sized matrix lapping at a large grain, subangular in shape.

I hypothesise that TV1 displays a continuous matrix structure, with the halloysite tubules, plates and spheres making up the basis of the microstructure, and allowing for the embedment of larger grains within.

8.3.2.4 Pore sizes and shapes

The TV1 samples analysed were found to have a porosity of 41 %. This porosity could be observed in the SEM imagery, which showed an open fabric (**Figure 8.43** and **8.44**). The samples contained a large number of irregularly shaped clay minerals and angular grains, and their open structure due to dominant edge to edge (EE) contacts allowed for the occurrence of multiple pores between individual grains and aggregates. These pores were typically between 0.1 and 0.3 μm in size, thus classifying the pores as ultra to micro-pores, usually less than 1 μm in size. Some larger pore spaces could be seen however, likely occurring as a result of material collapse (**Figure 8.45**).

The connectivity of the pores was challenging to determine however, but based upon the observation of the open, loose structure of many of the TV1 materials analysed, an assumption can be made that the likelihood of pores being interconnected is high.

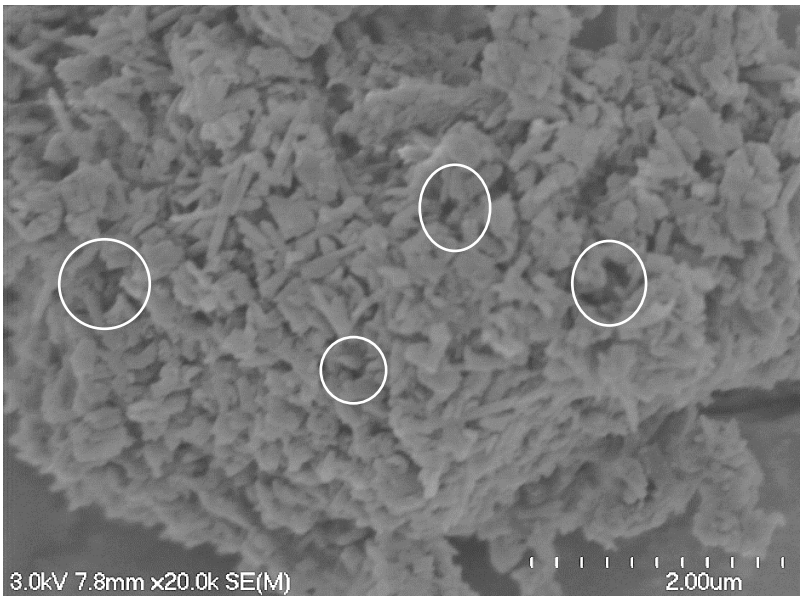

Figure 8.43. SEM image showing the presence of pores within the TV1 samples within the matrix. These pores typically range from 0.12 to 0.47 μm in size, classifying them as micro-pores.

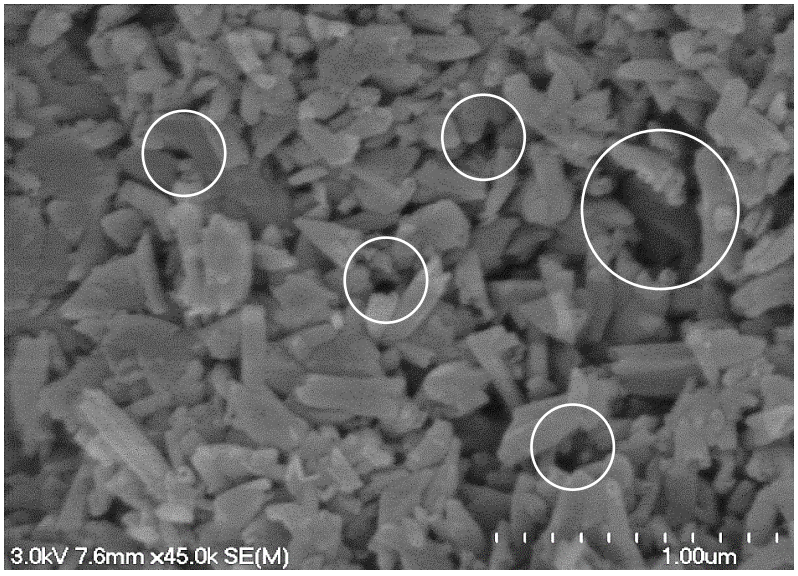

Figure 8.44. SEM image showing the presence of pore spaces within the clay-sized matrix. The pores measure between 0.08 and 0.24 μm in size, indicated by white circles. These sizes class the pores as ultra- to micro-pores.

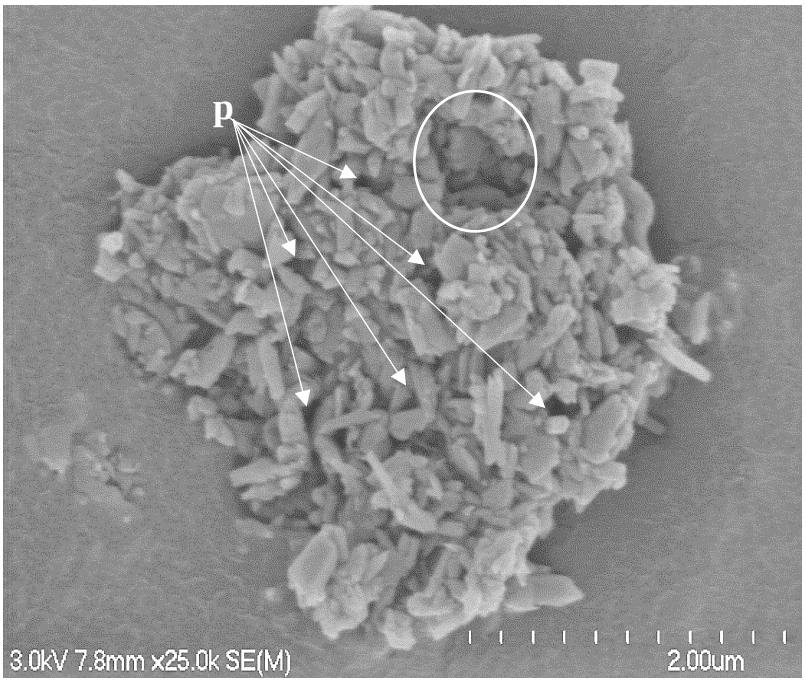

Figure 8.45. SEM image showing the presence of a number of pores (p) within an individual clay microaggregate, with a large pore being observed to the top right of the aggregate (denoted by white circle). This pore was measured to be 0.63 μm in size, still classifying it as a micro-pore.

8.3.3.1 Elementary particle associations

8.3.3.1.1 Clay minerals

Like DRAB1 and TV1, TV2 had a combination of interacting halloysite morphologies including tubules, irregular plates, and polygonal spheres (**Figure 8.46**). The different morphologies interact with one another in a similar manner to DRAB1, with the tubules (between 0.15 and 1 µm in size) encouraging a loose fabric by the dominance of face to edge (FE) and edge to edge (EE) contacts. The open structure is infilled with polygonal spheres (between 0.1 and 0.15 µm) and small irregular plates (between 0.2 and 0.4 µm) in the gaps. The spheres and plates had no definite orientation, and tended to contact the tubules. Small irregular plates and tubules of differing sizes were most common in TV2, with small spheroids apparently being more common in this sample compared with DRAB1 and TV1. The plates are generally arranged in race to face (FF) contacts upon one another, and the spheroids dominantly showing EE contacts. Identifying the exact orientations and contacts of the spheroids was again challenging due to the shape and nature of the morphology (**Figure 8.46** and **8.47**).

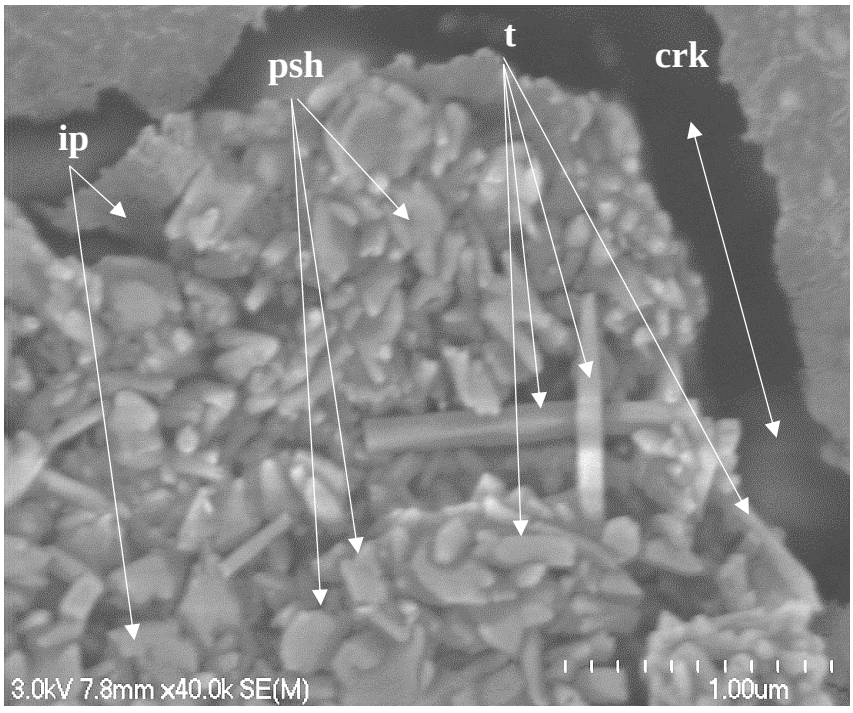

Figure 8.46. SEM image showing the interaction of multiple halloysite morphologies together to produce the clay-sized matrix. Note the presence of irregular plates (ipl), tubules (t), and polygonal spheroids (psh). Observe the crack (crk) produced from desiccation as a direct result of sample preparation.

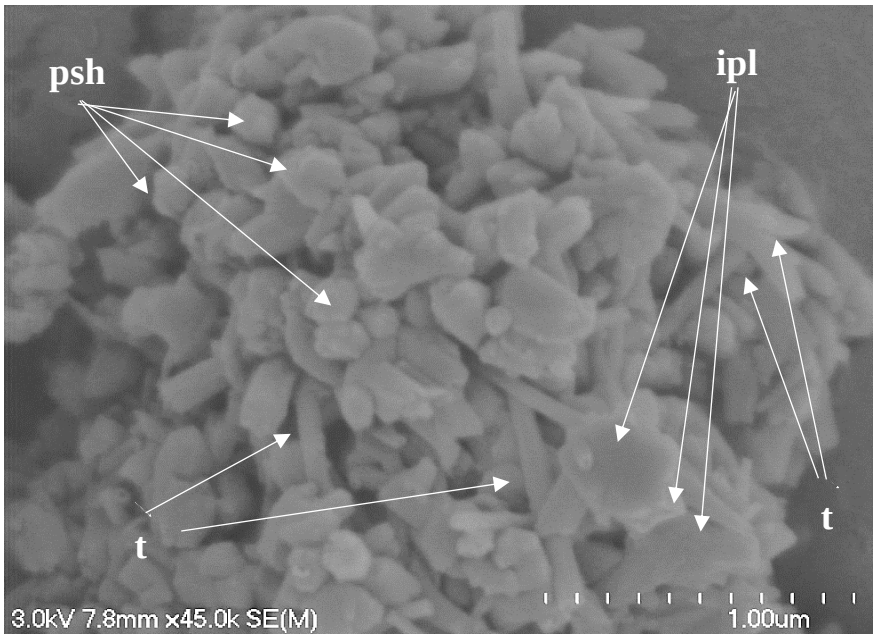

Figure 8.47. SEM image depicting the halloysite morphologies interacting with one another within the TV2 samples. Note the dominance of EE contacts for the tubules (t), FF contacts for the plates (ipl), and the general EE contacts of the spheres (psh). Identified globular arrangements of spheroids show closer arrangements however, but the identification of faces is challenging, therefore specific contacts are not easy to identify.

8.3.3.1.2 Grains

TV2 tended to have more grains isolated from the clay-sized groundmass compared with TV1 and DRAB1, indicative of the more granular nature of TV2 (**Figure 8.48** to **8.52**). These grains were relatively clean on the exposed surfaces, with only small amounts of surface matrix materials present upon the grains (**Figure 8.49**). The main grains observed appeared to be angular volcanic glass that had experienced differing degrees of weathering, and subangular quartz crystals (**Figure 8.50** and **8.51**). These crystals and glass tended to represent the silt and sand-sized grain fraction. Some grains were found to be embedded within the clay-sized matrix, particularly in the more cohesive portions of the sample (**Figure 8.53**).

A large square grain was identified within the more granular portion of the sample (**Figure 8.54**). This square fragment appeared to have a similar structure to that of the halloysite books identified. This structure was highly defoliated and porous, with large gaps between the individual layers. This unidentified mineral was generally isometric in size, measuring ~ 100 µm in diameter and length. The grain appears to resemble a large feldspar grain, with cleavage planes (**chapter 2**).

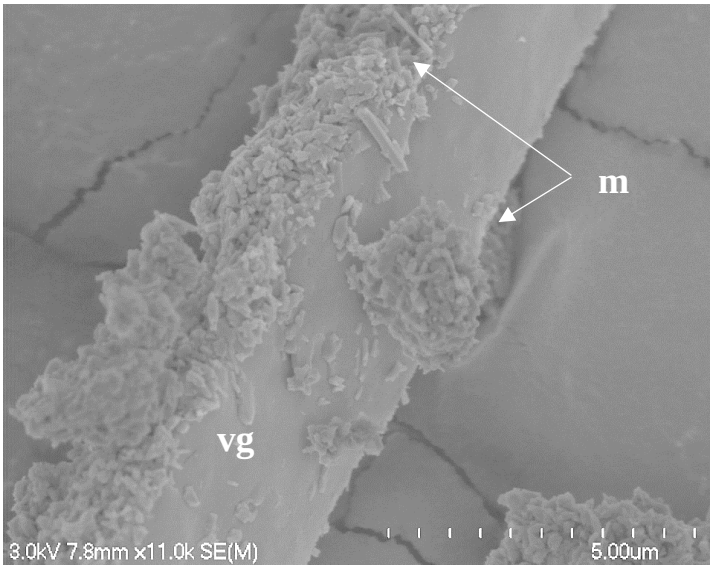

Figure 8.48. SEM image showing an example of a volcanic glass (vg) grain within the TV2 material. Note the relatively clean surface, with very little clay-sized matrix (m) upon the surface of the grain.

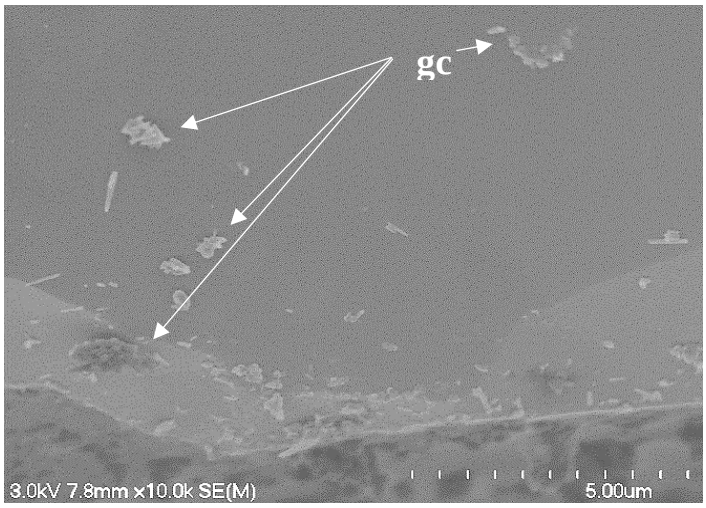

Figure 8.49. SEM image showing an example of the close-up texture of a hypothesised volcanic glass grain. Note the general absence of clay-sized matrix surrounding or embedding the grain, only very limited grain coatings (gc) are scattered upon the grain surface.

Figure 8.50. SEM image showing a large grain of slightly weathered volcanic glass (wvg), 313 μm in length and μm in diameter. Note the presence of small clay-sized microaggregates upon the surface of the grain (highlighted by white circles) and the presence of potential vermicular book formations to the left of the image (denoted by white circles). These were isolated from one another.

Figure 8.51. SEM image showing a volcanic glass shard isolated from any clay-sized matrix within the TV2 materials. The glass grain measures 306 μm in length, and 193 μm in diameter.

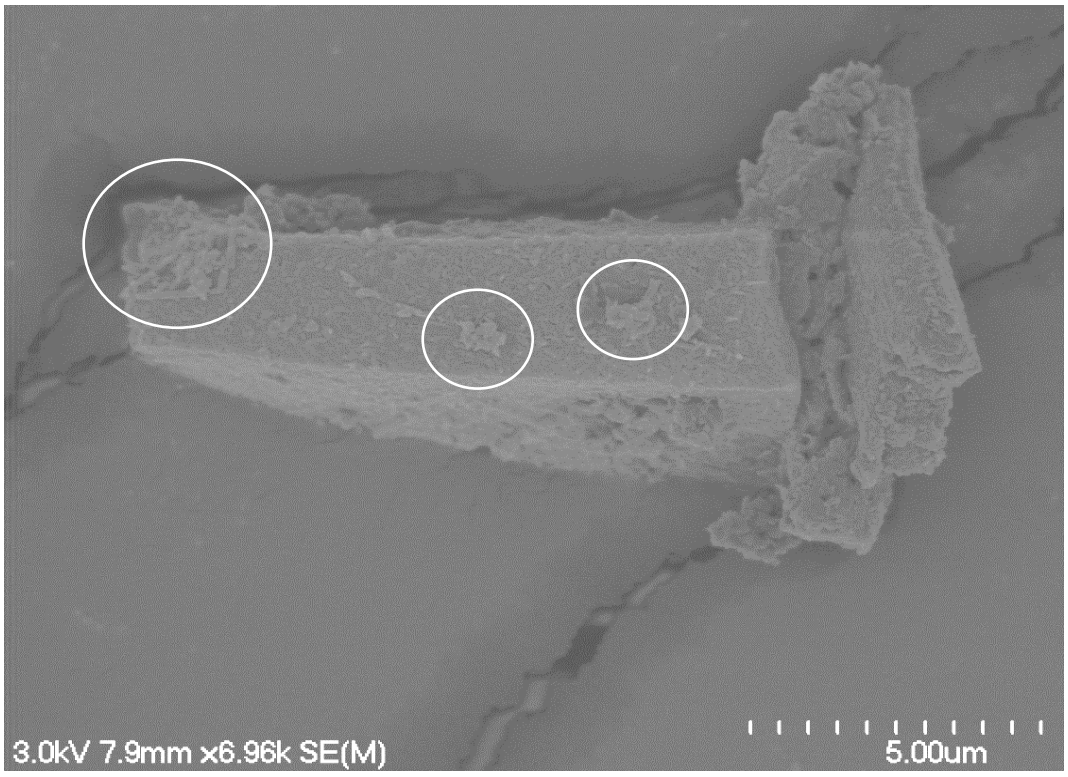

Figure 8.52. SEM image showing a sand sized grain, 11.3 μm in length and 7.8 μm in diameter. The presence of clay-sized microaggregates and matrix can be observed, denoted by white circles.

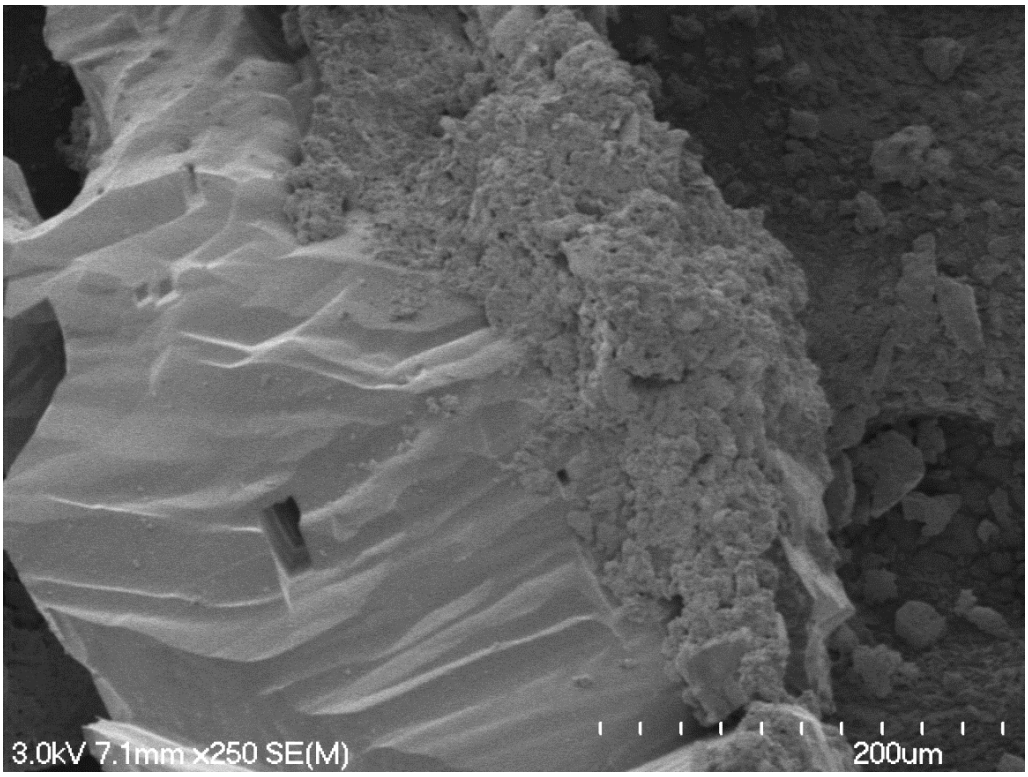

Figure 8.53. SEM image depicting a volcanic glass grain with distinctive conchoidal fracturing upon the surface, Note the presence of clay-sized matrix (m) coating the right hand side of the grain. Also of interest is the rectangular pore shape within the middle of the grain, measuring 40 µm in size. I hypothesise this space could have occurred due to preparation of the sample leading to the removal of a crystal that was present within the glass shard.

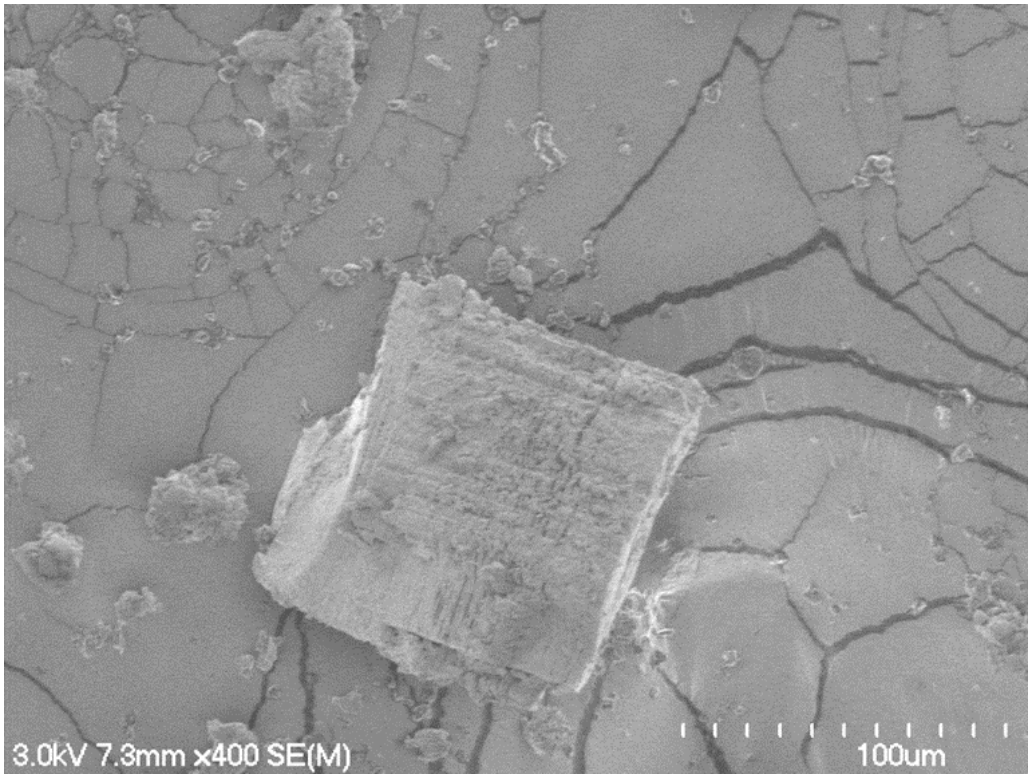

Figure 8.54. SEM image showing an overview of the unidentified isometric mineral found within the more cohesive portion of TV2. This mineral measured ~100 µm in length and ~100 µm in diameter.

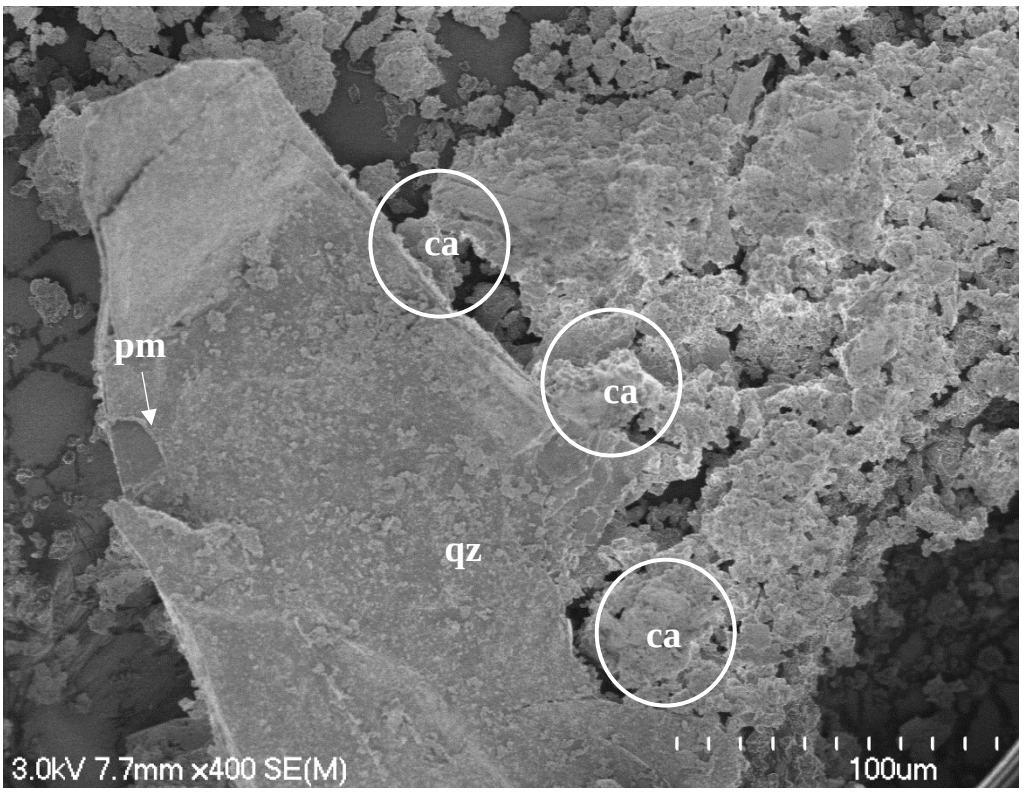

Figure 8.55. SEM image showing the interaction between a large grain, thought to be quartz (qz), and some clay-sized groundmass which appears to be disturbed. Note the gaps between the grain and matrix, indicating a loose connection between the interacting structures, and only few connector assemblages (ca). A pluck mark can also be identified upon the grain (pm), likely occurring as a result of sample preparation.

8.3.3.2 Elementary Particle arrangements

8.3.3.2.1 Matrix

The groundmass in TV2 consisted of predominantly clay-sized halloysite clay minerals of different morphologies. When identified, the tubules interacted with both FF and FE contacts, whilst the plates mainly interacted with FF contacts. The spheroids tended to dominantly interact with EE contacts. It was likely that more contact types existing within the materials, but could not immediately be identified. Connector assemblages were also observed (**Figure 8.55**).

8.3.3.2.2 Microaggregates

The main microaggregates present within TV2 were similar to those of TV1. Typically, small clusters of clay-sized material could be observed, in addition to halloysite book formation.

The clay microaggregates tend to be isometric in shape, generally measuring ~ 1.5 μm in size. The microaggregates are all less than 10 μm in size (**Figure 8.56** and **8.57**).

Halloysite book formations were common in TV2, and were found most frequently in these samples, as compared to DRAB1 and TV1. The book formations were generally vermicular in shape, and both fully formed and partially formed formations could be observed (**Figure 8.58**, **8.59**, **8.60** and **8.61**).

These books typically did not show any dominant orientation, rather being isolated from one another and connected to small aggregates of clay-sized matrix (**Figure 8.58**). No evidence of connection between halloysite book formations could be identified within the TV2 samples observed.

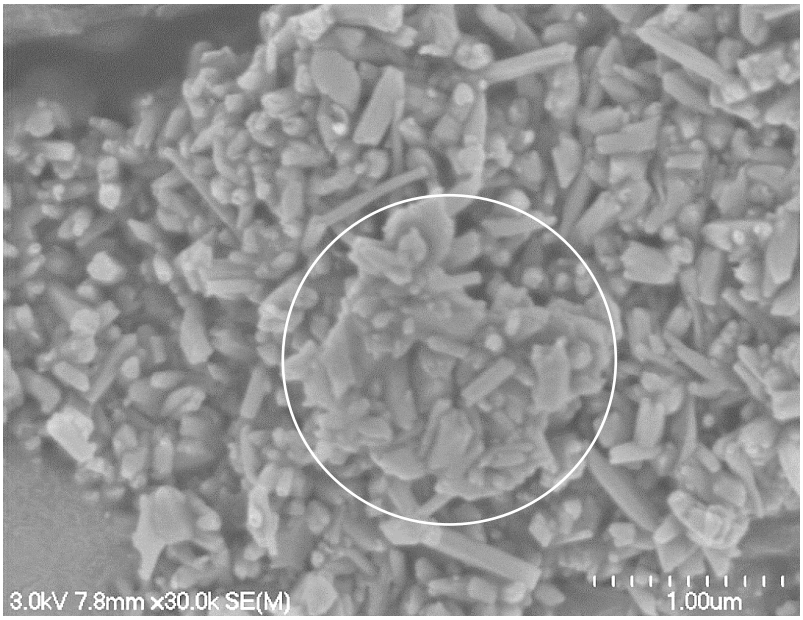

Figure 8.56. SEM image showing a typical clay microaggregate structure found within the TV2 samples analysed. The microaggregate consists of interacting halloysite tubules, polygonal spheres and irregular plates.

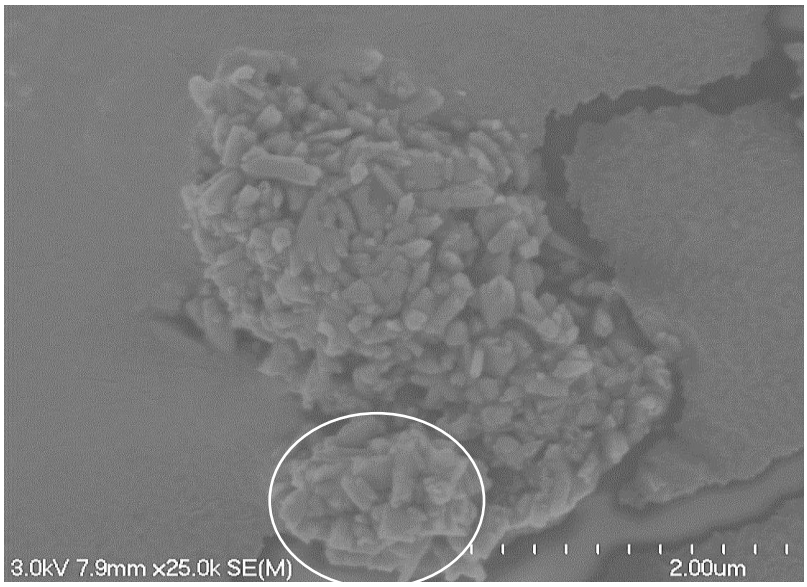

Figure 8.57. SEM image highlighting the presence of an identifiable clay microaggregate within a larger clay-sized matrix portion of TV2 material. The microaggregate is isometric, measuring ~5 μm in length and ~5 μm in diameter.

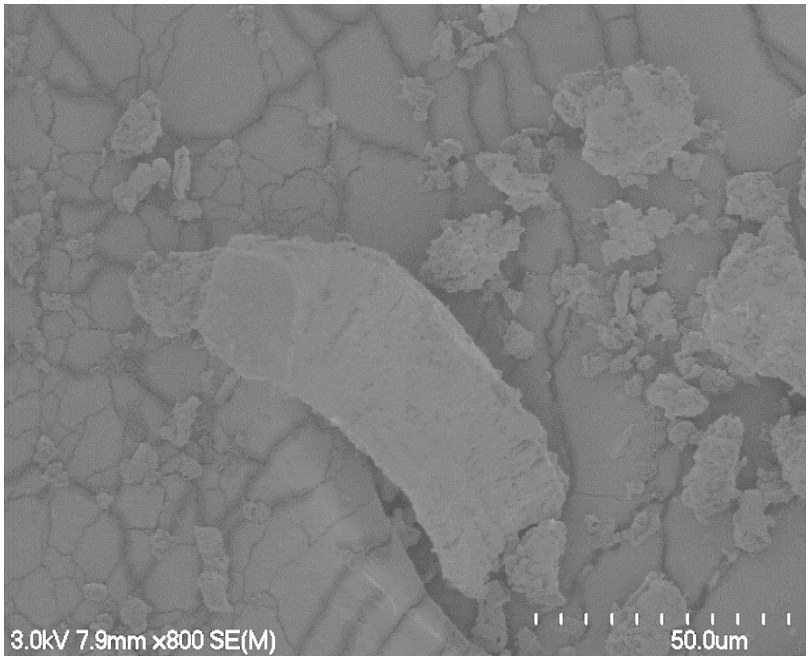

Figure 8.58. SEM image showing a typical vermiform book formation within the TV2 material analysed. Note the attached clay microaggregate to the base of the book, likely attached through clay connectors. The book measured 84 μm in length and 31 μm in diameter.

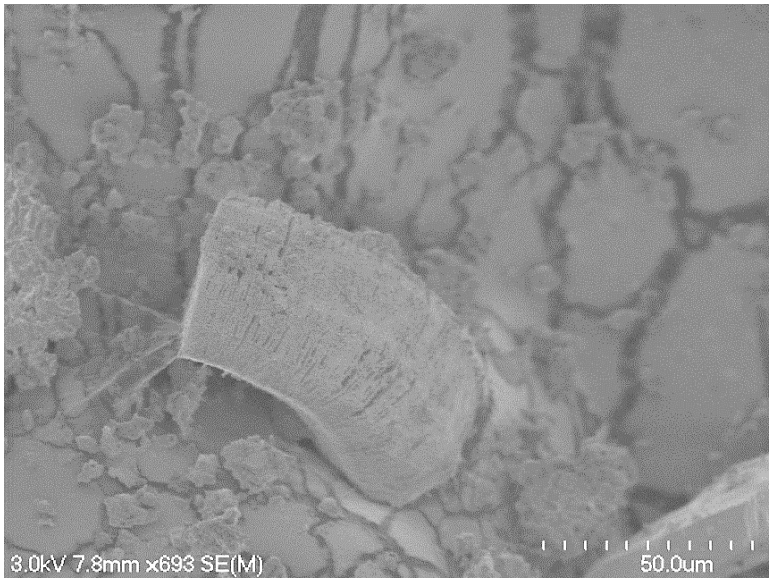

Figure 8.59. SEM image showing another example of the vermiform book formations analysed within the TV2 samples. This book formation measured 82.1 μm in length and 41 μm in diameter.

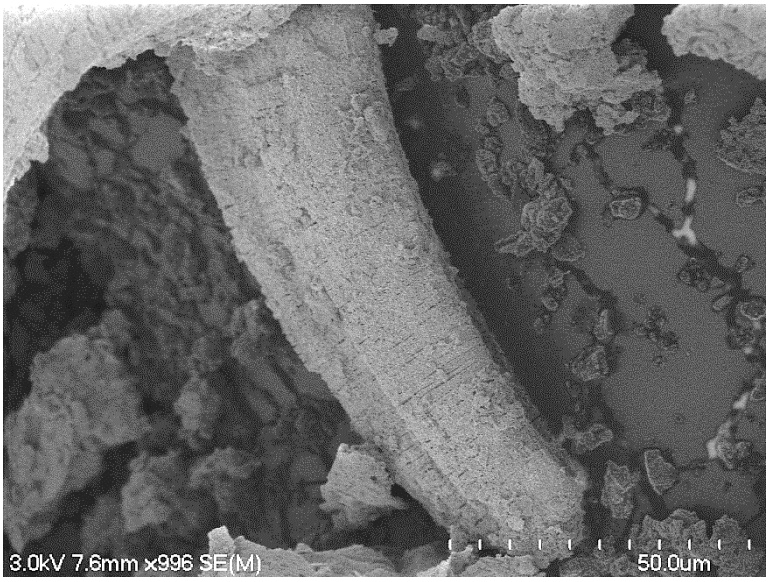

Figure 8.60. SEM image depicting a straighter halloysite book formation identified within TV2. Note the radiation out of some clay sized matrix to the top of the image, and apparent connection to more clay-sized material at the bottom of the image. The book formation measured 105 μm in length, and 31 μm in width.

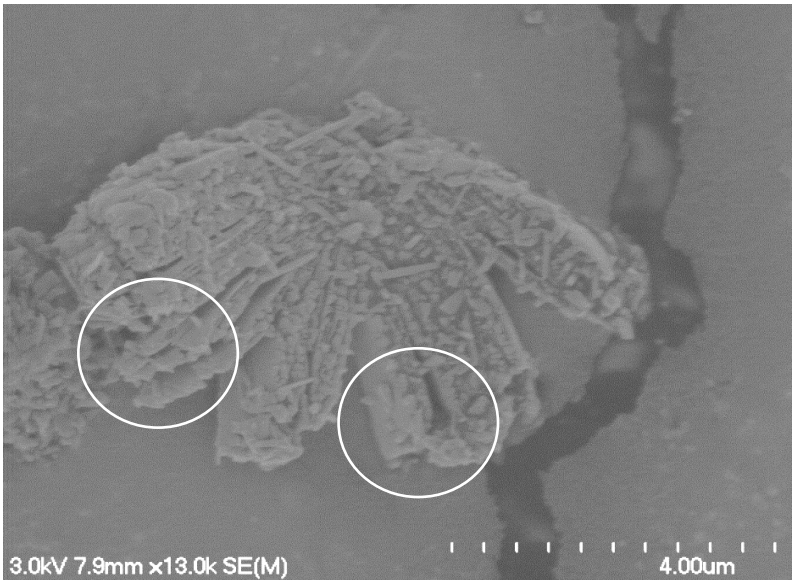

Figure 8.61. SEM image depicting a potential defoliated or partially formed halloysite book. Note the characteristic defoliated layers at the edge of the formation, as indicated by the white circles. The defoliated structure measured 7.2 μm in length and 4.8 μm in diameter. This formation is very heavily covered in clay-sized matrix.

8.3.3.3 Overall Particle associations

The overall particle associations identified within TV2 differ from those of DRAB1 and TV1. Whilst it was common to observe grains embedded within a clay-sized groundmass in DRAB1 and TV1, grains tended to be largely isolated from the groundmass, with only light grain coatings present upon the grain surface (**Figure 8.51**). Some embedded grains were identified, however these were much less common.

The books were typically observed isolated from one another and were commonly seen radiating from small amounts of clay-sized groundmass surrounding some portions of the base of the formations (**Figure 8.58**, **8.59**, **8.60** and **8.61**). The books also tended to have some grain coatings upon them and experienced some defoliation at the edges of individual platy layers (**Figure 8.62**).

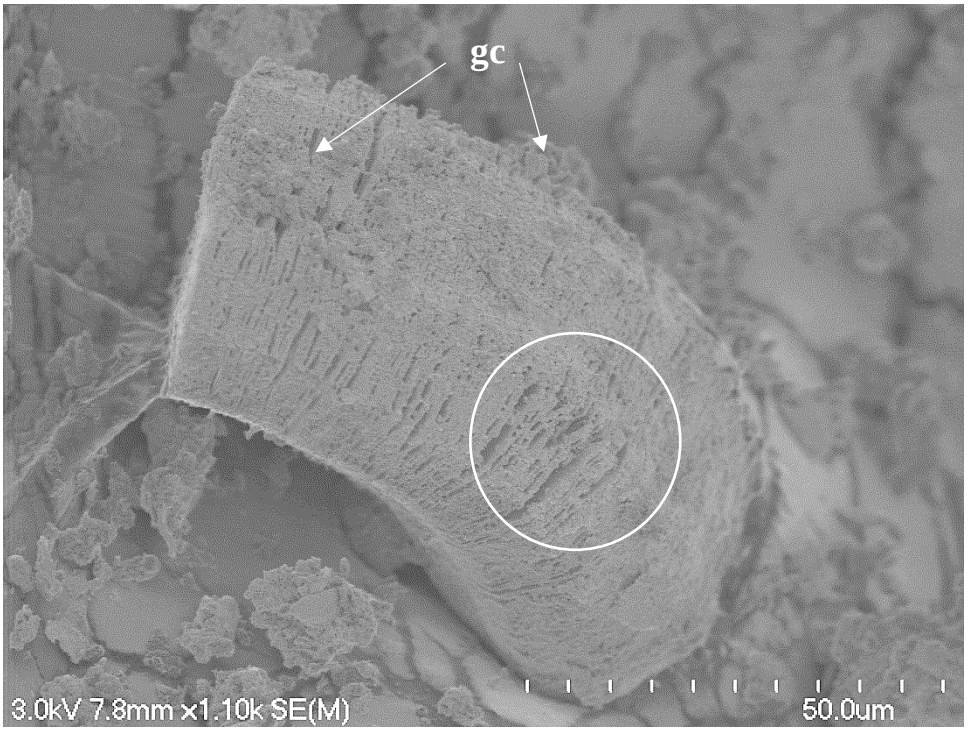

Figure 8.62. SEM image highlighting the defoliation of some of the individual plate layers making up the book formation (highlighted by white circle). Minor grain coatings (gc) can be observed upon the surface of the formation.

One book appeared to be in the process of formation (**Figure 8.61**). This formation process is hypothesised to occur following a short period of drying, where the plate formations shrink together to form a more book-like structure (Cunningham et al., 2016).

The grains and book formations also appeared to be larger than those identified in DRAB1 and TV1. This difference could relate to the degree of transport and sorting the samples have experienced, in addition to the particle componentry of the samples.

The connector assemblages seen holding the foliated layer structures together (**Figure 8.63**) measured between ~ 1 µm and ~2 µm in length. Weak connections were also identified between the apparent clay-sized matrix and larger grains in the more cohesive portions of the sample (**Figure 8.55**).

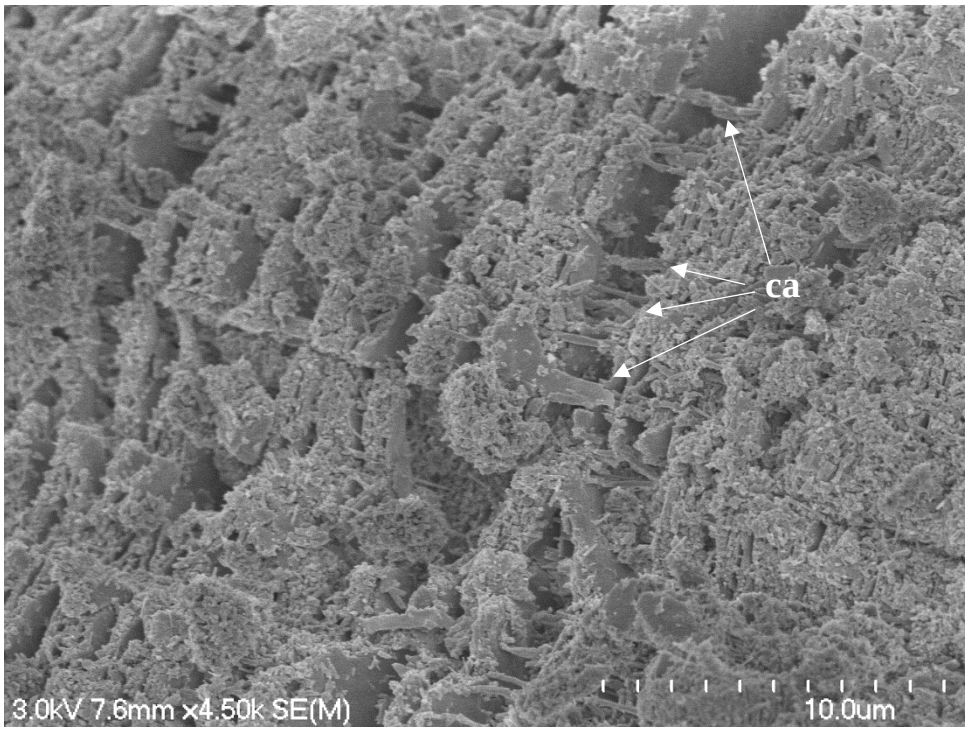

Figure 8.63. SEM image showing the extent and density of clay connector assemblages (ca) within the isometric mineral identified within TV2. These connectors measured between 1.1 µm and 2.3 µm in size. Note the highly foliated and porous nature of the mineral.

The combination of halloysite tubules, plates, spheroids and books dominated the groundmass of the TV2 samples analysed. The groundmass analysis is consistent with Beattie's 1990 definition of a continuous matrix. The large grains that were generally isolated were more consistent with a discontinuous matrix classification.

8.3.3.4 Pore shapes and sizes

TV2 had a high porosity (51 %). This can be observed within the SEM images of the microaggregates and clay-sized groundmass, which showed the open structure (**Figure 8.64** and **8.65**). The interactions of the differing halloysite particles results in loose contacts, producing

numerous small pores within the surface. These pores were typically less 5 μm in size, generally ranging between ~ 0.09 and ~ 0.4 μm, classifying them between ultra- and micro-pore sizes. Porosity was also identified within the halloysite tubules, identified by their hollow ends (**Figure 8.66**). These tubes were generally classed as ultra-pores, less than 0.1 μm in size. Porosity was also observed within the defoliated plates of the books, dominantly being identified as ultra-pores (**Figure 8.67**).

The true extent of the connectivity of the pores is unknown however, but the pores appeared to extend fairly deeply into the groundmass. The hollow halloysite tubules also appeared to extend quite deep into the microaggregates where they were identified. Similarly to TV1, the open structure made the likelihood of the pore spaces being interconnected higher (Wyatt, 2009).

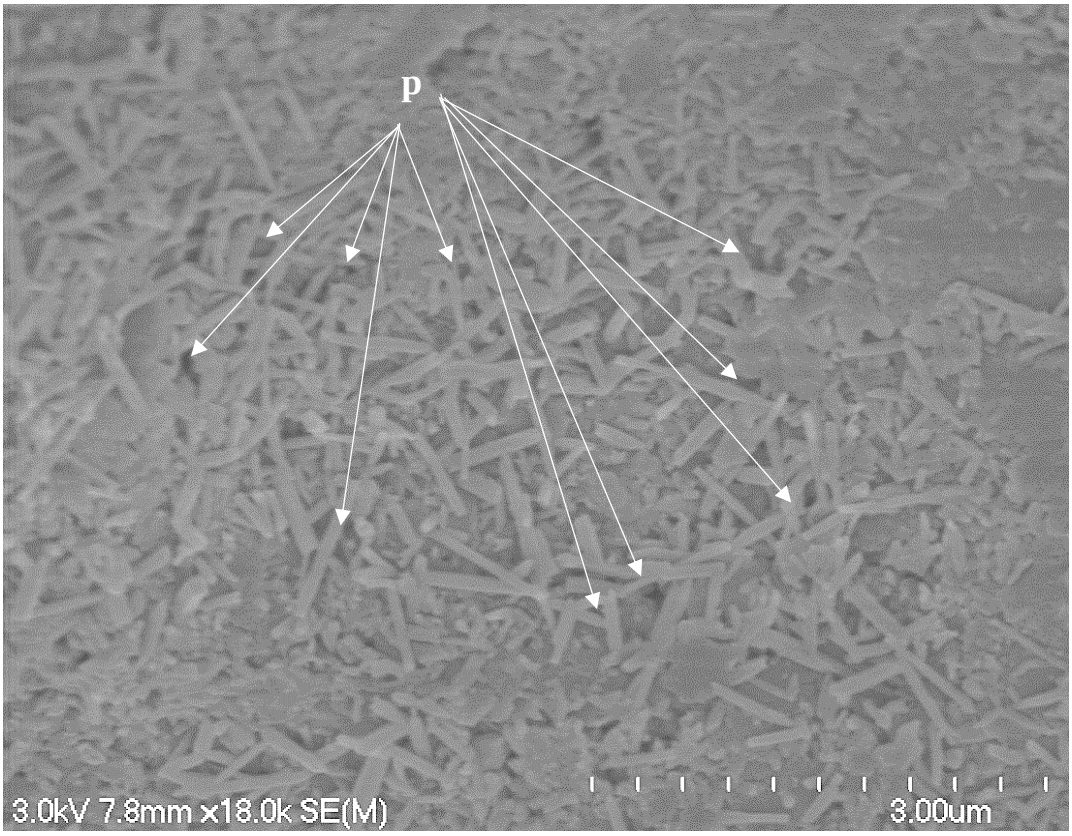

Figure 8.64. SEM image depicting the porous nature of the TV2 material. Pores are denoted by p, and range between 0.12 μm and 0.4 μm in size, classifying them as micropores.

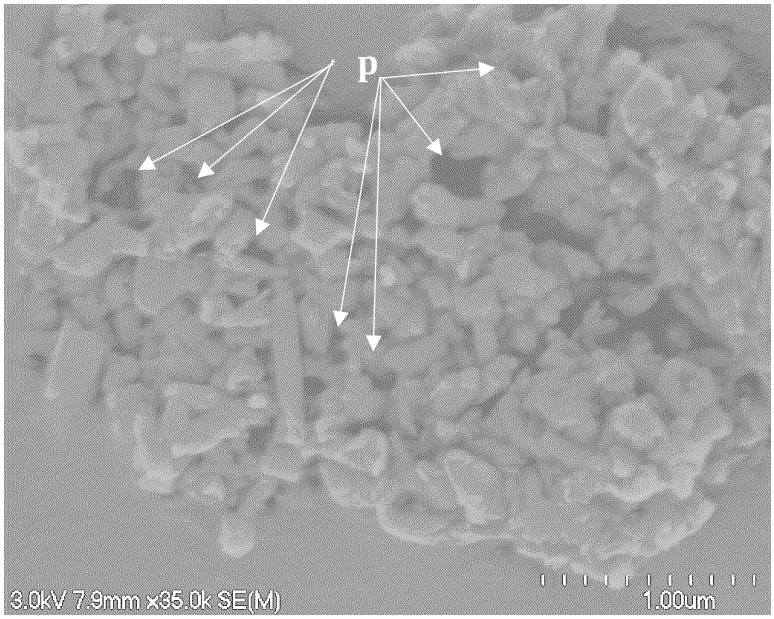

Figure 8.65. SEM image showing the porous nature of a clay microaggregate identified within the TV2 material analysed. The pores varied between 0.09 μm and 0.2 μm in size, classifying them as ultra- to micro-pores.

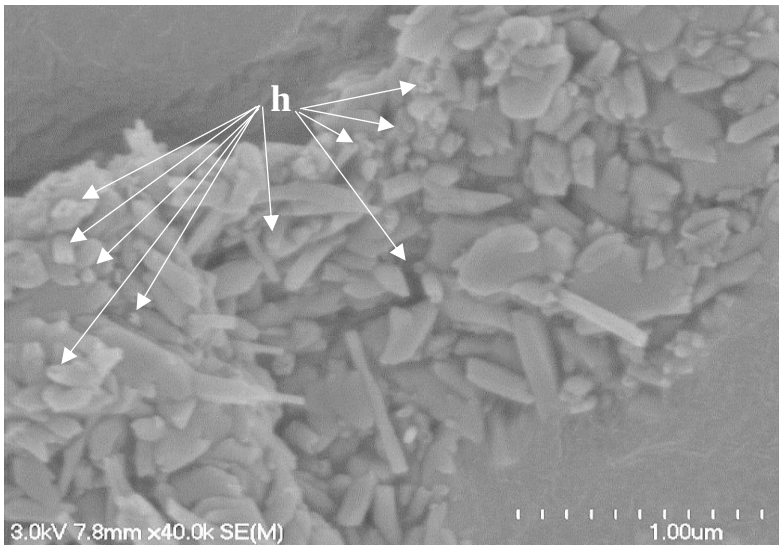

Figure 8.66. SEM image showing the extent of porosity within the halloysite tubules, as indicated by the hollow ends (h).

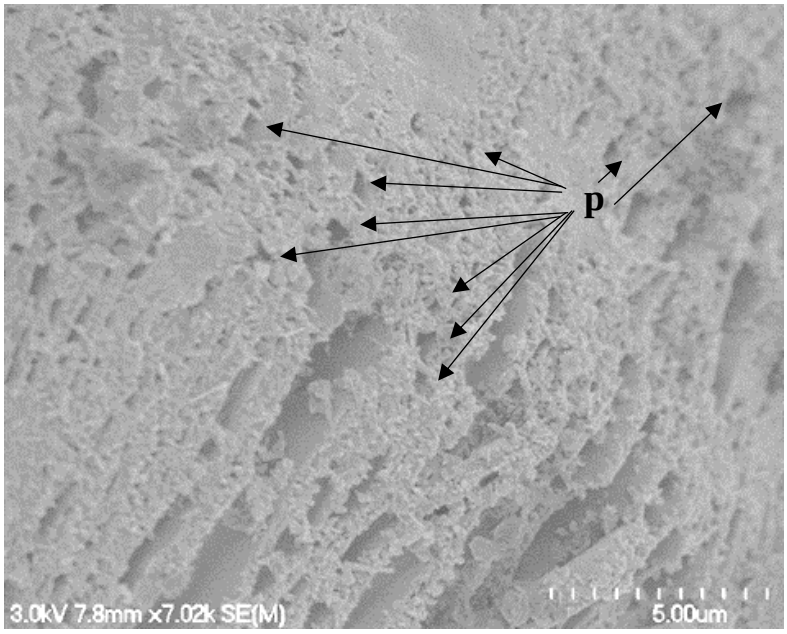

Figure 8.67. SEM image showing the extent of the porosity (p) identified within the foliated layers of the halloysite book formations. These pores were generally ultra to micro-pores in size.

8.4 Overall determination of microfabrics

The factors analysed for each of the samples throughout this chapter can in theory be used to determine the overall characteristic microfabrics of the samples. Historically, however, the microfabric is used to classify sedimentary materials into geometric classifications, which were often dictated by the history of formation (Huppert, 1986, 1987). Common modes of classification utilised by Huppert (1986) (**Table 2.6**) relate to sedimentary deposits, using geological history and geomechanical data relating specifically to the rock formation. I believe the samples in this study show sedimentary characteristics, therefore the classification can be used.

All three samples contained interacting halloysite morphologies which dominated the microfabric of the material. DRAB1 contained a combination of predominantly short tubules, hexagonal and irregular plates, and polygonal spheres. TV1 and TV2 had similar morphologies, but contained a greater abundance of long tubules compared with DRAB1, and also contained book formation. Larger silt and sand sized and grains were commonly seen embedded within the background matrix for DRAB1 and TV1. TV2 showed a greater abundance of isolated grains with very little clay matrix interactions, compared with the other two samples. Few clay connector assemblages were seen connecting the aggregates in all three samples, and typically showed an open microfabric.

The porosity of the samples were high, and pores were predominantly ultra to micropores which dominantly occurred between the clay minerals or within the clay-sized matrix. The hollow end of tubules also provided additional porosity, in the form of ultra-pores. The porosity of TV2 was significantly higher than that of DRAB1 and TV1 (67 %), and this was evident, with an abundance of pores within the microaggregates and the clay-sized groundmass. These pores were similar in size compared with TV1 and DRAB1, predominantly ultra to micropore in size.

The loose packing observed between the tubules, spheroids and plates results in loose contacts that were predominantly edge to edge (EE) and face to edge (FE) producing an open microfabric. However, some parallel face to face (FF) arrangements were observed for the tubules within the sample for DRAB1 and TV1, producing a denser degree of packing in these areas. TV2 appeared to have a greater dominance of FE contacts between tubules compared with the other samples, producing a more open microfabric structure.

DRAB1 and TV1 showed a continuous groundmass, evidenced by the lack of definable boundaries between differing grain size fractions within the material. TV2 conversely showed a discontinuous groundmass, as the silt and sand-sized grains could be observed in isolation from the more cohesive portions of the sample in many cases.

Taking into account these factors, I believe DRAB1 and TV1 show characteristics of a "matrix" structure (**Figure 8.68**), which has been observed in sensitive soil materials observed by Keam (2008) and Wyatt (2009). The characteristics of the samples are consistent between Huppert's 1986 definition of both microfabrics (Beattie, 1990). TV2, however, I believe differs from the other two samples, and shows a microfabric more consistent with "skeletal" to "matrix" arrangements (**Figure 8.68** and **8.69**).

A summary of the results from this chapter is presented in **Table 8.1**.

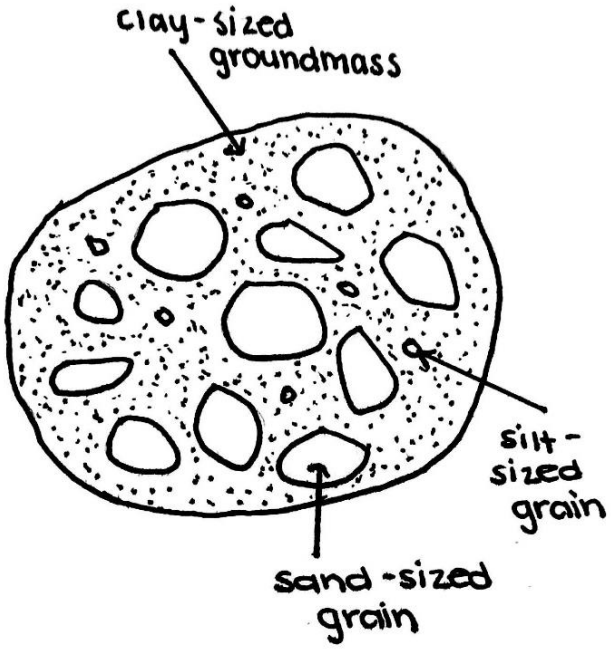

Figure 8.68. Simplified diagram depicting the general arrangement of a matrix microstructure, with silt and sand-sized grains being held within a dense clay-sized groundmass (Adapted from Beattie, 1990).

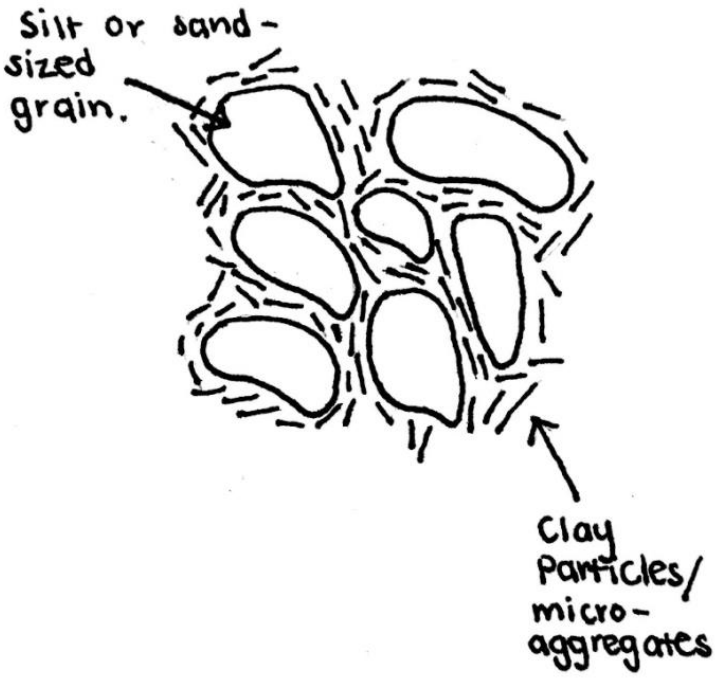

Figure 8.69. Simplified diagram showing the general arrangement of a skeletal microfabric, showing the interactions of the clay-sized matrix and the sand and silt-sized grains (Adapted from Beattie, 1990).

Table 8.1. Table summarising the microfabric classification derived from SEM analysis in the samples in this study.

Sample	Primary structural elements	Overall particle associations	Pore size (μm)	Pore size classification	Microfabric type
DRAB1	Dominance of clay-sized matrix materials, some silt and sand-sized grains.	Silt and sand-sized grains embedded within clay-sized matrix.	0.2 – 0.9	Micro-pore	Continuous matrix
TV1	Dominance of clay-sized matrix materials, some silt and sand-sized grains.	Silt and sand-sized grains embedded within clay-sized matrix.	0.1 – 0.3	Micro-pore	Continuous matrix
TV2	Clay-sized matrix and silt and sand-sized grains.	Silt and sand-sized grains isolated from clay matrix, or embedded within matrix	0.09 – 0.4	Ultra to micro-pore	Discontinuous skeletal and matrix

8.5 Summary of chapter

The SEM imagery produced determined halloysite to be the main clay mineral within the samples. A combination of tubules, spheroids, plates and vermicular ‘books’ were observed.

The interactions of the clay morphologies with one another, and the larger grains were analysed, with the most common interactions consisting of tubules predominantly laid in a subdued open structure with predominantly edge to edge contacts, with polygonal spheres and hexagonal to irregular plates. The plates identified within the materials tended to have face to face contacts, and could be seen to form into book formations, particularly in TV2. The spheroids identified were typically polygonal in shape and were predominantly interacting with one another in face to face and face to edge contacts. The characteristics of each sample were analysed and were related to characteristics of the ‘matrix’, ‘honeycomb’ and ‘skeletal’ sedimentary microstructure characteristics identified by Huppert (1986).

Chapter 9
Discussion

9.1 Introduction

This chapter discusses the findings of tests completed upon The Puketoka Formation soil taken from two sites in Hamilton. The history and sampling procedures for the materials are discussed. The geomechanical and mineralogical results are compared to previous studies, and the influence they have on one another assessed. The cause for sensitivity in these materials is hypothesised. The engineering recommendations are then discussed, in addition to any areas where future research would be beneficial.

9.2 History of the materials used

The materials sampled within this study were identified to be of volcanic origin, being derived from ancestral pyroclastic flow events (Kamp & Lowe, 1981). Evidence of weathering and reworking was also identified using SEM and thin section imagery. The material is likely a non-welded ignimbrite, identified by the presence of quartz, cristobalite and volcanic glass within the x-ray diffraction results. The identified presence of halloysite within the samples is also indicative of in-situ weathering. Therefore, I hypothesise my samples likely represent a secondary reworked ignimbrite deposit, which I have inferred to be the Puketoka Formation of the Walton Subgroup.

The dominance of hydrated forms of halloysite in the samples also indicates a silicic parent material, such as rhyolitic pyroclastic deposits (Joussein et al., 2005; Wyatt, 2009). This is consistent with the Walton Subgroup materials being of terrestrial origin, being deposited following a period of active volcanism, likely from the Taupo Volcanic Zone (TVZ) (Kear et al., 1978).

In terms of key geotechnical characteristics, sensitive soils are associated with a set of characteristic values. DRAB1 and TV1 had moisture contents lower than the calculated liquid limits, diverging away from the characteristics of volcanically derived sensitive soils (**Table**

9.1). TV2, however, had a slightly higher moisture content than the calculated liquid limit (**Table 9.1**). This could be attributed to the time of year sampling took place (summer). Interestingly, this trend could also be observed in Moon and Blackstock's 2004 study upon the same materials.

The samples also were compared to more recent studies completed upon sensitive soil material from the Tauranga Region – Omokoroa and Matua, most notably the Bramley Drive landslide (**Table 9.1.**). The results show that differing parameters were comparable for the materials from this study, however no one study was completely comparable. This can sensibly be attributed to the natural variations that will arise between two different soil groups; despite a similar mode of formation, local variations in a multitude of environmental factors will strongly influence how the soils form and behave.

A comparison was also made with a CMW geotechnical report analysing the materials found at Temple View (CMW Geosciences, 2015). A number of borehole and test pit investigations were completed, and BH06 was selected as the comparative investigation, due to the similarity in depth (**chapter 5**, **Table 5.1**). Whilst the BH06 Atterberg limit results were comparable to the DRAB1 sample, TV1 and TV2 showed appreciable differences in the results. The particle componentry results were appreciably different however. I hypothesise this variation can be attributed to where within Temple View the samples were taken. Variation in soil materials can also exist over small scales, and due to the inter-fingering nature of the Walton Subgroup materials and the depositional history, this should also be expected (Nielsen et al., 1973; Phoon & Kulhawy, 1999). Therefore, whilst similarities to the already defined values for similar materials could be identified for the materials of this study, the three samples experienced some internal variability in all the results seen (**Table 9.1** and **9.2**), likely dependent upon the individual mineralogical and structural properties of the materials. The spatial variability of material over an area can also be a cause of the differences observed, and is a phenomenon documented in published studies (Nielsen et al., 1973; Phoon & Kulhawy, 1999). This should be considered, due to the distance between the sampling sites (~ 6 km). This variability can even occur at small scales, as identified by Mills in her 2016 study.

Generally, however, the materials used in this study were identified to be high plasticity silts (MH). High plasticity soils take a long period of time to consolidate, as observed in the triaxial testing undertaken for this study. High plasticity in soils also may impart a high shrink-swell regime, however, in low activity clays such as halloysite, very little volume change is observed.

9.3 Geomechanical results

Table 9.1 and **Table 9.2** summarises the measured geomechanical values for this study and published results on similar materials.

Table 9.1. Table summarising the geomechanical properties measured for this study, with summarised ranges produced from previous studies. The Puketoka Formation materials used in this study are from pyroclastic flow deposits that have been minimally reworked in some cases, whilst most of the soils analysed in previous studies are derived from air-fall deposits, therefore the results are comparative only.

Study	Sample & location	LL (%)	PL (%)	LI (%)	PI (%)	Activity	Wet bulk density (kg/m3)	Dry bulk density (kg/m3)	Particle density (kg/m3)	Moisture content (%)	Porosity (%)	Void ratio	Sand (60-2000) (%)	Silt (2-60) (%)	Clay (< 2) (%)	Sensitivity
This Study (2021)	DRAB1	75	41	0.1	34	1.79	1575.5	1057	2452	49	36	0.56	25.35	55.06	18.85	3.1-4.71
	TV1	59	48	0.1	11	0.81	1460.1	980	2487	49	41	0.69	5.56	81.12	13.32	3.75
	TV2	61	53	1.5	8.0	0.60	1069.4	645	1935	65	51	0.88	10.89	76.01	13.10	2.19-2.25
Wyatt (2009)	Tauriko Road cutting (TS)	81	57	2.4	24	-	1581	966	2591	115	77.3	3.40*	13*	81*	6*	5-20
	Otumoetai (OS)	90	47	1.5	43	-	1515	920	2686	104	75.1	3.02*	52*	65*	10*	6-14
Cunningham (2012)	Otumoetai (OS)	73	49	1.6	24	6.4	1505	807	2415	87	67	2	32.51	61.3	6.2	13
	Te Puna (TP)	89	46	1.4	44	14.7	1436	688	2220	109	69	2	20.90	76.1	2.9	11
	Pahoia Peninsula (PL)	53	35	2	18	3.2	1626	963	2570	69	62	1.6	17.05	77.1	5.8	10

Mills (2016)	Omokaroa landslide scarp (OM)	66	41	2.9	25	0.4	1320	-	2517	72	70	1.8	0	37	63	6-15
	Matua (M)	52	37	1.8	15	0.4	1690	-	2777	64	65	2.3	37	23	40	10
Robertson (2017)	Bramley Drive soil	92	78	0.4	25	1.11	-	-	-	-	-	-	-	-	-	-
Ranges from previous studies		**52 - 92**	**35- 78**	**0.4- 3**	**18 - 25**	**0.4 – 14.7**	**1320 - 1690**	**688 – 966**	**2220 - 2777**	**64 - 109**	**62 – 77.3**	**1.6 – 3.4**	**0 - 52**	**23 – 77.1**	**2.9 – 63**	**6 - 15**

^ = values taken from characteristic activity calculated for halloysite (Wyatt, 2009).
*= maximum value calculated from multiple samples of the same material (Wyatt, 2009).
- = Not measured in study.
= Average taken from multiple studies (Wyatt, 2009)

Table 9.2. Summary table of the triaxial data gained throughout this study, in addition to a number of other studies, mainly based in the Tauranga region. Summarised ranges from the previous studies are included. It is to be noted that the Tauranga soils are largely formed by air-fall tephra deposits, whilst the Puketoka Formation materials formed from a combination of pyroclastic flow events and fluvial reworking, therefore the comparisons are relative only. PWP = pore water pressure, mSC = minor strain softening, contractive failure, MSC = moderate strain softening, contractive failure, SSC = strain softening, contractive failure, HSC = high strain softening, contractive failure, Dil = dilation.

Study:	Sample & location	Confining pressure (kPa)	Max corrected deviator stress (kPa)	Peak effective cohesion (c')	Peak effective friction angle (φ'(°)	Percentage axial strain at failure (***ε***), (%)	Calculated R, R' angles (°)	PWP response during shear	Post failure response	Failure type observed
This study (2021)	DRAB1	100	128	37	27	1.81	19.3, 57.8	Normally consolidated	MSC	Shear band
		170	141			2.44			MSC	Shear band
		270	233			6.51			SSC	Shear band
	TV1	130	144	0	38	4.82	28.7, 61.2	Normally consolidated	MSC	Intermediate – shear band
		170	167			16.35			MSC	Intermediate
		230	233			16.35			MSC	Intermediate - shear band
Wyatt (2009)	Tauriko Road cutting (TS), Bay of Plenty, NZ	20-300	73.4-294.5	12-24	27.-31	2.1-7.2	-	Normally to over consolidated*	MSC-SSC	Shear band
	Otumoetai (OS), Bay of Plenty, NZ	20-300	64.2-368.4	5-35	26-39	1.7-20.1	-		MSC-SSC	Shear band
Cunningham (2012)	Omokaroa (OS), Bay of Plenty, NZ	100-300	104.5 – 240.2			1 - 9	-		mSC - MSC	Intermediate, barrel and shear band

Cunningham (2012) cont.	Te Puna (TP), Bay of Plenty, NZ	50-150	197.3 – 268.2	8-19[+]	28-41[+]	5 - 8	-	Normally to over consolidated[#]	mSC - HSC	Wedge to shear band
	Pahoia Peninsula (PL), Bay of Plenty, NZ	50-150	106.7 – 138.5			3 - 7	-		HSC	Intermediate, barrel and shear band
Mills (2016)	Omokoroa (OM1), Bay of Plenty, NZ	140-355	179-383	26[^]	31[^]	1.9-3.5	29.5, 60.5	Normally consolidated	MSC-SSC	Shear band to shear-wedge
	Matua (M1), Bay of Plenty, NZ	75-255	131-250	17	32	2.2-4.4	29, 61		Dil-MSC	Barrel, wedge and shear band
Robertson (2017)	Bramley Drive, Bay of Plenty, NZ	205-355	121.34-196.9	27	19	1.6-5.3	31, 59	Normally consolidated	-	Barrel to shear band
Ranges from previous studies		**50 - 355**	**64.2 - 383**	**0-35**	**19 - 41**	**1 – 20.1**	**19.3 – 31, 57.8 – 61.2**	**Normally to over consolidated**	**Dil - HSC**	**Barrel, wedge, intermediate, shear band**

*= Over-consolidated response observed for OS1, OS2, OS3 and OS4 at 20-55 kPa confining pressure (Wyatt, 2009).
#= Over-consolidated response observed for TPS1, TPS2 and TPS3 at 50-150 kPa confining pressure (Cunningham, 2012).
^ = Average values taken from four different test runs (Mills, 2016).
+= Average values taken from multiple different tests (Cunningham, 2012).
-= Not measured in this study.

9.3.1 Atterberg limits, activity and particle componentry results

The Atterberg limits results determined that the three samples are consistent with published values from previous studies, detailed in **chapter 5**. These values are characteristic of volcanically-derived soils and were first defined through two key studies completed by Bain in 1971 and Wesley in 1973. The studies focused upon defining the Atterberg limits for a pure halloysite clay (Bain, 1971), and halloysite-rich soils (Wesley, 1973). This was a key observation made for both Bain's (1971) and Wesley's (1973) studies. More recent studies (Moon, 2016; Mills, 2016; and Robertson 2017) also share the same trend. Key results can be seen in **Table 9.1.**

The high plastic and liquid limits obtained for the samples of this study indicate a large amount of water is contained within the soils occurs before the key rheological changes that define the limits occurs. This is readily driven off when the soils are oven dried (Bain, 1971).

The large amount of water is hypothesised to be contained within the halloysite clay minerals and relates to morphology. A high incidence of tubular halloysite particles allows for a large proportion of water being adsorbed upon internal surfaces, which therefore is unable to either physically interact and lubricate the individual clay particle contacts, or interact electrostatically with clay surfaces (Bain, 1971; Moon, 2016). Therefore, this additional water does not contribute to plasticity development (Bain, 1971). Halloysitic soils have been characterised to have low plasticity indexes as a result (Bain, 1971; Wesley, 1973; Moon, 2016). Low plasticity indexes are indicative of low activity minerals (Moon, 2016). Activity relates to the interactions taking place between the surfaces of the clay minerals and the cations within the double layer of water (Moon, 2016). The activity for the samples was measured (**Table 9.1.**). The active to normal activity values observed for DRAB1 and TV1 could be a result of observed higher plasticity indexes compared with TV2, and the soils likely remain plastic for a wider range of moisture contents compared with the less plastic TV2 sample. The activity values are in agreement with the previously published ranges for Tauranga soils (**Table 9.1**).

The plasticity index also relates to the clay content within the soil. Low plasticity has a run-on effect, imparting the materials with a low cation exchange capacity, and a low shrink-swell capacity as a result (Bain, 1971). The low cation exchange capacity leads to a low

remoulded shear strength; a key parameter for definition as a sensitive soil (Joussein et al., 2005; Moon et al., 2013; Moon et al., 2015).

The particle componentry of the samples also influenced the Atterberg limit values gained. DRAB1 had the highest clay content of all the samples in addition to the greatest proportion of sand-sized particles. TV1 was distinctly siltier, as was TV2, but TV2 was sandier than TV1 (**Table 9.1.**). These values are in agreement with the observations made by Wyatt in 2009, where many of the tephra materials from Tauranga had a clay content less than 10 %. Wyatt postulated however that the clay particles were likely underestimated in the particle sizer analysis, due to the dominance of halloysite within the SEM imagery taken. This was due to the potential for clay aggregations to persist during particle size analysis, even following the application of Calgon solution (Wyatt, 2009). These observations are similar to what was experienced during this study; as despite a relatively low clay content calculated in the particle size analysis, I observed a clay-matrix dominated microstructure in each sample through SEM imagery (**chapter 8**). However, very little evidence exists for this hypothesis, therefore for the purpose of this study I will accept the particle size analysis results as correct, and interpret them as such.

Based upon these findings, it can be hypothesised that the soil materials analysed during the course of this study would behave in a similar manner to previously studied halloysite-rich sensitive soils, based upon similar Atterberg limits, activity and particle componentry results.

The mode of formation of the Puketoka Formation and Walton Subgroup materials differs from the Tauranga sensitive soils studied however (pyroclastic flow and fluvial reworking versus air-fall tephra deposits). I believe that the materials of this study likely experienced some degree of weathering and reworking, based upon the lack of sorting identified within the thin sections produced for the samples, in addition to the dominant ‘matrix’ structure observed through SEM imagery. Literature suggests that the Puketoka Formation materials were weathered in-situ, and experienced minimal reworking as a result (Selby and Lowe, 1992; Moon and Blackstock, 2004).

9.5.2 Particle and bulk density, porosity, and moisture content

Table 9.1 summarises key results. The samples of this study had higher particle density values compared with the Tauranga sensitive soils was evident, particularly for the DRAB1 sample. A higher particle density could have occurred due to a higher proportion of

heavy particles within the sand fraction of the materials (Jacquet, 1990). However, the sand fraction of the samples was not analysed specifically, therefore this can only be an assumption.

Conversely, TV2 had a lower measured particle density than that of published values defined by previous studies (**Table 9.1**) (Wyatt, 2009; Mills, 2016; Moon et al., 2017). This low particle density could be attributed to a lack of heavy materials within the sand-sized fraction of the material.

The bulk density at field moisture content values for DRAB1 and TV1 (**Table 9.1.**) were within the previously published ranges for halloysite-dominated sensitive soils (**Table 9.1.**). TV2 however fell below this. The reduced amount of clay within TV2 could have influenced the amount of moisture being held within the material, as less clay would lead to an overall reduced capacity for moisture to be held.

Oven dry bulk density was also calculated for these samples. The trends matched those of the wet bulk densities, with DRAB1 being the most dense and TV2 being the least dense (**Table 9.1.**). For DRAB1 and TV1, the high oven dried bulk density values relate to a lower porosity value. The lower oven dried bulk density of TV2 compared with DRAB1 and TV1 resulted in a higher porosity. The values all fall into the published values for halloysite-dominated sensitive soil materials (33 – 71 %) (**Table 9.1**) (Selby, 1993; Moon & Blackstock, 2004; Mills, 2016; Moon et al., 2017).

The moisture content values reflect the differences in porosity (**Table 9.1.**). These values again were within the accepted range for halloysite-dominated soil materials (**Table 9.1**) (Moon et al., 2017). Moisture content and porosity values relate to where water is contained within the soil materials. An open structure and dominance of hollow tubules was observed in SEM images of the samples of this study, thus encouraging porosity (**chapter 8**) (Moon et al., 2015). This produces a soil with a high porosity, but a low permeability. An open framework is predisposed to sensitivity as a result (Arthurs, 2010; Moon et al., 2015; Cunningham et al., 2016).

9.6 Triaxial testing

The mode of origin of the triaxial samples indicates that the soils have not experienced significant elevated overburden stresses, therefore remain normally consolidated in most cases (Moon, 2016; Cunningham et al., 2016).

9.6.1 Pore water pressure response

Figure 2.11 (**chapter 2**) summarises the soil response of clays under differing degrees of consolidation, and the subsequent response of the pore water pressure (PWP). An appreciable positive change in pore water pressure was characteristically observed during shear of the materials, indicating that water was being expelled from the sample as it sheared. This correlates to a reduction in sample volume and is characterised by a left tracking trend on the p' versus q' plots produced. All three confining pressures for both samples produced a positive pore water pressure change consistent with a slightly over consolidated soil (**chapter 2**).

This trend is consistent with previous observations made by Konrad & Sawitzki in 1994 upon lab-created clay and silt mixture soils with 15 % clay content, and more recently by Mills in 2016 and Robertson in 2017, regarding sensitive soil materials in the Tauranga Region. Wyatt (2009) and Cunningham's (2012) studies also generally show a normally consolidated response, however some samples, particularly at lower confining pressures (50 –200 kPa), were more prone to over-consolidated responses (**Table 9.2**). The pressures used in this study were significantly higher (130 – 270 kPa), likely resulting in the difference in responses seen.

9.6.2 Response to shearing stress

The deviator stress at the soil failure point (**Table 9.2**) values were agreeable with the values gained by Wyatt (2009), Cunningham (2012), Mills (2016), and Robertson (2017) in their studies for similar confining pressure values. The peak deviator stress values were observed to increase as confining pressures increased.

Higher confining pressures in this study generally correlated with an increase in effective stresses in the pre-peak strain hardening region, followed by failure at the peak deviator stress, and subsequent effective stress decrease. This becomes more pronounced at higher confining pressures and could be observed for the DRAB1 170 kPa test, and the TV1 130 and 230 kPa tests. This was also observed by Mills (2016).

The failed cores generally showed some form of shear band formation following failure, except for the TV1 170 kPa test, which formed a complex intermediate potential wedge failure. The clay content within a soil sample has been proven to dictate the type of failure experienced by the soil (Konrad & Sawitzki, 1994).

Both DRAB1 and TV1 generally show a rapid rise on the p'-q' plots produced (**chapter 7**) in the pre-peak strain hardening region, before reaching the peak value, where failure occurred. This was indicative of the samples contracting following failure, and experiencing some degree of strain softening. This similarly was observed by Mills (2016). The samples generally followed this trend, except for the TV1 170 kPa test, where deviation to the left occurred, before tracking back to the right, indicating partial sample dilation (Gylland et al., 2014).

The slightly over consolidated behaviours of the materials could also be attributed to the dominant composition. The dominance of non-plastic silt within the samples influences the behaviours of the materials under shear stresses, as does clay. The presence of silt in material increases pore water pressure changes whilst decreasing the compression as a function of void ratio, whilst higher clay contents encourage sample contraction, and decreases dilation (Konrad & Sawitzki, 1994). This was observed in the samples of this study, as the samples tended to be silt-dominated (**Table 9.1.**) and displayed a large positive change in pore water pressure throughout the shear stage of testing. Whilst some degree of compression was observed by the samples upon the shear graphs, the void ratio of the materials was low (**Table 9.1.**), and the observed pore water changes were appreciable, fitting the classification of a silt-dominated material under Konrad & Sawitzki's (1994) guidelines.

Table 9.2 summarises the key values. Effective shear strength is influenced by the moisture content, pore water pressure, mineralogy, and external environmental factors (Alias et al., 2014). As a result, variance is expected between the samples.

Effective cohesion is appreciably higher for DRAB1 than TV1 (**Table 9.2**). This is expected, due to the higher proportion of clays within DRAB1. These values are consistent with previously published studies in halloysite-rich soils (**Table 9.2**), however, the published values display a large range. The effective friction angle for TV1 is higher than DRAB1 which can potentially be explained through the amount of silt present in TV1. Silt content is hypothesised to influence the triaxial response of a material during testing (**chapter 2**).

9.6.3 Strain softening failure types

The following strain softening descriptions were suggested by Mills in her 2016 study, relating to the response of the soil cores during shear. The framework has been also adopted in this study to analyse the failed triaxial soil core behaviour. Two failure types are identified:

strain softening contractive failure (SSC), and moderate strain softening contractive failure (MSC).

9.6.3.1 Strain softening, contractive failure (SSC)

Strain softening, contractive failure (SSC) is discussed in detail in **chapter 2.** SSC failures generally result in strain localisation related with the formation of shear bands within the soil material. Shear bands were observed in the form of deformed soil material in many of the samples of this study (**chapter 5**). The formation of shear bands usually occurs near an area of weakness within the soil, such as where material changes occur, concentrations of particular materials, and where material properties differ (Gylland, 2013a; Mills, 2016). This was observed in multiple samples tested throughout the course of this study (**Table 9.2**), particularly with manganese concentrations identified within the soils (**Figure 9.1**).

Figure 9.1. Image showing the extent of strain localisation (shear band formation) occurring within areas of manganese concentrations within a failed triaxial core sample (DRAB1 130 kPa).

Strain softening, contractive (SSC) failures produce characteristic responses on stress-strain, stress path and pore water pressure graphs (**chapter 2**). In previous literature, higher confining pressures generally correlated with a sharper peak being produced upon both the stress-strain and p'-q' plots, in addition to the production of a higher pore water pressure (Mills,

2016). This was observed in the DRAB1 270 kPa test. This is consistent with the higher confining pressure theory suggested by Mills (2016).

Previous literature, namely Wyatt's 2009 and Cunningham's 2012 studies, indicate that the soil material being tested also influences the results seen, as the SCC failure type was observed at lower confining pressures (20-150 kPa) within both studies. Conversely, Mills stated in their 2016 study that SCC failures were limited to higher confining pressures, as more rapid accumulation of pore pressure occurs in the areas of weakness, which subsequently produces a more sudden strength loss within the material, due to the plastic straining and deformation of material within the shear zone (Gylland et al., 2014). These tests were all completed upon sensitive soil material located within the Tauranga Region however. Based upon these observations and characteristics, I cannot say with any certainty that all my samples tested fall into this category, as the described responses are not necessarily characteristic of an SSC failure. Therefore, I hypothesise that the majority of my samples failed in a manner more characteristic of moderate strain softening, contractive failure.

9.6.3.2 Moderate strain softening, contractive failure (MSC)

Samples failing in a moderate strain softening, contractive failure (hereafter referred to as MSC) show similar characteristics as an SSC failure, but less pronounced. The graphs also differ slightly, with the stress-strain curves showing a greater peak curvature, with minimal significant drops in deviator stress following the peak (Mills, 2016). The pore water pressure response also either flattens or rises slightly following failure (Mills, 2016).

The samples of this study I believe show a response in agreement with MSC failure types, based on the responses of the graphs and the failure types observed on the cores.

The increased curvature of the stress-strain curves for MSC failures in this study is potentially indicative of the strain being exerted accumulating in a more uniform manner compared to an SSC failure. The p'-q' plots tend to show some degree of contraction at failure, which indicates that the pore pressure had some time to dissipate out of the sample, meaning that contraction and deformation of the sample was not necessarily concentrated to one specific area. However, the MSC response still allowed for the formation of shear bands, meaning the pore water pressure did not drop enough to become negative, and reduce the contraction observed.

Failure types commonly observed for MSC failures are the same as SSC failures (**Table 9.2**). Contraction of the samples does not necessarily guarantee the development of shear band features, as was observed by Cunningham in his 2012 study. The lack of shear band development potentially occurs for a number of reasons, including the potential for weaker regions to exist within the sample, leading to the development of strain in these areas to produce a barrel failure rather than a localised shear band formation, in addition to a lower shear rate allowing time for pressure to dissipate somewhat and reduce the likelihood of strain localisation occurring (Gylland et al., 2013b; Mills, 2016). Additionally, barrel failures have been evidenced to occur more commonly at higher confining pressures, based upon Konrad & Sawitzki's 1994 research. Lower clay contents were also indicated by Konrad & Sawitzki (1994) to have an influence on barrel failure modes. The critical cut – off identified for changes in behaviour in terms of kaolinite clay content was around 15 – 30 % total clay content, based upon published literature (Konrad & Sawitzki, 1994). As a result, brittle shear failures are expected in soils with higher clay contents (Konrad & Sawitzki, 1994).

No apparent barrel failures were observed within this study, however, but the formation of an intermediate style of failure occurred for the TV1 170 kPa test. This failure mode could be attributed to the same parameters as barrel formations, but with a lesser degree of pressure dissipation occurring, allowing for only a small area of the sample, potentially containing areas of weakness, to fail, by comparison with Gylland et al., (2013b).

I believe that the majority of the samples tested within this study display characteristics consistent with MSC failure. The responses of the graph, in addition to the physical failures the cores displayed were consistent with this mode of failure, as compared with SSC failures. The studies by Wyatt (2009), Cunningham (2012) and Mills (2016) did not appear to classify any of their samples into this failure category, indicating a notable difference in the failure characteristics of the sensitive soil materials found in the Tauranga region, versus the Puketoka Formation. This shows there is a difference between the materials of this study and the Tauranga materials, and could relate to the structure and arrangement of the materials differing between the two differing groups. Further testing upon the same materials to confirm my hypothesis is recommended.

9.7 Thin section analysis

To further analyse the zones of failure, thin sections of the triaxial failure zones were analysed. Unfortunately, only three thin sections were usable for the final analysis. Details of the process can be found in **Appendix 3.1.4.**

The specific angles of the R and R' shear propagation calculated for this study differ between DRAB1 and TV1 (**Table 9.2**). The difference in the observed angles could relate to the failure type, as neither TV1 sample developed true shear band failures compared with DRAB1, rather intermediate to juvenile zones of shear. In the case of the TV1 230 kPa sample, the shears had not propagated with enough clarity to determine the angles of interaction between different shear types. As a result, the true extent of the failure may not have been captured upon the thin section slides. These R and R' shears propagate during differing times of shear to produce the PDS and were observed connecting the PSZ with the secondary shears in most cases.

9.8 Mineralogical (microstructure) results

9.8.1 XRD

All three samples analysed through bulk sample XRD were found to contain similar compositions containing quartz, augite, volcanic glass, and some cristobalite. The presence of large concentrations of silicic materials was expected, as halloysite favours formation within a silica rich environment. This is discussed in detail in **chapter 2**. Under this model, halloysite forms preferentially in Si-rich environments, under a moisture regime that retains water within the soil for much of the year (Churchman and Lowe, 2012; Cunningham et al., 2016).

9.9 Scanning electron microscope

9.9.1 Morphologies and sensitivity

All three samples contained a mixture of halloysite morphologies interacting with one another to form a loose open structured clay matrix in addition to forming many of the irregular

microaggregates (**chapter 8**). It has been inferred differing morphologies influence the sensitivity, in particular, mushroom-capped spheroids (**chapter 2**).

Whilst no mushroom capped forms of halloysite spheroids were identified within the samples analysed, spheroids were identified. It can be inferred as a result that the sensitivity is governed to a degree by the morphology identified within the samples.

The formation of multiple different morphologies of halloysite relates to the mineralogical composition within the materials, and the local geological factors acting upon the soils (Cunningham et al., 2016). Halloysite morphologies also have been suggested to form in relation to Fe content of the material (Joussein et al., 2005; Wyatt; 2009). These can manifest as manganese concretions, and were observed within this study (**Figure 9.1**). Manganese has also been hypothesised to influence the failure characteristics of a soil (**chapter 2**). Interestingly, book formations were also observed in TV1 and TV2.

Book formations are also usually indicative of kaolinite, as discussed in multiple pieces of published literature (**chapter 2**) (Dixon, 1989; White & Dixon, 2002). A detailed analysis of the XRD clay traces was completed for the samples of this study (**chapter 7**). In the case of TV1 and TV2, it is hypothesised that the blocky books identified could potentially be halloysite. The plates making up the books are arranged in a face to face manner on top of one another. Review of the XRD results, and previous studies of book formations (Wyatt, 2009; Cunningham, 2012) produced a hypothesis consistent with halloysite. The geological characteristics of the Puketoka Formation and Walton Subgroup also leans toward the formation of halloysite, being classified as highly weathered, poorly welded ignimbrites, with evidence of localised reworking within individual layers (White et al., 2015). The permeability of the material is low, yet porosity is high, due to the interactions of halloysite clay minerals. Literature also states, although irregularly, that halloysite can exist in book forms (Churchman & Theng 1984; Noro 1986; Joussein et al., 2005; Wyatt, 2009).

9.9.2 Orientation

A predominance of edge to edge and face to edge contacts at significant angles encourages an open structure, often with high porosity and is predisposed to collapsibility as a result (Moon, 2015). This open structure is dependent upon the morphology, and halloysite tubules are the most common form to show this arrangement (Wyatt, 2009; Cunningham et al., 2016), with plates and spheres oftentimes filling some of the gaps produced by the tubular

arrangement. This phenomenon was commonly observed in all three of the samples analysed in this study, with TV2 showing it most dominantly. This arrangement has been compared as similar to the flocculated structure first described by Lambe in 1958 (Wyatt, 2009).

This orientation additionally influences the geomechanical properties observed for the soils. The highly porous nature observed via SEM in all three samples but was particularly prominent in TV2 (**Figure 9.2**).

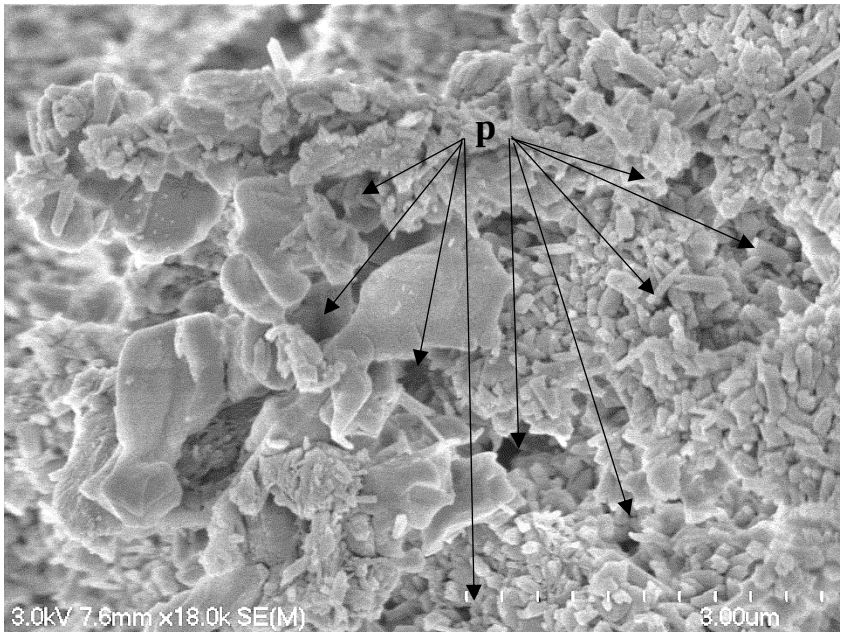

Figure 9.2. SEM image highlighting the porosity of TV2 at microscale. Note the presence of multiple pores (p), ranging between 0.1 µm and 1.5 µm in size, classifying them as ultra- to micropores.

The void ratios of the samples also related to the microstructure. TV2 had the greatest void ratio whilst DRAB1 had the lowest (**Table 9.1**). The images supported these observations. The open microstructure of the samples encourages porosity, and the tubule morphologies add additional pore spaces to the material which allows for the additional storage of water.

9.9.3 Microfabric and weathering influences

The SEM imagery also provided evidence into the geological history and formation processes the materials had undergone. The Walton Subgroup has several sub-types, dependent upon location and depth, including the Puketoka Formation (Kear & Schofield, 1964; Kear et al., 1978; White et al., 2015). Arthurs (2010) produced a diagram depicting the common grain and material inclusions expected within weathered pyroclastic soil material, following his investigation of multiple sensitive soil materials across the Tauranga region (**chapter 2**). The

materials within this study showed a number of features consistent with Arthurs' observations, confirming the volcanic nature of the material.

The degree and manner of weathering experienced by the grains identified within the SEM images could provide evidence into the identification of the differing formations within the Walton Subgroup. The presence of argillized volcanic glass in TV2 is consistent with descriptions of the Puketoka fluvatile and lacustrine deposits (Kear et al., 1978). The light yellowish grey colouration of the subtype identified during the site visit (**chapter 4**) is also consistent with historic observations made (Kear et al., 1978). The absence of pumice observed within TV2 is interesting however. From this, I believe the materials analysed within this study ae consistent with the Puketoka Formation, rather than the Karapiro Formation of the Walton Subgroup.

The matrix microfabric identified in all three samples (**chapter 8**) is indicative of a sedimentary material that has experienced environmental reworking to alter the clay-sized fabric within the material.

9.10 Relationship between geomechanical and mineralogical results

Graphs for this section can be found in **Appendix 9.1.**

9.10.2 Void ratio, porosity and bulk density

9.10.2.1 Shear strength and void ratio

No correlation could be observed between peak vane strength and void ratio in this study, likely due to a low amount of measurements taken in the field. However, in Wyatt's 2009 study, a weak negative relationship is displayed (R^2 = 0.64) (**Figure 9.3**). Additional studies by Cunningham (2012) and Mills (2016) are also included on **Figure 9.3**. The samples of this study fall well below the trend line of Wyatt. The graph shows with clarity that the Puketoka Formation materials behave differently from Tauranga sensitive soils.

The morphology within the samples influenced the peak vane strength gained. TV1 had the greatest peak strength value measured (120 kPa), likely influenced by the arrangement and orientation of the differing halloysite morphologies. The density of tubules, plates and

spheroids within TV1, in addition to occasional book formations forming an interacting subdued arrangement, with the book formations producing predominant face to face contacts. This arrangement encourages the area available for electrostatic attraction between the clay particles (Wyatt, 2009).

In comparison, DRAB1 was dominated by halloysite tubules, arranged in an open structure with plates and spheroids infilling gaps. The dominance of edge to edge or face to edge contacts produced a weaker framework for interactions through electrostatic bonds (White & Dixon, 2002). This resulted in a lower peak strength reading.

TV2 similarly had a lower peak strength reading, likely caused by the open arrangement of the halloysite morphologies DRAB1 also showed lower peak strength, but also had a high number of identified pores, which in turn indicated a lower density within the material, which subsequently reduced the frictional resistance of the materials (Wyatt, 2009).

A graph showing the remoulded strength trends for the samples of this study, in addition to the results gained by Wyatt (2009), Cunningham (2012), and Mills (2016) was also produced, and can be found in **Appendix 9.1.** Wyatt's (2009) remoulded strength trendline showed a marginally closer correlation ($R^2 = 0.71$), however, the Puketoka Formation materials still differ, with the results of this study showing a lower remoulded strength compared with previous Tauranga studies, and the remoulded strength displays no apparent relationship with the void ratio of the samples.

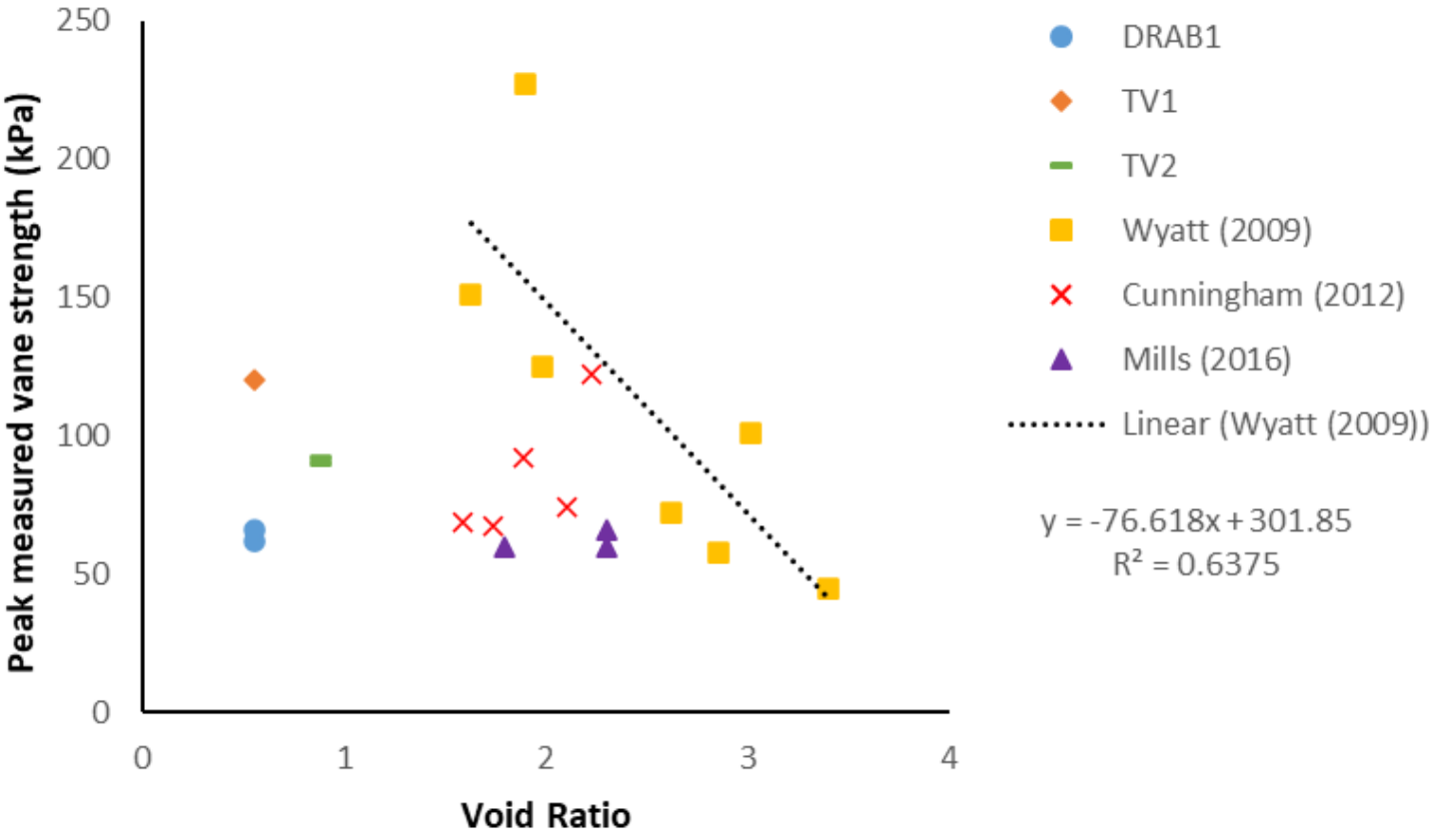

Figure 9.3. Graph depicting the relationship between the void ratio, and the peak measured vane strength (kPa), using results gained from this study, and the results of multiple studies completed in Tauranga sensitive soils.

9.10.2.2 Porosity and permeability

The results of this study indicate porosity is lower for the Walton Subgroup materials, when compared with the Tauranga Sensitive soils (**Table 9.1**). As a result, the coefficient of permeability was also calculated to be lower when compared to previously published values for halloysite-dominated materials (**chapter 7,**

Table 7.5). This is expected, as fewer physical pores present within the material reduces the likelihood of inter-connection between pores overall, thus producing a lower overall permeability.

9.10.2.3 Sensitivity and void ratio

The relationship between void ratio and sensitivity is summarised in **Figure 9.4**. A weak positive relationship ($R^2 = 0.5237$) is observed using Wyatt's (2009) data to determine trends. The Puketoka Formations' sensitivity falls well below the trend, indicating a different response between void ratio and sensitivity for these materials, compared with the Tauranga samples.

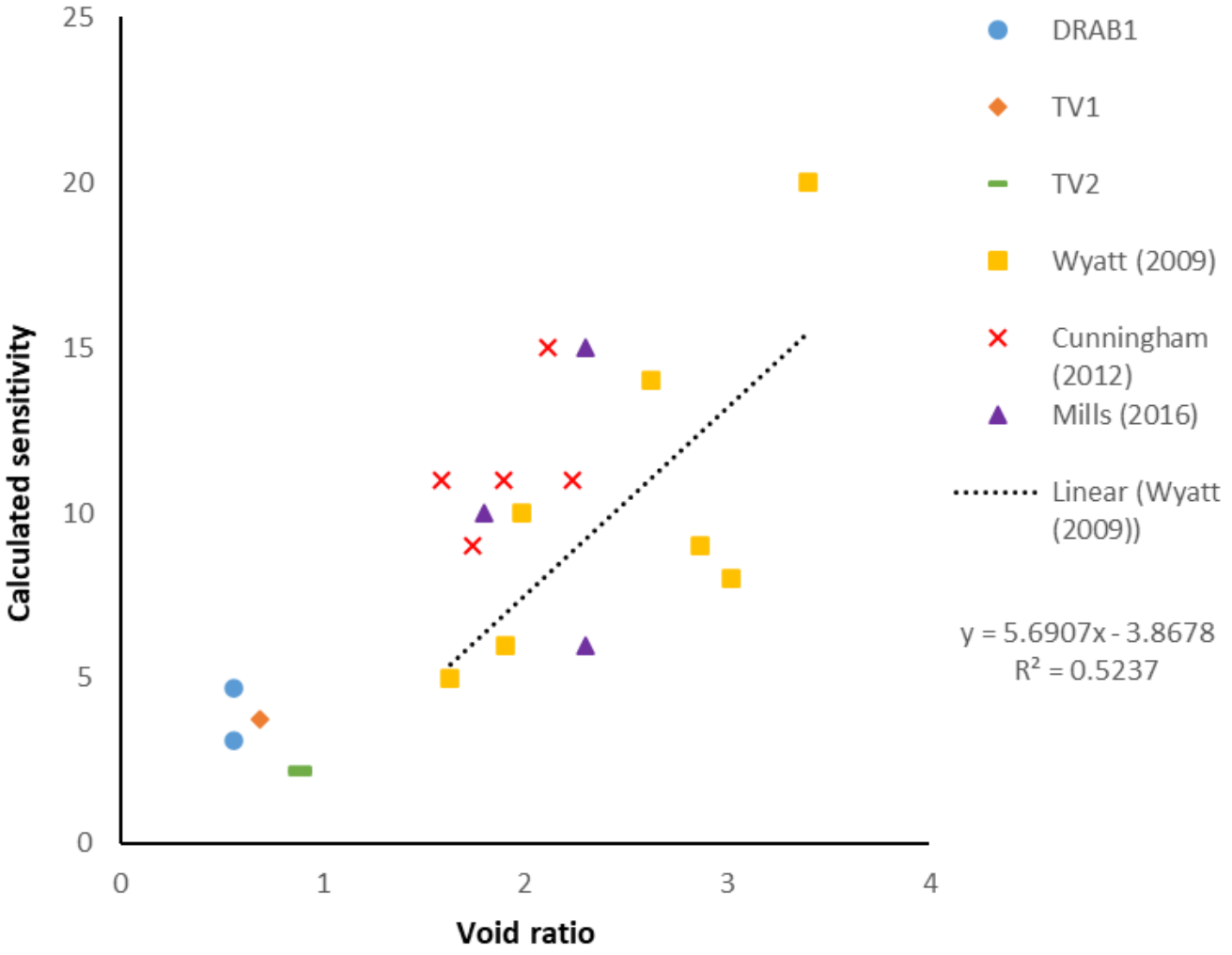

Figure 9.4. Graph summarising the relationship between void ratio and calculated sensitivity for the samples of this study, in addition to Wyatt (2009), Cunningham (2012) and Mills (2016).

In summary, the Puketoka Formation materials analysed in this study are hypothesised to be minimally reworked pyroclastic silts of rhyolitic origin. The Walton Subgroup materials are predominantly silt, with ~10 % clay (**Table 9.1**). The clay minerals were identified to be predominantly halloysite, with some kaolinite (**chapter 6**). The clay minerals had a number of

differing morphologies, influencing the microfabric observed for the samples (**Table 8.1**), in addition to the classification properties (**Table 5.1**). The response of the materials to triaxial testing showed a predominant moderate strain, contractive failure type (**Table 9.2**). The strength observed for the Puketoka Formation samples classifies them as moderately sensitive to sensitive. The Puketoka Formation samples show a lower peak strength for a given void ratio when compared with Tauranga sensitive soils but show a slightly higher sensitivity for a given ratio when compared to the Tauranga soils.

Therefore, I believe that the mode of formation and the degree of weathering and reworking the Puketoka Formation materials have experienced may influence the sensitivity they display.

9.11 What influences Puketoka Formation sensitivity?

Throughout this study, the Puketoka Formation materials have generally shown both geomechanical and mineralogical properties in keeping with published ranges expected for halloysite-dominated sensitive soil materials (**chapter 8**). However, some properties, particularly the particle componentry, peak and remoulded strengths and void ratios differ from these previous studies. These differences raise a question to determine the main cause of sensitivity for the materials of this study, compared with soils of the Tauranga Region.

I hypothesise that the depositional history of the Puketoka Formation and the Walton Subgroup has played a significant part in the development of sensitivity. The materials were theorised to have been deposited as a pyroclastic flow event. Following deposition, a large period of non-deposition followed.

As discussed in depth in **chapter 2,** the Walton Subgroup is generally classified into two layers; the highly bedded Karapiro Formation, which shows evidence of fluvatile and bedded plain deposits; and the Puketoka Formation conversely represents a primary ignimbrite, homogenous in composition.

The Puketoka Formation can experience localised reworking however, from environmental factors such as stream movement, wind, rain, and other environmental conditions. Due to the lack of soil forming processes (pedogenesis), this reworking is minimal. I believe that the samples of this study have experienced some degree of reworking over geological history. I believe, based on the observations of this study, the descriptions of the materials are more consistent with that of the Puketoka Formation rather than the Karapiro

Formation, as I have previously alluded to in this study. However, the definitions of the Karapiro and Puketoka Formation are dated, therefore the accuracy of these classifications has been brought into question in recent years. Therefore, I believe the deposits analysed in this study are representative of a secondary reworked ignimbrite that has experienced some degree of fluvial reworking over time.

The occurrence of reworking within the samples likely reduces the overall homogeneity of the samples, however marginal. However, the impacts of reworking upon a material are still widely unknown, therefore the impact upon the observed mineralogies, microstructure and subsequent geotechnical properties is poorly understood.

I hypothesise reworking influences how the individual particles within the soil mass behave, in terms of grain sorting and the development of bedding within the materials. Evidence of sorting could be seen in the thin section analysis, with DRAB1 appearing to have the greatest degree of variance between grain sizes. TV1 however appeared to have a slightly more uniform grain size of ~800 µm (**Figure 9.5**). Grain sorting influences porosity and permeability, with more well sorted sediments being more porous and permeable compared with poorly sorted sediments. TV1 appears to show thin sections in keeping with those produced in previous studies using Tauranga sensitive soil materials (Mills, 2016; Robertson, 2017), whilst DRAB1 varies, with a large variance in grains being observed (**Figure 9.5**).

Bedding between differing depositional layers is also commonly observed in outcrops across the Hamilton Basin. Bedding was observed at both sites sampled, in particular at Dixon Road Roundabout (**Figure 4.2** and **4.3**). It is likely these beds formed in response to reworking, with materials of differing densities being arranged as the reworking agent moved through the soil.

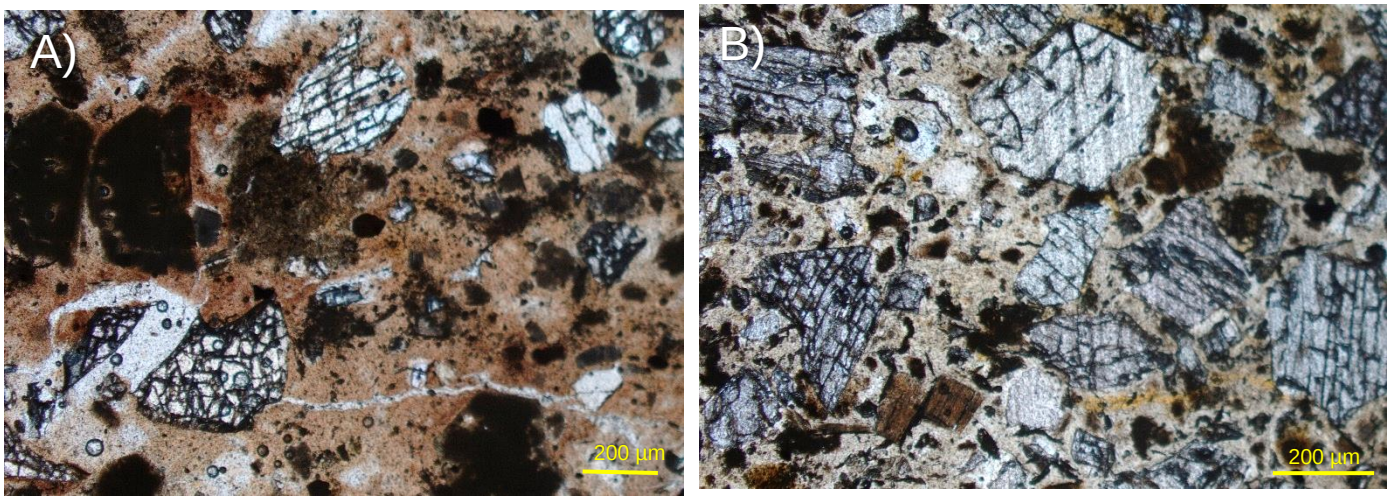

Figure 9.5. Thin section images showing the sorting and apparent weathering and sorting of the larger grains in both TV1 (A) and DRAB1 (B). TV1 appears to contain more uniform sized, sub-rounded grains; conversely, DRAB1 contains much more variance in sizes of grains, and appear more angular compared with TV1.

Arthurs (2010) alluded to reworking of pyroclastic materials across Tauranga to have an influence on sensitivity. Similarly, I believe there could be some benefit in the determination of reworking in these materials, and to assess whether the properties seen are influenced by the process. The sensitive Tauranga materials studied extensively in recent history could provide a viable source, as recent research (Cunningham et al., 2016; Kluger et al., 2017) has alluded to the differences in soil layers being attributed to different levels of material reworking following deposition.

In addition to reworking, the degree of weathering the samples have experienced may influence a number of characteristics. The Puketoka Formation and wider Walton Subgroup materials were deposited recently in geological history (**chapter 2**). The Tauranga soils were also deposited around the same time (~1 Ma). However, the soils of Tauranga show evidence of experiencing a greater degree of weathering, compared with the soils of this study. This is evidenced in the SEM imagery (**chapter 8**). Whilst some degree of weathering was observed, the weathering features were generally shallow, and grains appeared largely intact. In this study, thin section imagery also supports this (**chapter 7** and **Appendix 7.4**), with the clay groundmass remaining cohesive, and grains displaying some weathering joints, but remaining intact. The lack of eutaxitic textures, characteristic of primary ignimbrite deposits should also be noted, as the dominance of matrix structures throughout the samples observed in this study indicate a sedimentary deposit that experienced some degree of reworking.

The individual grains within the thin sections also appeared angular to sub-angular, whilst in studies' such as Mills (2016), the grains appeared more sub-rounded to rounded (**Figure 9.6**). The degree of weathering, and to a lesser degree, transport of the materials, can be inferred from the shape of the particles, which therefore provides evidence that the Puketoka Formation appear to have experienced a lesser degree of weathering compared to the Tauranga materials.

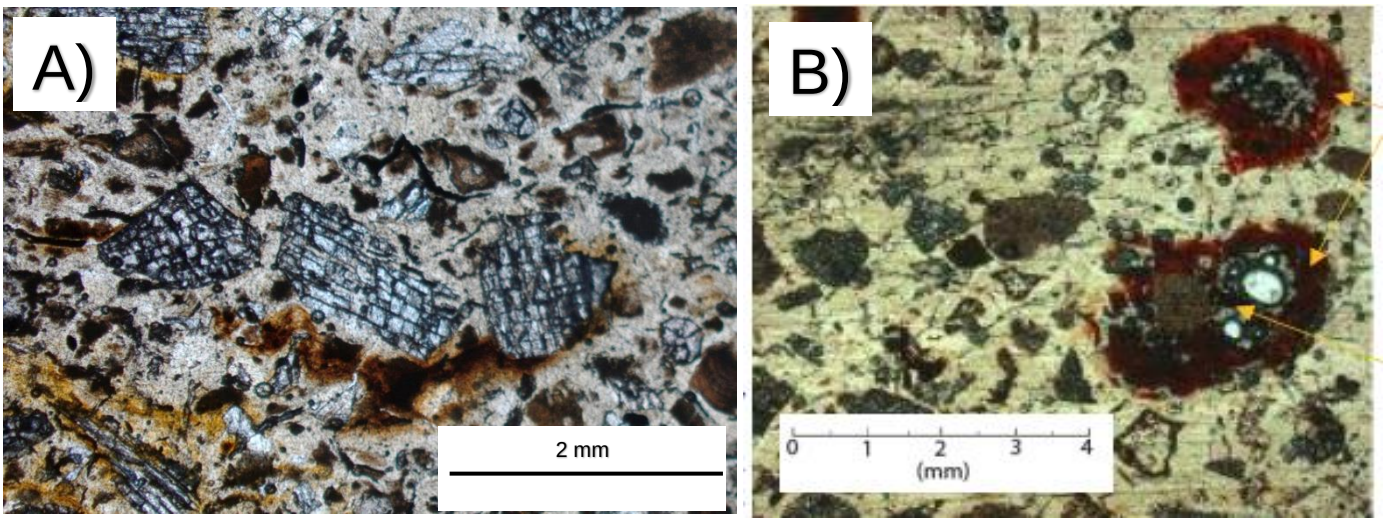

Figure 9.6. Thin section imagery showing the differences in apparent weathering on different grains within materials from the A) Puketoka Formation (DRAB 270 kPa) and the B) Tauranga sensitive soils (M1) (Mills, 2016). Note the lack of eutaxitic structures in either thin section, indicative of the sedimentary nature of the materials.

Weathering also likely influenced the formation of clay within the materials. The clay-sized particle concentrations for the samples of this study are generally different from the values gained from studies conducted with Tauranga soils (**Table 9.1**) Wyatt's (2009) study appears to be the most comparable, however, he highlighted that the particle size analyses completed upon the samples were likely underestimating the amount of clay, due to aggregation effects (Wyatt, 2009). Therefore, these values are likely not accurate. The silt-sized particle contents also appear much higher for the materials of this study, compared with the Tauranga soils. Generally, the Tauranga soils have a greater amount of clay-sized particles than the Puketoka Formation, and fewer silt-sized particles. This indicates a potential difference in the source of the materials. The soils of Tauranga are airfall deposits, whereas the Walton Subgroup were derived from pyroclastic flows. Both deposits likely experienced some degree of transport, but the Tauranga sediments likely experienced a greater degree, based on the particle shapes observed in the thin sections. Additionally, the Tauranga materials potentially experienced a greater degree of weathering, as clay forms as a result of weathering, through mineral dissolution (Kluger et al., 2017).

Halloysite has been hypothesised to form through chemical weathering in Si-rich environments (**chapter 2**). Halloysite forms through the transformation of morphologies over time (**chapter 2**). The higher incidence of tubules within the samples analysed indicates the early stage of weathering experienced. Compared with other studies (Wyatt, 2009;

Cunningham, 2012) where microstructure was analysed, the Puketoka Formation contains comparatively fewer plates and books, being dominated by tubules, with some spheroids. The presence of halloysite book formations in TV2 is indicative of a different degree of weathering. Halloysite books (**chapter 2**) are indicative of late-stage weathering in halloysite, forming through the aggregation of plates. This might provide a line of evidence to identify the weathering conditions TV2 experienced, in relation to other factors such as the geographic location, and the original in-situ depth of the material.

The predominance of tubules will have an influence upon the geomechanical properties seen (**chapter 9**). SEM imagery undertaken in this study identified a dominance of tubules in every sample (**chapter 8**). Compared with the previous works of Wyatt (2009) and Cunningham (2012) on Tauranga soils, the majority of Wyatt's samples (TS1, TS2, OM1 – 4) appear to be tubule-dominated, similar to this study. Cunningham's Tauriko samples showed the same trend. However, Wyatt's TS3, in addition to Cunningham's OS1-2 and TPS1 were dominated by either halloysite spheroids or plates, rather than tubules. Therefore, I hypothesise the material collected at Tauriko (from tephra-fall deposits of the Matua Subgroup) likely experienced a similar degree of weathering as the Puketoka Formation and the wider Walton Subgroup. The samples taken at Omokoroa and Te Puna were conversely taken from undifferentiated tephra deposits of the Matua Subgroup, and potentially experienced a greater degree of deep weathering leading to an alteration in the halloysite morphologies seen. In general, I believe the materials within the Tauranga Region have experienced a greater degree of weathering compared with the Puketoka Formation studied. This could be as a result of the estuarine influence within the Tauranga Region, resulting from the actions of the ocean, compared to the inland Hamilton Basin.

A higher density of tubules correlates with a more open microfabric arrangement, which in turn encourages a greater degree of porosity. This is widely accepted in the literature (Joussein et al., 2005; Wyatt; 2009; Moon et al., 2015; Cunningham et al., 2016; Kluger et al., 2017). Higher porosity relates to lower bulk density and predisposes the material to collapse through more spaces being filled with air or water. The moisture content is also reduced, as water is stored in small pores that are not readily accessible, rather than in thin films around the negatively charged clay minerals. The combination of high porosity, low cation exchange capacity and an open microfabric result in less cohesion, and subsequently lower peak strength. Additionally, when the material collapses, water stored in the pores is released, lubricating the

spaces between the clay minerals and further reducing cohesion, producing a low remoulded strength value.

The low porosity leads to a lower permeability in the Puketoka Formation materials, compared with the Tauranga soils. The materials in this study were a magnitude lower than the previously published values for Tauranga soil materials (10^{-8} – 10^{-9} m/s) (Moon et al., 2013). This reduced permeability will have an appreciable influence on the drainage and moisture characteristics of the soil. Water is likely held for extended periods of time within the Puketoka Formation materials and influences the response to disturbance and remoulding.

The dominant microfabric seen across all three samples was characteristic of the 'matrix' style, based upon Huppert's (1986) definition for sedimentary deposits. This relates to the sorting of the materials; and matrix microstructures tend to occur in materials that are poorly sorted (Vernon, 2018). Wyatt (2009) and Cunningham (2012) similarly observed matrix microfabrics, in addition flocculated, honeycomb (Wyatt, 2009), skeletal and turbulent (Cunningham, 2012) microfabrics. Neither Wyatt nor Cunningham completed thin section analyses in their studies, therefore the relative sorting cannot be directly compared between studies. The influence of reworking upon the differing sediments will likely have influenced the degree of sorting seen, therefore this additionally needs to be considered.

Void ratio is used in engineering literature rather than porosity; therefore the two are interchangeable. Void ratios for this study are lower when compared with sensitive soil materials derived from Tauranga (**Table 9.1**). A lower void ratio reduces the compression a material experiences when undergoing shear stresses, due to the greater amount of physical soil present within the material, reducing the amount of space to be filled by material under changing stress condition.

Void ratio relates to the strength of the soil (**Figure 9.3**). Void ratio is generally accepted to be influenced by the particle size distribution, particle shape, and overall microfabric of a material (Xu et al., 2019). These factors in turn influence the shear resistance of the soil (Xu et al., 2019). Evidence shows the Puketoka Formation materials are more granular than soils from Tauranga, and the degree of weathering less, resulting in more angular grains observed. The higher incidence of angular grains indicates a lower overall clay content as a result, and the strength of the material becomes derived from the frictional resistance between the interactions of the grains. In-situ field vane testing is predominantly used for cohesive materials however, with alternate methods (scala penetrometer) being used for more granular materials. Therefore, I hypothesise, for mixed materials such as the Puketoka Formation, that contain an appreciable

amount of clay-sized particles, but a higher amount of silt and sand-sized particles, a field vane test may underestimate the true strength reading, as a result of the higher presence of grains, which gain strength through frictional bonding forces rather than cohesion. The use of additional data, such as the undrained shear strength from cone penetration testing (CPT) and triaxial tests can produce a more comprehensive dataset. This is a beneficial course of action for large-scale projects, such as the Dixon Road Roundabout, as it provides multiple lines of evidence regarding the relative strength of a soil material.

The remoulded strengths tended to be comparable for the Puketoka Formation and Tauranga soils, however (**Table 9.1**). This could have occurred as a result of the reduced amount of clay within the soil to begin with, and the impact of the dominant halloysite tubule morphology reducing the impact of sensitivity, through a lower degree of alteration following remoulding. Tubules have generally been accepted in the literature to impede soil sensitivity through better interactions and connections to one another, compared to more spheroidal morphologies (Kluger et al., 2017). The void ratio also influenced the calculated sensitivity of the material as a direct result, and in keeping with the other findings, the Walton Subgroup sensitivity generally tended to be lower compared with Tauranga (**Table 9.1**).

Therefore, taking into account all of the results observed, I believe sensitivity in the Puketoka Formation, moreover the Walton Subgroup materials is governed by the degree of reworking and weathering the samples have experienced, which in turn has influenced the main morphology of the sensitive halloysite clay minerals, which subsequently influences the microfabric, porosity and permeability of the samples, in addition to the geomechanical properties the materials display. The apparent dominance of tubules impedes sensitivity somewhat, and this is observed in the quantitative relationship between void ratio and sensitivity (**Figure 9.4**). The dominant failure mechanism observed (MSC) throughout triaxial testing also indicates the sensitivity of the soil materials, and was the characteristic response identified in this study, which differs compared with the response generally observed for the Tauranga soil materials. However, the peak strength observed for these samples is lower compared with the Tauranga studies. I believe this could be the case for a number of reasons. Cerato & Lutenegger (2004) hypothesised that a number of factors influences undrained field vane testing in soft to stiff clays. Results hypothesised the perimeter ratio (a ratio between blade thickness and vane diameter) was inversely proportional to the vane strength measured. I believe this, coupled with likely differences in the stress distributions have led to variance in results observed, as the amount of soil impacted through these tests will have differed as a

result, in addition to the amount of soil remoulded through the force of the vane breaking down the inter-particle bonds of the soils.

I believe that testing of the materials using the same shear vane under the same conditions for both the Puketoka Formation and Tauranga soils would be beneficial to provide a more direct comparison, and further developing the sensitivity hypotheses for the Walton Subgroup materials. Additional testing of the differing formations within the Walton Subgroup would also be beneficial.

9.12 Engineering recommendations

Considering the hypothesised controls of sensitivity for the Puketoka Formation materials, remediation strategies need to be considered. Hamilton contains several slopes derived from geological formation processes (hills, riverbank features). However, these are not in the same magnitude as the slopes observed in Tauranga, therefore, the risk of failure following a disturbance is not considered to be as significant.

The Puketoka Formation materials, due to their sensitivity, are deemed unsuitable for use as fill in most earthworks' specifications, as the material does not meet the required specifications by itself. The porous nature and poor permeability of the halloysite-rich soil also make it unsuitable. The longevity of these remediation techniques within and past the design life of around 50 years for volcanic materials such as the Puketoka Formation has not been extensively researched, therefore could provide some future large-scale research to further understand the impacts of remediation over a long period.

9.12.1 Current remediation strategies for sensitivity

Chapter 2 outlined that the current commercial remediation strategies for sensitivity rely largely upon in-situ remediation. Techniques tend to centre around five main modes of remediation: replacement, densification, solidification, reinforcement and drainage (MBIE, 2017). However, a multitude of factors including cost, composition of the materials and depth of the target layers will influence the methods that can be utilised. The specific characteristics of the site, dependent upon the job that is being completed, also need to be considered.

9.12.2 Why in-situ remediation may not be effective

The common remediation strategies for sensitive soil materials may not necessarily be suitable, due to the sensitive nature of the Puketoka Formation materials. The characteristics presented within this thesis could potentially have an impact on which strategies will be effective. Compaction, lime, potassium compound dosing and drainage were selected as remediation strategies with the potential to be beneficial to the Puketoka Formation.

9.12.2.1 Compaction and consolidation

Compaction (**chapter 2**) aims to increase soil density through the re-arrangement of soil particles within a material, through the removal of air. This is a rapid process and is completed through the movement of plant across the soil surface. The properties of the Puketoka Formation encourage a low level of compaction, therefore require less working to produce a compaction level that meets the requirements of a building specification.

Consolidation of the soil materials also needs to be considered. Consolidation is controlled by a soils' moisture content and measured density, which in turn is influenced by the materials porosity (which relates to void ratio). The Puketoka Formation was identified to have a low void ratio, therefore the degree of compaction will decrease compared with soils with a high void ratio, such as the Tauranga soil materials, as a result of fewer pore spaces to become filled with soil material (Kear et al, 1978). As a result, whilst a reduced need for compaction is beneficial in engineering terms, the halloysite tubules that dominate the Puketoka Formation have the potential to release ultra-pore water when crushed, leading to a lubrication of the clay particles and an additional loss of internal cohesive strength. Research into grain crushing in weak materials (pumiceous (NZ, Japan), and carbonates (China)) is a current area of interest in the engineering community, therefore, whilst the hypothesised crushing in the Puketoka Formation materials is at a much smaller scale, it could provide an area of future focused research.

As a result, I believe compaction is an effective general strategy for surface level soil stabilisation in-situ, given that a sufficient stockpile of material exists to use for blending with the weaker materials more prone to failure. For the Puketoka Formation however, the potential for the release of excess water could hinder the effectiveness of compaction. Stabilisation at

depth by compaction is also less viable, therefore additional methods should be explored. Consolidation of the soil is also effective for the long-term stabilisation of soil materials through the movement of pore water, but in low permeable soils such as the Puketoka Formation, consolidation is expected to take an extended period of time, therefore is likely to require additional measures to enhance the materials' consolidation response.

9.12.2.2 Lime application

The application of lime upon soil has a number of effects considered beneficial (

Table 9.3). A study completed by Dibble (1991) with allophanic soil materials determined that the soils reacted with lime to produce a higher shear strength, a reduced plastic and liquid limit, and reduced linear shrinkage. These are similar observations as made in more recent literature (NZ Forest Owners Association, 2011; MBIE, 2017). The extremely low permeability of the Puketoka Formation would potentially not benefit from a further reduction in material permeability in a fill setting, as excess water would become more susceptible to runoff, leading to additional problems in the long-term impacts of the construction project.

Lime interacts with soils in a manner of ways (**chapter 2**). However, a consideration of the irreversible drying of halloysite interlayer water needs to be made. Very little literature exists about the relationship between dehydrated halloysite and observed sensitivity but is an area of research I believe is beneficial to assess further, as the deliberate drying of halloysite soils prompting an irreplaceable loss of water may prove beneficial to improved strength within the material and could have some practicability for use as fill material when mixed with more cohesive materials, or may be more receptive to cementing agents such as lime.

Table 9.3. Summary table detailing the effects of lime application upon cohesive soils (NAASRA, 1986; NZ Forest Owners Association, 2011).

Process:	Effects:
Lime application (Slaked and Burnt)	Reduced plasticity Decreased susceptibility to changes in moisture Improved strength Decreased permeability Increased shear modulus

9.12.2.3 Potassium Chloride dosing

Robertson's (2017) study analysed the impacts of potassium chloride (K_2CO_3) amongst other compounds on soil material from Tauranga. Historical studies determining the impact of potassium compound dosing is discussed in **chapter 2**. He found the shear strength of the materials increased and hypothesises this occurred through the intercalation of the potassium ions within the halloysite basal spacing, displacing the water and expanding the crystal lattice (Robertson, 2017). This in turn was found to increase the particle contact area, causing an increase in cohesion and friction angle (Robertson, 2017). The increased basal spacing within the halloysite particles allows for a greater accommodation of pore water fluid, and reduces the amount of pore water pressure generated through stress application (Robertson, 2017).

The impact of potassium compound dosing upon the Puketoka Formation and wider Walton Subgroup has not been investigated, therefore provides an opportunity for future research, and to determine if the materials behave in the same manner as Tauranga sensitive soils.

Additionally, the testing of potassium-based phosphorus compounds on the materials to determine if a change in properties occurs could also be beneficial. Halloysite is characterised by having substantial phosphate retention capabilities, therefore insights into the impacts of dosing could provide some useful information.

9.12.2.4 Prefabrication vertical drainage

Prefabrication vertical drains (PVDs) were discussed in depth in **chapter 2**. PVDs aim to decrease consolidation time for materials through the lateral transmission of pore water pressure (Turukmane et al., 2019). Drainage appears to be a viable solution for stabilisation in lieu of cementing remediation strategies, which exacerbate some undesirable characteristics of the soil.

The installation of drains could be beneficial for the Puketoka Formation soils, as the excess pore water pressure released during remoulding could be transferred laterally and carried away vertically through the drain. The low permeability of the materials may increase the time needed for primary consolidation to occur however, therefore significant preloads may also be required to increase the rate in which consolidation occurs. This preloading may

encourage disturbance within the near surface soil layers, leading to loss of strength in the materials. The in-situ installation of the drains may also encourage disturbance (Thurukmane et al., 2019). Therefore, I believe it would be beneficial to simulate the in-situ installation of the drain in Puketoka Formation material, and monitor the effects over a set time period, such as 12 months.

Drainage installation relies heavily upon the specific properties of the soil, therefore is unlikely to be beneficial as a general solution. A site-specific assessment likely needs to be made in each case, which reduces the economic feasibility of the drains.

9.12.2.5 Alternate uses of Puketoka Formation material

The Puketoka Formation has material properties that make it somewhat undesirable for use as a cohesive construction fill, and make it challenging to remediate.

However, the properties of the materials could be utilised for differing applications aside from construction fill. Typically, low permeability cohesive fills are deemed suitable for landfill liners. A number of parameters need to be met in order for the material to be deemed suitable (**Table 9.4**). The Puketoka Formation samples, in particular DRAB1, have parameters in line with those needed for landfill liner materials (**Table 9.1**) (Trenter, 2001). The maximum or optimum permeability is usually in the magnitude of 10^{-9} m/s (NRA, 1992; Trenter, 2001). The calculated permeability for the Puketoka Formation are either within these values (TV1 130 and 230 kPa) or lower (10^{-10} m/s). However, it should be noted that the method for calculating the coefficient of permeability in this study was indirect, therefore the estimates cannot be relied on. A more direct measurement would be required to confirm the Puketoka Formations' suitability.

Therefore, I believe there would be some benefit in direct measurement of the permeability, and the analysis of the Puketoka Formation as a landfill liner material, using simulated ion leachate products. This could provide a use to materials deemed unsuitable for use for construction purposes. A comparison of the material both with and without stabilisation with agents like lime or potassium solutions would also be beneficial, to determine if these agents positively increase the response of the materials, through factors such as an increase in pH, which aids in the absorption of ions by the liner material (Trenter, 2001). This was noted

in Robertson's 2017 thesis, where an increase in pH aided in the absorption of potassium compounds within the halloysite soils of the Tauranga region.

Table 9.4. Table summarising the desired parameters for materials to be used as landfill liners (NRA, 1992; Trenter, 2001).

Parameter	Optimum limits
Plasticity index	≥ 20 %
Activity	≥ 0.3
Percentage fines	≥ 10 %
Percentage gravel	≤ 30 %
Maximum particle size	50 mm

9.13 Opportunities for future relevant research

The results of this study provide a dataset that highlights the characteristic geotechnical behaviours expected for the Puketoka Formation and the minerals within the soils. Further opportunities for research based upon the findings of this study are outlined here.

9.13.1 Degree of weathering and evidence of reworking analysis

The sensitivity of the Puketoka Formation and the wider Walton Subgroup soils have been hypothesised to be controlled by the morphology of the materials, influencing the porosity, permeability and measured strength. The degree of weathering and potential reworking the materials experienced likely influenced this. Quantitative characterisation of the amount of weathering the soils have experienced, through analysis of clay contents of multiple samples, the relative abundances of mafic and felsic silicate minerals, and any published data within the geological record of the area could provide viable evidence. Reworking could similarly be investigated, and characteristics relating to the sorting and microstructure of the materials analysed, and potentially related to the macro-scale features that potentially indicate reworking, such as the bedding of material.

9.13.2 Liquefaction potential of the identified sensitive materials

The discovery of the extensive fault network beneath the Hamilton basin has raised questions regarding the resilience of current infrastructure if an earthquake event were to hit the city, and the susceptibility of the materials making up the Hamilton basin to liquefaction. This is of interest, due to the inherent properties of the Puketoka Formation. The silt-sized particle dominance in all three samples is appreciable (>50 %), therefore has a potential to liquefy. However, the age, weathering and depth characteristics of the Puketoka Formation somewhat reduces this risk, thus reducing the probability of significant liquefaction occurring following an earthquake event. However, I believe there is some benefit of a comprehensive assessment of the present day liquefaction susceptibility of the Puketoka Formation materials.

9.13.3 Further analysis of halloysite morphologies

The assessment of which halloysite morphology contributes the most to the sensitivity of the Walton Subgroup material could be beneficial. Previous literature has historically proven that spheroidal halloysite has been present in failed material following landslide events worldwide (Smalley et al., 1980; Tanaka, 1992). This has been further proven more locally, in the Tauranga Region (Cunningham et al., 2016). Therefore, I believe it would be beneficial to further study the morphologies within the Puketoka Formation and wider Walton Subgroup materials, to determine if any characteristic layer is associated with higher sensitivity.

9.13.4 Assessment of current in-situ remediation strategies

I believe it would be beneficial to further assess the current widely used in-situ remediation strategies used to remediate the soil material, and potentially test the different strategies in a lab-based setting, to determine the relative effectiveness against one another for the Puketoka Formation. Lime is a logical starting point, following Dibble's (1991) research regarding lime stabilisation in allophanic soils highlighting the lack of information regarding the effects of lime addition to soils of varying allophane contents, and the amount of lime needed to make an impact upon soil properties, and whether it would be economically viable to dose large amounts of soil material (Dibble, 1991).

Robertson's 2017 study assessed the use of potassium chloride (K_2CO_3) to stabilise the sensitive soil layer identified within Omokoroa. Dosing the Puketoka Formation with the same potassium compounds could provide evidence into whether the impact is specific to the properties of the Tauranga soil, or has the potential to have wider applicability.

9.13.5 Impacts of dehydrated halloysite

Very little literature exists regarding the impacts of dehydrated halloysite upon the strength and sensitivity characteristics of soil material. Lab-based tests on dehydrated halloysite soils could provide some quantitative data to be compared. The influence of dehydration upon remediation strategies such as lime addition could also be beneficial to assess further.

9.13.6 Specific engineering parameter development – Cone Penetration Testing (CPT)

The data gained from cone penetration testing (CPT) can be used to directly solve a variety of engineering problems. For differing material types, differing reliabilities for different problems can be observed (Robertson & Cabal, 2015).

No specific parameters exist for determining CPT properties for the Walton Subgroup materials. Generally, in programs such as CLiq and CPeT-IT, a general set of parameters for a select region or area of interest are used. However, individual layers or groups do not tend to be quantified. Results are generated from the CPT trace data, and a generic soil behaviour type attached to each differing soil layer. However, whilst small-scale variations can be determined by the CPT through changes in the sleeve friction, pore water pressure and cone resistance readings, only one set of calculation parameters is used to assess an entire CPT trace. The parameters inputted for analysis (peak ground acceleration and maximum earthquake magnitude), in the case of the Hamilton Basin, are based off calculations completed prior to the discovery of the extensive fault network. As a result, these values may be underestimating the impact of the earthquakes on the materials of the Hamilton Basin. CPT data also defines layers based on the characteristic sleeve friction, pore water pressure and sleeve friction values. This does not account for the relative densities of different particle sizes. The results of this

study have identified the importance of the relative densities of clay, silt and sand-sized particles on the geotechnical behaviours of the materials, including the strength characteristics.

The CPT data populated can then be used for additional analyses, such as slope stability in SLIDE. SLIDE uses the calculated friction angle, cohesion, groundwater level and slope angle to produce a model that can simulate the stability of the materials *in situ* in a slope. However, SLIDE is mainly used to assess the risks for materials situated on a slope, therefore materials on a flatter environment may not be accurately assessed as a result.

This can lead to a generalisation of how a soil profile behaves, disregarding any differences arising from differing formations. As a result, often a conservative approach is taken to specific engineered designs, which can be in excess of what is required for stabilization or retention. This approach may not be beneficial in some cases, and over-engineering the soil materials may lead to economic losses which could have been avoided.

The shear strength parameters gained for this study (**chapter 7, *Table 7.3***) could provide some indication of suitable parameters to be used to analyse the Puketoka Formation materials in programs such as CLiq and CPeT-IT, to determine the liquefaction potential of the materials, and as a basis for further analysis in stability programs such as SLIDE. However, due to the limited repeated tests completed, these values can be used as an indication only, and provide a starting point for future focused research.

The development of specific parameters for differing formations could provide a more accurate assessment of in-situ soil behaviour, which could lead to more tailor-made recommendations and designs being produced. This could streamline designs and create a potential for cost saving by all parties involved, from the time taken to produce designs, to the implementation and construction costs of designs that are more site-specific (Day, K., Personal Communication, 31st January 2021).

9.14 Summary

The results of this study has led to the identification of a number of differences in properties between the Puketoka Formation of the Walton Subgroup and sensitive soils previously studied. This has led to a hypothesis being developed determining that the degree of reworking and weathering likely influenced the sensitivity observed in the Puketoka Formation samples. The low measured porosity, permeability, and strength values of the

Puketoka Formation are hypothesised to have developed through the geological history of the materials.

The identified remediation strategies commonly used in engineering practice has been discussed, and the lack of relevant literature regarding halloysite-rich soils. Lime stabilisation is widely used and has been found to decrease plastic limit, porosity, increase strength, and reduce linear shrinkage. Whilst a strength increase would be beneficial to the low strength Puketoka Formation materials, reduced porosity would not, due to the already low values calculated. Drainage has the potential to be a suitable option for remediation of large-scale deposits, however, whilst it has been hypothesised to aid in the dissipation of excess pore water pressure of low permeability soils, limited relevant literature exists for the impacts in halloysite-rich soils.

Chapter 10
Conclusion

The presence of sensitive soils within the Hamilton Basin causes issues for engineers, as these materials are susceptible to loss of strength, and can lead to significant damage if left untreated. The sensitive soils within the Hamilton Basin are derived from volcanic material, classified as the Puketoka Formation of the Walton Subgroup, and the hypothesised in-situ reworking and weathering of the materials contributes to the sensitivity observed.

The aim of this thesis was to determine the characteristic mineralogical and microstructural properties of the Puketoka Formation, in addition to completing a set of laboratory based geomechanical tests to provide a characteristic set of classification results, and to determine whether the Puketoka Formation materials show similarities to previously studied sensitive soil materials, such as those found in Tauranga.

The bulk and particle density values were generally characteristic of sensitive soil materials, based on previously published values. The samples had lower observed densities overall, compared with previous studies completed. Particle size distribution results indicated all three samples tested were silt-dominated, with varying proportions of clay and sand-sized particles. All samples were consistent with published values for silt content within sensitive materials derived from volcanic activity. The activity of the samples differed between inactive to active, dependent on the particle componentry of the material.

XRD analysis indicated that all three samples contained varying amounts of halloysite, plagioclase, cristobalite, quartz and volcanic glass. This is consistent with the materials expected from a pyroclastic flow deposit, and the presence of halloysite confirms the materials' origin in the geological history of the Hamilton Basin. One sample (TV2) was seen to also contain kaolinite clays. Scanning Electron Microscope (SEM) imagery taken provided evidence of several different hypothesised halloysite clay morphologies, including tubules, spheroids, plates and vermiform books. The interactions were analysed, and it was determined the samples show microfabrics generally consistent with matrix and skeletal arrangements. TV2 also contained the greatest abundance of book features, potentially indicative of kaolinite.

Atterberg limits indicated all three samples fell within the “MH” category, indicative of high plasticity, inorganic silts and clays with a liquid limit greater than 50 % (Carter & Bentley, 2016).

Triaxial results indicated two main failure types were experienced by the samples, either shear band formation, or intermediate failures. Contraction of material was observed in all tests. Generally, positive changes in pore water pressure were experienced. The responses relate to the differing clay and silt contents of the samples, with greater silt content influencing the effective cohesion and friction angles observed. The void ratio of the samples also influenced the degree of compression experienced by the materials. Thin section results showed the development of some Riedel shear features, indicating a degree of strain softening experienced by the materials.

The results of this thesis research have provided a set of data that can be used as an additional reference point in the determination and analysis of the Puketoka Formation materials. This study has also provided a potential hypothesis into why the Puketoka Formation within the Walton Subgroup differ from the Tauranga soils in terms of sensitivity, relating to the relative weathering and reworking the Walton Subgroup has experienced compared with the Tauranga soils. The Puketoka Formation was found to be less weathered, less permeable, more poorly sorted and produced a lower peak strength value compared with the Tauranga materials, which I believe was influenced by the amount of reworking the Puketoka Formation underwent following deposition. Whilst the main halloysite morphologies between both the Puketoka Formation and previously studied Tauranga soils were similar (tubules), the Puketoka Formation contained appreciably less spheroidal and plate forms of halloysite, compared with Tauranga. The dominance of tubules influences the sensitivity observed within the materials, through the arrangement of the tubules within the microfabric, the extent of bonding between the clay particles through surface area interactions, and the amount of these bonds that withstand the remoulding of the material.

Because the Puketoka Formation is used as a material for construction, the current *in situ* remediation processes have been analysed, and I believe that strategies encouraging secondary consolidation and the movement of pore water, such as through the installation of prefabrication vertical drains would be beneficial for mitigating the risks posed by soil materials such as the Walton Subgroup.

Further research is suggested and encouraged to further build upon the data presented here. Some further research ideas include:

- Determination of the extent of reworking and weathering experienced by the Walton Subgroup materials;
- the assessment of the liquefaction potential of these silt-dominated materials following the recent discovery of the complex fault system running beneath the Hamilton Basin;
- the potential identification of the main halloysite morphology causing sensitivity within the soil, in a similar manner to that of the Tauranga sensitive soil materials
- further assessment into porosity and relative weathering impacts upon observed sensitivity;
- impacts of dehydrated halloysite on the engineering parameters of the Walton Subgroup materials.
- the assessment of current in-situ remediation strategies in relation to their effectiveness upon the Walton Subgroup, and the suggestion of alternative uses for removed material; and
- the development of more specific parameters for use in engineering programs such as CPeT - IT or CLiq to better estimate the engineering characteristics of the Walton Subgroup materials.

The results of this thesis research may also provide a viable and useful guide for a number of groups, including Waikato University Alumni that are researching similar topics, and for local engineering consultancy firms to better determine the relative risk of sensitive soils complicating the planning and construction monitoring phases, particularly with the emerging evidence of the extensive fault system running under much of Hamilton. These developments, and any research undertaken in the future, may aid in providing the information needed for the updating and re-evaluation of existing methodologies and processes undertaken, to provide a basis for future approaches by relevant parties.

References

BS 1377-8: 1990: *Methods of test for soils for civil engineering purposes. Shear strength tests (effective stress).*

ISO/TS 17892-12:2004a, *Geotechnical investigation and testing — Laboratory testing of soil — Part 1: Determination of water content.*

ISO/TS 17892-12:2004b, *Geotechnical investigation and testing — Laboratory testing of soil — Part 2 – Determination of density in fine-grained soils.*

ISO/TS 17892-12:2004c, *Geotechnical investigation and testing — Laboratory testing of soil — Part 12: Determination of Atterberg limits.*

Abuhajar, O., El Naggar, M. H., & Newson, T. (2010). Review of available methods for evaluation of soil sensitivity for seismic design. In *Fifth International Conference on Recent Advances in Geotechnical Earthquake Engineering and Soil Dynamics, 24-29 May, San Diego, CA* (Paper No. 1.32b). https://scholarsmine.mst.edu/icrageesd/05icrageesd/session01b/27

Ahlgren, S. G. (2001). The nucleation and evolution of Riedel shear zones as deformation bands in porous sandstone. *Journal of Structural Geology*, *23*(8), 1203-1214.

Åhnberg, H., Larsson, R., & Holmén, M. (2013). Degradation of clay due to cyclic loadings and deformations. In *Proceedings of the 18th International Conference on Soil Mechanics and Geotechnical Engineering ICSMGE, Paris, France* (pp. 1411-1414).

Anantanasakul, P., & Roth, C. (2018). Undrained behavior of silt-clay transition soils with varying degrees of overconsolidation. *Journal of GeoEngineering, 13*(1), http://dx.doi.org/10.6310/jog.201803_13(1).1.

Arthurs, J. M. (2010). *The nature of sensitivity in rhyolitic pyroclastic soils from New Zealand.* MSc thesis, University of Auckland, New Zealand.

Bain, J. A. (1971). A plasticity chart as an aid to the identification and assessment of industrial clays. *Clay Minerals*, *9*(1), 1-17.

Beattie, A. G. *Petrological controls on the geomechanical behaviour of coal measure soft rock, Waikato, New Zealand.* MSc thesis, University of Waikato, Hamilton, New Zealand.

Bell, F.G. (1988). Stabilisation and treatment of clay soils with lime Part 1 – basic principles. *Ground Engineering*, *21*: 22-30.

Bell, F.G. (1989). Lime stabilisation of clay soils. *Bulletin of the International Association of Engineering Geology*, *39*: 67-74.

Blue Wallace Surveyors Limited (2021). *The Meadows*. http://www.bluewallace.co.nz/projects/the-meadows/

Boulanger, R. W., Idriss, I. M. (2006). Liquefaction susceptibility criteria for silts and clays. *Journal of Geotechnical and Geoenvironmental Engineering*, *132*(11), 1413-1426.

Briaud, J. L. (2013). *Geotechnical Engineering: Unsaturated and Saturated Soils*. Somerset, NJ, USA: John Wiley & Sons.

Brindley, G. W. (1980). Order-disorder in the clay mineral structures. In G. W. Brindley & G. Brown (Eds.), *Crystal Structures of Clay Minerals and their X-Ray Identification* (pp. 125-196). London, U.K.: Mineralogical Society.

Byerlee, J. (1992). The change in orientation of subsidiary shears near faults containing pore fluid under high pressure. *Tectonophysics, 211*(1), 295-303.

Carter, M., & Bentley, S. P. (2016). *Soil Properties and their Correlations*. Chichester, U.K.: John Wiley & Sons.

Casagrande, A. (1948). Classification and identification of soils. *Transactions of the American Society of Civil Engineers, 113*, 901-930.

Cerato, A. B., & Lutenegger, A. J. (2004). Disturbance effects of field vane tests in a varved clay. In A. V. da Fonseca & P. W. Mayne (Eds.), *Geotechnical and Geophysical Site Characterization: Proceedings of the Second International Conference on Site Characterization, ISC-2, Porto, Portugal, 19-22 September, 2004* (pp. 861-867): Millpress.

Chapel Hill Analytical & Nanofabrication Laboratory (2007). *Hitachi S-4700 SEM Training and Reference Guide.* https://chanl.unc.edu/wp-content/uploads/sites/18385/2019/02/S4700.pdf

Churchman, G. J., Pontifex, I. R., & McClure, S. G. (2010). Factors influencing the formation and characteristics of halloysites or kaolinites in granitic and tuffaceous saprolites in Hong Kong. *Clays and Clay Minerals*, *58*(2), 220-237.

Churchman, G. J., & Lowe, D. J. (2012). Alteration, formation, and occurrence of minerals in soils. In *Handbook of Soil Sciences: Properties and Processes* (pp. 1-72). CRC Press.

CMW Geosciences. (2015). *Proposed Temple View Eastern development Tuhikaramea Road, Temple View, Hamilton Geotechnical Interpretive Report*. https://www.hamilton.govt.nz/our-services/planningguidanceandresourceconsents/publicly-notified-applications/Documents/LDS%20Application%20Appendix%204%20CMW%20Geosciences%20Geotech%20Interpretive%20report.pdf

Cunningham, M. J. (2012). *Sensitive rhyolitic pyroclastic deposits in the Tauranga region: Mineralogy, geomechanics and microstructure of peak and remoulded states.* PhD thesis, University of Waikato, Hamilton, New Zealand.

Cunningham, M. J., Lowe, D. J., Wyatt, J. B., Moon, V. G., & Churchman, G. J. (2016). Discovery of halloysite books in altered silicic Quaternary tephras, northern New Zealand. *Clay Minerals, 51*(3), 351-372.

Cuomo, S. (2014). New Advances and Challenges for Numerical Modelling of Landslides Of the Flow Type. *Procedia Earth and Planetary Science*, 9(*C*), 91-100.

Dibble, W. H. (1991). *Lime stabilisation of an allophanic soil.* PhD thesis, University of Waikato, Hamilton, New Zealand.

Edbrooke, S. W. (Ed.). (2005). *Geology of the Waikato area* (p. 68). Institute of Geological & Nuclear Sciences.

Firoozi, A. A., Olgun, C. G., Firoozi, A. A., & Baghini, M. S. (2017). Fundamentals of soil stabilization. *International Journal of Geo-Engineering*, *8*(1), Article No. 26.

Gillott, J. (1979). Fabric, composition and properties of sensitive soils from Canada, Alaska and Norway. *Engineering Geology*, *14*(*2*), 149-172.

Goodary, R., Lecomte-Nana, G. L., Petit, C., & Smith, D. S. (2012). Investigation of the strength development in cement-stabilised soils of volcanic origin. *Construction and Building Materials*, *28*(1), 592-598.

Gylland, A. S., Long, M., Emdal, A., Sandven, R. (2013a). Characterisation and engineering properties of Tiller clay. *Engineering Geology*, *164*, 86-100

Gylland, A. S., Rueslåtten, H., Jostad, H. P., & Nordal, S. (2013b). Microstructural observations of shear zones in sensitive clay. *Engineering Geology*, *163*, 75-88.

Gylland, A. S., Jostad, H. P., & Nordal, S. (2014). Experimental study of strain localization in sensitive clays. *Acta Geotechnica, 9*, 227-240

Hamilton City Council (2020). *Peacocke SH3 Roundabout*. https://www.hamilton.govt.nz/our-city/city-development/peacocke/upcoming-works/Pages/Peacocke-SH3-Roundabout.aspx

Hamilton City Council (2021). *Temple View Zone Urban Design Guide*. https://www.hamilton.govt.nz/our-council/council-publications/districtplans/ODP/appendix1/Pages/1.4.9-Temple-View-Zone-Urban-Design-Guide.aspx

Harris, W., & White, N. G. In A. L. Ulery & L. R. Richard Drees (Eds.), *Methods of Soil Analysis Part 5—Mineralogical Methods* (pp. 81-115).

Head, K. H., & Epps, R. J. (1980). *Manual of soil laboratory testing* (Vol. 1, No. 2).

London: Pentech Press.

Helle, T. E., Nordal, S., Aagaard, P., & Lied, O. K. (2015). Long-term effect of potassium chloride treatment on improving the soil behavior of highly sensitive clay—Ulvensplitten, Norway. *Canadian Geotechnical Journal*, *53*(3), 410-422.

Helle, T. E. (2017). *Quick-clay landslide mitigation using potassium chloride.* PhD thesis, Norwegian University of Science and Technology (NTNU), Norway.

Hillier, S., & Ryan, P. C. (2002). Identification of halloysite (7 Å) by ethylene glycol solvation: the 'MacEwan effect'. *Clay minerals*, *37*(3), 487-496.

Huppert, F. (1986). *Petrology of soft tertiary sedimentary rocks and its relationship to geomechanical behaviour Central North Island, New Zealand.* PhD thesis, University of Auckland, New Zealand.

Impact Test Equipment (2016). *50kN triaxial load frame - digital with fully variable speed limit*. Retrieved from: http://www.impact-test.co.uk/products/3182-50kn-triaxial-load-frame-digital-with-fully-variable-speed-limit/

Jacquet, D. (1990). Sensitivity to remoulding of some volcanic ash soils in New Zealand. *Engineering Geology*, *28*(1-2), 1-25.

Joussein, E., Petit, S., Churchman, J., Theng, B., Righi, D., & Delvaux, B. (2005). Halloysite clay minerals—a review. *Clay minerals*, *40*(4), 383-426.

Kamp, P. J., & Lowe, D. J. (1981). Quaternary stratigraphy, landscape, and soils of the Hamilton Basin. In *Geological Society of New Zealand Annual Conference* (pp. 14-28). University of Waikato.

Katz, Y., Weinberger, R., & Aydin, A. (2004). Geometry and kinematic evolution of Riedel shear structures, Capitol Reef National Park, Utah. *Journal of Structural Geology*, *26*(3), 491-501.

Keam, M. J. (2008). *Engineering geology and mass movement on the Omokoroa peninsula, Bay of Plenty, New Zealand.* MSc thesis, University of Auckland, New Zealand.

Kear, D., Schofield, J. C., & Couper, R. A. (1978). *Geology of the Ngaruawahia subdivision.* New Zealand Geological Survey. Bulletin new series no.88. Department of Scientific and Industrial Research, Wellington, New Zealand.

Kluger, M. O., Seibel, D., Moon, V., Kreiter, S., Hepp, D. A., De Lange, W., Jorat, E., Mörz, T. (2015). *The role of halloysite morphology on undrained shear strength and sensitivity of volcanic ashes in New Zealand*. Presented at the InterCoast Workshop, Bremen.

Kluger, M. O., Moon, V. G., Kreiter, S., Lowe, D. J., Churchman, G. J., Hepp, D. A., ... & Mörz, T. (2017). A new attraction-detachment model for explaining flow sliding in clay-rich tephras. *Geology*, *45*(2), 131-134.

Kluger, M. O., Jorat, M. E., Moon, V. G., Kreiter, S., de Lange, W. P., Mörz, T., ... & Lowe, D. J. (2020). Rainfall threshold for initiating effective stress decrease and failure in weathered tephra slopes. *Landslides, 17*(2), 267-281.

Konrad, J. M., & Sawitzki, D. G. (1994). Undrained behaviour of clay-silt mixtures in triaxial compression. In *13th International conference on soil mechanics and foundation engineering* (pp. 33-38).

Kuman, D. (2019). *Determination of optimum moisture content and degradation of shear strength over time for Hamilton ash materials.* PhD thesis, University of Waikato, Hamilton, New Zealand.

Lefebvre, G. (1996). Soft sensitive clays. In K. A. Turner & R. L. Schuster (Eds.), *Landslides: Investigations and Mitigation* (Chapter 24, pp. 607-619). Washington, D.C.: National Academy Press.

Lowe, D. J. (1981). Late Quaternary tephras in the Hamilton Basin, North Island, New Zealand. In *Tephra Workshop (1980)* (pp. 67-73). Victoria University of Wellington.

Lowe, D. J. (Ed.). (1994). *Intra-conference and Post-conference Tour Guides*. Waikato Print, University of Waikato, Hamilton, New Zealand..

Lowe, D. J. (1995). Teaching clays: from ashes to allophane. In Churchman, G.J.; Fitzpatrick, R.W.; Eggleton, R. A. (eds.). *Clays controlling the environment*. Proceedings of the 10th International clay conference 1996, vol 2, Oral papers. CSIRO Publishing, Melbourne.

Lowe, D. J. (2010). Introduction to the landscapes and soils of the Hamilton Basin. In D. J. Lowe, V. E. Neall, M. Hedley, B. Clothier & A. Mackay (Eds.), *Guidebook for pre-conference North Island New Zealand "Volcanoes to ocean" 26th-30th July, 2010, 19th World Congress of Soil Science: soil solutions for a changing world: Brisbane Australia 1-6 August 2010* (pp. 1.14-1.61): New Zealand Society of Soil Science.

Lowe, D. J., Lanigan, K. M., & Palmer, D. J. (2012). Where geology meets pedology: Late Quaternary tephras, loess, and paleosols in the Mamaku Plateau and Lake Rerewhakaaitu areas. In A. Pittari (Ed.), *Field Trip Guides, Geosciences 2012 Conference, Hamilton, New Zealand. Geoscience Society of New Zealand Miscellaneous Publication 134B* (pp. 2.1−2.45).

Lowe, D. R. (1975). Water escape structures in coarse-grained sediments. *Sedimentology*, 22(*2*), 157-204.

Marcucci, E. C., & Hynek, B. M. (2014). Laboratory simulations of acid-sulfate weathering under volcanic hydrothermal conditions: Implications for early Mars. *Journal of Geophysical Research: Planets*, *119*(3), 679-703.

Malvern Instruments Ltd. (2013). Mastersizer 3000 User Manual. Worcestershire: United Kingdom.

McCraw, J., & Geoscience Society of New Zealand, issuing body. (2011). *The wandering river: Landforms and geological history of the Hamilton Basin* (Guidebook (Geoscience Society of New Zealand); no. 16).

McNamara, G. (2003). *The Presence of Allophanes in Soils and Its Effects on Long Term Stabilized Strength of Fiji Roading Materials*. Auckland: Materials and Stabilising Consultancy.

Meilani, A., & Fikri, F. (2020). Analysis of settlement prediction due to preloading and vertical drain applications on runway construction. In *E3S Web of Conferences* (Vol. 156, p. 02002). EDP Sciences.

Mills, P. (2016). *Failure mechanisms in sensitive volcanic soils in the Tauranga Region, New Zealand.* MSc thesis, University of Waikato, Hamilton, New Zealand.

Ministry of Business, Innovation and Employment (2017) *Earthquake Geotechnical Engineering Practice – Module 5: Ground Improvement of Soils Prone to Liquefaction.*

Moon, V. G. (1989). *Relationships between the geomechanics and petrography of ignimbrite.* PhD thesis, University of Waikato, Hamilton, New Zealand.

Moon, V., & Blackstock, H. (2004). A methodology for assessing landslide hazard using deterministic stability models. *Natural Hazards*, *32*(1), 111-134.

Moon, V. G., Cunningham, M. J., Wyatt, J. B., Lowe, D. J., Morz, T., & Jorat, M. E. (2013). Landslides in sensitive soils, Tauranga, New Zealand. In C. Y. Chin (Ed.), *Hanging by a thread? Lifelines, infrastructure and natural disasters. Proceedings of the 19th NZGS Symposium, 20-23 November, 2013, Queenstown New Zealand* (Vol. 38, pp. 537-544).

Moon, V. G., Lowe, D. J., Cunningham, M. J., Wyatt, J., Churchman, G. J., de Lange, W. P., ... & Tommasi, P. (2015). Sensitive pyroclastic-derived halloysitic soils in northern New Zealand: interplay of microstructure, minerals, and geomechanics. In *Volcanic Rocks and Soils. Proceedings of the International Workshop on Volcanic Rocks and Soils, Lacco Ameno, Ischia Island, Italy* (pp. 3-21). Taylor & Francis, London, UK.

Moon, V. (2016). Halloysite behaving badly: Geomechanics and slope behaviour of halloysite-rich soils. *Clay Minerals, 51*(3), 517-528.

Moon, V. G., Mills, P. R., Kluger, M. O., Lowe, D. J., Churchman, G. J., de Lange, W. P., … Mörz, T. (2017). Sensitive pyroclastic soils in the Bay of Plenty, New Zealand: Microstructure to failure mechanisms. In G. J. Alexander & C. Y. Chin (Eds.), *Proceedings 20th New Zealand Geotechnical Society Symposium, 23-26 November, 2017, Napier, New Zealand* (pp. 1-8): New Zealand Geotechnical Society.

Morgenstern, N. R., & Tchalenko, J.S. (1967). Microscopic Structures in Kaolin Subjected to Direct Shear. *Geotechnique, 17*, 309-328.

Multiquip (2012). *Soil Compaction Handbook*: Carson, USA: Multiquip Incorporated.

Murphy, C.P. (1985). Faster methods of liquid-phase acetone replacement of water from soils and sediments prior to resin impregnation. *Geoderma*, *35*: 39--45.

NZ Forest Owners Association (2011). *Forest Road Engineering Manual:* Wellington, New Zealand.

New Zealand Geotechnical Society. (2005). *Field description of soil and rock*. Retrieved from: https://fl-nzgs-media.s3.amazonaws.com/uploads/2016/06/NZGS-2005-Field-description-of-soil-and-rock.pdf.

Parfitt, R.L. (1990). Allophane in New Zealand - A review. *Soil Research*, 28, 343-360.

Phoon, K.-K., & Kulhawy, F. H. (1999). Characterization of geotechnical variability. *Canadian Geotechnical Journal*, *36*(4), 612-624.

Podor, R., Ravaux, J., & Brau, H. P. (2012). In situ experiments in the scanning electron microscope chamber. In V. Kazmiruk (Ed.), *Scanning Electron Microscopy* (Chapter 3). IntechOpen.

Rees, S. (2013). *Part One: Introduction to Triaxial Testing*. GDS Instruments.

Robertson, P. K., & Cabal, K. L. (2015). *Guide to Cone Penetration Testing for Geotechnical Engineering*. (6th ed.). Signal Hill, CA: Gregg Drilling & Testing.

Robertson, T. P. (2017). *Is there a salty solution to sensitive soil sliding in the Bay of Plenty, New Zealand?* PhD thesis, University of Waikato, Hamilton, New Zealand.

Robinson, F. (2016). Variation in rhyolitic magma composition linked with fractionation from a common source: Insights from the Rotoiti eruption, Taupo Volcanic Zone, New Zealand. *International Geology Review*, 58(*16*), 1967-1982.

Sachan, A., & Penumadu, D. (2007). Identification of Microfabric of Kaolinite Clay Mineral Using X-ray Diffraction Technique. *Geotechnical and Geological Engineering*, *25*(6), 603-616.

Selby, M. J., & Lowe, D. J. (1992). The middle Waikato Basin and hills. In J. M. Soons & M. J. Selby (Eds.), *Landforms of New Zealand* (2nd ed., Chapter 10, pp. 233-255). Auckland, New Zealand: Longman Paul.

Selby, M. (1993). Rock-slope processes. In *Hillslope Materials and Processes* (Chapter 15, pp. 320-355). Oxford, U.K.: Oxford University Press.

Shi, B., Wu, Z., Inyang, H., Chen, J., & Wang, B. (1999). Preparation of soil specimens for SEM analysis using freeze-cut-drying. *Bulletin of Engineering Geology and the Environment*, *58*(1), 1-7.

Smalley, I. J. R., Ross, C.W., Whitton, J.S. (1980). Clays from New Zealand support the inactive particle theory of soil sensitivity. *Nature, 288*, 576-577.

Tanaka K. (1992) Slope hazards and clay minerals. *Journal of the Clay Science Society of Japan (Nendokagaku), 32*, 16–22.

Terzaghi, K. (1925). *Erdbaumechanik auf Bodenphysikalischer Grundlage Deuticke*. Vienna.

Thakur, V. (2011). Numerically observed shear bands in soft sensitive clays. *Geomechanics and Geoengineering: An International Journal*, *6*(2), 131- 146.

Thakur, V., Degago, S. A., Oset, F., Aabøe, R., Dolva, B. K., Aunaas, K., ... & L'Heureux, J. S. (2014). Characterization of post-failure movements of landslides in soft sensitive clays. In *Landslides in sensitive clays* (pp. 91-103). Springer, Dordrecht.

Thakur, V., L'Heureux, J., & Locat, A. (2017). *Landslides in Sensitive Clays - From Research to Implementation*. Advances in Natural and Technological Hazards Research (Vol. 46). Cham, Switzerland: Springer.

Theng, B. (2012). The Clay Minerals. In *Developments in Clay Science* (Vol. 4, Chapter 1, pp. 3-45). Elsevier.

Toksoz, D., & Yilmaz, I. (2019). A fuzzy prediction approach for swell potential of soils. *Arabian Journal of Geosciences*, *12*(23), 1-10.

Trenter, N. A. (2001). *Earthworks: A guide*. London: Thomas Telford.

Turukmane, R., Gulhane, S., Kolte, P., & Chaudhary, B. (2019). Prefabrication vertical drain for soft soil consolidation. *Technical Textiles International, 62*. 27-29.

Vernon, R. H. (2018). *A Practical Guide to Rock Microstructure*. Cambridge, U.K.: Cambridge University Press.

Ward, W.T. (1972) Pleistocene ash in the Waikato basin: Ages implied by changes in sea level. *New Zealand Journal of Geology and Geophysics, 15*(4), 678-685.

Wesley, L. D. (1973). Some basic engineering properties of halloysite and allophane clays in Java, Indonesia. *Geotechnique*, *23*(4), 471-494.

White, N. G., & Dixon, J. B. (2002). Kaolin–serpentine minerals. In J. B. Dixon & D. G. Schulze (Eds.), *Soil Mineralogy with Environmental Applications* (Vol. 7, Chapter 12, pp. 389-414). Madison, WI: Soil Science Society of America.

White, P. A., Tschritter, C., Rawlinson, Z., Moreau, M., Dewes, K., & Edbrooke, S. (2015). *Groundwater Resource Characterisation in the Waikato River Catchment for Healthy Rivers Project.* Technical Report 2018/33. Waikato Regional Council, Hamilton, New Zealand.

Whitton, S. J., & Churchman, J. G. (1987). *Standard Methods for Mineral Analysis of Soil Survey Samples for Characterisation and Classification in NZ Soil Bureau.* NZ Soil Bureau Scientific Report 79. Department of Scientific and Industrial Research, Lower Hutt, New Zealand.

Wyatt, J. B. (2009). *Sensitivity and clay mineralogy of weathered tephra-derived soil materials in the Tauranga region.* MSc thesis, University of Waikato, Hamilton, New Zealand.

Xu, Z., Xu, N., & Wang, H. (2019). Effects of particle shapes and sizes on the minimum void ratios of sand. *Advances in Civil Engineering*, *2019*' Article ID: 5732656.